REPORT DOCUMENTATION PAGE

Form Approved
OMB No 0704-0188

1. AGENCY USE ONLY (Leave blank)	2. REPORT DATE	3. REPORT TYPE AND DATES COVERED
		FINAL

4. TITLE AND SUBTITLE
First International Symposium on Long Wavelength Infrared Detectors: Physics and Applications

5. FUNDING NUMBERS
61102F
2305/FS

6. AUTHOR(S)
Dr Calvo

7. PERFORMING ORGANIZATION NAME(S) AND ADDRESS(ES)
Electrochemical Society, Inc
Pennington, NJ 08534-2896

8. PERFORMING ORGANIZATION REPORT NUMBER
AFOSR-TR- 95 0158

9. SPONSORING/MONITORING AGENCY NAME(S) AND ADDRESS(ES)
AFOSR/NE
110 Duncan Avenue Suite B115
Bolling AFB DC 20332-0001

10. SPONSORING/MONITORING AGENCY REPORT NUMBER
F49620-94-1-0003

11. SUPPLEMENTARY NOTES

12a. DISTRIBUTION/AVAILABILITY STATEMENT
APPROVED FOR PUBLIC RELEASE: DISTRIBUTION UNLIMITED

12b. DISTRIBUTION CODE

13. ABSTRACT (Maximum 200 words)

A CONFERENCE WAS HELD

~~XXXXXXXXXXXXXXXXXXXXXXXXXXXX~~
~~SEE FINAL REPORT ABSTRACT~~

19950323 146

14. SUBJECT TERMS	15. NUMBER OF PAGES
	16. PRICE CODE

17. SECURITY CLASSIFICATION OF REPORT	18. SECURITY CLASSIFICATION OF THIS PAGE	19. SECURITY CLASSIFICATION OF ABSTRACT	20. LIMITATION OF ABSTRACT
UNCLASSIFIED	UNCLASSIFIED	UNCLASSIFIED	UNCLASSIFIED

The Electrochemical Society, Inc.

184th Meeting Program

Including:

Dielectric Science & Technology/Electronics Joint Recent News Papers
State-of-the-Art Program on Compound Semiconductors XIX
Fullerenes: Chemistry, Physics, and New Directions V
Micromachining and 3-D Nanostructures
General Society Student Poster Session

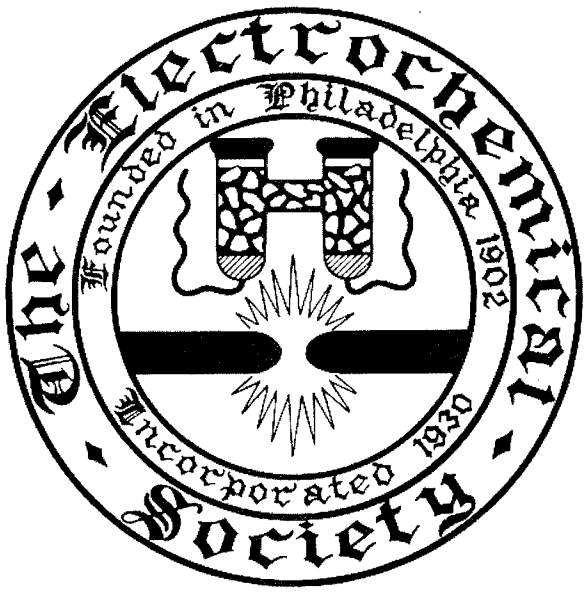

Sheraton New Orleans Hotel
New Orleans, Louisiana
October 10-15, 1993

WELCOME

It is a pleasure to welcome you to the 184th Meeting of The Electrochemical Society, Inc. This Meeting offers a first rate technical program, combined with the fascinating history, fine food, great jazz, beautiful gardens, and other scenic sites for which New Orleans is famous. The Meeting will open on Monday morning with Professor Richard E. Smalley of Rice University delivering The Electrochemical Society Plenary Lecture entitled, "From Buckyballs to Bucky Tubes: New Possibilities in Nano-Technology". The technical program for this Meeting consists of 35 symposia with 752 technical papers scheduled for presentation, including a Recent News Paper Session and the Society's first General Society Student Poster Session.

You are invited to participate not only in our extensive technical program but also in the many other activities planned for this Meeting. The events of the 184th Meeting will provide you with a forum to network and to exchange information, knowledge and awareness of the latest scientific and technical developments with your fellow colleagues from around the world.

On behalf of The Electrochemical Society, Inc., I would like to take this opportunity to express our gratitude to all the individuals who made this Meeting a success. We hope that you will be stimulated by the technical program and will enjoy the many other activities that will take place over the next five days.

Cordially,

Robert P. Frankenthal

Robert P. Frankenthal
President, The Electrochemical Society, Inc.

The Classic New Orleans Plantation Home

A New Orleans Favorite - The Jazz Trio

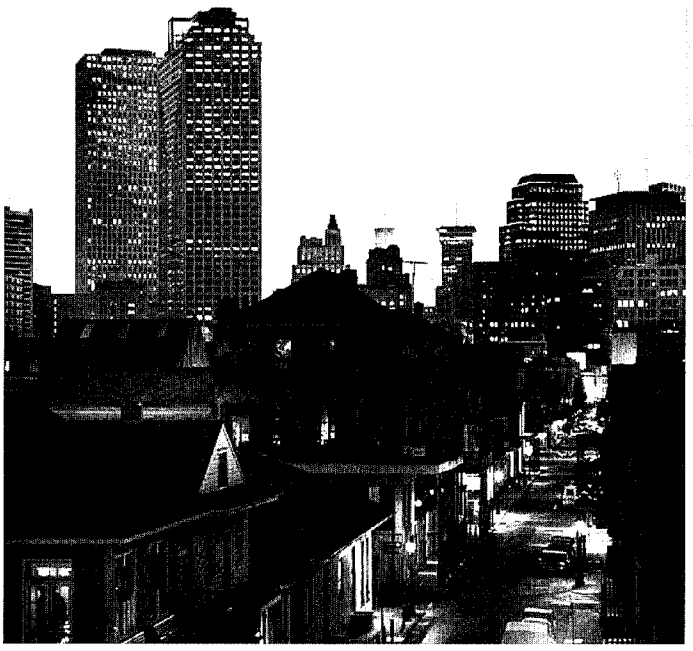

The City at Night - The New Orleans Sky Line

New Orleans

(continued from previous page)

to natives of New Orleans, there's no such thing as a meal too huge to top off with fresh beignets at a sidewalk cafe in the French Quarter.

New Orleans and South Louisiana constitute one of the world's great musical regions. New Orleans is best known for jazz, which made some of its most crucial evolutionary leaps here. Traditional jazz remains healthy as well, and is nurtured at places such as Preservation Hall and the Palm Court Jazz Cafe. Rhythm and blues became an art form in New Orleans some 40 years ago and is still flourishing. Catching an evening of some of the hottest music in the world is simply a matter of taking a stroll down the block.

For an exciting afternoon, climb aboard the St. Charles Avenue streetcar, a national historical landmark and, at more than 150 years old, the oldest continuously operating street railway system in existence. The up-town route runs beneath huge arching oaks, past the handsome mansions of the Garden District, the campuses of Loyola and Tulane Universities, and the luxuriant lawns of Audubon Park, home of the world famous Audubon Zoo.

Not everyone comes to New Orleans to sample its cuisine, listen to jazz, or delve into its history. New Orleans hosts several national sporting events annually, attracting top players from around he world. The Super Bowl, the grandest of sporting events, has taken place in New Orleans more often than in any other city. New Orleans' own football team, the Saints, plays in the Superdome. The Fair Grounds Race Track is the third oldest in the U.S. and home of Risen Star, the 1988 Belmont and Preakness winner. New Orleans has plenty of excitement for sports enthusiasts, whether they are active participants or strictly spectators.

A great many attractions await you in New Orleans, Queen of the Mississippi. Enjoy them all and let the good times roll! ■

* *Photos courtesy of the Greater New Orleans Tourist & Convention Commission*

Tuesday, October 12

Awards and Recognition Session

At this session the following awards will be presented: the Gwendolyn B. Wood Local Section Excellence Award, the F.M. Becket Memorial Award to P. Agarwal and the Norman Hackerman Young Authors' Awards to D. Bonham and E. Aydil. Also, Wayne L. Worrell will be recognized for his term as President. Several Divisional Awards will also be presented, including the H. H. Uhlig Award to H. Isaacs and the Battery Division Research Award to E. Peled. The Carl Wagner Memorial Award will be given to J. Jorne and J.-M. Savéant will receive the Olin Palladium Award at this session. Also, the 1993 class of Society Fellows will be recognized.

Olin Palladium Award Address

Following the Awards and Recognition Session, J-M. Savéant will deliver the Olin Palladium Award Address "Electron Transfer and Bond Breaking."

Olin Palladium Award Reception

Immediately following the Address, a reception will be held in Grand Ballroom A on the 5th Floor to honor Dr. Savéant. Those attending the Session and the Address are invited to attend and greet the medalist.

Jazzin' on the Mississippi

A visit to New Orleans is incomplete without a ride on the "Mighty Mississippi" River. An exclusive charter of the John James Audubon Yacht will be arranged to include a food festival buffet, one drink, and a cash bar. A jazz band will entertain on the top deck. A great way to see New Orleans. Buses depart from the front entrance of the Sheraton at 6:15 PM for the cruise that begins at 7 PM. Prices are: $48.00 for Adults and $42.00 for Children.

SCHEDULE OF COMMITTEES

Sunday, October 10

1:00 PM Seventh International Symposium on Silicon Materials Planning Committee - *Edgewood, 4th Floor*
2:00 PM Electronics Division Subcommittee on Silicon Dioxide/Silicon Interface - *Crescent, 4th Floor*
3:00 PM Electronics Division Subcommittee on Compound Semiconductors - *Southdown, 4th Floor*
3:00 PM Electronics Division Subcommittee on ULSI Science and Technology - *Felicity, 4th Floor*
3:30 PM Vittorio de Nora Award Subcommittee - *Aurora, 4th Floor*
4:00 PM Electronics Division Award Subcommittee - *Crescent, 4th Floor*
5:00 PM External Awards Subcommittee - *Felicity, 4th Floor*
5:00 PM Corrosion Monograph Committee - *Bayside A, 4th Floor*
5:30 PM Corrosion Division Executive Committee - *Southdown, 4th Floor*
5:30 PM Electronics Division Technical Program Planning Subcommittee - *Aurora, 4th Floor*
6:00 PM Battery Division Executive Committee - *Crescent, 4th Floor*
7:00 PM Henry B. Linford Award Subcommittee - *Felicity, 4th Floor*
7:00 PM Dielectric Science & Technology Division Executive Committee - *Bayside B, 4th Floor*
7:00 PM Council of Local Sections - *Ponchartrain Ballroom D, 3rd Floor*
7:00 PM Sensor Group Executive Committee - *Bayside A, 4th Floor*
7:00 PM Luminescence & Display Materials Division Executive Committee - *Edgewood, 4th Floor*
8:00 PM Electronics Division Executive Committee - *Aurora, 4th Floor*

Monday, October 11

7:30 AM Dielectric Science & Technology Division Symposium Planning Committee - *Gallier House, 4th Floor*
7:30 AM High Temperature Materials Division Executive Committee - *Felicity, 4th Floor*
7:30 AM Industrial Electrolysis & Electrochemical Engineering Division Executive Committee - *Oakley, 4th Floor*
10:30 AM Education Committee - *Oakley, 4th Floor*
1:30 PM Society Meeting Committee - *Oakley, 4th Floor*
2:00 PM New Technology Subcommittee - *Gallier House, 4th Floor*
4:00 PM Honors & Awards Committee - *Oakley, 4th Floor*
4:00 PM Ad Hoc Committee on Meeting Content and Format - *Crescent, 4th Floor*
4:30 PM Division/Group/Local Section Representatives to Individual Membership Committee - *Gallier House, 4th Floor*
4:30 PM *Interface* Advisory Board - *Felicity, 4th Floor*
6:00 PM Dielectric Science & Technology Division Governing Body/ Long Range Planning Committee - *Southdown, 4th Floor*
7:00 PM Energy Technology Division Executive Committee - *Gallier House, 4th Floor*
8:00 PM Electrodeposition Division Executive Committee - *Felicity, 4th Floor*

Tuesday, October 12

7:30 AM Symposium Subcommittee - *Walt Whitman, 5th Floor, Waterbury Conference Center*
7:30 AM **Journal** Editorial Board - *Felicity, 4th Floor*
9:00 AM Publication Committee - *Oakley, 4th Floor*
10:30 AM Executive Session of the Individual Membership Committee - *Gallier House, 4th Floor*
1:30 PM Technical Affairs Committee - *Oakley, 4th Floor*

Wednesday, October 13

7:30 AM Solid State Monograph Committee - *Esterwood, 4th Floor*
7:30 AM Finance Committee - *Oakley, 4th Floor*
7:30 AM Council of Past Presidents' Breakfast - *Gallier House, 4th Floor*
10:00 AM Ways & Means Committee - *Oakley, 4th Floor*
12:00 PM Contributing Membership Committee - *Oakley, 4th Floor*
1:30 PM Financial Policy Advisory Committee - *Gallier House, 4th Floor*
4:00 PM Nominating Committee - *Gallier House, 4th Floor*

Thursday, October 14

7:30 AM Solid State Division/Group Chairmen's Breakfast (Dielectric Science and Technology Division Host) - *Oakley, 4th Floor*
9:00 AM Board of Directors' Meeting - *Grand Ballroom B, 5th Floor*

LUNCHEONS AND BUSINESS MEETINGS

Monday, October 11

12:15 PM Battery Division Luncheon & Business Meeting - *Waterbury Ballroom, 2nd Floor*
12:15 PM High Temperature Materials Division Luncheon & Business Meeting - *Armstrong Ballroom, 8th Floor*

Tuesday, October 12

12:15 PM Corrosion Division Luncheon & Business Meeting - *Waterbury Ballroom, 2nd Floor*
12:15 PM Sensor Group Luncheon & Business Meeting - *Armstrong Ballroom, 8th Floor*

Wednesday, October 13

12:15 PM Electrodeposition Division Luncheon & Business Meeting - *Waterbury Ballroom, 2nd Floor*
12:15 PM Luminescence & Display Materials Division Luncheon & Business Meeting - *Armstrong Ballroom, 8th Floor*

TECHNICAL SESSION CHAIRMEN ORIENTATION

All Session Chairmen and Vice-Chairmen are urged to attend an orientation breakfast on the day of their sessions. The breakfast is scheduled from 7:30 AM to 8:30 AM in the Lagniappe Lounge, 2nd Floor. All Session Chairmen and Vice-Chairmen will be sent the necessary information and materials needed to conduct their Technical Sessions. Should you have any questions or specific problems that you would like to discuss, a member of the Society Headquarters Staff will be available in the Lagniappe Lounge for the times indicated above on the day of your participation.

NONTECHNICAL REGISTRANTS PROGRAM

For details of the evening social events, please refer to the category to the category GENERAL FUNCTIONS in this program.

Headquarters for the Nontechnical Registrants will be located in the Lagniappe Lounge, 2nd Floor, of the Sheraton New Orleans Hotel, Monday, October 11 through Thursday, October 14. Those individuals registered as Nontechnical Registrants are cordially invited to a continental breakfast each morning from 8:30 AM to 10:00 AM, Monday through Thursday.

During this period, plans can be made with old and new acquaintances to enjoy one of the many sightseeing tours available through **Hotard Destination Services New Orleans**, the exclusive tour operator for the Society's 184th Meeting. The Tour Registration Desk will be located in the Meeting Registration Area in the Third Floor Foyer of the Sheraton New Orleans Hotel. The tour registration hours are: Sunday - 2:00 PM to 7:00 PM, Monday through Thursday - 8:00 AM to 11:00 AM. Buses for all tours depart from the front entrance of the Sheraton New Orleans Hotel at the scheduled times listed below. Please feel free to contact Hotard Destination Services New Orleans (2838 Touro Street, New Orleans, LA 70122, Phone: (504) 944-0253, Toll Free: (800) 553-4895, or Fax: (504) 944-0253) directly with your questions regarding any of the tours listed below. Call between the hours of 9:00 AM and 5:00 PM Central Time, Monday through Friday. Please mention that you are attending the 184th Meeting of The Electrochemical Society in New Orleans.

Plenary Lecturer and Award Recipient Biographies

Richard E. Smalley to Deliver Plenary Lecture

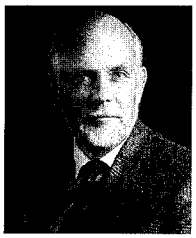

Richard E. Smalley, a Professor of both the Chemistry and Physics Departments at Rice University in Houston, Texas, is well known for his research in the development of new experimental physical techniques for investigating a broad range of questions in chemical physics. Among his most notable discoveries have been the detection and characterization of C_{60}, or buckminsterfullerene, a soccerball-shaped molecule representative of an entire class of molecules, fullerenes, the generation and study of metal-containing fullerenes, and development of a new approach to surface science and catalysis based on small surface bound clusters of atoms.

A prolific writer, with over 160 papers published on chemical physics, Dr. Smalley received his B.S. degree in chemistry from the University of Michigan in 1965. He then went to work for Shell as a research chemist for four years before attending Princeton University, from which he received a Ph.D. in 1973. After graduation, Dr. Smalley moved to the University of Chicago for a postdoctoral period where, with L. Wharton and D. Levy, he pioneered one of the most powerful techniques in chemical physics; supersonic beam laser spectroscopy.

In 1976, Dr. Smalley joined the faculty of Rice University, where he has risen rapidly through the academic ranks, being named to the Gene and Norman Hackerman Chair in Chemistry in 1982. A founder of the Rice Quantum Institute in 1979, Dr. Smalley has served as the chairman of this interdisciplinary Institute since 1986.

Recognized by many as one of the premier scientists in his field, Dr. Smalley has been honored with many awards and with election to a number of associations and societies. Among these are: Election to the National Academy of Sciences in 1990 and the American Academy of Arts and Sciences in 1991; Recipient of the 1991 Irving Langmuir Prize in chemical physics, the 1992 International Prize for New Materials, shared with his colleagues R. Curl and H. Kroto, the 1992 E.O. Lawrence Award of the DOE, the 1992 Robert A. Welch Award in Chemistry, and, most recently, the 1992 Southwest Regional Award of the American Chemical Society.

At Rice University, Dr. Smalley has made pioneering advances in the development of new experimental techniques, such as super-cold pulsed beams and ultrasensitive laser detection techniques, and has applied these techniques to a broad range of vital questions in chemical physics. He is currently working on the development of a new approach to surface science and catalysis. In this new "molecular surface science", small clusters of metals of only 10 to 100 atoms, are used as tiny molecular models of the bulk surface. These models are large enough to display real surface chemistry and physics, but small enough for theorists to handle at a detailed and predictive level.

Jean-Michel Savéant to Receive Olin Palladium Award

Jean-Michel Savéant, a native of Rennes, Brittany, France, received his Doctorat-es-Sciences degree in 1966 from the Ecole Normale Supérieure, where he remained to perform research after graduation, being named Vice-Director of the Chemistry Laboratories in 1967. In 1971 he took a position as Professor of Chemistry at the Université Denis Diderot, where he formed the Laboratoire d'Electrochimie Moléculaire. In 1985 he was named as Directeur de Recherche of the Centre National de la Recherche Scientifique at this laboratory. In 1988 and 1989 Dr. Savéant was a Distinguished Fairchild Scholar at the California Institute of Technology and, in 1993, was elected "Membre Correspondent" of the Academy of Sciences.

Interested in many areas of Molecular Electrochemistry, Dr. Savéant has studied, among other things, the systematic investigation of reaction mechanisms in organic and coordination electrochemistry, the catalysis of chemical reactions by electrons from an electrode, mostly in the field of nuceophilic substitutions, the dynamics of electron transfer in assemblies of redox centers, simple and general modeling of the dynamics of dissociative electron transfer, the factors governing concerted and stepwise mechanisms in reactions where electron transfer and bond breaking are coupled, and the electrochemistry of free radicals. These various studies have allowed Dr. Savéant to progressively build a general understanding of the relationships between single electron transfer and chemical reactivity. This knowledge, acquired on electrochemical grounds, has enabled Dr. Savéant to contribute to many other fields of chemistry, materials science, solid state ionics, and electronics.

Jacob Jorné to be Honored with Carl Wagner Award

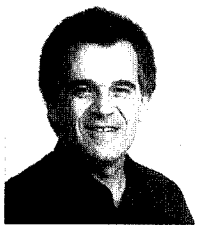

Jacob Jorné, a native of Israel, received his B.S. in chemical engineering from Technion, Israel Institute of Technology, in 1963. He then entered service in the Israeli Army as a Lieutenant, serving until 1967 when he returned to Technion to obtain his M.S. in chemical engineering in 1968. He then moved to the University of California at Berkeley where he obtained his Ph.D. in 1972 under the direction of Charles Tobias. In 1972 he became a Professor at Wayne State University , where he stayed until 1982, when he moved to the University of Rochester as Professor of Chemical Engineering.

Professor Jorné's research is mostly concerned with electrochemistry and microelectronics processing, encompassing a wide variety of areas such as battery research and modeling, flow batteries, alkali metals in nonaqueous solvents, electrodeposition, oscillations and multiplicity in electrochemical systems, plasma etching, and stability of ecosystems.

With his efforts to introduce chemical engineering concepts to electrochemistry, Dr. Jorné helped in the development of a new class of batteries; flow batteries. His fundamental work on the zinc-chlorine battery has resulted in a significant improvement in energy efficiency and contributed to advancing the position of flow batteries as viable candidates for energy conversion and load leveling applications. His work on the interaction between natural and forced convection is of importance, both fundamentally and practically, in the development of various flow batteries and energy storage devices.

Dr. Jorné's pioneering research with Charles Tobias on the the thermodynamics and kinetics of the alkali metals in propylene carbonate provided fundamental information for future research and development of the alkali metal batteries which are rapidly gaining commercial importance. His work on the morphological stability of electrodeposition led to attempts to suppress dendrites and protrusions by hydrodynamic means. Presently, Dr. Jorné is analyzing the morphology of electrode-

to his work with ring-disk electrodes, he developed new electroplated magnetic alloys for use in recording heads. He designed plating tools capable of providing excellent thickness and compositional uniformity over large substrates and wafers of the type used in the manufacture of electronic components. During the last several years, Dr. Andricacos and his co-workers have pioneered the application of plating to chip metallization and interconnection offering significant cost, reliability, and environmental advantages over other processes such as evaporation and chemical vapor deposition traditionally employed in these areas.

An Adjunct Associate Professor at Columbia University since 1990, Dr. Andricacos is also the Chairman of the Metropolitan New York Local Section of the Society. He has authored more than 25 articles in the Journal, written a book chapter on magnetically soft materials, and has been awarded a patent in magnetic recording. At this time he is working on a book on electrochemical technology in thin films. ■

The 1993 Electrochemical Society Fellows

The fourth class of Fellows of The Electrochemical Society will be introduced and honored at the Fall Meeting of the Society during the Awards and Recognition Session, Tuesday, October 12, 1993, at 4:30 PM in the Grand Ballroom C of the Sheraton New Orleans Hotel.

***Richard P. Buck**, in recognition of his contributions to the advancement of the science of theoretical electrochemistry, his leadership in electrochemical science and technology, and participation in Society affiars .*

Dr. Buck, an Adjunct professor of Biomedical Engineering and Mathematics in the School of Medicine at the University of North Carolina at Chapel Hill, received his B.S. in chemistry from the California Institute of Technology in 1950. After graduation he continued his studies at CalTech, receiving an M.S. in chemistry in 1951 before moving to MIT, where he earned a Ph.D. in chemistry in 1954.

Dr. Buck then returned to California and joined Chevron Research Corp. as a Research Scientist working on sensor technology. In 1965 Dr. Buck moved to Beckman Instruments, where he was a Senior Scientist. After two years with Beckman, he took a position with the University of North Carolina as an Associate Professor of Chemistry, and was elevated to the position of Professor of Chemistry in 1975.

Since then Dr. Buck has served as a Visiting Professor at the University of Bristol, Bristol, England (1976-1977), at the Imperial College in London, England (1987), and at the Bundeswher University of Munich, Munich, Germany (1989 to 1991). He has also served as the Chairman of the Society's Sensor Group (1990-1992), and as the Chairman of the Commission on Electroanalysis for the International Union of Pure and Applied Chemistry and was the winner of the von Humboldt Preis of the West German von Humboldt Stiftung (1989-1990).

Dr. Buck has written almost 300 papers on subjects ranging from the theory of ion selective electrodes, solid and gel ion exchangers, field effect devices, transport of mixed conductors, layer and membrane systems, quartz microbalance studies of surface processes, and various analytical methods.

***Larry R. Faulkner**, in recognition of his contributions to the understanding of the electron and energy transfer processes in organized chemical systems, for the invention and design of the cybernetic potentiostat, for the co-authorship (with A.J. Bard) of "Electrochemical Methods: Fundamentals and Applications", and for his leadership in Society affairs.*

Dr. Faulkner is Professor of Chemistry and Dean of the College of Liberal Arts and Sciences at the University of Illinois at Urbana-Champaign. He received his B.S. degree from Southern Methodist University (1966), and a Ph.D. from the University of Texas at Austin (1969).

After completing his graduate work, Dr. Faulkner accepted an assistant professorship at Harvard University, where he worked until 1973, when he joined the faculty at the University of Illinois. A Professor of Chemistry since 1979, Dr. Faulkner spent the 1983-1984 academic year at the University of Austin, returning to the University of Illinois in 1984 as Head of the Department of Chemistry.

Dr. Faulkner's research efforts have spanned more than 25 years and have involved diverse areas. From the mid 1960s to the early 1980s he was active in studies of chemiluminescence arising from very energetic electron transfer reactions in solution, and he contributed to the evolution of mechanistic understanding about the way in which fast electron transfer can yield excited states. In the early 1970s he became interested in the prospects for assembling chemical devices from thin films of molecular materials. Since then, most aspects of his research have concerned the problems of molecular organization and communication of energy and information is supermolecular assemblies. His group has contributed to the knowledge about semiconduction and electrochromism in phthalocyanine thin films, exciton diffusion in organized assemblies of dyes in polymeric matrices, and photoredox processes in zeolites. His activities over the last decade have emphasized electrodes modified with thin films of polymers containing redox centers. A particular focus has been on the kinetic limitations to the motion of electrons in the films. Dr. Faulkner has also maintained an interest in advanced electrochemical instrumentation, working with his group on the invention of the cybernetic potentiostats commercialized by Bioanalytical Systems. Recent research has concerned electrochemical measurements in new domains, including crystalline samples and systems at high pressure. Research is now proceeding in his group on nanosecond timescale electrochemistry at ultramicroelectrodes and on the kinetics of fundamental interfacial processes.

A Society member since 1973, Dr. Faulkner has served on the Executive Committee and as Chairman of the Physical Electrochemistry Division (1979-1987), and on various award selection committees. He has also organized and participated in numerous technical symposia, served as a Divisional Editor of the Journal (1975-1980) and was the recipient of the Young Author's Award in Electrochemical Science and Technology in 1975. Most recently Dr. Faulkner has served the Society as Vice-President (1988-1991) and as President (1991-1992).

Dr. Faulkner was a founder, member of the Board of Directors, and Treasurer of the Society for Electroanalytical Chemistry, a member of the Committee on Science of the ACS, a Titular Member of Commission I.3 (Electrochemistry) of IUPAC, and served on the Selection and Scheduling Committee of the Gordon Research Conferences. He is the Vice-President of the International Society of Electrochemistry and a Fellow of the AAAS.

Dr. Faulkner has served on numerous advisory panels, most recently on the Chinese University Project, sponsored by the

1957, both from the Swiss Federal Institute of Technology. After working with the DuPont Company on polymers and intermediates for three years, he went to the University of California at Berkeley to perform postgraduate studies for two years. In 1961 he accepted a position at the Lawrence Berkeley Laboratory as a Staff Senior Scientist and in 1971 was named as Associate Division Director, a position which he held until 1991. A lecturer in the Department of Chemical Engineering at the Berkeley Campus from 1966 to 1991, Dr. Muller has held numerous positions in the Society. Among them: Chairman of the San Francisco Local Section (1971), Chairman of the Physical Electrochemistry Division (1990), and Chairman of the DeNora Award Committee. Dr. Muller has also been involved in the organization of two Society Meetings in San Francisco.

Dr. Muller is also associated with the International Society of Electrochemistry, where he has held several offices, the Optical Society of America, the American Chemical Society, the Swiss Chemical Society, and AAAS.

Over the years Dr. Muller has studied many different aspects of electrochemistry, including corrosion layers and alkali metals in nonaqueous media, the acceleration of electrochemical mass transfer, the nucleation and growth of thin metal films, and the electrochemical machining of metals, carbides, and borides. More recently, Dr. Muller has worked on the development and use of optical techniques for the study of electrode surfaces, thin films, and boundary layers. During that research he has built a fast, self-compensation spectroscopic ellipsometer and has developed optical models for deriving physical properties of surface layers from the measurements during their nucleation and growth.

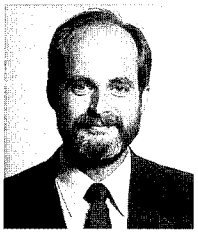

***Carlton M. Osburn**, in recognition of his pioneering work on thin film insulator reliability, development of scaled semiconductor devices, and service to the Society.*

Dr. Osburn received a B.S. in engineering sciences in 1966, a M.S. in aeronautics, astronautics, and engineering sciences in 1967, and a Ph.D. in electrical engineering in 1970, all from Purdue University. After graduation, he went to work at the IBM T.J. Watson Research Center as a Research Staff Member studying the dielectric properties of insulators. In that position he was involved extensively in research on the dielectric properties of thin insulators on silicon for MOSFET applications, a subject on which he has published many papers. In 1973, Dr. Osburn became Manager of the Silicon Process Studies Group, and, in 1976, was named Manager of the Exploratory Fabrication Technology area, with responsibility for research studies and fabrication of advanced semiconductor devices. In this capacity he was responsible for managing the Yorktown silicon processing facility and IBM's submicron VHSIC program.

In 1983, Dr. Osburn took a position as Professor of Electrical and Computer Engineering at North Carolina State University on assignment as Director of Advanced Semiconductor Technology at the Microelectronics Center of North Carolina. At MCNC he is responsible for directing manufacturing technology research programs in advanced silicon device design and fabrication, working on process integration of scaled CMOS devices and thin oxide and shallow junction formation among other things. Also a CEI Europe and UC Berkeley Extension instructor, Dr. Osburn teaches VLSI fabrication technology at NCSU and offers the course over the National Technological University network.

With over 95 papers and 23 patents and patent publications, Dr. Osburn is well known in his field. In the past he has been honored with the 1975 Thomas D. Callinan Award of the Dielectrics and Insulation Division of the Society, the 1989 Maurice Simpson Award of the Institute of Environmental Sciences, and the 1991 Electronics Division Award of the Society's Electronics Division, which he received for his pioneering studies of thin insulator reliability and development of process technologies for scaled semiconductor devices.

A member of the Society since 1970, Dr. Osburn has served on several symposia organizing committees and in a number of Divisional and Society committees. He is also a senior member of IEEE and Sigma Xi.

***Robert A. Rapp**, in recognition of his contributions to the science and technology of high-temperature materials and in the corrosion of materials, for exemplary teaching, and for service to the Society.*

Dr. Rapp, of The Ohio State University, received his B.S. degree with honors in metallurgical engineering from Purdue University in 1956 and was the first recipient of the University's John Bray Award, given to the outstanding senior in metallurgical engineering. During the summer of 1956 he worked on the brazing of stainless steels as a metallurgist at the Westinghouse Corporation in Pittsburgh. He then entered the Carnegie Institute of Technology (now CMU) as the Thompson Products (now TRW) Fellow, obtaining an M.S. degree in 1958 and a Ph.D. in August of 1959.

Upon graduation, Dr. Rapp was awarded a Fulbright Post-Doctoral Scholarship to study in Germany, where he conducted research under the guidance of Professor Carl Wagner at the Max Planck Institut fur Physikalische Chemie. After his fellowship, Dr. Rapp served on active military duty as a First Lieutenant and Research Metallurgist in the Aerospace Research Laboratory at Wright-Patterson Air Force Base in Ohio. There he conducted research on the high-temperature oxidation of metals and high-temperature electrochemical studies.

In September 1963, Dr. Rapp joined the Department of Metallurgical Engineering at The Ohio State University as an Assistant Professor, where he was promoted to Associate Professor in 1966 and to Professor in 1969, when he was chosen by the students at Ohio State to receive the Mars G. Fontana Outstanding Teacher Award.

Primarily interested in chemical, extractive, and high-temperature processes in metals, Dr. Rapp served on a NASA Advisory Panel for Materials in Aircraft Engines from 1968 to 1971, three committees of the Materials Advisory Board of the National Academies of Science and Engineering, as Chairman for four conferences and reviews of the Department of Energy, and as Chairman of the Society's Corrosion Division (1986-1988). He currently serves on the Editorial Boards for the journals *Corrosion*, *Oxidation of Metals*, and the *Journal of The Electrochemical Society*. He was Chairman of the Gordon Conference on Corrosion in 1977 and Chairman of a NACE International Conference on High-Temperature Corrosion in 1981.

A Guggenheim Fellow during the 1972-1973 academic year, Dr. Rapp studied and taught at the Ecole Nationale Superieure d'Electrochimie, in Grenoble, France. A member of two US-Japan seminar teams, Dr. Rapp has presented eight plenary lectures at international meetings abroad and has been a Visiting Lecturer at a dozen laboratories in China in 1980 and 1982.

A devoted researcher, Dr. Rapp has published over 185 technical papers concerned with high-temperature reactions of

The recipient of numerous national and international awards for his work, Dr. Zuman has been honored with the Heyrovsky Medal twice (1960 and 1990), the A.A. Benedetti-Pichler Award of the American Micromechanical Society (1975), the Gold Medal of the Electroplaters Society (1976), and the J.B. Beccari Medal from the University of Bologna (1991) among others. A member of the Society since 1954, Dr. Zuman served as an officer of the Organic and Biological Electrochemistry Division from 1981 to 1987 . He is also a Fellow of the Royal Society of Chemistry as well as of the Chemical Institute of Canada.

Dr. Zuman's research interests involve the use of polarography and other electrochemical techniques to investigate mechanisms of organic reactions, including fast reactions occurring in the vicinity of the electrode and slower reactions that take place in bulk solution. Early studies were devoted to carbonyl compounds, whereas more recent studies have focused on the chemistry of nitro and nitroso compounds. Much of his work has involved reactions in strongly acidic and alkaline media.

The author of over 320 papers and 15 books on his research activities, Dr. Zuman has served on the editorial board of the Journal of The Electrochemical Society as well as that of seven other publications. ■

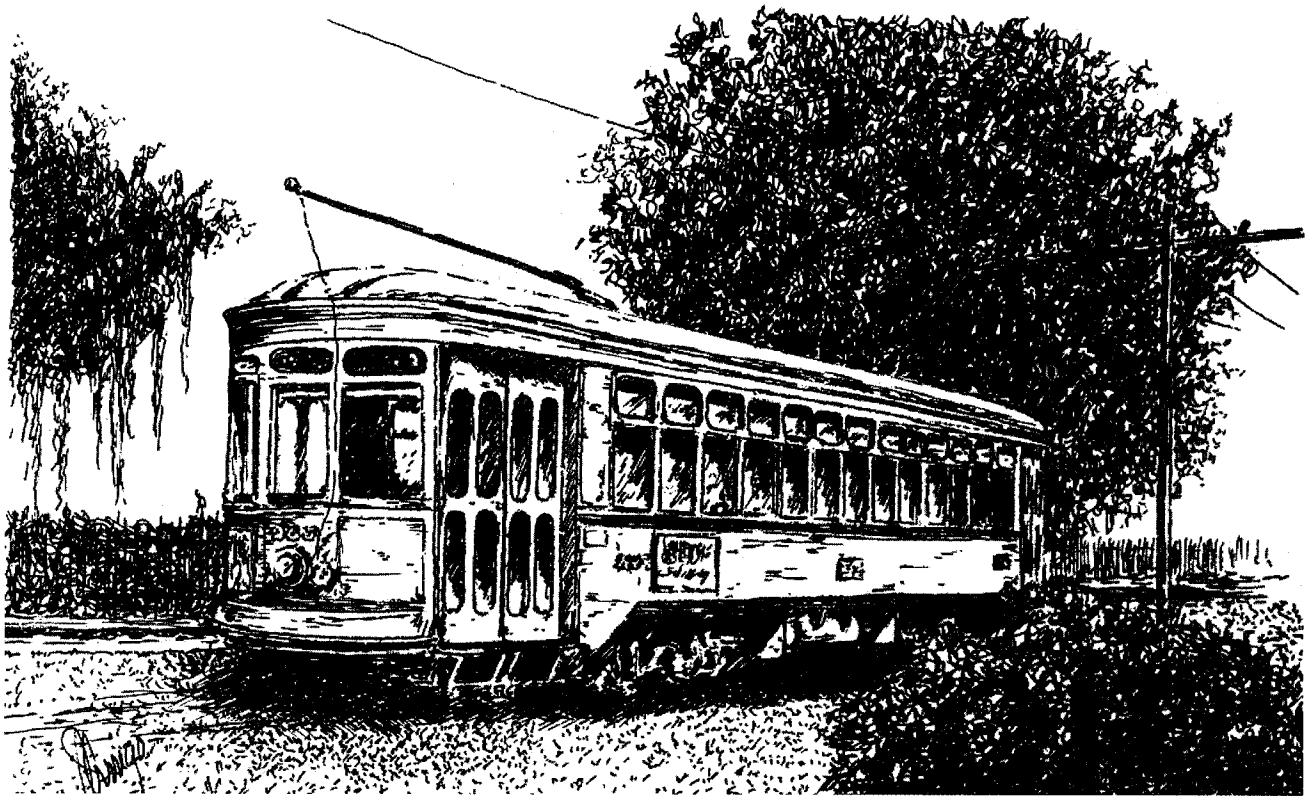

Schedule of Technical Sessions
184th Meeting of The Electrochemical Society, Inc.
New Orleans, Louisiana, October 10-15, 1993

SYMPOSIA	Monday, Oct. 11		Tuesday, Oct. 12		Wednesday, Oct. 13		Thursday, Oct. 14		Friday, Oct. 15	
	AM	PM	AM	PM	AM	PM	AM	PM	AM	PM
BATTERY										
Lithium Batteries	Ponchartrain A, Third Floor Abs. 1-5	Ponchartrain A, Third Floor Abs. 6-11	Ponchartrain A, Third Floor Abs. 12-17	Ponchartrain A, Third Floor Abs. 18-21	Ponchartrain A, Third Floor Abs. 22-27	Ponchartrain A, Third Floor Abs. 28-33	Ponchartrain A, Third Floor Abs. 34-39			
Rechargeable Alkaline Batteries	Ponchartrain B, Third Floor Abs. 40-45	Ponchartrain B, Third Floor Abs. 46-55	Ponchartrain B, Third Floor Abs. 56-62	Ponchartrain B, Third Floor Abs. 63-67						
General Session					Ponchartrain B, Third Floor Abs. 68-75					
CORROSION										
Corrosion and Corrosion Prevention in Seawater Environments			Grand Ballroom A, Fifth Floor Abs. 76-84	Grand Ballroom A, Fifth Floor Abs. 85-90						
General Session					Grand Ballroom A, Fifth Floor Abs. 91-100	Grand Ballroom A, Fifth Floor Abs. 101-111				
CORROSION/BATTERY/ENERGY TECHNOLOGY										
Corrosion in Battery and Fuel Cell Systems		Grand Ballroom A, Fifth Floor Abs. 112-118								
DIELECTRIC SCIENCE AND TECHNOLOGY/ELECTRONICS										
First International Symposium on Long Wavelength Infrared Detectors and Arrays: Physics and Applications	Bayside A, Fourth Floor Abs. 119-122	Bayside A, Fourth Floor Abs. 123-128	Bayside A, Fourth Floor Abs. 129-135	Bayside A, Fourth Floor Abs. 136-139	Bayside A, Fourth Floor Abs. 140-148					
High Permittivity Materials							Rosella, Fourth Floor Abs. 149-155	Rosella, Fourth Floor Abs. 156-163	Rosella, Fourth Floor Abs. 164-168	
Joint General Session	Rosella, Fourth Floor Abs. 169-174	Rosella, Fourth Floor Abs. 175-182	Rosella, Fourth Floor Abs. 183-189							
Joint Recent News Paper Session				Rosella, Fourth Floor 723-729						
ELECTRODEPOSITION										
Electrodeposition of Semiconductor Materials							Grand Ballroom D, Fifth Floor Abs. 190-195	Grand Ballroom D, Fifth Floor Abs. 196-203		
Manufacturing Technology in Electrodeposition					Grand Ballroom D, Fifth Floor Abs. 204-211	Grand Ballroom D, Fifth Floor Abs. 212-218				
Second International Symposium on *In-Situ* Characterization of Electrodeposition Processes					Grand Ballroom E, Fifth Floor Abs. 219-223	Grand Ballroom E, Fifth Floor Abs. 224-228				
Third International Symposium on Magnetic Materials, Process and Devices	Grand Ballroom E, Fifth Floor Abs. 229-233	Grand Ballroom E, Fifth Floor Abs. 234-243	Grand Ballroom E, Fifth Floor Abs. 244-249	Grand Ballroom E, Fifth Floor Abs. 250-254						
ELECTRONICS										
State-of-the-Art Program on Compound Semiconductors XIX							Bayside A, Fourth Floor Abs. 623-629	Bayside A, Fourth Floor Abs. 630-634		

Plenary Session—Grand Ballroom C—(9:00 AM-10:00 AM)

Awards & Recognition Session—Grand Ballroom C—(4:30 PM-6:00 PM)

Schedule of Technical Sessions-3

SYMPOSIA	Monday, Oct. 11		Tuesday, Oct 12		Wednesday, Oct. 13		Thursday, Oct. 14		Friday, Oct. 15	
	AM	PM	AM	PM	AM	PM	AM	PM	AM	PM
LUMINESCENCE AND DISPLAY MATERIALS/ DIELECTRIC SCIENCE AND TECHNOLOGY	Plenary Session—Grand Ballroom C—(9:00 AM-10:00 AM)			Awards & Recognition Session—Grand Ballroom C—(4:30 PM-6:00 PM)						
Nonlinear Optics and Materials								St. Charles B, Third Floor Abs. 484-488	St. Charles B, Third Floor Abs. 489-493	
PHYSICAL ELECTROCHEMISTRY										
Electrochemistry in Unconventional Media and in Media Under Extreme Conditions					Ponchartrain D, Third Floor Abs. 494-498	Ponchartrain D, Third Floor Abs. 499-504	Ponchartrain D, Third Floor Abs. 505-509	Ponchartrain D, Third Floor Abs. 510-515		
General Session							Bayside B, Fourth Floor Abs. 516-522	Bayside B, Fourth Floor Abs. 523-526		
PHYSICAL ELECTROCHEMISTRY/DIELECTRIC SCIENCE AND TECHNOLOGY/ELECTRONIC/LUMINESCENCE AND DISPLAY MATERIALS										
Porous Silicon					Aurora, Fourth Floor Abs. 527-534	Aurora, Fourth Floor Abs. 535-542				
PHYSICAL ELECTROCHEMISTRY/ELECTRODEPOSITION										
Electroless Deposition	Grand Ballroom D, Fifth Floor Abs. 543-546	Grand Ballroom D, Fifth Floor Abs. 547-556								
PHYSICAL ELECTROCHEMISTRY/ORGANIC AND BIOLOGICAL ELECTROCHEMISTRY/BATTERY										
Electrochemistry in Nonaqueous Media	Ponchartrain D, Third Floor Abs. 557-560	Ponchartrain D, Third Floor Abs. 561-566	Ponchartrain D, Third Floor Abs. 567-571	Ponchartrain D, Third Floor Abs. 572-575						
PHYSICAL ELECTROCHEMISTRY/SENSOR/CORROSION										
Microelectrodes and Microenvironments: Fundamentals and Applications	Ponchartrain C, Third Floor Abs. 576-579	Ponchartrain C, Third Floor Abs. 580-586	Ponchartrain C, Third Floor Abs. 587-592	Ponchartrain C, Third Floor Abs. 593-596	Ponchartrain C, Third Floor Abs. 597-603	Ponchartrain C, Third Floor Abs. 604-609				
SENSOR/PHYSICAL ELECTROCHEMISTRY										
Fundamental Processes in Ion-Selective Electrodes and Other Ion-Sensors							Ponchartrain C, Third Floor Abs. 610-616	Ponchartrain C, Third Floor Abs. 617-622		
NEW TECHNOLOGY SUBCOMMITTEE										
Fullerenes: Chemistry, Physics and New Directions V	Rhythms, Second Floor Abs. 635-638	Rhythms, Second Floor Abs. 639-646	Rhythms, Second Floor Abs. 647-653	Rhythms, Second Floor Abs. 654-658	Rhythms, Second Floor Abs. 659-665	Rhythms, Second Floor Abs. 666-674	Rhythms, Second Floor Abs. 675-680	Rhythms, Second Floor Abs. 681-688	Rhythms, Second Floor Abs. 689-690	
Micromachining and 3-D Nanostructures	St. Charles A, Third Floor 729-731	St. Charles A, Third Floor 732-740	St. Charles A, Third Floor 741-748	St. Charles A, Third Floor 749-751						
ALL DIVISIONS AND GROUPS										
General Society Student Poster Session		Armstrong Ballroom, Eighth Floor Abs. 691-722								

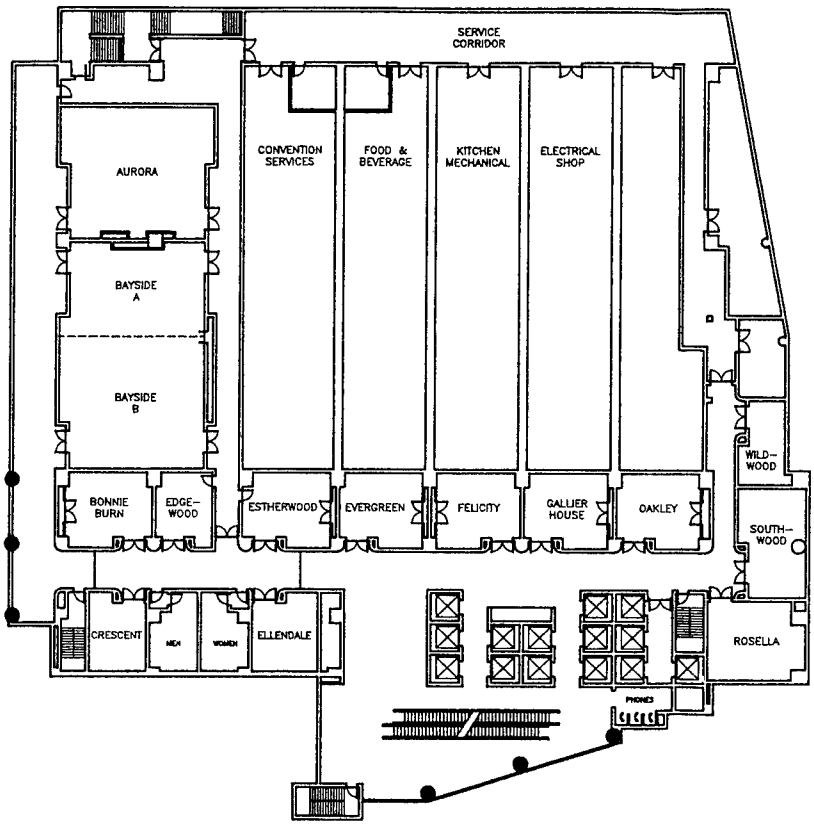

Fourth Floor

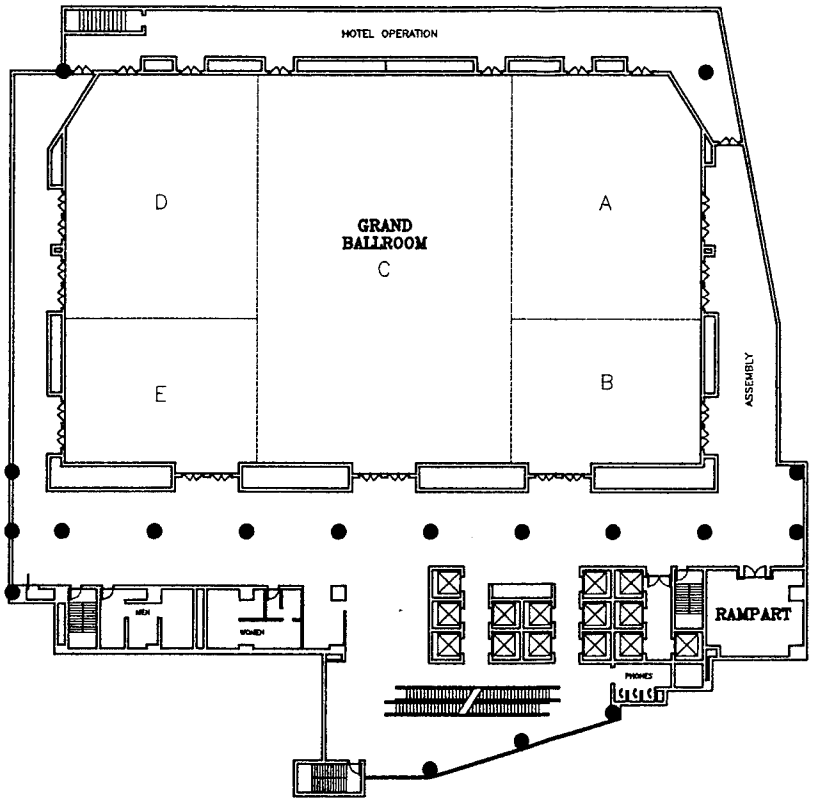

Fifth Floor

MONDAY CONTINUED

FIRST INTERNATIONAL SYMPOSIUM ON LONG WAVELENGTH INFRARED DETECTORS AND ARRAYS: PHYSICS AND APPLICATIONS

Dielectric Science and Technology/Electronics

F. Radpour, Chairman; V. S. Swaminathan, Vice-Chairman
Bayside A, 4th Floor

M. O. Manasreh, Chairman; R. S. Balcerak, Vice-Chairman

JOINT GENERAL SESSION

Dielectric Science and Technology/Electronics

R. Jaccodine, Chairman; A. Harrus, Vice-Chairman
Rosella Room, 4th Floor

Contamination Control

A. Harrus, Chairman; R. Jaccodine, Vice-Chairman

Insulators and Deposited Films

THIRD INTERNATIONAL SYMPOSIUM ON MAGNETIC MATERIALS, PROCESSES, AND DEVICES

Electrodeposition

L. T. Romankiw, Chairman; Y. Nakamura, Vice-Chairman
Grand Ballroom E, 5th Floor

D. A. Herman, Chairman; C. A. Ross, Vice-Chairman

MONDAY CONTINUED

2:35 Photocured Gelled Electrolytes for Li Battery Applications - G. Nagasubramanian, D. Shen, R. Surampudi, and G. Halpert 374

2:55 Conducting Polymer/Graphite Fiber Composites for High Charge Density Battery Electrodes - B. M. Coffey, P. V. Madsen, T. O. Poehler, and P. C. Searson 375

3:15 *In Situ* Spectroelectrochemical Studies on Poly(1,8-Diaminonaphthalene) - S.-M. Park, M. Ruan, and Y.-B. Shim 376

3:35 Fifteen-minute intermission

3:50 Sulfonated Polyaniline: A Conducting Polymer Electrode for Ion Transfer Batteries - R. Koetz, C. Barbero, and M. C. Miras 377

4:10 Ternary Polymer Electrolytes: A New Approach to Polymer Electrolyes - R. D. A. Paulmer and A. R. Kulkarni 378

ELECTROCHROMIC MATERIALS

Energy Technology/Luminescence and Display Materials

D. M. MacArthur, Chairman; K.-C. Ho, Vice-Chairman
Bayside B, 4th Floor

2:00 A Robust Completely Inorganic Electrochromic Window for Building Applications - R. B. Goldner, F. O. Amtz, K. Dickson, T. E. Haas, S. Slaven, and P. Zerigian 385

2:25 Laminated Electrochromic Window Based on Nickel Oxide, Tungsten Oxide, and a Gel Electrolyte - B. Scrosati, S. Passerini, C. Holmblad, and T. Bartlett 386

2:50 Commercial Developments in Electrochromics - H. Byker 387

3:15 Fifteen-minute intermission

3:30 Tungsten Oxide-Prussian Blue Electrochromic System Based on a Proton-Conducting Polymer Electrolyte - K.-C. Ho, T. G. Rukavina, and C. B. Greenberg 388

3:55 Digital Simulation of an Electrochromic Device - J. C. Lopez Tonazzi and C. L. Pershing 389

4:20 Spectroelectrochemistry of Reversible Electrodeposition Electrochromic Materials - J. P. Ziegler and B. M. Howard 390

HIGH TEMPERATURE BEHAVIOR OF CERAMICS, INTERMETALLICS, AND COMPOSITES

High Temperature Materials

D. A. Shores, Chairman; R. A. Rapp, Vice-Chairman
Senate/Walker Percy Amphitheater, 3rd Floor

Metals and Intermetallics

2:00 The Effect of Substrate Grain Growth on High Temperature Oxidation of Pure Nickel - R. A. Rapp and J. Shen 416

2:20 The Stability of a Protective Oxide Scale on a Binary Alloy with Scale Dissolution or Evaporation - G. Wang 417

2:40 The Effect of Yttrium on the Oxide Spalling Behavior of Cast Ni-30Cr Alloy - Y. Zhang and D. A. Shores 418

3:00 The Formation of α-Al_2O_3Scales on β-NiAl at 1400 and 1500^0 C - B. A. Pint and L. W. Hobbs 419

3:20 Ten-minute intermission

3:30 The Effect of Oxidation Time on the Grain Boundary Segregation of Zr in Alpha-Al_2O_3 Scales Grown on β-NiAl - B. A. Pint, A. J. Garratt-Reed, and L. W. Hobbs 420

3:50 Oxidation-Resistant Boron- and Germanium-Doped Silicide Coatings for Titanium - B. V. Cockeram and R. A. Rapp 421

4:10 High Temperature Oxidation of Alloys in the Presence of HF Vapor - M. McNallan, Y. W. Chang, E. Dewing, and D. Creber 422

4:30 The Simultaneous Oxidation-Sulfidation Resistance of a Cr-Nb Alloy - J. C. Duncan and L. W. Hobbs 423

HIGH TEMPERATURE LAMP CHEMISTRY III

High Temperature Materials/Luminescence and Display Materials

E. G. Zubler, Chairman; W. van Erk, Vice-Chairman
St. Charles B, 3rd Floor

10:00 Lamp R&D Needs and Directions - H. Horster 436

10:50 Computer Modeling of Halogen Incandescent Lamp Chemistry - M. J. Abbott, D. L. Trindell, and R. Devonshire 437

11:15 IR Laser Measurements of HBr near the Filament of a Tungsten Halogen Lamp - L. Bigio and P. Y. Chang 438

11:40 Thermochemical Properties of Some Phosphorus Compounds Pertinent to Lamp Chemistry - D. L. Hildenbrand and K. H. Lau 439

K. Hilpert, Chairman; T. R. Brumleve, Vice-Chairman

2:00 Effects of Natural Convection on Envelope Temperature and Tungsten Transport in a 100 W Filament Lamp - P. Y. Chang 440

2:25 Application of CARS to the Investigation of Non-LTCE in Halogen Lamps - J. R. Woodward and R. Devonshire 441

2:50 Ripening of Y_2O_3 Particles in W-5wt% Y_2O_3 Composites - X. Zheng, R. A. Rapp, V. Mehrotra, H. S. Betrabet, and P. D. Goodell 442

3:15 Ten-minute intermission

3:25 The High Temperature Corrosion of Tungsten by Carbon Dioxide - G. M. Forsdyke, D. M. Jenkins, and J. S. Ogden 443

3:50 Wall Blackening in Metal Halide Lamps Containing Scandium or Rare-Earth Iodide - W. van Erk, P. H. L. M. Cobben, and P. Bennema 444

4:15 Damage to the Cathodes of HPS Lamps Suffered during Sealing - F. Nagel and M. Farkas-Jahnke 445

4:40 Aging of Ba_2SrWO_6 Cathode Emissive Material Used in HPS Lamps - F. Nagel, M. Farkas-Jahnke, and L. Petras 446

ELECTROLESS DEPOSITION

Physical Electrochemistry/Electrodeposition

A Damjanovic, Chairman; M. Paunovic, Vice-Chairman
Grand Ballroom D, 5th Floor

10:05 Introductory remarks

10:10 Formation Mechanism of Colloidal Pd-Sn Solutions - G. Stremsdoerfer, E. Queau, and J. R. Martin 543

10:40 Structural and Analytical Characteristics of Adsorbed Pd-Sn Colloids - M. Froment, E. Queau, J. R. Martin, and G. Stremsdoerfer 544

11:10 Self-Organization of Surface Microstructures during Electroless Metal Plating - K. G. Weil 545

11:40 Modeling and Response Surfaces for Electroless Co Deposition Process - M. Paunovic, T. Nguyen, R. Mukherjee, C. J. Sambucetti, and L. T. Romankiw 546

M. Paunovic, Chairman; G. Stremsdoerfer, Vice-Chairman

2:00 Corrosion and Wear Resistance of ACD Ni-P and Co-P Bright Layers - P. L. Cavallotti, B. Bozzini, L. Battezzati, E. Lanzoni, and M. U. Ivanov 547

2:30 Electroless Deposition in the Electronic Industry: A Review - C. J. Sambucetti 548

3:00 Electroless Metal Deposition for Microelectronics - V. M. Dubin 549

3:20 STM Patterning and AFM Imaging of Self-Assembled Monolayer Films with Selective Electroless Metallization - S. L. Brandow, W. J. Dressick, T. S. Koloski, C. S. Dulcey, J. M. Calvert, C. R. K. Marrian, F. K. Perkins, and E. A. Dobisz 550

3:40 Ten-minute intermission

3:50 Patterned Self-Assembled Films for Selective Electroless Metallization - J. M. Calvert, W. J. Dressick, C. S. Dulcey, T. S. Koloski, M-S. Chen, G. S. Calabrese, J. H. Georger, and S. L. Brandow 551

4:10 A New Series of Inorganic Additives for Electroless Copper Plating Solutions - H. Akahoshi, M. Kawamoto, and A. Takahashi 552

4:30 Characterization of the Copper-Poly(tetrafluoroethylene) Interface - R. R. Rye, G. W. Arnold, and A. J. Ricco 553

4:50 Morphology of Electrolessly Deposited Pd Membranes and Its Effect on Hydrogen Permeability - J. Shu, B. P. A. Grandjean, and S. Kaliaguine 554

5:10 Modelization of Chemical Bath Deposition of Cadmium Sulfide Films - D. Lincot and R. Ortega-Borges 555

5:30 The Electroless Catalytic Properties of an Efficient Cr-Based Barrier for Cu Diffusion - M. D. Bruni 556

MONDAY CONTINUED

2:00 The Micromachining and 3-D Nanostructures Program and Abstracts will be published in the December issue of *INTERFACE* and included in the program booklet distributed at the Meeting. Copies of both the Micromachining and 3-D Nanostructures Program and Abstracts may be obtained from the Society Headquarters Office after September 1, 1993

GENERAL SOCIETY STUDENT POSTER SESSION
All Divisions and Groups

J. B. Talbot, Chairman; O. J. Gregory, Vice-Chairman
Armstrong Ballroom, 8th Floor
5:45 to 7:00 PM

Electrochemical Science and Technology

- The Effects of Organic Adsorbates on the Underpotential Deposition of Silver on Pt(111) - D. L. Taylor 691
- Impedance Characterization of Thin-Film Multisite Microelectrodes for *In Vivo* Electrochemical Analysis - A. S. Salian, S. S. Ang, and W. D. Brown 692
- Molecular Recognition with Self-Assembled Monolayers of Thiolated Cyclodextrins - J. Srinivasan 693
- Monitoring the Reactions of Surface Confined Monolayer Films Using QCM and FTIR Spectroscopy - W. A. Hayes and C. Shannon 694
- Toward Separation Based Sensor - C. D. Dunn and K. Ghowsi 695
- Circuit Modeling of Corrosion Properties of Ion Implanted Carbon Steel Using Electrochemical Impedance Spectroscopy - D. Vollmer, M. R. Madani, J. D. Garber, G. A. Glass, R. D. Braun, and F. H. Walters 696
- The Electrodeposition of Co, Cu, Fe, Hg, and Ni in the Room Temperature Aluminum Chloride-1-Methyl-3-ethylimidazolium Chloride Molten Salt - W. R. Pitner and C. L. Hussey 697
- An Electrochemical and Vibrational Spectroscopic Study of Self-Assembled Monolayers of Benzoquinone and Anthraquinone Derivatives - B. J. Clark and C. L. Hussey 698
- Investigation of the "Anomalous" Voltammetric Behavior of the Pt(111) Electrode in Sulfuric and Perchloric Acids by AC Impedance - R. L. Turner, L. R. Faulkner, K. Dobrowolska, and A. Wieckowski 699
- Electrochemical Corrosion Behavior of Ion Implanted Carbon Steel - Q. Zhang, R. D. Braun, M. R. Madani, and G. A. Glass 700
- Electrochemical Flow-Cell System for Atomic Layer Epitaxy of Thin Films of Compound Semiconductors - B. M. Huang and J. L. Stickney 701

GENERAL SOCIETY STUDENT POSTER SESSION
All Divisions and Groups

J. B. Talbot, Chairman; O. J. Gregory, Vice-Chairman
Armstrong Ballroom, 8th Floor
5:45 to 7:00 PM

Solid-State Science and Technology

- Integrated Force Arrays - J. E. Bousaba, J. D. Jacobson, and K. K. McKay 702
- High Resolution i-Line and Deep UV Photoresists with Significantly Enhanced Plasma Etch Resistance - J. Bousaba, L. Qushair, and J. Nickel 703
- Characterization of Plasma-Enhanced Chemical Vapor Deposited Diamond-Like Carbon Films - G. Sreenivas, S. S. Ang, W. D. Brown, R. K. Ulrich, and S. Nasrazadani 704
- Solar Cells: Solution Optimized n-GaAs/Aqueous Polyselenide Photoelectrochemistry - F. Forouzan and S. Licht 705
- Blanket Tungsten Deposition by APCVD - U. V. Patel, M. S. Haque, H. A. Naseem, and W. D. Brown 706
- AuTi Metallization of CVD Diamond Substrates for Multi-chip Module Applications - P. Chilakamarri, I. Meyyappan, H. Naseem, and W. D. Brown 707
- Deposition of a-SiN_x:H:F Films by PECVD for Use in Multijunction a-Si:H Based Solar Cells - S. G. Kizzar, H. A. Naseem, and W. D. Brown 708
- Silane Assisted PECVD of Fluorinated, Hydrogenated Germanium Carbon Alloy - P. R. Moffitt, H. A. Naseem, and W. D. Brown 709
- Preparation of Tl-Ba-Ca-Cu-O Thin Films by Laser Ablation and Low Temperature Annealing - S. Afonso, I. N. Chan, Y. Q. Tang, F. T. Chan, and G. S. Salamo 710
- Preparation of Superconducting $TlSr_2(Ca,Cr)Cu_2O_7$ Thin Films with Zero Resistance up to 100 K by Laser Ablation - K. Y. Chen, Y. Q. Tang, I. N. Chan, Y. J. Shi, Z. Y. Chen, A. Pigg, Z. Z. Sheng, G. J. Salamo, and F. T. Chan 711
- Deposition of Polycrystalline Silicon by PECVD at Low Temperatures - M. R. Sathish Kumar, H. A. Naseem, and W. D. Brown 712
- Defects Structure of ZnO/Ag Ceramic-Metal Two-Phase Material - S. Jiang and J. B. Wagner, Jr. 713
- A New Apparatus for Measuring the Ultimate Strain of Thin Films - G. Zhao and R. K. Ulrich 714
- Bubble Formation and Growth in Liquid Encapsulated Laser Chemical Vapor Deposition - Q. J. Chen and S. D. Allen 715
- Laser Assisted Particle Removal of Micron Sized Contaminants on Silicon Surfaces - L. A. Pollack, S. J. Lee, and S. D. Allen 716
- Laser Fabricated Fiber Optic Taps and Application to Sensors - C. H. Lee and S. D. Allen 717
- Diagnostics and Mechanisms in Laser Chemical Vapor Deposition of Tungsten - X. F. Zhang and S. D. Allen 718
- High Electron Mobility Transistors Grown by LP-MOCVD with p+ InGaAs Gate Layer - R. Hickman II and V. J. Kapoor 719
- InAlAs/InGaAs High Electron Mobility Transistor for MMIC Applications - W. S. Gaines and V. J. Kapoor 720
- Luminescence Quenching of Porous Silicon by Adsorbed Molecular Oxygen - J. Harper and M. J. Sailor 721
- Electroluminescence from a Polymer/Porous Silicon Contact - J. M. Lauerhaas and M. J. Sailor 722

TUESDAY, OCTOBER 12, 1993

12:15 P.M. Corrosion Division Luncheon and Business Meeting, Waterbury Ballroom, 2nd Floor.
12:15 P.M. Sensor Group Luncheon and Business Meeting, Armstrong Ballroom, 8th Floor.
4:30 P.M. Awards and Recognition Session, Grand Ballroom C, 5th Floor. Jean-Michel Saveant will deliver the Olin Palladium Award Address, "Electron Transfer and Bond Breaking."

BATTERY DIVISION RESEARCH AWARD ADDRESS
Battery

F. M. Delnick, Chairman; M. L. Kronenberg, Vice-Chairman
Ponchartrain Ballroom A, 3rd Floor

8:55 Introduction of the Award Recipient
9:00 **BATTERY DIVISION RESEARCH AWARD ADDRESS:** Lithium Composite Solid Electrolyte FeS_2 Bipolar Battery - E. Peled, D. Golodnitsky, J. Lang, and Y. Lavi 12

LITHIUM BATTERIES
Battery

Electrolytes

9:40 Enhanced Ion Dissociation of $LiCF_3SO_3$ by a New Carbonate Plasticizer: Raman and IR Studies - L. K. Hanson, X. Q. Yang, H. S. Lee, and J. McBreen 13
10:05 Conductivity of $Li_xMg_yAl_z(SO_4)_3$ as a New Lithium Ionic Conductor for a Solid-State Cell - T. Shodai, H. Ohtsuka, M. Ichimura, and J-i. Yamaki 14

TUESDAY CONTINUED

FIRST INTERNATIONAL SYMPOSIUM ON LONG WAVELENGTH INFRARED DETECTORS AND ARRAYS: PHYSICS AND APPLICATIONS

Dielectric Science and Technology/Electronics

G. S. Pomrenke, Chairman; M. E. Greiner, Vice-Chairman
Bayside A, 4th Floor

8:30	Grating Coupled III-V Quantum Well Infrared Photodetectors for Mid-Wavelength and Long-Wavelength Infrared Detection - S. S. Li	129
9:10	Efficiency of Grating Coupled AlGaAs/GaAs Quantum Well Infrared Detectors - J. Y. Andersson, L. Lundqvist, Z. F. Paska, J. Borglind, and D. Haga	130
9:50	Investigation of a Concentric-Ring Grating Coupler for Normal-Incidence Absorption in Quantum-Well Infrared Photodetectors - D. A. Cardimona and A. Singh	131
10:10	Optical Gratings for GaAs/AlGaAs Quantum Well Detectors - J. E. Scheihing and M. A. Dodd	132
10:30	Fifteen-minute intermission	
10:45	Barrier-Doped GaAs/AlGaAs Quantum Well Detector - M. A. Dodd and J. E. Scheihing	133
11:05	Tunneling Emitter Undoped Quantum-Well-Infrared Photodetector - K. M. S. V. Bandara, B. F. Levine, and M. T. Asom	134
11:25	Two-Mode InGaSb/GaSb Strained-Layer Superlattices, Infrared Photodetectors - Y. K. Su, S. M. Chen, and Y. T. Lu	135
11:45	Recent News	

R. L. Whitney, Chairman; J. R. Susko, Vice-Chairman

2:00	$In_{1-x}Tl_xSb$ for Long Wavelength Infrared Photodetectors - M. Razeghi, Y. H. Choi, P. T. Staveteig, and E. Bigan	136
2:40	InAsSb/InSb Strained Layer Superlattice Infrared Detector Technology - S. R. Kurtz	137
3:20	Ten-minute intermission	
3:30	The Role of Surface Tension in the Growth of InAsSb/InSb Superlattices by Molecular Beam Epitaxy - T. J. Drummond, S. R. Lee, and A. J. Howard	138
3:50	Bandstructure Calculation of InAs/InGaSb Type-II Strained Layer Superlattices - J. P. Loehr, B. Jogai, and D. N. Talwar	139

JOINT GENERAL SESSION

Dielectric Science and Technology/Electronics

R. Jaccodine, Chairman; A. Harrus, Vice-Chairman
Rosella Room, 4th Floor

Annealing, Conductivity, and Defects

9:00	The Influence of Dopant and Rapid Thermal Annealing on the Silicidation of Submicron Lines - P. D. Agnello and A. Fink	183
9:20	Increase in Conductivitity of As-Implanted Layers by Low Temperature (below 900C) RTA - A. Kalnitsky, R. MacNaughton, and J. Li	184
9:40	Characterization of As-Grown Crystallographic Defects in Czochralski Silicon Using Nonagitated Secco Etching - W. Wijaranakula and Y. Pan	185
10:00	Behavior of Defects in Boron Implanted/Oxidized Silicon - S. Sundaram and N. D. Theodore	186
10:20	Fifteen-minute intermission	
10:35	Reduction of Corrosion Defects on Metal Alloy Lithography Seen Immediately after Etch Processing - G. Gebara and K. Mautz	187
10:55	Solid Electrolytic Capacitor with Electron-Conducting Polymer Layers - F. Takei, H. Shiroto, and N. Sawatari	188
11:15	High Performance Capacitor with Rugged Surface Poly-Si Electrodes Formed by Two-Step Wet Etching - T. Hirota, M. Zenke, and K. Okamura	189

JOINT RECENT NEWS PAPER SESSION

Dielectric Science and Technology/Electronics

D. E. Bailey, Chairman; L. K. White, Vice-Chairman
Rosella Room, 4th Floor

2:00 The Joint Recent News Paper Program and Abstracts will be published in the December issue of *INTERFACE* and included in the program booklet distributed at the Meeting. Copies of both the Joint Recent News Paper Program and Abstracts may be obtained from the Society Headquarters Office after September 1, 1993.

THIRD INTERNATIONAL SYMPOSIUM ON MAGNETIC MATERIALS, PROCESSES, AND DEVICES

Electrodeposition

M. A. Russak, Chairman; P. L. Cavallotti, Vice-Chairman
Grand Ballroom E, 5th Floor

9:30	Thin Film Recording Disks with Textured Underlayers - M. Mirzamaani, C. V. Jahnes, and M. A. Russak	244
10:00	Remanent Magnetization Study of the CoCrPtB/Cr Thin Films - P. Glijer, J. M. Sivertsen, and J. H. Judy	245
10:20	Effect of Substrate Temperature on Microstructure and Noise Properties of CoCrTaPt/Cr Thin Film Media - K. Sin, J. M. Sivertsen, and J. H. Judy	246
10:40	Fifteen-minute intermission	
10:55	ECD Precious Metal - Cobalt Thin Films for Magnetic Recording Applications - P. L. Cavallotti, G. Zangari, G. Fontana, P. G. Maistro, and E. Terrenzio	247
11:15	Sputter Deposition of High Coercivity, C-Axis In-Plane Oriented-Barium Hexaferrite Thin Films for High Density Longitudinal Recording - X. Sui and M. H. Kryder	248
11:35	Electrodeposition of Thin Magnetic Co-W Coatings - V. S. Racinskas and L. V. Orlovskaya	249

D. S. Lashmore, Chairman; T. Miyazaki, Vice-Chairman

1:30	Giant Magnetoresistance of Fe-Ni-Co/Cu Multilayers - T. Miyazaki, H. Kubota, M. Sato, and S. Ishio	250
2:00	Giant Magnetoresistance and Film Morphology in Co/Cu Multilayers - S. Honda and M. Nawate	251
2:30	Magnetoresistance Measurements of Electrodeposited Multilayers - D. S. Lashmore, M. P. Dariel, L. Swartzendruber, and Y. Zhang	252
3:00	Magnetoresistance in Ni-Co-Cu/Cu Multilayers Electrodeposited on to (100) n-Type Gallium Arsenide Substrate - R. Hart and W. Schwarzacher	253
3:30	Electrodeposited Super Lattices of CoFe/Cu and NiFe/Cu on N-Type (111) Si Single Crystal Wafers - J. W. Chang and L. T. Romankiw	254

THE DEGRADATION OF ELECTRONIC DEVICES DUE TO DEVICE OPERATION AS WELL AS CRYSTALLINE AND PROCESS-INDUCED DEFECTS

Electronics

K. E. Bean, Chairman; T. J. Shaffner, Vice-Chairman
Grand Ballroom B, 5th Floor

Heterostructures

9:00	Reliability Issues due to Hot-Electron Effects in GaAs-Based MESFETs and HEMTs - E. Zanoni, C. Tedesco, A. Neviani, and G. Meneghesso	265
9:30	Temperature Dependent Performance Simulation and Failure Mechanisms of Heterostructure Field Effect Transistors and Inverter Circuits - J.-S. Kuo and A. Christou	266
9:50	Study of SiO_2/InP Structure Prepared by Direct Photo-CVD - Y. K. Su, S. C. Shei, C. J. Hwang, and M. Yokoyama	267
10:10	Fifteen-minute intermission	
10:25	Electronic Studies on SF_6 and O_2 Plasma-Etched $Si_{1-x}Ge_x$/Si p^+-n Heterojunction - W. Zhong, D. Misra, H. Amin, J. Gaudani, and H. Patel	268
10:45	Enhanced Diffusion of Arsenic along Misfit Dislocation in Epitaxial Si/Si(Ge) - N. Braga, A. Buczkowski, and G. A. Rozgonyi	269
11:05	Metastability of Electronic Properties of Misfit Dislocations in Si/Si(Ge) Heterostructures - A. Agarwal, S. Koveshnikov, and G. A. Rozgonyi	270

TUESDAY CONTINUED

10:20 Electrochromic Performance of Polyaniline Films Polarized in a pH 3 Electrolyte - A. Hugot-Le Goff and M. C. Bernard 394

10:45 Fractal Porosity and Lithium Ion Kinetics in Electrochromic Li_xWO_3 Thin Films - D. K. Benson, J.-G. Zhang, C. E. Tracy, A. W. Czanderna, and S. K. Deb 395

11:10 Electrodeposition of Nickel Oxyhydroxide Films Through Polymer Masks - M.-C. Yang, C.-K. Lin, C.-L. Su, and T.-C. Chou 396

11:35 On the Structural Properties of Electrochromic NiO_x - M. C. A. Fantini, I. C. Faria, R. M. Torresi, and A. Gorenstein 397

S. F. Cogan, Chairman; H. J. Byker, Vice-Chairman

2:00 Application of a Solid Polymer Electrolyte in One Square-Foot Electrochromic Devices - R. D. Varjian, M. Shabrang, and S. J. Babinec 398

2:25 Characterization of Nonstoichiometric Nickel Oxide Thin Film Electrodes for Electrochromic Devices - B. Scrosati and S. Passerini 399

2:50 Electrochromic Reaction in MnO_2 Films Polarized in Neutral Solution - A. Hugot-le Goff, M. C. Bernard, S. Cordoba-Torresi, and T. B. Vu 400

3:15 Characterization and Performance of Codeposited Nickel/Tungsten Trioxide Electrochromic Films - A. C. C. Tseung and J. Syed-Bokhari 401

3:40 Study by Laser Probe Deflection of the Ionic Mechanism in Nickel Oxide Thin Films - J.-C. Giron and C. M. Lampert 402

HIGH TEMPERATURE BEHAVIOR OF CERAMICS, INTERMETALLICS, AND COMPOSITES

High Temperature Materials

N. S. Jacobson, Chairman; M. McNallan, Vice-Chairman
Senate/Walker Percy Amphitheater, 3rd Floor

Ceramics and Composites I

8:30 Strength Retention of NT154 Silicon Nitride Exposed to High Temperature Oxidation and Hot Corrosion Environments - T. E. Strangman and D. S. Fox 424

9:00 Lifetime Prediction of Engineering Ceramics and Composites in High Temperature Corrosion Environments - M. H. Van de Voorde 425

9:30 Environmental Effects on the Flexure Strength of HIPed Silicon Nitride at Elevated Tempeatures - A. A. Wereszczak, K. Breder, M. K. Ferber, T. P. Kirkland, and P. Khandelwal 426

9:50 High Temperature Subcritical Crack Growth of SiC/SiC Composites - C. F. Windisch, Jr., R. H. Jones, and C. H. Henager, Jr. 427

10:10 Ten-minute intermission

10:20 The Oxidation of Silicon Carbide in 0.5 Atmosphere Water Vapor - E. J. Opila 428

10:40 Stability of Si-Ti-C-O (Tyranno) Fibers in Air and High Temperature High Pressure Water - Yu. G. Gogotsi and M. Yoshimura 429

11:00 Hydrothermal Corrosion and Strength Degradation of Sialon Ceramics - T. Yoshio and K. Oda 430

A. Nagelberg, Chairman; S. C. Singhal, Vice-Chairman

Ceramics and Composites II

2:00 Oxidation Behavior of Reaction-Formed Silicon Carbide Ceramics - L. U. Ogbuji and M. Singh 431

2:20 Corrosion of Mullite and Mullite-Coated SiC by Sodium Salts - N. S. Jacobson, K. N. Lee, and T. Yoshio 432

2:40 A Study of Vanadium Hot Corrosion Reactions of Ceria Using Thermogravimetric Analysis - R. F. Reidy and R. L. Jones 433

3:00 The Oxidation Behavior of ZrO_2 Reinforced $MoSi_2$ Composites at 1500°C - P. Beatrice, W. L. Worrell, and J. J. Petrovic 434

3:20 Mass Spectrometric Study of the High Temperature Vaporization of $LaCrO_3$ - K. Hilpert, D. Kobertz, M. Miller, and H. Nickel 435

HIGH TEMPERATURE LAMP CHEMISTRY III

High Temperature Materials/Luminescence and Display Materials

H. Horster, Chairman; D. L. Hildenbrand, Vice-Chairman
St. Charles B, 3rd Floor

9:00 Measurement of Enhanced Thulium Abundance in Metal Halide Discharge Lamps - M. J. Shea, W. M. Keeffe, C. W. Struck, and A. E. Feuersanger 447

9:25 Analysis and Thermochemistry of the Vapor of the NaBr-$DyBr_3$ System - K. Hilpert and M. Miller 448

9:50 Study of the Heterocomplexes in the Vapor of the Na-Sn-Br-I System and Their Relevance for Metal Halide Lamps - K. Hilpert, M. Miller, and U. Niemann 449

10:15 Ten-minute intermission

10:25 Modeling Multicomponent Metal Halide Systems - S. A. Mucklejohn and A. T. Dinsdale 450

10:50 An Assessment of the Thermochemical Parameters for the Lanthanide Triiodides - S. A. Mucklejohn, R. Devonshire, and D. L. Trindell 451

11:15 Coherent Anti-Stokes Raman Scattering (CARS) Studies of Metal Halides - D. L. Trindell, S. Greiff, and R. Devonshire 452

11:40 Incandescent Radiation from Clusters: A Novel Type of Light Source - R. Scholl 453

W. M. Keeffe, Chairman; R. Devonshire, Vice-Chairman

2:00 On the Lithium Loss of LiI Containing Metal-Halide Lamps - F. Nagel and L. Bencze 454

2:25 On the Chemical Processes in Zr Containing Fluorescent Tube Emission Mix - F. Nagel, M. Farkas-Jahnke, and J. Meszaros 455

2:50 Ten-minute intermission

3:00 Zn-Hg Amalgams for Fluorescent Lamps: Vapor Pressure, Thermodynamics, and Lamp Performance - T. R. Brumleve, S. C. Hansen, and L. G. Kaczorowski 456

3:25 A Self-Consistent Model for the Medium Pressure Mercury and Mercury Rare Gas Discharge - G. Zissis, N. Bashlov, V. Milenin, and M. Stambouli 457

THE ELECTROCHEMISTRY OF MANGANESE

Industrial Electrolysis and Electrochemical Engineering/Battery/Physical Electrochemistry

M. P. Grotheer, Chairman; L. Bai, Vice-Chairman
Grand Ballroom D, 5th Floor

10:15 Introductory remarks

10:20 Compositions for Rechargeable Leclanche Cells - B. Schumm, Jr. 458

10:40 A Study of the Rechargeability of Modified MnO_2 - X. Xi 459

11:00 The Mechanism Studies of the Reduction and Reoxidation of Rechargeable Chemically Modified MnO_2 Battery Cathode Material. I. - D. Y. Qu, L. Bai, B. E. Conway, Y. H. Zhou, and W. A. Adams 460

11:20 The Mechanism Studies of the Reduction and Reoxidation of Rechargeable Chemically Modified MnO_2 Battery Cathode Material. II. - D. Y. Qu, L. Bai, B. E. Conway, and W. A. Adams 461

11:40 Manganese Oxides as 3 V and 4 V Cathodes for Rechargeable Lithium Cells - M. Yoshio, H. Noguchi, H. Kurimoto, K. Suzuoka, and A. Kozawa 462

B. Schumm, Jr., Chairman; L. Bai, Vice-Chairman

2:00 Lithiated Manganese Oxide for Rechargeable Nonaqueous Batteries - M. Broussely, P. Biensan, A. Lecerf, J. C. Rousche, J. B. Soupart, and P. Botkovitz 463

2:20 The Electrochemical Modulation Reflectance Spectrum Characteristics of MnO_2 Film Electrodes - Y. Wang, J. Tian, and L. Gu 464

2:40 An Aluminum/Permanganate Battery for Electric Vehicles - S. Licht and D. Peramunage 465

3:00 Electrowinning of Manganese Metal - M. P. Grotheer and T. W. Clapper 466

3:20 Open discussion

WEDNESDAY, OCTOBER 13, 1993

12:15 P.M. Electrodeposition Division Luncheon and Business Meeting, Waterbury Ballroom, 2nd Floor.
12:15 P.M. Luminescence and Display Materials Division Luncheon and Business Meeting, Armstrong Ballroom, 8th Floor.

LITHIUM BATTERIES
Battery

M. A. Dzieciuch, Chairman; W. Li, Vice-Chairman
Ponchartrain Ballroom A, 3rd Floor

Li^+ Cells

N. Doddapaneni, Chairman; K. Gaffney, Vice-Chairman

Li^+ Cells (cont'd)

GENERAL SESSION
Battery

S. C. Levy, Chairman; C. F. Holmes, Vice-Chairman
Ponchartrain Ballroom B, 3rd Floor

GENERAL SESSION
Corrosion

E. McCafferty, Chairman; P. Kovacs, Vice-Chairman
Grand Ballroom A, 5th Floor

A. J. Davenport, Chairman; J. R. Scully, Vice-Chairman

WEDNESDAY CONTINUED

THE DEGRADATION OF ELECTRONIC DEVICES DUE TO DEVICE OPERATION AS WELL AS CRYSTALLINE AND PROCESS-INDUCED DEFECTS

Electronics

G. A. Rozgonyi, Chairman; H. Tsuya, Vice-Chairman
Grand Ballroom B, 5th Floor

Electrical

THIRD INTERNATIONAL SYMPOSIUM ON CLEANING TECHNOLOGY IN SEMICONDUCTOR DEVICE MANUFACTURING

Electronics/Dielectric Science and Technology

V. Menon, Chairman; R. J. Nemanich, Vice-Chairman
Grand Ballroom C, 5th Floor

Gas-Phase Cleaning - Part I

C. R. Helms, Chairman, A. Velaga, Vice-Chairman

Gas-Phase Cleaning - Part II

THERMAL-TO-ELECTRIC ENERGY CONVERSION AND STABILITY OF REFRACTORY MATERIALS

Energy Technology/High Temperature Materials

M. A. Ryan, Chairman; D. L. Jacobson, Vice-Chairman
Senate/Walker Percy Amphitheater, 3rd Floor

ELECTROCHROMIC MATERIALS

Energy Technology/Luminescence and Display Materials

H. J. Byker, Chairman; C. M. Lampert, Vice-Chairman
Bayside B, 4th Floor

WEDNESDAY CONTINUED

11:40	Mechanism of Selective Porosification at Heterojunctions in Group IV Multilayer Structures - T. George, R. W. Fathauer, W. T. Pike, E. W. Jones, and A. Ksendzov	534

M. Tomkiewicz, Chairman; C. Levy-Clement, Vice-Chairman

2:00	Formation Mechanisms of Porous Silicon - V. Lehmann	535
2:20	Anodization of p-Type Si: Theoretical Analysis - Y. Kang and J. Jorne	536
2:40	Computer Simulations of Pore Growth in Silicon - J. Erlebacher, K. Sieradzki, and P. C. Searson	537
3:00	Impedance of Porous Si - W. M. Shen, M. Tomkiewicz, A. Lagoubi, and C. Levy-Clement	538
3:30	The Microstructure and Formation Mechanism of Porous Silicon - F. M. Ross, P. C. Searson, and J. M. Macaulay	539
3:50	Microstructure of Porous n-Type Silicon Formed by Photoelectrochemical Etching - A. Albu-Yaron, D. Bouchet, N. Brun, C. Colliex, and C. Levy-Clement	540
4:10	Porous Gallium Arsenide and Porous Silicon: A Comparison - J. M. Macaulay, J. A. Liddle, and P. C. Searson	541
4:30	Characterization of Porous SiC - J. S. Shor, I. Grimberg, L. Bemis, M. Macmillan, W. J. Choyke, B. Z. Weiss, and A. D. Kurtz	542

MICROELECTRODES AND MICROENVIRONMENTS: FUNDAMENTALS AND APPLICATIONS

Physical Electrochemistry/Sensor/Corrosion

B. R. Shaw, Chairman; R. J. Nowak, Vice-Chairman
Ponchartrain Ballroom C, 3rd Floor

8:30	Ultraslow Diffusion to Electrodes - R. W. Murray, M. W. Poupart, Z. Porat, O. Haas, and C. Velazquez	597
9:00	AC Admittance Techniques Using Ultramicroelectrodes in Media of High Resistance - M. Fedurco, W. R. Fawcett, and M. Opallo	598
9:30	Electrochemistry at Microelectrodes in Supercritical Chlorodifluoromethane - D. E. Tallman and S. A. Olsen	599
10:00	Electrochemical Studies in Nonconventional Conditions - M. I. Montenegro, M. F. Bento, M. D. Geraldo, M. J. Medeiros, D. Pletcher, and C. Amatore	600
10:30	Ten-minute intermission	
10:40	A New Kind of Viscometer Based on the Electrochemical Measurement of Diffusion-Limited Currents at Microelectrodes and Microelectrode Arrays - S. Fletcher, R. L. Deutscher, and V. A. Vicente-Beckett	601
11:10	Electrocatalysis with Metal Microparticles in a Synthetic Glassy Carbon Host - R. L. McCreery, N. Pocard, D. Alsmeyer, M. Huston, W. Huang, and M. Callstrom	602
11:40	Electrified Microheterogeneous Catalysis: With and Without Zeolite-Supported Microelectrodes - D. R. Rolison and J. Z. Stemple	603

H. S. White, Chairman; R. M. Penner, Vice-Chairman

2:00	Nanometer-Scale Electrochemical Synthesis of Electronic Materials Using the Scanning Tunneling Microscope - W. Li, G. Hsiao, S. Lee, J. A. Virtanen, and R. M. Penner	604
2:30	Toward the Refinement of Nanoband Electrodes: Chemically Enhanced Metal Nucleation as Studied by Scanning Probe Microscopy - R. L. McCarley and D. J. Dunaway	605
3:00	Imaging and Modification of Au(111) Monoatomic Steps with the Atomic Force Microscope - J. C. Brumfield, C. A. Goss, E. A. Irene, and R. W. Murray	606
3:30	Fifteen-minute intermission	
3:45	Luminescence Imaging of Electrode Microenvironments - R. C. Engstrom and J. E. Vitt	607
4:15	Observations of Corrosion Pit Initiation on Aluminum Using Microelectrodes - K. Hebert, Y. Tak, and I. Obi	608
4:45	Disk Microelectrodes Fabricated by Excimer Laser Micromachining - B. J. Seddon and H. H. Girault	609

FULLERENES: CHEMISTRY, PHYSICS, AND NEW DIRECTIONS V

New Technology Subcommittee

P. A. Cahill, Chairman; J. C. Withers, Vice-Chairman
Rhythms Room, 2nd Floor

Chemistry/Electrochemistry

8:30	Fullerenes in Rocks - P. R. Buseck and T. Daly	659
9:00	Coupling of Redox and Acid-Base Reactions in the Electrochemistyr of C_{60} - D. H. Evans, S. A. Larke, and P. J. Fagan	660
9:30	Spectroscopic Characterization of Electrochemically Prepared Fullerene Films - P. W. Faguy, W. N. Richmond, F. Xu, A. Borman, and T. F. Guarr	661
10:00	Electrochemical Properties of Reduced Fullerenes - T. F. Guarr, M. S. Meier, V. K. Vance, and M. Clayton	662
10:30	Magnetic Properties of Some Solid C_{60} Salts - M. T. Jones, P. Buolas, R. Subramanian, W. Kutner, and K. M. Kadish	663
11:00	Fifteen-minute intermission	
11:15	Solvent, Supporting Electrolyte and Substituent Effects on the Electrochemistry of Fullerenes - K. M. Kadish	664
11:45	Regioselective Electrosynthesis of Alkylated C_{60} Derivatives: A Novel Method for Controlled Functionalization of Fullerenes - K. M. Kadish, C. Caron, R. Subramanian, F. D'Souza, W. Kutner, and M. T. Jones	665

R. Malhotra, Chairman; J. R. Shapley, Vice-Chairman

Theory

1:30	A Computational Model for Fullerene Chemistry - B. Doust, D. A. Jelski, J. R. Bowser, and T. F. George	666
2:00	Theoretical Studies of Fullerene Derivatives - K. Raghavachari	667
2:30	Evaluation of Linear and Nonlinear Optical Properties of Fullerenes - A. Rosen and E. Westin	668
3:00	Fullerene Annealing and Fragmentation: A Tale of Handles and Sticks - G. E. Scuseria	669
3:30	Pinching Reactions of Carbon Rings - D. L. Strout and G. E. Scuseria	670
4:00	Fifteen-minute intermission	
4:15	Energetics of Fullerene Molecules and Nanotubes - J. Tersoff	671
4:45	Molecular Dynamics Simulations of C_{60} Fragmentation - C. Xu and G. E. Scuseria	672
5:15	Tight-Binding Molecular Dynamics Simulation of Compression of C_{60} Solid - B. L. Zhang, C. Z. Wang, K. M. Ho, and C. T. Chan	673
5:45	Ionization Potentials and Electron Affinities of Fullerenes - R. S. Ruoff, D. Tomanek, and Y. Wang	674

THURSDAY, OCTOBER 14, 1993

LITHIUM BATTERIES

Battery

M. Binder, Chairman; J. McBreen, Vice-Chairman
Ponchartrain Ballroom A, 3rd Floor

Other Advanced Li Cells

9:00	Gas Plasma Treatment of Cathodes to Improve Li/SO_2 Cell Performance - R. J. Mammone, T. B. Reddy, M. Binder, and E. P. Thurston	34
9:25	Parametric Analysis of Lithium Oxyhalide Spirally Wound Cells Utilizing the Taguchi Approach to Experimental Design - E. S. Takeuchi and P. J. Size	35
9:50	High Rate Lithium/Thionyl Chloride Bipolar Battery Development - P. G. Russell and F. Goebel	36
10:15	Fifteen-minute intermission	
10:30	Reduction of Voltage Delay in Li/$SOCl_2$ Cells after Partial Discharge and Storage - A. P. Johnson, S. Sekido, and C. R. Schlaikjer	37
10:55	EC Based Electrolytes for the Graphite Negative Electrode - H. Mao, P. Juric, and U. von Sacken	38

3:40 Gunn Diodes Resistance Measurements by Galvanomagnetic Method - A. Wolkenberg, T. Przeslawski, J. Klamka, and Z. Tkaczyk 634
4:00 Open Discussion/Recent News

THIRD INTERNATIONAL SYMPOSIUM ON CLEANING TECHNOLOGY IN SEMICONDUCTOR DEVICE MANUFACTURING
Electronics/Dielectric Science and Technology

T. Ohmi, Chairman; P. Patruno, Vice-Chairman
Grand Ballroom C, 5th Floor

General Cleaning - Part II

9:00 A New Cleaning Concept for Particle and Metal Removal on Si Surfaces - M. Meuris, S. Verhaverbeke, P. W. Mertens, H. F. Schmidt, A. Rotondaro, M. M. Heyns, and A. Philipossian 341
9:30 Prevention of Microroughness on the Si Wafer Surface in Buffered Oxide Etchant by a Surfactant Addition - M. Miyamoto, N. Kita, S. Ishida, and T. Tatsuno 342
9:50 Ultrathin Oxide Formation Using Chemical Oxide Passivation - K. Nakamura, T. Futatsuki, K. Makihara, and T. Ohmi 343
10:10 Peculiarities of Hot Phosphoric Acid Used in the Etching of Silicon Nitride - W. Syverson and M. J. Fleming 344
10:30 Impact Study of the Use of ULSI, VLSI, and MOS Grade Chemicals in the RCA Cleaning Process on MOS and Bipolar Devices - F. Tardif, J. P. Joly, T. Lardin, A. Tonti, P. Patruno, D. Levy, and W. Sievert 345
10:50 Contamination Removal by a Wafer Spin Cleaning Process with an Advanced Chemical Distribution System - N. Yonekawa, S. Yasui, F. Kunimoto, F. W. Kern, Jr., and T. Ohmi 346
11:10 Characterization of Quick Dump Megasonic Cleaner for VLSI Planarization RIE Post-Clean Process - P. Wang and D. Bell 347
11:30 The Effects of HF-Cleaning Prior to Silicon Wafer Bonding - Y. Backlund, K. Ljungberg, and A. Soderbarg 348
11:50 The Effect of Dissolved Oxygen and Dissolved Ozone in Ultrapure Water on N^+- Doped Polycrystalline Silicon to N^+- Doped Crystalline Silicon Contact Resistance - M. J. Satterfield, B. Anthony, G. Huffman, and F. Walczyk 349

W. Syverson, Chairman; M. J. Satterfield, Vice-Chairman

General Cleaning - Part III

1:30 Silicon Surface Roughening by the Decomposition of Hydrogen Peroxide - H. F. Schmidt, M. Meuris, P. W. Mertens, S. Verhaverbeke, M. M. Heyns, L. Hellemans, I. Snauwaert, and K. Dillenbeck 350
1:50 A Study of Various Surface Pretreatments and Their Effect on Electrical Characteristics of Subsequently Grown Film - K. W. Morinville, R. Kauffman, R. C. Hawthorne, and D. Korn 351
2:10 Studies of Rinse Efficiencies in Wet Cleaning Tools - R. Spearow, J. Rosato, and C. R. Helms 352
2:30 The Effect of Increased Chemical Temperature in a Centrifugal Spray Processor - K. K. Christenson 353
2:50 The Use of Centrifugal Force to Improve Rinsing Efficiency - K. K. Christenson 354

LIGHTING, DISPLAY, AND IMAGING TECHNOLOGY: PHOSPHOR SYNTHESIS, COATING, AND SCREENING
Luminescence and Display Materials

C. G. A. Hill, Chairman; V. B. Reddy, Vice-Chairman
St. Charles B, 3rd Floor

CRT and Other Phosphors

8:30 Introductory remarks
8:35 Infrared Emitting Rare-Earth Aluminum Oxide Phosphors - H. Tamaki and M. R. Royce 477
9:00 Measurement of Adhesion of Electrophoretically Deposited Phosphor Coatings - M. J. Shane, J. B. Talbot, M. Le, E. Sluzky, and K. R. Hesse 478
9:25 Aging and Thermoluminescence in Flying Spot Scanner CRT Phosphors - M. S. Waite and C. Brass 479
9:50 High Resolution Phosphor Screens by Electrophoretic Deposition - R. P. Rao and D. C. Ketchum 480
10:15 Fifteen-minute intermission
10:30 Photo- and Low-Voltage Cathodoluminescence of MN^{+2} Activated $ZnGa_2O_4$ Phosphors - L. E. Shea, R. K. Datta, and J. J. Brown, Jr. 481
10:55 Saturation Behavior of Zinc Sulfide Thin Films Grown by Metal Organic Chemical Vapor Deposition - M. Shiiki, H. Matsukiyo, and O. Kanehisa 482
11:20 Phosphors for Displays - T. Welker 483

NONLINEAR OPTICS AND MATERIALS
Luminescence and Display Materials/Dielectric Science and Technology

S. W. Koch, Chairman; S. I. Najafi, Vice-Chairman
St. Charles B, 3rd Floor

2:00 Quantum Dot Figure of Merit for All-Optical Switching Applications - E. M. Wright 484
2:30 Spectral Hole Burning and Confinement-Enhanced Biexciton Binding Energy in Semiconductor Quantum Dots - N. Peyghambarian, K. I. Kang, A. D. Kepner, S. V. Gaponenko, Y. Z. Hu, and S. W. Koch 485
3:00 Doped Nanocrystals of Semiconductors: A New Class of Luminescent Materials - R. N. Bhargawa and D. Gallagher 486
3:30 Quantum Dots: Quasi-Atom Optoelectronics - G. W. Bryant 487
4:00 Optical Properties of Semiconducting Nanocrystals: Correlation with Precipitation Stages - S. V. Gaponenko, U. Woggon, W. Langbein, and C. Klingshirn 488

ELECTROCHEMISTRY IN UNCONVENTIONAL MEDIA AND IN MEDIA UNDER EXTREME CONDITIONS
Physical Electrochemistry

R. M. Corn, Chairman; S. E. Creager, Vice-Chairman
Ponchartrain Ballroom D, 3rd Floor

9:00 Electrochemistry in Ambient Temperature Chloroaluminate Ionic Liquids: An Overview for the Uninitiated! - R. A. Osteryoung 505
9:30 Electrochemical Reduction of Azobenzyne and Azoxybenzene from Molten Acetamide at 85°C - R. Saraswathi and R. Narayan 506
10:00 Electrochemical Measurements of Diffusion Coefficients of Redox-Labeled Poly(Ethyleneglycol) Dissolved in Poly (Ethyleneglycol) Melts - O. Haas, Ch. Valasquez, Z. Porat, and R. W. Murray 507
10:30 Fifteen-minute intermission
10:45 Clusters and Complexes in Polymer Electrolytes: EXAFS Studies - J. McBreen, I.-C. Lin, X. Q. Yang, and H. S. Lee 508
11:15 A Study of Anodic Processes at Carbon Electrodes in Alumina-Cryolite Melts by Means of Cyclic Voltammetry - S. S. Djokic, B. E. Conway, and T. F. Belliveau 509

J. Leddy, Chairman; C. Shannon, Vice-Chairman

1:30 Adsorption, Orientation, and Reaction at Liquid-Liquid Electrochemical Interfaces as Studied by Optical Second Harmonic Generation - R. M. Corn, D. A. Higgins, and R. N. Naujok 510
2:00 Fabrication and Characterization of Microelectrodes Using STM - C. Shannon, V. Cammarata, and U. Demir 511
2:30 Electric Field Effects on Surface Elimination Reactions Involving Self-Assembled Monolayers - R. J. Forster and L. R. Faulkner 512
3:00 Fifteen-minute intermission
3:15 Diffusionless Electrochemistry of Self-Assembled Cytochrome/Alkanethiolate/Gold Monolayer Structures - E. F. Bowden, R. A. Clark, S. Song, and M. J. Tarlov 513
3:45 Electrochemistry of Single Monolayer Langmuir-Blodgett Films on Electrodes - M. Majda, P. Krysinski, T. Hanna, and R. Chamberlain 514
4:15 Migration Effect and IR Correction during Linear Sweep Voltammetry - S. L. Keller, J. W. Van Zee, and J. W. Weidner 515

FRIDAY, OCTOBER 15, 1993

HIGH PERMITTIVITY MATERIALS

Dielectric Science and Technology/Electronics

B. Gnade, Chairman; J. Chapple-Sokol, Vice-Chairman
Rosella Room, 4th Floor

9:00	Electrodes Systems for Ferroelectric Capacitor Structures in DRAMs - A. I. Kingon, H. Al-Shareef, and S. Summerfelt	164
9:30	Chemical Vapor Deposition of (Ba,Sr)TiO_3 - M. Yoshida, H. Yamaguchi, T. Sakuma, Y. Miyasaka, P.-Y. Lesaicherre, and A. Ishitani	165
10:00	Physicochemical Properties of RF Magnetron-Sputtered Lead Zirconate Titanate Thin Fllms - B. Agius, E. Cattan, B. EA Kim, and F. Varniere	166
10:30	Microstructural Analysis of a Ge Barrier Layer at the $BaTiO_3$/Si Interface - E. G. Jacobs, Y. Rho, R. F. Pinizzotto, S. R. Summerfelt, and B. E. Gnade	167
10:50	Investigation of Electrode Materials for Metal-Ferroelectric-Pt Capacitors for DRAM Applications - J. Kim, R. Khamankar, C. Sudhama, J. Lee, S. Summmerfelt, and B. Gnade	168
11:10	Open Discussion/Recent News	

NONLINEAR OPTICS AND MATERIALS

Luminescence and Display Materials/Dielectric Science and Technology

S. I. Najafi, Chairman; S. W. Koch, Vice-Chairman
St. Charles B, 3rd Floor

9:00	Circular Grating Lasers in Quantum Well Structure - M. Fallahi, M. Dion, F. Chatenoud, I. M. Templeton, and K. A. McGreer	489
9:30	Quantum Confinement and Strain Effects in Nonlinear Semiconductor Gain Media - W. W. Chow	490
10:00	Semi-Insulating Materials and Epitaxy for Advanced Optoelectronics - D. G. Knight	491
10:30	Gain and Absorption in Semiconductor Amplifiers - R. Binder, A. Knorr, E. M. Wright, and S. W. Koch	492
11:00	Photophysics of Light Emitting Polymer Diodes - L. Rothberg, M. Yan, J. W. P. Hsu, T. M. Jedju, A. Dodbalapur, H. H. Kim, T. M. Miller, M. Galvin, and F. Papadimitrakapoulos	493
11:30	Recent News	

FULLERENES: CHEMISTRY, PHYSICS, AND NEW DIRECTIONS V

New Technology Subcommittee

B. I. Dunlap, Chairman; S. W. McElvaney, Vice-Chairman
Rhythms Room, 2nd Floor

Physics/Chemistry

9:00	Production of Fullerenes in Nitrogen Media - O. M. Vovk, L. A. Vaschenko, O. A. Boryak, M. V. Kosevich, G. V. Andrievsky, and V. S. Shelkovsky	689
9:30	X-Ray Dilatometry of C_{60} - A. P. Isakina, A. I. Prokhvatilov, and M. A. Strzhemechny	690
10:00	Open Discussion/Recent News	

14 Conductivity of $Li_xMg_yAl_z(SO_4)_3$ as a New Lithium Ionic Conductor for a Solid-State Cell: *T. Shodai* and *H. Ohtsuka,* NTT Interdisciplinary Research Laboratories, Tokai-mura, Ibaraki-ken, 319-11 Japan, *M. Ichimura,* NTT Interdisciplinary Research Laboratories, Musashino-shi, Tokyo-to, 180 Japan, *J.-i. Yamaki,* NTT Interdisciplinary Research Laboratories, Tokai-mura, Ibaraki-ken, 319-11 Japan

The composition of $Li_{3.3}Mg_{0.6}Al_{0.5}(SO_4)_3$ shows the highest conductivity and the lowest activation energy of $Li_xMg_yAl_z(SO_4)_3$ system. The conductivity is 4×10^{-5} S/cm at 100°C and 1×10^{-6} S/cm at 25°C. The activation energy is 0.41 eV in the 25-200°C temperature range. In addition, it is clear that $Li_xMg_yAl_z(SO_4)_3$ system is a Li ionic conductor. $Li_{3.3}Mg_{0.6}Al_{0.5}(SO_4)_3$ is stable with Li metal under 180°C. $Li_xMg_yAl_z(SO_4)_3$ system is very promising as a solid electrolyte for a solid-state cell.

15 Effect of Electrolyte Composition on Carbon Electrode Performance: *C.-K. Huang, S. Surampudi, G. Halpert,* and *D. Shen,* JPL, Pasadena, CA 91109

The electrochemical intercalation of lithium into carbon was investigated in several mixed solvent electrolytes containing ethers and carbonate. The results obtained so far indicate that electrolyte decomposition occurs at the carbon electrode surface during the initial stages of the discharge process. The extent ot decomposition was significantly dependent on the electrolyte composition. Electrolytes containing a higher percentage of EC showed higher electrolyte decomposition. The cells containing more EC in the electrolyte showed higher rate capability. Hence, a tradeoff in the electrolyte composition may be necessary to obtain higher rate capability and to minimize electrolyte decomposition at the carbon electrode.

16 Ionic Conductivity of Polymer Electrolyte Using Modified Carbonate as Plasticizer in Poly(ethylene oxide): *X. Q. Yang, H. S. Lee,* and *J. McBreen,* Brookhaven Natl. Lab., Upton, NY 11973, *Z. S. Xu* and *T. A. Skotheim,* Moltech Corp., Stony Brook, NY 11794-2275, and *Y. Okamoto,* Polytechnic Univ., Brooklyn, NY 11201

A new type of plasticizer, modified carbonate(MC), has been synthesized. It was done by attaching three ethylene oxide units on 4 position of ethylene carbonate group. By adding 50% weight of this plasticizer into the PEO-$LiCF_3SO_3$ complex, the ionic conductivity reached 10^{-5} s/cm at room temperature. The mixture forms a homogeneous electrolyte and can be cast into freestanding films with good mechanical properties. Temperature-dependent conductivity measurement and thermal analysis show that this plasticizer uniformly increased the ionic conductivity of the entire polymer electrolyte system. This plasticizer also enhanced ion pair dissociation.

17 Electrochemical Measurements of Li-Si-Ca Alloy in LiCl-KCl Electrolyte at 426°C: *G.E. Lagos, J. Parada, G. Crisostomo,* and *J. Corvalan,* Dept. of Mining Eng., Univ. of Chile, Santiago, Chile

Electrochemical measurements of Li-Si-Ca alloy have been made in an LiCl-KCl electrolyte at 426°C, to assess the behavior of this material as a negative electrode of a high specific power battery of the type Li alloy/molten salt/metal sulfide. Potential *vs.* composition plots of coulometric titration of lithium into $CaSi_2$, showed that there are several plateaus, some of which can be attributed to three phase equilibria. The specific energy of this material, after 42 atomic percent of lithium had been titrated was measured to be 437 wh/kg. According to the ternary diagram, it should be possible to titrate up to 75% atomic percent of lithium.

Tuesday PM

18 The Electrochemistry of Lithium in Nonaqueous Solvents: Past and Future Trends: *J. Jorne,* Dept. of Chem. Eng.. Univ. of Rochester, Rochester, NY 14727

A review of past efforts and present trends in the research of lithium in nonaqueous solvents is presented. The fundamental studies of the earlier years (1960-1980) resulted in the development of primary lithium batteries. The present efforts to develop rechargeable lithium batteries must identify the delicate balance between containing the reactivity of lithium and maintaining its high energy density. Current approaches include the formation of insertion and intercalation lithium compounds, and the use of aprotic solvents and solid polymer electrolytes. The electrochemistry of lithium in propylene carbonate is reviewed historically as a guideline for future research and development of lithium batteries.

19 Novel Stable Highly Conductive Electrolytes for Lithium Batteries: *L. A. Dominey,* Covalent Ass., Inc., Woburn, MA 01801

Improvements in Li polymer and liquid electrolyte conductivity and stability are needed. Toward that goal we have prepared and characterized several new Li salts and studied them as both liquid and polymer electrolytes. We present results for electrolytes containing $LiC(SO_2CF_3)_3$, $LiC(SO_2CF_3)_2F$, $LiC(SO_2CF_3)_2SO_2CH_3$, and $LiC(SO_2CH_3)_3$. Of this set. $LiC(SO_2CF_3)_3$ is the most conductive and also possesses excellent oxidative stability. The role of low levels of Li salts as high voltage corrosion inhibitors is discussed.

20 Boron Substituted Carbons as Anodes for Lithium Ion Cells: *B. Way* and *J. Dahn,* Dept. of Physics, Simon Fraser University, Burnaby, BC, Canada V5A 156

It is important that the specific capacity of carbons used as anodes in Li-ion cells be as large as possible. Here we show that for $z = 0.10$ in B_zC_{1-z}, reversible specific capacities of 0.40 Ah/g for Li/B_zC_{1-z} cells can be attained. This is 50% larger than for pure carbon prepared under the same conditions.

21 Characterization of Lithium-Ion Rechargeable Cell after Charge and Discharge Cycling: *K. Tanaka,* Sony Corp. Research Center, Material Research Dept., 174, Fujitsuka-cho, Hodogaya-ku, Yokohama, 240, Japan, *M. Itabashi, M. Aoki, S. Hiraka, K. Kataoka,* Sony Corp. Research Center, Material Characterization Dept., 134, Koudo-cho, Hodogaya-ku, Yokohama, 240 Japan, *S. Fujita, K. Sekai,* and *K. Ozawa,* Sony Corp. Research Center, Battery Group R&D Div., 174, Fujitsuka-cho, Hodogaya-ku, Yokohama, 240, Japan

The lithium-ion rechargeable cell, with a nongraphitizable carbon anode, $LiCoO_2$ cathode and the propylene carbonate (PC)-diethyl carbonate (DEC) (1:1 by volume)/1*M* $LiPF_6$, after charge and discharge cycling, has been characterized by using impedance measurement, SEM, EDX, XPS, GC/IR/MS, and solid-state NMR in order to clarify the slight decrease of discharge capacity accompanied by charge and discharge cycling. It was found that the slight decrease of the discharge capacity is due to the carbon anode mainly.

Wednesday AM

22 Overcharge Protection of Lithium Ion Rechargeable Batteries: *Y. Yamamoto, H. Kato,* and *Y. Nishi,* R&D Dept., Sony Energytec Inc., Koriyama-shi, Fukushima 963-05, Japan

Lithium ion rechargeable cells shows sufficient safety characteristics under the recommended charging voltage of 4.1-4.2 V. In the case of overcharging a cell, however, a safety device has been desired to prevent the cell from thermal runaway. In order to improve the safety characteristics of an overcharged cell, anti-overcharging materials were investigated in this study which decompose electrochemically on overcharging with the gas evolution. The gas pressure works upon a safety device to terminate charging. It was found that Li_2CO_3 is a useful material for this purpose.

23 Lithium Polymer Rocking Chair Batteries: *B. Scrosati, F. Croce,* and *S. Passerini,* Dipartimento di Chimica, Universita di Roma, 00185 Rome, Italy

The rocking chair batteries under present development generally use lithiated carbon Li_xC_6 as the lithium-sink electrode, a lithium metal oxide $LiMo_2$ (M = Co, Ni, Mn) as the lithium-source electrode, and liquid organic solutions as the electrolyte. This overall configuration, although very appealing in terms of practicity and cost, is far from being the best choice since it is affected by some operational problems, mainly connected to the electrolyte and of anode. As a possible alternative configuration, we have assembled a rocking chair cell where titanium disulfide was the negative electrode and lithium cobalt oxide was the positive electrode, while the electrolyte was a PAN-EC/PC, $LiClO_4$ polymer membrane, to achieve a TiS_2/PAN-EC/PC, $LiClO_4$ / $LiCoO_2$ overall cell structure. Preliminary results indicated that this novel type rocking chair battery operates at room temperature with a promising response in terms of cyclability and reliability.

24 Performance Characteristics of Lithium Cobalt Dioxide Cathodes in Polymer-Based Lithium Rechargeable Cell: *W. Li, H.-P. Lin,* and *D. L. Chua,* Alliant Techsystems Inc., Power Sources, Horsham, PA 19044, *S. House,* United States Air Force, Phillips Laboratory (VTPC), Kirtland AFT, NM 87117-6008

This paper describes characterization and development of a polymer-based lithium rechargeable cell system using high voltage lithium cobalt dioxide cathode. Included is a discussion of the polymer electrolyte with enhanced room temperature conductivity and a wide operating temperature range, and the properties of lithium cobalt dioxide cathode. The performance characterization of the polymer-based Li/Li_xCoO_2 cells indicated good rate capability and long cycle life.

25 Electrochemical Impedance Analysis of Vanadium Pentoxide Xerogel during Lithium Insertion and Release: *H. K. Park,* and *W. H. Smyrl,* Corrosion Res. Cntr., Dept. of Chem. Eng. & Mat. Sci., Univ. of Minnesota, Minneapolis, MN 55455

Electrochemical impedance has been employed to characterize the processes of charge transfer and diffusion in thin spon-coated xerogel films of vanadium pentoxide. Diffusion coefficients vary from 4×10^{-10} to 4×10^{-11} cm^2/s at low and high Li insertion concentrations, respectively. The charge transfer resistance increases more than one order of magnitude as well. High charge-transfer resistance at high lithium composition may limit the utilization of the xerogel at these conditions.

26 Composition and Morphology Studies of V_6O_{13} Cathodes: *A. Louis Xidis, R. T. Atanososki, B. B. Owens,* and *W. H. Smyrl,* Corrosion Res. Cntr., Dept. of Chem. Engr. and Material Sci., Univ. of Minnesota, Minneapolis, MN 55455

V_6O_{13} is considered a most promising candidate for the cathode material in high energy density rechargeable lithium batteries. V_6O_{13} has the advantages of a high cell voltage *vs.* lithium and also the ability to insert many lithium ions per unit weight ($x = 8$ at full discharge in $Li_xV_6O_{13}$). The present investigation is directed toward the relationship between performance and the morphology of nonstoichiometric V_6O_{13} (V_6O_{13+y}) cathodes to determine optimum structure.

27 Lithium Insertion Vanadium Pentoxide Xerogel Cathodes: *R. T. Atanasoski, B. B. Owens, H.-K. Park,* and *W. H. Smyrl,* Corrosion Res. Cntr., Dept. of Chem. Eng. & Mat. Sci., Univ. of Minnesota, Minneapolis, MN 55455

Vanadium pentoxide xerogels have shown promising electrochemical properties as a rechargeable Li^+ insertion cathode. The Li/V_2O_5 xerogel system has a high open-circuit potential and is reversible. The material can be readily processed in the form of thin films suitable for large-scale industrial fabrication. With future applications in mind, our aim is to assess the relationship between the specific energy and power of the $Li_xV_2O_5$XRG films produced by spin-coating technique.

Wednesday PM

28 Voltage Variation with Temperature for $Li/SOCl_2$ & Li/MnO_2 Cells Using a Nonsteady State Method: *M. L. Kronenberg,* and *N. C. Liberto,* MSA, Sparks, MD 21152

In view of the interest in the electrochemical behavior of metal hydrides a $Pd_{0.85}Ni_{0.15}$ wire electrode was prepared and activated by a Pd surface layer deposited electrochemically. The hydriding and dehydriding behavior of the electrode was characterized by cyclic voltammetry. The discharge kinetics of $\beta Pd_{0.85}Ni_{0.15}H_x$ were determined. The contribution of the βPdH_x phase was quantitatively accounted for. At high driving forces (E = 300-400 mV) the primary rate limiting process was concluded to be diffusion of the H atom in the bulk electrode. (This work was supported under U.S. DOE contract No. DE-AC02-76CH00016.)

44 Nonstoichiometric Hydride-Forming AB_5 Battery Materials: *R. E. F. Einerhand* and *P. H. L. Notten,* Philips Research Laboratories, 5600 JA Eindhoven, The Netherlands

Nonstoichiometric hydride-forming compounds with the $CaCu_5$ crystal lattice structure can be obtained by annealing of $LaNi_5Cu$. An increasing degree of nonstoichiometry is observed with increasing annealing temperature. Materials combining excellent long-term cycling stability and fast hydrogen reaction kinetics are obtained. Partial replacement of lanthanum by copper-containing dumbbell pairs is crucial to obtain these characteristics.

45 Rechargeable Batteries with Amorphous *NiZr* Hydride Electrodes: *M. Ciureanu, J. O. Strom-Olsen, D. H. Ryan, P. Rudkowski,* and *G. Rudkowska,* Dept. of Physics, McGill University, Montreal, PQ, Canada H3A 2T8

Rapidly quenched *NiZr* alloys have been used as anodes in Ni/hydride batteries in two morphological forms: ribbons, obtained by melt spinning, and fibers, obtained by melt extraction. The main battery characteristics—hydrogen storage capacity, cycle life, rate capability, self-discharge rate—are presented. Differences between the two types of anodes are emphasized and discussed. The parallel decay of charge retention and open-cell potential with storage time are discussed in terms of the site-distribution theory for hydrogen storage in amorphous alloys.

46 Sn-Modified AB_5-Type Alloys Prepared by Mechanical Alloying and Arc-Melting Methods for Hydride Electrodes: *K. M. Petrov, A. A. Rostami, A. Visintin,* and *S. Srinivasan,* Cntr. for Electrochem. Sys. and Hydrogen Res., Texas A&M Univ., College Station, TX 77843, *J. J. Reilly, J. R. Jonson,* Dept. of Applied Science, BNL, Upton, NY 11973, and *R. B. Schwarz* and *P. B. Desch,* Cntr. for Mat. Sci., LANL, Los Alamos, NM 87545

The arc-melting and mechanical alloying (MA) were used to prepare hydrogen storage alloy materials, based on the AB_5 system. Materials prepared by both techniques are compared here with respect to: (*i*) structure and phase identity of the alloy samples, characterized by x-ray diffraction, (*ii*) gas-phase hydrogen absorption/desorption capabilities of the alloy; and (*iii*) electrochemical characteristics, such as capacity, rate capability, capacity retention, and cycle life. The results show the significant similarities of the gas-phase and electrochemical characteristics of the alloys prepared by the two methods.

47 Optimization of Structure and Composition of Metal-Hydride Electrodes, using Sn-Modified AB_5-Type Alloys: *K. M. Petrov, S. Srinivasan, A. A. Rostami, A. Visintin,* and *A. J. Appleby,* Cntr. for Electrochem. Sys. and Hydrogen Res., Texas A&M Univ. College Station, TX 77843-3402

We report on the development of metal hydride electrodes, using Sn-modified AB_5 type alloy, for Ni/MH_x batteries. To optimize the composition (active material and additive) and structure of metal hydride electrode, additives, such as Teflonized carbons (Vulcan-XC-72, Norit-NK, etc.), acetylene black (XC-35), and copper were evaluated. The increase in electrode parameters with active carbons was attributed to the flexible 3D networks with an intimate and a stable contact between the active alloy particles as well as the reduction of some oxidized alloy particles by the active carbon.

48 Surface Composition of a Misch-Metal Based AB_5 Compound: *M. E. Fiorino, K. Konstadinidis, R. Opila,* and *W. C. Fang,* AT&T Bell Labs., Murray Hill, NJ

The surface composition of a prototypical AB_5 compound, $MmNi_{3.5}Al_{0.8}Co_{0.7}$, has been studied in detail after cycling using x-ray photoelectron spectroscopy. Although the surface film, which contains oxidized lanthanum, cerium, and magnesium, is complex, as is the substrate from which it is formed, no obvious correlation exists between film compopsition and substrate stability. The rate capability of this material can be attributed to the presence of not only metallic nickel but also metallic cobalt.

49 A High Energy Density Ni-MH Battery Using a Pasted Type Nickel Electrode and a MmNiAlCo Alloy Electrode: *M. Ohnishi, Y. Matsumura, M. Kuzuhara, M. Watada,* and *M. Oshitani,* Yuasa Corp., Central Lab., Takatuki, Osaka, 569, Japan

A high energy density Ni-MH battery has been developed. The capacity of the metal hydride electrode has been increased from the previous version by using MmNiAlCo alloy whose contents of rare-earth elements are optimized. The surface of the alloy after cycling was investigated by TEM and SIMS analysis. The energy density of the nickel electrode has been increased from the previous version by using Cd-free high density nickel hydroxide powder.

50 Preparation and Electrochemical Characterization of Amorphous $LaNi_x$ Thin Film Electrodes: *Y. T. Cheng, Y. Li,* and *M. A. Habib,* Dept. of Phys. Chem., GM NAO R&D Cntr., Warren, MI 48090-9055

Amorphous $LaNi_x$ ($1 \leq x \leq 5.5$) thin films have been fabricated by electron-beam evaporation in a UHV system and characterized by electrochemical cycling. The maximum reversible hydrogen storage capacity is about 165 mAh/g for films over a wide range of composition ($3 \leq x \leq 5.5$) and thickness. The 500 Å thick films can be cycled up to 500 cycles before their discharge capacity decreases to half of the maximum value, while 6000 Å thick films can last for more than 2000 cycles.

51 Impedance Analysis of Boiler-Plate Ni/H_2 Cells as a Function of Electrolyte Concentration, Dept. of Discharge, and Cycle History. I. Experimental Setup and Initial Results: *S. M. Lipka,* Dept. of Ocean Engineering, Florida Atlantic Univ., Boca Raton, FL 33431 and *M. A. Reid,* NASA Lewis Research Center, Cleveland, OH 44135

Electrochemical impedance was obtained on boiler-plate Ni/H_2 cells as a function of depth of discharge, discharge rate, and electrolyte concentration (26 and 31% KOH). The cells were cycled for about 100 cycles under a 40% low earth orbit regime prior to obtaining impedance spectra. Details of the experimental methodology are presented.

52 Impedance Analysis of Boiler-Plate Ni/H_2 Cells as a Function of Electrolyte Concentration, Depth of Discharge, and Cycle History: II. Results of Long-Term Cycling: *M. A. Reid,* NASA Lewis Research Center, Cleveland, OH 44135 and *S. M. Lipka,* Florida Atlantic Univ., Boca Raton, FL 33431

Two boiler-plate Ni/H_2 cells were cycled in a 40% low earth orbit (LEO) regime, one using 26% KOH, the other with 31% KOH. Impedance measurements showed no difference until 3000 cycles, when at high depths of discharge, the kinetic resistances of the 31% cell became much larger than that of the 26% KOH cell. This result is consistent with other findings that cells with 31% KOH have shorter lifetimes than cells with 26% KOH. Cycling has reached 4500 cycles and is continuing.

53 Characterization and Comparison of New and Cycled Ni/H_2 Cells Using Electrochemical Impedance Spectroscopy: *K. S. Nechev* and *S. M. Lipka,* Dept. of Ocean Engineering, Florida Atlantic Univ., Boca Raton, FL 33431

Impedance measurements were made on boiler-plate nickel-hydrogen cells containing new and cycled nickel electrodes. A model was developed and experimental data was fit to an equivalent electrical circuit. Various electrochemical parameters (*e.g.,* faradaic capacitance and resistance, adsorption capacitance and resistance, and diffusional characteristics) of the nickel-hydrogen battery were studied as a function of depth of discharge, discharge rate, and electrolyte concentration.

54 Self-Discharge in the Nickel-Hydrogen Cell: *A. H. Zimmerman,* and *M. V. Quinzio,* The Aerospace Corp., Los Angeles, CA 90009

The mechanisms which have been proposed to account for the high self-discharge rate of the nickel-hydrogen cell have been reviewed. The data support a real contribution of three mechanisms to the overall self-discharge rate in this cell. These three processes are: oxygen evolution and recombination, direct chemical reaction, and a proton-mediated electrocatalytic process. Experiments have indicated that each of these processes can contribute significantly to the overall self-discharge, at rates depending on state of charge, hydrogen pressure, and cell operating temperature.

55 Advanced Nickel-Hydrogen Battery Design Concepts for Spacecraft Power System Applications: *D. K. Coates, P. S. Hoofnagle,* and *C. L. Fox,* Eagle-Picher Industries, Inc., Advanced Systems Operation, Joplin, MO 64802

Advanced nickel-hydrogen cell and battery designs are being manufactured and tested for spacecraft power system applications. These advanced design concepts have been developed in response to the higher power level requirements of the Space Station Freedom, large communications satellites, Strategic Defense space platforms, and other high power, space-based applications. The designs include common pressure vessel (CPV), single pressure vessel (SPV), and dependent pressure vessel (DPV) technology.

56 Inelastic Neutron Scattering Studies of Active Material from Discharged Ni Positive Plates: *J. Eckert, LANSCE,* Los Alamos National Lab., Los Alamos, NM 87545, *R. Varma,* Los Alamos Technol. Office/Rocky Flats, Golden, CO 80401-0013, *L. Diebolt,* Dept. of Chem., Arizona State Univ., Tempe, AZ 85281, and *M. Reid,* NASA Lewis Res. Cntr, Cleveland, OH 44135

We have carried out vibrational spectroscopic studies by inelastic neutron scattering (INS) on several samples of nickel hydroxide from cycled battery plate materials as well as β-$Ni(OH)_2$ to determine the form and importance of excess protons in the lattice on the battery activity. All plate material was predominantly β-phase as expected, but several vibrational bands could be identified with the presence of varying amounts of α-phase $Ni(OH)_2$. Some additional features in the vibrational spectra could be attributed to lattice-incorproated water molecules, and these appear related to the cycling history of the battery.

57 Investigation of the Origin of Nickel Electrode Fading: *S. I. Joles, L. Sokolov,* and *B. C. Cornilsen,* Dept. of Chemistry, Michigan Technological Univ., Houghton, MI 49931

Faded electrodes from Ni/H_2 boilerplate test cells have been characterized using x-ray diffraction, Raman, and photoacoustic-FTIR spectroscopy, with the objective of identifying phases present which contribute to fading. A nickel electrode can lose capacity, *i.e.,* fade, on prolonged standing in KOH electrolyte. Identification of phases which may cause fading is critical to understanding and eliminating this loss of capacity. The results reported here show, for the first time, a correlation between β-nickel hydroxide content, hydrogen percharge, and battery failure.

58 Performance Enhancement of the Nickel Foam Electrode: *J. Babjak, V. A. Ettel, M. A. Mosoiu,* and *P. Kalal,* INCO Ltd., Sheridan Park, Mississauga, Ont. L5K 1Z9, Canada

The discharge capacity of ~190 mAh/g of the electrode mass or up to 680 mAh/cm^3 of the electrode volume has been attained with an electrode fabricated from INCO extrafine nickel foam substrate (cell diam ~350 μm)

neering Div., Univ. of Medicine and Dentistry of New Jersey-Robert Wood Johnson Medical School, Piscataway, NJ 08854

The classical method of determining pore structure of battery electrodes, bone, and other porous objects is by infusion of mercury under high pressure. A new method developed at the Frumkin Institute of Electrochemistry in Moscow is based on determining the distribution of a wetting liquid between the test sample and a standard sample with a known pore size distribution curve. We compare data taken by mercury porosimetry and the new method. The elimination of mercury makes the determination of pore structure more environmentally benign and also eliminates the problem of amalgamation with mercury of those electrodes which alloy.

71 Krypton *vs.* Nitrogen in Surface Area Measurements of Silver-Zinc Battery Plates: *V. L. Hammersley,* Crane Div., Naval Surface Warfare Center, Crane, IN 47522-5001

The determination of surface area of whole battery plates was performed using two different gases as the adsorbate. A comparison of results was made using krypton and nitrogen on the same silver oxide cathodes and zinc anodes. Low surface area samples require krypton. A relationship was determined between nitrogen and krypton in order to report previous nitrogen surface area data in terms of krypton.

72 Rechargeability of $Ag/RbAg_4I_5/Me_4NI_5$ Solid State Batteries: *M. Morita,* Dept. of Applied Chemistry & Chemical Engineering, Yamaguchi University, Tokiwadai, Ube 755, Japan, *R. Atanasoski* and *B. B. Owens,* Corrosion Res. Center, Dept. of Chemical Engineering and Materials Science, Univ. of Minnesota, Minneapolis, MN 55455

Silver solid-state primary cells based on the solid electrolyte $RbAg_4I_5$ and tetramethylammonium polyiodide cathodes were developed 20 years ago. These cells are capable of long-life operation as primary batteries. By use of careful charge control, it is possible to reform the polyiodide complex in the Ag/Me_4NI_5 system. Reversible behavior is indicated for shallow cycling at intermediate depths of discharge.

73 Implications of Fuel Crossover in Direct Methanol Fuel Cells: *S. R. Narayanan, E. Vamos, S. Surampudi, H. Frank,* and *G. Halpert,* Jet Propulsion Lab., Pasadena, CA 91109

The consequences of fuel crossover to the cathode have been examined in a new liquid-feed type direct methanol fuel cell developed at JPL. All the methanol crossing over to the cathode is completely oxidized to carbon dioxide. The rate of evolution of carbon dioxide has been used to determine the crossover rate and a crossover parameter characteristic of the membrane-electrode assembly. The rate of crossover increases with increasing fuel concentration and temperature. While higher fuel concentrations favor the kinetics of methanol oxidation, the increased crossover lowers the cell voltage. The effect of crossover on the utilization of methanol is discussed.

74 The Development of Pt-Ru Catalyzed Activated Charcoal Electrodes for the Direct Oxidation of Methanol in an Alkaline Methanol-Air Fuel Cell: *G. A. Pathanjali* and *R. F. Chireau,* High Energy Batteries (India) Ltd., R&D Laboratories, Mathur 622 515, Inida

Our objective is to develop porous electrodes using Pt-Ru bimetal catalyzed high-surface-area activated charcoal substrate, as anodes, for the electrochemical oxidation of methanol. These electrodes are intended for use in direct-feed liquid methanol fuel cells. A study was made of the effect of methanol concentration, electrolyte (KOH) concentration, and temperature of the anolyte, on the behavior of these electrodes during anodic and cathodic polarization. The results of electrode evaluation show that these electrodes are effective and show promise for use as anodes for the electrochemical oxidation of methanol in alkaline methanol-air fuel cells.

75 Charge-Discharge Characteristics of Activated Carbon/Carbon Composite Electrodes for Electric Double-Layer Capacitor: *Y. Kibi* and *J. Tabuchi,* NEC Corp., Fundamental Res. Labs., Miyamae-ku, Kawasaki 216, Japan, *T. Saito,* NEC Corp., Circuit Component Div., 1120 Shimokuzawa, Sagamihara 229 Japan, and *A. Ochi,* NEC Corp., Fundamental Res. Labs., Miyamae-ku, Kawasaki 216, Japan

Charge-discharge characteristics of AC/C composite electrodes for electric double-layer capacitors (EDLCs) have been improved. The size and total volume of open pores in the electrodes can be controlled by burning out polymer spheres. The ac impedance and the dc capacitance indicate that the electrodes using polymer spheres can follow rapid charge-discharge. The EDLCs with these AC/C composite electrodes are promising for use in a new supplementary power source.

CORROSION AND CORROSION PREVENTION IN SEAWATER ENVIRONMENTS

Corrosion

Tuesday AM

76 Analysis of Solutions in Crevices: Alloy C276 and Inconel 625 in Natural Seawater: *F. D. Bogar, E. McCafferty,* and *P. M. Natishan,* Naval Research Lab., Washington, DC 20375-5343 and *E. D. Thomas,* Naval Research Laboratory, Key West, FL 33041-1739

The chemistry of solutions contained within modeled and real crevices on Inconel 625 and alloy C276 in chloride environments, including natural seawater, were determined by thin-layer chromatography (TLC). X-ray photoelectron spectroscopy was used to determine the surface compositions of samples before and after crevice corrosion. The bulk composition of the alloy, the solubilities of the reaction products, and the formation of nonprotective films determined the pH and chemistry of the crevice solutions.

77 Modeling the Factors Contributing to the Initiation and Propagation of the Crevice Corrosion of Alloy 625: *R. S. Lillard* and *J. R. Scully,* Ctr. for Electrochem. Sci. and Eng., Dept. of Mat. Sci. and Eng., Univ. of Virginia, Charlottesville, VA 22903

The initiation and propagation of crevice corrosion of alloy 625 in both chlorinated and nonchlorinated ASTM artifical seawater has been investigated. Remote crevice assembly experiments demonstrate that the galvanic couple potential must be shifted sufficiently positive to initiate crevice corrosion in this alloy. The couple potential in nonchlorinated ASTM artificial seawater may not increase sufficiently in a 30 day period. This shift in potential can be achieved by the addition of chlorination. The origins of these observations are examined with computer modeling of current and potential distributions in model crevices and mass transport calculations.

78 Evaluation of Calcium Silicate and Calcium Aluminate Concretes for Internal Pipeline Protection: *R. G. Buchheit, T. E. Hinkebein,* and *P. F. Hlava,* Sandia National Labs., Albuquerque NM 87185 and *D. G. Melton,* La Que Center for Corrosion Technology, Inc., Wrightsville Beach, NC 28480

A variety of industrial-standard and experimental concretes are being evaluated for use in brine disposal pipelines operated by the U.S. Strategic Petroleum Reserve (SPR). This paper reports on interim performance results from on-going studies involving an American Petroleum Institute (API) standard calcium silicate-based (CS) concrete and a commercially available calcium aluminate-based (CA) concrete. Samples exposed to nonflowing SPR brine in the field were returned to the laboratory at regular intervals for analysis. Electron probe microanalysis (EPMA) determined the dept of brine penetration and the amount of concrete deterioration. Corrosion occurring at steel pipe/concrete interfaces during exposure to simulated brine has been studied on laboratory-constructed specimens using electrochemical impedance spectroscopy (EIS).

79 Characterization of Polyester Powder Coatings on Steel Substrates by Electrochemical Impedance Spectroscopy: *E. Potvin* and *L. Brossard,* Institut de Recherche de Hydro-Québec, Varennes, Qué, Canada J3X 1S1

Polyester powder coatings are considered to prevent corrosion of electrical equipment in contact with the atmosphere. Painted panels of mild steel and stainless steel were exposed to different aggressive environments to test their performance by using electrochemical impedance spectroscopy (EIS). The main parameters under consideration were the formulation of the coatings and the coating thickness. The EIS technique is a powerful tool for investigating the behavior of such coatings.

80 Corrosion Monitoring in Salt Water Using Electrochemical Noise Analysis: *F. Mansfeld, H. Xiao,* and *L.-T. Han,* Corrosion and Environmental Effects Lab. (CEEL), Dept. of Materials Science and Engineering, University of Southern California, Los Angeles, CA 90089-0241

Electrochemical noise analysis (ENA) has been evaluated as a tool for corrosion monitoring in salt water. Iron in NaCl solutions which were aerated, deaerated, or aerated with $NaNO_2$ added as inhibitor was used as a model system. Potential and current noise data were obtained at the beginning of each hour for a 24-h period. Statistical and spectral analyses were performed resulting in noise resistance values. For the noise resistance $R_n = \delta V/\delta I$, where δV and δI are the rms values of potential and current, respectively, similar values as for the polarization resistance R_p obtained with electrical impedance spectroscopy (EIS) at the end of the test were obtained. The spectral noise resistance R_{sn} obtained from spectral analysis of ENA had values similar to R_n. These concepts have been applied to corrosion monitoring of iron with different surface pretreatments exposed to dilute abiotic and biotic solutions. (This project has been funded by Montana State University under subcontract No. 2914350-1).

81 Assessment of the Protective Properties of Marine Coatings by Electrochemical Noise Techniques: *G. P. Bierwagen* and *D. J. Mills,* Dept. of Polymers and Coatings, North Dakota State University, Fargo, ND 58102, *D. E. Tallman,* Dept. of Chemistry, NDSU, Fargo, ND 58105, and *B. S. Skerry,* The Sherwin-Williams Co., Cleveland Technical Center, Cleveland, OH 44113

Monitoring the electrochemical noise (ECN), the spontaneous potential and current fluctuations developed between paris of painted metal surfaces immersed in electrolyte, affords one insight into the corrosion protection afforded by the paints. Corrlations between ECN parameters for painted panels and the lifetimes in seawater provided by experimental marine paints are presented. Total marine paints systems consists of grit-blasted steel + multiple primer layers + topcoat. Performance data for similar systems exposed to more conventional accelerated corrosion test methods are also presented.

82 Electrochemical Impedance Spectroscopy as a Tool to Evaluate Degradative Processes in AS4/Nylon 6 Composites Nondestructively: *J. F. McIntyre, S. M. Lipka,* and *R. Haniyur,* Dept. of Ocean Engineering, Florida Atlantic Univ., Boca Raton, FL 33431

Electrochemical impedance spectroscopy was used to characterize moisture absorption in a carbon-reinforced nylon composite exposed to aqueous chloride solution at ambient and high pressures. Electrochemical impedance spectroscopy was able to distinguish a well-consolidated composite from a poorly consolidated composite. The carbon-nylon composite exhibited porous electrode behavior after one day of immersion at both ambient and high pressures. High pressure accelerated porous electrode development by forcing electrolyte into the composite. Electrochemical impedance spectroscopy was used to follow progressive damage that was induced electrochemically.

96 Role of Copper on Corrosion Behavior of Hydrotalcite-Coated Al Alloys: *C. A. Drewien, K. R. Zavadil,* and *R. G. Buchheit,* Sandia National Lab., Albuquerque, NM 87185

Aluminum alloys coated with hydrotalcite pass salt-spray tests if copper is not present in the alloy; alloys containing copper suffer severe pitting and general corrosion. The presence of copper in the alloy leads to copper surface enrichment during standard surface pretreatment operations. In particular, deposition of copper onto the aluminum alloy surface occurs in the nitric acid deoxidation bath. Copper influences the corrosion behavior of aluminum in nitric acid solutions, and copper incorporates itself into the coating, possibly reducing the formation and growth of hydrotalcite on copper-containing aluminum alloys.

97 Adsorption of Water on Gold Surface: *S. Lee, R. W. Staehle,* and *W. H. Smyrl,* Corrosion Res. Cntr, Univ. of Minnesota, Minneapolis, MN 55455

In atmospheric corrosion of nuclear waste canister materials, such as copper, nickel, and iron, relative humidity has an important role as a rate-controlling factor. Gold, unlike other metals, does not form any known surface oxides under practical atmospheric corrosion environments and retains its surface characteristics throughout adsorption experiments. This trait enabled us to study only the adsorption of water without any surface change due to oxidation or roughening. The quartz crystal microbalance (QCM) technique was used to measure the adsorption of water on a gold surface with RH ranging from 0 to 100% at 7, 20, 45, 70, and 90°C. The adsorption isotherms can be explained well by the slab theory of Frankel, Halsey, and Hill (FHH) at 7 and 20°C. At higher temperatures, however, the data points deviate significantly from the FHH model at intermediate and high RH regions and the FHH model must be refined.

98 *In Situ* Neutron Reflectometry Study of Titanium Anodization: *D. G. Wiesler* and *C. F. Majkrzak,* NIST, Gaithersburg, MD 20899

The growth of anodic oxide on Ti has been studied by neutron reflectometry *in situ*, during formation in dilute (0.1*N*) H_2SO_4. Neutron reflectometry measures a weighted density profile of a flat sample as a function of depth over a range of ~2 to 200 nm. We use these profiles to track the evolution of anodized Ti as a function of time and anodizing potential. We find that the oxide has a density midway between anatase and rutile, and that the oxide thickness at a rate of 1.5 nm/V.

99 Anodic Oxidation of Iron in Alkaline Solutions: *H. Zhang* and *S-M. Park,* Dept. of Chemistry, Univ. of New Mexico, Albuquerque, NM 87131

The anodic oxidation of iron has been studied in alkaline media by using cyclic voltammetric, rotating ring-disk electrode, and *in situ* spectroelectrochemical techniques. While four anodic and cathodic cyclic voltammetric peaks (CV) may be observed at times, three cathodic CV peaks are observed for four anodic peaks under usual experimental conditions. Results obtained from these studies are consistent with the conclusion that iron is oxidized to: Fe(II) at the least positive anodic CV peak, Fe_3O_4 at the second peak, δ-FeOOH at the third peak, and Fe_3O_4 at the most positive anodic peak below the δ-FeOOH layer. Corresponding cathodic CV peaks were identified for all these anodic processes but not for the most positive one. Evidence supporting the conclusion and detailed mechanisms for the iron oxidation is presented.

100 Mechanism of Atmospheric Corrosion of Copper in the Presence of Submicron Ammonium Sulfate Particles: *R. E. Lobnig, R. P. Frankenthal, D. J. Siconolfi,* and *J. D. Sinclair,* AT&T Bell Laboratories, Murray Hill, NJ 07974-0636

The corrosion of copper contaminated with submicron-sized particle of $(NH_4)_2SO_4$ has been studied in air-H_2O gas mixture at 300 and 373 K and relative humidities below, at and above the critical relative humidity (CRH) of $(NH_4)_2SO_4$ by SEM, x-ray diffraction, scanning Kelvin probe, and IR spectroscopy. Below the CRH, the particles do not affect the oxidation of copper. At and above the CRH, initially Cu_2O forms. Over the oxide, one of the basic copper sulfates—brochantite, antlerite or langtite—grows, depending on the amount of $(NH_4)_2SO_4$ deposited and the temperature. The corrosion mechanism is discussed.

Wednesday PM

101 The Effect of Sulfur on the Corrosion of Iron in Calcium Nitrate: *C. F. Windisch, Jr., D. R. Baer, M. H. Engelhard,* and *T. F. Soran,* Pacific Northwest Laboratory, Richland, WA 99352

Grain boundary impurities influence IGSCC of metals including Fe; however, in most cases, the mechanisms for the corrosion processes and, in particular, the role the impurities play in these mechanisms are not completely known. Toward an understanding of these mechanisms, studies were conducted to determine the effect of S on the corrosion of Fe in $Ca(NO_3)_2$ solutions at 60°C. Electrochemical polarization experiments in conjunction with surface analyses employing ultrahigh vacuum transfer showed that S, when above a threshold amount, accelerated the corrosion of Fe when polarized at passive potentials. In addition, the corrosion rate was zeroth order with respect to S; a relatively large fraction of the S was incorporated in the corrosion product film and remained in the film in a reduced state; the corroson film was thicker when more S was present in the metal; and the concentration of S in the film was also greater for thicker films.

102 Electrochemical Studies of Orthopaedic Implant Alloys and Their Metallic Constituents: *P. Kovacs,* Orthopaedic Research Dept., Smith & Newphew Richards Inc., Memphis, TN 38116

To provide a coherent treatment of major performance issues associated with the use of metalic materials in the human body, the spontaneous passivation of various orthopaedic implant alloys, and their metallic alloying elements was studied by EIS and potentiodynamic polarization. The results obtained in lactated Ringer's solution at 37°C are in complete agreement with *in vivo* test results from the literature, and demonstrate the superior electrochemical behavior of Ti, Zr, Nb, and Ta, as well as that of Ti-13Nb-13Zr, a new alloy developed for biomedical implant applications. The superior electrochemical behavior and biocompatibility of these metals and the new titanium alloy can be directly attributed to the excellent protective ability and extremely low solubility of oxides and hydroxides formed.

103 Distributions of Microstructural Sensitization Levels in AISI 304 Stainless Steel and Its Influence on Intergranular Stress Corrosion Cracking: *M. A. Gaudett* and *J. R. Scully,* Cntr. for Electrochem. Sci. and Eng., Dept. of Mat. Sci. and Eng., Univ. of Virginia, Charlottesville, VA 22903-2442

Distributions in grain boundary Cr depletion levels were characterized for 304SS after various sensitizing heat-treatments. The IGSCC susceptibility of 304SS was then examined at the same sensitization levels in a 0.5*M* H_2SO_4 + 0.01*M* KSCN solution. An abrupt decrease in IGSCC cracking resistance was observed when greater than 23% of the grain boundaries were active. A well-connected intergranular fracture path was observed under these conditions. Interpreting these findings in the context of bond percolation theory, they are consistent with the presence of a one-dimensional percolation threshold for IGSCC.

104 Electrode Kinetics of Pit Initiation on Aluminum: *E. McCafferty,* Naval Research Lab., Washington, DC 20375

A mathematical model for pit initiation is described which takes into account adsorption of chloride ions on the oxide surface, penetration through the oxide film, and interaction with the underlying substrate. Two differnt mechanisms for chloride transport through the oxide film are considered: transport by means of oxygen vacancies and penetration via water channels. Mathematical expressions are derived which correctly describe: (*i*) the variation in pitting potential with chloride ion concentration at constant pH, and (*ii*) the variation in pitting potential with pH at constant chloride ion concentration.

105 A Microelectrode Sensor for Surface Monitoring and Dynamics of Electrode Reactions: *A. Brodsky, L. Burgess,* and *W. Reinhardt,* Dept. of Chemistry, University of Washington, Seattle, WA 98195

The practical use of microelectrode sensors is still in a preliminary state because of stability problems and the lack of a firm theory base for interpretation of corresponding signals. We propose construction of a stable to the external perturbations sensor, which is a sensor consisting of a generator microelectrode in the form of a narrow strip with macroscopic length placed on the surface of the macroscopic collector, metallic or semiconductor, electrode. The exact solution of the corresponding diffusion problem is given. Such a sensor should allow the measurement of rapid electrode reaction characteristics.

106 Influence of Fluoride Ion on Corrosion of Steels in H_2SO_4 or CH_3COOH Solutions Containing KF: *I. Sekine, H. Usui, S. Kitagawa,* and *M. Yuasa,* Dept. of Industrial Chemistry, Science University of Tokyo, 2641 Yamazaki, Noda, Chiba 278, Japan, *L. Silao,* Chemical Engineering Dept., De La Salle University, Manila, Philippines

Corrosion behavior of mild steel (SS 400) and stainless steels (types 430 and 304) in H_2SO_4 or CH_3COOH solution containing KF was investigated. The corrosion rate of SS 400 in KF-H_2SO_4 solution decreased with KF. SS 400 and type 430 were corroded in KF-CH_3COOH solutions. In higher concentration of KF, these corrosion rates decreased. This is due to decrease H^+ in acid. Type 304 was scarcely corroded in KF-CH_3COOH solutions because of a formation of stable passive film.

107 *In Situ* Spectroelectrochemical Studies on Corrosion of Brass Electrodes in Alkaline Solutions: *S. N. Hoier,* Sandia National Lab., Albuquerque, NM 87185 and *B.-S. Kim* and *S.-M. Park,* Dept. of Chemistry, Univ., of New Mexico, Albuquerque, NM 87131

Corrosion behavior of brass electrodes has been studied in alkaline solutions with cyclic voltammetric (CV) and *in situ* spectroelectrochemical experiments. Results obtained from CV experiments show that there are four anodic and three cathodic processes. It is shown by spectroelectrochemical experiments that two anodic CV peaks at the more negative potentials result from the oxidation of zinc while two other peaks arise from the copper oxidation. The Cu(II)-oxide/hydroxide generated at the most positive anodic CV peak oxidizes Zn effectively, resulting in protection of copper. Of the three cathodic peaks, the most positive one results from the reduction of Cu(I)-oxide/hydroxide, while the other two peaks are from the zinc reduction.

108 Polyamino-benzoquinone(PAQ) Polymers: A New Class of Corrosion Inhibitors for Mild Steel: *K. L. N. Phani, S. Pitchumani, S. Muralidharan, S. Ravichandran,* and *S. V. K. Iyer,* Central Electrochemical Research Institute, Karaikudi 623 006, India

A new polymer, namely polyamino-benzoquinone (PAQ) synthesized electrochemically has been found to be an excellent corrosion inhibitor for mild steel in 1*N* H_2SO_4. The corrosion inhibitive action of the polymer has been assessed by weight loss method, polarization technique, hydrogen permeation measurements and ac impedance spectra which show that the synthesized polymer provides corrosion inhibition efficiency of >90% and this is achievable by the use of minimal amount of polymer, *i.e.*, 300 ppm. The mechanism of corrosion inhibitive action of the polymer is found to be through a formation of protective film with time.

109 Studies on the Corrosion Behavior of Mild Steel in Acidic Solutions in the Presence of Chelating Agents: *S. Muralidharan* and *S. V. K. Iyer,* CECRI, Radioelectrochemistry Lab., Karaikudi 623 006, India, and *M. A. Quraishi,* Dept. of Applied Chemistry, Z. H. College of Engineering Technology, Aligarh Muslim Univ., Aligarh, India

Monday PM

123 128 × 128 GaAs/AlGaAs Multiple Quantum Well Infrared Focal Plane Array: Demonstration of Background-Limited Sensitivity at 35 Kelvin: *L. J. Kozlowski, G. M. Williams,* and *R. E. DeWames,* Rockwell International Science Center, Thousand Oaks, CA 91360

We report the first demonstration at low operating background of background-limited infrared photodetctor (BLIP) long wavelength infrared (LWIR) sensitivity with ~9 μm starting GaAs/AlGaAs multiple quantum well focal plane arrays (FPA). A mean D^* of 4.51×10^{13} cm-Hz$^{1/2}$/W was obtained at 35 K and 1.2×10^{10} photon/cm^2-s background on a 128 × 128 FPA with gate modulation readout. The sensitivity corresponds to 75% of BLIP for the measured effective quantum efficiency of ~1%.

124 Long Wavelength Infrared Imaging Using Miniband Transport Multiple Quantum Well Infrared Detectors: *W. A. Beck, J. W. Little, A. C. Goldberg,* and *T. S. Faska,* Martin Marietta Lab., Baltimore, MD 21227

We will show 128 × 128 long wavelength infrared (LWIR) imagery using miniband transport (MBT) GaAs/AlGaAs multiple quantum well (MQW) detectors. Laboratory measurements indicate that the best MBT MQW focal plane arrays (FPA)s have a temporal noise equivalent temperature difference (NETD) of 15 mK and a fixed pattern NETD of 30 mK (for a 10°C calibration interval) when operated at 60 K in an f/2 camera system. The videotape contains night imagery of people, cars, airplanes, and a moving M-48 tank.

125 Very Long Wavelength Intersubband Infrared Hot Electron Transistor: *S. D. Gunapala,* JPL, CIT, Pasadena, CA 91109

Very long wavelength infrared (IR) detectors and imaging systems are required in many space applications such as atmospheric IR sounder (AIRS) and tropospheric emission spectrometer (TES) instruments, which will be used in NASAs Earth Observation System (EOS). The wavelength of the infrared radiation required in these applications range from 3 to 16 μm. We present here the results of a 16 μm infrared hot electron transistor, which may meet the AIRSs very long wavelength IR detector requirements.

126 N- and P-Type AlGaAs/GaAs Superlattice Infrared Detector Structures: Interplay of Design, Materials and Characterization Issues: *A. Majerfeld, E. Mao, B. W. Kim, Z. H. Lu, E. G. Oh, T. McCormick,* and *S. A. Dickey,* Dept. of Electrical and Computer Engineering, Univ. of Colorado, Boulder, CO 80309-0425

We address some of the intricate interplay between theoretical design requirements, epitaxial growth and materials limitations, and the characterization of key structural, electrical, and optical parameters of AlGaAs/GaAs multiquantum-well (MQW) and superlattice (SL) structures for 10 μm infrared photodetectors (IRPD). The possibility of normal incidence operation for p-type IRPDs makes it necessary to consider both n- and p-type MQW and SL structures. The results of a rigorous theoretical analysis of p-type SLs is presented, which indicates that it should be possible to obtain large absorption coefficients for 10 μm normal incident light.

127 Normal Incidence Detection Using AlAs/AlGaAs Quantum Wells: *J. E. Scheihing,* and *M. A. Dodd,* Wright Lab., Solid State Electronics Directorate, WPAFB, OH 45433, and *G. J. Sullivan, C. W. Farley,* and *R. W. Grant,* Rockwell Science Cntr., Thousand Oaks, CA 91358

AlGaAs/AlAs quantum well detector structures were grown on (111)B GaAs substrates and fabricated into 100 μm^2 detectors. These detectors are sensitive to normally incident radiation without the need for a grating due to the anisotropic nature of the effective mass tensor. Measurements are performed on these samples and performance comparisons are made to conventional grating-coupled GaAs/AlGaAs quantum well detectors.

128 Normal Incidence p-Type InGaAs/InGaAlAs Strained Quantum Well Infrared Photodetectors: *C. Lee, W. Zhou, K. K. Choi, W. Chang,* Army Research Lab.-EPSD, Fort Monmoutn, NJ 07703, *L. F. Eastman,* Cornell Univ., Ithaca, NY 14850, *N. J. Sauer* and *T. Y. Chang,* AT&T Bell Lab., Holmdel, NJ 07733

We have designed, fabricated, and investigated a new normal incidence, InP-based, p-type, InGaAs/InGaAlAs, tensile-strain, multiple quantum well three terminals, infrared photodetector. This detector uses hole intersubband absorption from a nearly degenerate first light and heavy hole subbands to be extended (unconfined) states, to enhance the absorption of the normal incident light. Preliminary results yield a responsivity of $R = 7 \times 10^{-4}$ A/W with a detectivity, $D^* = 1.5 \times 10^9$ cm Hz$^{1/2}$/W at ~9 μm and 10 K.

Tuesday AM

129 Grating Coupled III-V Quantum Well Infrared Photodetectors for Mid-Wavelength and Long-Wavelength Infared Detection: *S. S. Li,* Dept. of Electrical Engineering, University of Florida, Gainesville, FL 32611

We present four types of novel grating coupled III-V quantum well infrared photodetectors (QWIPs) for 2-14 μm detection. These dual mode (photovoltaic and photoconductive) operation QWIPs were grown by the MBE technique using GaAs/AlGaAs, AlAs/AlGaAs, and InGaAs/InAlAs material systems. Based on the enhanced bound-to-continuum (EBTC) and bound-to-miniband (BTM) intersubband transition schemes, these detectors exhibit large optical absorption coefficient, low dark current, and high detectivity in the 3-5 and 8-12 μm detection bands. A normal incidence type-II QWIP using an indirect AlAs/AlGaAs grown on (110) GaAs substrate for multicolor detection in the 2-18 μm wavelength range is also presented.

130 Efficiency of Grating Coupled AlGaAs/GaAs Quantum Well Infrared Detectors: *J. Y. Andersson, L. Lundqvist, Z. F. Paska, J. Borglind,* and *D. Haga,* Swedish Institute of Microelectroncis, S-164 21 Kista, Sweden

The efficiency of grating coupling of radiation into quantum well infrared detectors is investigated theoretically and experimentally, with special emphasis on the influence of detector mesa size, due to its importance for high resolution focal plane arrays. The absorption quantum efficiency η and detectivity D^* are measured for detectors with crossed gratings and a waveguide, as a function of different detector parameters, including mesa area and grating type. For a mesa size = 50 μm one obtains η = 60% and $D^* = 5.7 \cdot 10^{10}$ cm Hz$^{1/2}$ W^{-1}, for detectors optimized with respect to D^*, at 80 K operating temperature, which demonstrates the superior coupling efficiency even for small mesa dimensions. Different optical coupler configurations are discussed and their efficiency compared.

131 Investigation of a Concentric-Ring Grating Coupler for Normal-Incidence Absorption in Quantum-Well Infrared Photodetectors: *D. A. Cardimona,* and *A. Singh,* Air Force Phillips Laboratory, Passive Sensors Branch, PL/VTRP, Kirtland AFB NM 87117-5776

In this paper, we theoretically investigate the potential of a concentric-ring grating etched on the surface of a multiquantum-well infrared photodetector pixel for coupling normally incident radiation into the radially propagating TM modes that are required for absorption by direct-gap n-type GaAs/AlGaAs quantum wells. We determine the grating and pixel parameters that maximize this absorption, and calculate the increased efficiency due to the distributed feedback nature of the structure.

132 Optical Gratings for GaAs/AlGaAs Quantum Well Detectors: *J. E. Scheihing,* and *M. A. Dodd,* Wright Lab., Solid State Electronics Directorate, WPAFB, OH 45433

Methods to increase the coupling efficiency of optical gratings for ue in GaAs/AlGaAs quantum well detectors are currently under investigation. Both etched and deposited metal gratings are being explored. Front-illuminated detectors employing linear gratings with 2 μm lines and spaces are used as a reference standard and are compared to two-dimensional configurations. In addition, the use of a thin (50 Å) metal layer for the enhancement of surface plasmon generation is reported.

133 Barrier-Doped GaAs/AlGaAs Quantum Well Detector: *M. A. Dodd,* and *J. E. Scheihing,* Wright Lab., Solid State Electronics Directorate, WPAFB, OH 45433

The doping profile of a (λ_p = 8.6 μm) quantum well infrared detector was altered to increase optical absorption. This structure is of the bound-to-continuum design and utilizes undoped GaAs wells and doped AlGaAs barriers. The result was a device with λ_p = 12.05 μm and dark current in the nA range. Optical response with a signal-to-noise ratio of better than 10:1 was achieved at temperatures as high as 150 K.

134 Tunneling Emitter Undoped Quantum-Well-Infrared Photodetector: *K. M. S. V. Bandara, B. F. Levine,* and *M. T. Asom,* AT&T Bell Labs., Murray Hill, NJ 07974-0636

An extensive series of measurements and theoretical analysis are presented on an undoped single quantum-well-infrared photodetector. The well is filled by electron tunneling through the thin emitter barrier resulting in several novel characteristics compared with the usual directly well-doped detectors. These include a unity optical gain and a dramatic drop in the well carrier density (and responsivity) at high bias when the bound state in the well drops below the emitter conduction bandedge.

135 Two-Mode InGaSb/GaSb Strained-Layer Superlattices, Infrared Photodetectors: *Y. K. Su, S. M. Chen,* and *Y. T. Lu,* Depts. of Electrical Engineering and Physics, National Cheng Kung University, Tainan, Taiwan, China

An interesting two-mode photodetector was constructured using $In_{0.19}Ga_{0.81}Sb$/GaSb strained-layer superlattice (SLS). Such a structure is, at the same time, of type I for heavy-hole and type II for light-hole. Mini-subbands in $In_{0.19}Ga_{0.81}Sb$/GaSb SLS have been calculated for the first time using the modified Kronig-Penney model, and as a function of well width at 300 K. A 10-period $In_{0.19}Ga_{0.81}Sb$/GaSb SLS structure can be applied as two-mode photodector with near zero and reverse bias. This phenomenon can be proved by spectral response of the structure grown by low pressure metalorganic chemical vapor deposition (MOCVD). The wavelength of dominant absorption peaks are 1.92 and 1.77 μm at near zero and reverse bias, respectively. The experimental data have good agreements with the theoretical deductions.

Tuesday PM

136 $In_{1-x}Tl_xSb$ for Long Wavelength Infrared Photodetectors: *M. Razeghi, Y. H. Choi, P. T. Staveteig,* and *E. Bigan,* CQD, Dept. of EECS, Northwestern Univ., Evanston, IL 60208

A new generation of long wavelength infrared detectors based on III-V semiconductors are rapdily emerging as more reliable and cost-effective alternatives to HgCdTe, facilitated by the advancements made in epitaxial growth techniques such as metallorganic chemical vapor deposition. The growth and characterization of $In_{1-x}Tl_xSb$, a new III-V alloy, for long wavelength infrared detector applications are presented.

137 InAsSb/InSb Strained Layer Superlattice Infrared Detector Technology: *S. R. Kurtz,* Div. 1315, Sandia National Laboratories, Albuquerque, NM 87185

Based on demonstrated detectivity, InAsSb strained-layer superlattices (SLSs) are the most advanced of the SLS infrared detector technologies, and InAsSb SLS detectors offer the promise of a III-V based photovoltaic technology to compete with HgCdTe. The physics of these type II SLS detectors is common to other SLS detector technologies, and the materials and processing problems that we have encountered may be "rediscovered" in competing

Lead scandium tantalate (PST) thin layers were prepared by a sol-gel method. Perovskite phase development and preferred orientation were studied by XRD. Dense insulating thin layers formed as low as 750°C. Dielectric properties as a function of temperature and frequency are reported. PST showed typical relaxor behavior with a maximum relative permittivity between 2000-4000. Ferroelectric properties were obtained.

152 Formation of Crystalline-Oriented PZT by a New Sol-Gel Technique: *K. Aoki, Y. Fukuda, K. Numata* and *A. Nishimura,* ULSI Technology Development, Texas Instruments Japan Limited, 2350 Kihara Miho-mura, Inashiki-gun, Ibaraki-ku 300-04, Japan

A new sol-gel technique has been developed to obtain <100> oriented PZT films on Pt/Ti/SiO_2/Si substrates, It is found that the oriented PZT films show excellent electrical characteristics. A leakage current of 240 nm thick film is as low as 7 nA/cm^2 at 3 V, which is an order of magnitude lower than the best reported La- and Fe-doped PZT films.

153 Advanced Oxide Etching Using a Silicon Electrode: *C.H. Yang,* IBM Corp., East Fishkill, NY 12533, and *G. Schwartz,* Lam Research Corp., East Fishkill, NY 12524-2505

To improve product throughput, yield and applications, a silicon electrode was installed in Lam's single oxide system as part of a joint development effort between Lam and IBM Corp. A significant reduction of ≥0.3 μm particles was observed after extensive RF hours. In contrast to the graphite electrode, which is a carbon producer, the silicon electrode is a fluorine consumer. A significant difference in the etch rate is observed when the results are measured on blanket *vs.* patterned oxide. The advantage of using the silicon electrode as a fluorine consumer is demonstrated in the enhancement of selectivity of oxide to silicon or oxide to nitride.

154 Low Temperature Electrochemical Synthesis and Dielectric Characterization of $BaTiO_3$ Thick Films Using Nonalkali Electrolytes: *S. Venigalla, P. Bendale,* and *J. H. Adair,* Dept. of Materials Science and Engineering, University of Florida, Gainesville, FL 32611-2066

Homogeneous, polycrystalline, $BaTiO_3$ films of several micron thickness have been synthesized on Ti substrates by an electrochemical process using nonalkali electrolytes, at temperatures as low as 55°C. Effect of various processing parameters, such as solution chemistry, atmosphere, current density, and cell potential, temperature and deposition time have been discussed. Use of tetraethylammonium hydroxide, a nonalkali base reagent to adjust solution pH, has resulted in films having improved dielectrric properties as opposed to the films prepared with NaOH. Microstructural and dielectric characteristics of the films heat-treated under various conditions have also been reported.

155 Deposition and Characterization of Photoconductive PZT Thin Films: *C. T. Lin, L. Li* and *J. S. Webb,* Dept. of Chemistry, Northern Illinois University, DeKalb, IL 60115-2862, *M. S. Leung* and *R. A. Lipeles,* The Aerospace Corp., Los Angeles, CA 90009-2957

Deposition by aqueous acetate solution (DAAS) technique was used to synthesize highly crystalline thin films of undoped and iron-doped $Pb(Zr_{0.53}Ti_{0.47})O_3$ [PZT] perovskites on sapphire and Pt substrates at 600°C. The defect chemistry of ferroelectric/photoconductive PZT thin films was investigated by photocurrent action and 77 K emission spectroscopy, and P-E hysteresis loop measurements. The photoconductivity measured at visible wavelengths was enhanced for the thermally diffused, but not the precursor processed-doped materials.

Thursday PM

156 Deposition, Annealing, and Characterization of High-Dielectric Constant Metal Oxide Films: *H. Treichel,* Siemens Components, Essex Jct., VT 05452, *A. Mitwalsky, G. Tempel,* and *G. Zorn,* Siemens Corporation, Corporate Research and Development, 8000 Munich, Germany, *D. A. Bohling, K. R. Coyle, B. S. Felker,* and *M. George,* Air Products and Chemicals Inc., IGD Electronics, Allentown, PA 18195, *W. Kern,* Werner Kern Associates, East Windsor, NJ 08520, *A. P. Lane,* Texas Instruments, SPL, Dallas, TX 75265, and *N. P. Sandler,* Lam Research, Fremont, CA 94538

Films of Ta_2O_5, Nb_2O_5, Al_2O_3, HfO_2, ZrO_2, and TiO_2 have been fabricated by use of different precursor materials, deposition processes, and annealing techniques. New data of fundamental properties are reported and related to practical features that are of importance in device design and manufacturing of advanced, highly integrated circuits. This overview may facilitate the choice of an optimal combination of precursor, deposition process, and annealing procedure for a specific application of these metal oxide films in microelectronics.

157 Integration of Ta_2O_5 Capacitors for Advanced 256 Mb Stocked DRAMs: *P. C. Fazan, V. K. Mathews,* and *G. S. Sandhu,* Micron Semiconductor, Inc., Boise, ID 83706-9698, *N. Sandler,* LAM Research Corp., Freemont, CA 94538

A full CVD-deposited Ta_2O_5 capacitor structure is proposed for 256 Mb DRAMs. The integration issues of this structure using CVD-poly-Si/RTN/CVD Ta_2O_5/CVD/TiN are discussed. Their electrical properties and, in particular, the effect of post Ta_2O_5 or post TiN deposition anneals are presented.

158 Suppression of Grain Growth and Surface Roughness of MOCVD Ta_2O_5 Films in a Stacked Gate Structure: *E. Yoon, M. E. Thomas,* and *Ren P. Kovacs,* National Semiconductor, Santa Clara, CA 95052

This paper reports the enhanced dielectric properties afforded by the suppression of grain growth and surface roughness in multilayered Ta_2O_5/SiO_2 dielectric composite structures. These composite films can be integrated in IC processes providing high dielectric constants (permittivity) and breakdown strength. It has been observed by using TEM and AFM analyses that the thicker Ta_2O_5 films (>20 nm) have larger grain sizes and rougher surface morphologies after annealing above 750°C. Subsequently, dielectric leakage current increases with the film thickness. To suppress this structural change, multiple alternating layers of thin Ta_2O_5 (<10 nm) and SiO_2 (<2 nm) have been fabricated and studied. The incorporated Ta_2O_5 films in the multilayer scheme maintain similar structural characteristics to thin single-layer films. These composite films have demonstrated leakages of 10^{-6} A/cm^2 at 3 MV/cm with an effective dielectric constant above 15. This structure can be scaled to any thickness by stacking as many alternating layers as required with no significant dielectric strength degradation.

159 Tantalum Oxide and Ferroelectric Thin Films by Metallorganic Decomposition: *E. P. Giannelis, M. W. Russell, G. T. Kraus,* Dept. of Mat. Sci., and Eng., Cornell Univ., Ithaca, NY 14853

Ta_2O_5 and $Pb(Ti, Zr)O_3$ thin films were deposited by decomposition of metallorganic precursors and characterized by ion-beam analysis (Rutherford backscattering and forward recoil spectrometry), transmission electron microscopy, and electrical measurements. Precursor chemistry, substrate type, and heat-treatments were varied to optimize the electrical behavior of the films. The dielectric and ferroelectric properties of the films are presented and discussed in terms of the corresponding chemistry and film microstructure.

160 Electronic and Ionic Charge Transport in High Permittivity Materials: *D. M. Smyth,* Mat. Res. Cntr., Lehigh Univ., Bethlehem, PA 18015

Both holes and oxygen vacancies can contribute significantly to charge transport in insulating perovskite titanates. While the magnitude of the ionic conduction depends solely on the impurity content, the hole contribution also depends on the temperature and oxygen activity of equilibration, and on the carrier mobility. The latter is determined by band conduction in the alkaline earth titanates, while a hopping mechanism prevails in lead-based compounds. Charge transport is reviewed using both classes of materials as examples.

161 Control of Physical and Electrical Properties of Sol-Gel Processed, Lead Titanate-Based Thin Films: *C. J. Smart, D. B. Beach, A. Grill, R. Laibowitz, T. Shaw,* and *J. Viggiano,* IBM T.J. Watson Research Center, Yorktown Heights, NY, 10598

By a combination of established sol-gel techniques and some novel processing details, we have been able to control some important physical and electrical properties of thin films of PZT, PLZT, and PMN-PT. Substrate choice, precursor solution composition and additives, and annealing conditions were found to be critical in obtaining the desired (perovskite) crystalline phase. AC capacitance and loss tangent as well as dc current-voltage characteristics were measured and correlated with processing conditions.

162 Reliability of Titanate Thin Films for ULSI DRAM Applications: *X. Chen* and *A. I. Kingon,* Dept. of Mat. Sci. and Eng., NCSU, Raleigh, NC 27695-7907

Dielectric breakdown of both $Pb(Zr_xTi_{1-x})O_3$ (PZT) and $Ba(Sr_xTi_{1-x})O_3$ (BST) thin films, which have potential applications in ULSI DRAMs because of their high permittivity, are studied. The emphasis is on the effects of top contact material, contact area, and contact thickness on the self-healing behavior of breakdown. Statistical distribution of breakdown field and time to breakdown also are studied. Both breakdown mechanism and the relevance of the results to the practical applications are discussed.

163 Electrical Properties of $SrTiO_3$ Thin Films Deposited by Laser Ablation: *P. Bhattacharya, T. Komeda, K. Park,* and *Y. Nishioka,* Texas Instruments, Tsukuba R&D Center, Tsukuba, Ibaraki 305, Japan, *S. Summerfeld* and *B. Gnade,* Texas Instruments, Central Research Lab, Dallas, TX 25265

$SrTiO_3$ thin films were deposited by laser ablation on Pt/SiO_2/Si substrates at different substrate temperatures. The leakage currents of crystalline films were higher than amorphous films. Electron-trapping centers were observed at the surface of deposited films by the constant-current injection method. The presence of electron-trapping centers was correlated with x-ray photoelectron spectroscopic (XPS) measurements of O1s peak from the surface of deposited films.

Friday AM

164 Electrodes Systems for Ferroelectric Capacitor Structures in DRAMs: *A. I. Kingon* and *H. Al-Shareef,* North Carolina State University, Materials Research Center, Raleigh, NC 27695-7919, *S. Summerfelt,* Materials Science Laboratory, Texas Instruments, Dallas, TX 75265-5936

New high permittivity materials are being considered for application in ULSI dyanamic random access memory (DRAMs). The electrodes in these devices are critical to their performance. Candidate materials are evaluated in two categories: metals and metal oxides. Emphasis is placed upon two materials, *viz.*, Pt and RuO_2. The issues discussed include thermal stability, adhesion, diffusion barriers, and the effect on electrical properties of the capacitors.

165 Chemical Vapor Deposition of (Ba, Sr)TiO_3: *M. Yoshida, H. Yamaguchi, T. Sakuma,* and *Y. Miyasaka,* Fundamental Research Laboratories, NEC Corp., 4-1-1 Miyazaki, Miyamae-ku, Kawasaki, Kanagawa 216, Japan, *P.-Y. Lesaicherre* and *A. Ishitani,* ULSI Device Development Laboratories, NEC Corp., 1120 Shimokuzawa, Sagamihara, Kanagawa 229, Japan

The chemical vapor deposition (CVD) of (Ba, Sr)TiO_3 thin films is surveyed. Films are prepared using titanium isopropoxide, barium and stronium tetramethylheptanedionate complexes, and oxygen. The characterization of the film crystal structure, surface morphology, step coverage, and the electri-

179 Step-coverage Simulation for Tetraethylortho silicate/Ozone Atmospheric Pressure Chemical Vapor Deposited Borosilicate Glass and Borophosphosilicate Glass: *K. Fujino,* Semiconductor Process Lab., Minato-ku, Tokyo 108, Japan, and *Y. Egashira, Y. Shimogaki,* and *H. Komiyama*, Dept. of Chemical Engineering, Faculty of Engineering, Univ. of Tokyo, Bunkyo-ku, Tokyo 113, Japan

The analytical step-coverage simulation has been applied successfully to the tetraethylortho silicate/ozone ($TEOS/O_3$) atmospheric pressure chemical vapor deposited (APCVD) borosilicide glass (BSG) and borophosphosilicate glass (BPSG) films of superior step-coverage using the same simulation procedures as for the SiO_2 and phosphosilicate glass (PSG) films, whose simulation is presented already. The simulated curves exhibited good fit to the experimental ones if the sticking probabilities were 0.0019 and 0.0025 for BSG and BPSG, respectively. Both CVD reactions were limited by the reactant diffusion.

180 Optimization of TEOS/Ozone Films to Minimize Hot Electron Effects in High Performance Integrated Circuit Technology: *W. J. Hsia* and *S. Yeh,* LSI Logic, Inc., Santa Clara, CA, and *J. Foggiato, J. Park,* and *S. Fisher,* Quester Technology, Inc., Fremont, CA

With smaller geometries and higher circuit sensitivity to stray ions, the presence of moisture in the intermetal dielectric (IMD) films has been attributed to device degradation due to hot electron effects. Several techniques are being employed to minimize the moisture absorption of the films as well as reduce the inherent moisture content during deposition. One effective method employs plasma treatment with various gases showing improvement in the moisture absorption resistance (MAR) of the films. In turn, the film deposition conditions are being optimized to increase the MAR resulting in lower moisture levels. An array of techniques are described substantiated by experimental data. Devices with these films have been evaluated and the levels of improvements noted. With these optimal deposition conditions, TEOS/ozone films have demonstrated suitability for IMD applications for high density integrated circuits.

181 Chem-Mechanical Polishing Planarization Concerns Surrounding CeO_2 Slurry: *R. Mattox,* Motorola Inc., Mesa, AZ 85052

Chem-Mechanical polishing (CMP) has gained considerable interest as a technique for planarization of multilevel metal circuitry. The technique has been proven as a feasible method for obtaining virtually global planar interlevel dielectric structures. Fumed silica slurry has been the slurry of choice, however, cerium oxide slurry was chosen here as an alternative slurry material. A four-level metal test structure was fabricated and potential concerns of physical damage, redeposition, and alkaline contamination were evaluated. The results on these three issues are discussed.

182 Fabrication and Evaluation of Indium Tin Oxide Semiconductor Structures: *E. Lisicka-Skrzek, K. A. Vineberg, W. Coyne,* and *O. Berolo,* Communication Res. Cntr., Ottawa, ON, Canada K2H 8S2

Indium-Tin Oxide (ITO) transparent thin films have been characterized for the fabrication of optoelectronic detectors. We are the first to report the microlithographic patterning of these RF sputtered thin films by standard lift-off procedures. Measurements of sheet resistance and optical transmittance are reported as a function of anneal temperature. The diode characteristics such as barrier height and ideality factor on standard GaAs metal semiconductor field effect transistor (MESFET) material have been measured and compared with Ti-Pt-Au Schottky diode parameters on the same material.

Tuesday AM

183 The Influence of Dopant and Rapid Thermal Annealing on the Silicidation of Submicron Lines: *P. D. Agnello* and *A. Fink,* IBM T.J. Watson Res. Cntr., Yorktown Heights, NY 10598

$TiSi_2$ must undergo a transformation from the high resistivity C49 phase to the low resistivity C54 phase for applications where it is used as a gate conductor. Temperature control and wafer-to-wafer reproducibility during momentary annealing via rapid thermal annealing (RTA) is critical for $TiSi_2$ *S*elf *A*ligned si *LICIDE* (SALICIDE) processing for deep submicron complimentary metal oxide semiconductor (CMOS). A process modification to achieve improved wafer-to-wafer and within-wafer temperature reproducibility is demonstrated. It has the additional benefit to the $TiSi_2$ salicide process of enabling anneals of reduced duration, enhancing silicide transformation to the desired phase without leading to agglomeration. The affect of heavy n-type doping and vanishing process window at physical linewidths of 0.25 μm is discussed.

184 Increase in Conductivity of As-Implanted Layers by Low Temperature (below 900°C) Rapid Thermal Annealing: *A. Kalnitsky, R. MacNaughton,* and *J. Li,* SGS-Thomson Microelectronics, Carrollton, TX 75006

We report an increase in conductivity of As-implanted layers achieved by rapid thermal activation of As at temperatures below the temperature of junction anneal [900°C, N_2, furnace, performed prior to rapid thermal annealing (RTA)]. This effect is interpreted in terms of residual inactive As reaction with vacancies generated during the heat-treatment. Proposed model gives the value of the activation energy (5.65 eV) for the process as well as the interpretation of the meaning of this activation energy. An estimate of the activation energy for As diffusion also is obtained. This work shows that efficient activation of implanted As can be achieved at temperatures well below 900°C.

185 Characterization of As-Grown Crystallographic Defects in Czochralski Silicon Using Nonagitated Secco Etching: *W. Wijaranakula* and *Y. Pan,* Research and Development Dept., SEH America, Inc., Vancouver, WA 98682

A characterization of as-grown crystallographic defects, referred to as "flow pattern defects," in as-received and annealed Czochralski silicon wafers using nonagitated Secco etching was performed. As-received Czochralski silicon wafers are observed to contain as-grown defects on the order of 5×10^6 defects/cm^3. The defect density reduces during a high temperature annealing. In addition, it is observed that the etching rate of silicon depends strongly upon the grown-in defect density.

186 Behavior of Defects and Boron Implanted/Oxidized Silicon: *S. Sundaram,* and *N. David Theodore,* Motorola Inc, Mesa, AZ 85202

The microstructural behavior of boron-implanted silicon is investigated for varying doses and energies of implant, with and without post-implant oxidation. Damage bands formed upon annealing vary with varying implant and oxidation/anneal conditions. Different damage bands arise due to end-of-range implant-damage, exceeding dopant solid-solubility, and due to later coalesence of interstitials freed from the first band during annealing. An oxidation step increases the density and distribution of defects in the defect bands in a manner consistent with oxidation-induced injection of interstitials into the silicon.

187 Reduction of Corrosion Defects on Metal Alloy Lithography Seen Immediately after Etch Processing: *G. Gebara,* and *K. Mautz,* Motorola, Inc., SPS, Austin, TX 78762

Corrosion defects on submicron lithography are a significant limitation of semiconductor manufacturing. The defects studied occurred as corrosion byproduct residues protruding from the sidewalls, seen immediately after exiting the metal etch reactor. Processing factors found significant in producing corrosion defects were: (*i*) metal thickness, (*ii*) overetch step chlorine flow and step time, (*iii*) wafer back-side condition, (*iv*) photoresist type, (*v*) wafer position, (*vi*) metal contacting substrate, and (*vii*) pattern density polymer encapsulation, done *in situ* after metal etching was effective in preventing these defects.

188 Solid Electrolytic Capacitor with Electron-Conducting Polymer Layers: *F. Takei, H. Shiroto,* and *N. Sawatari,* Fujitsu Lab., Ltd., Atsugi 243-01, Japan

The solid electrolytic capacitor we developed has excellent characteristics and is easily fabricated with new electron-conducting polymer layers: soluble polyaniline(SPAn) and polypyrrole. SPAn was synthesized chemically, and coated on the capacitor element with dip-coating. The polypyrrole layer was formed over the polyaniline layer using an electrochemical technique. Because of the high conductivity of the SPAn layer, the equivalent series resistance was reduced to half of the conventional polypyrrole capacitor. The number of manufacturing processes is one third that of conventional methods.

189 High Performance Capacitor with Rugged Surface Poly-Si Electrodes Formed by Two-Step Wet Etching: *T. Hirota, M. Zenke,* and *K. Okamura,* VLSI Manufacturing Engineering Div., NEC Corp., 1120, Shimokuzawa, Sagamihara, Kanagawa 229, Japan

This paper describes stacked capacitors with rugged surface poly-Si storage electrodes formed by two-step wet etching which meet the requirements for high density DRAMs. To rough the surface of poly-Si electrode, novel combination of H_3PO_4 solution treatment (1st step etching) and light Si etching (2nd step etching) was used. Using this technique, more than twice the storage capacitance can be obtained with simple stacked capacitor, and it shows excellent electrical properties.

ELECTRODEPOSITION OF SEMICONDUCTOR MATERIALS
Electrodeposition

Thursday AM

190 Structure of Chemically Deposited Cadmium Sulfide Films: *M. Froment,* UPR15 CNRS, Physique des Liquides et Electrochimie, 75252 Paris Cedex 05, France, *D. Lincot* and *R. Ortega Borges,* Laboratoire d'Electrochimie Analytique et Appliquée, Ecole Nationale Supérieure de Chimie Paris, 75231 Paris Cedex 05, France

Cadmium sulfide films have been deposited chemically at near room temperature in aqueous ammonia solutions using thiourea as the sulfur source. The structure of the layers and the growth mechanism are studied by using high resolution transmission electron microscopy (HRTEM). The layers deposited on carbon/Cu grids are formed of well-defined crystallites with the hexagonal structure. HRTEM images display atomic projections in the [0001] and [1120] directions. The presence of stacking faults is discussed in relation to CdS polymorphism. The CdS structure is also dependent on the nature of three substrates: Si, GaAs, InP. Either cubic or hexagonal structures are observed. When deposited on (111) InP, RHEED observations reveal an hexagonal CdS epitaxial growth.

191 Electrodeposition of Selenium Containing Semiconductors. I. Copper Selenides: *J. Vedel, S. Rouquette-Sanchez, L. Thouin,* and *S. Massaccesi,* Laboratoire d'Electrochimie, ENSCP, F-75231 Paris Cedex 05, France

The electrodeposition of copper selenides at room temperature is studied using voltammetry, x-ray diffraction, and composition analysis. These semiconductors do not follow the general scheme observed by other compounds like CdTe. The selenium needs the presence of copper to be deposited, even at potential lower than its standard redox potential. Two potential ranges were determined. In the first one, the deposit composition is fixed by the precursor diffusion. In the second range, at the most negative values, copper (II) is reduced as Cu_2Se and the excess of Se(iV) as H_2Se.

192 Electrodeposition of Selenium Containing Semiconductors. II. Copper Indium Diselenide: *J. Vedel,* S. Rouquette-Sanchez,

NJ 08875, *H. Meyer, W. Meyer,* and *R. Schumacher,* Atotech Deutschland GmbH, W1000 Berlin, Germany

Principally, classical wet chemical analytical techniques characterize the bulk concentrations in the liquid phase. For solutions which are in contact with surfaces an interfacial region is formed in which a potential and concentration gradient is formed. In this region the concentration, *e.g.,* of metal ion in electrodeposition solutions, can deviate significantly from the bulk concentration of the liquid phase. The changing interfacial concentration can be determined by *in situ* techniques. We have developed and employed various techniques which allow the *in situ* examination of galvanic and electroless metallization processes. The following techniques were applied: cyclovoltammetric stripping (CVS), microgravimetry with oscillating quartz crystals, microtopography with a coherent light source and/or with various scanning techniques based on tunneling and atomic force microscopy. In some instances a combination of *in situ* and bulk techniques were applied. The results are discussed and compared with those obtained by classic wet chemical techniques.

206 Steady-State-Bath-Control Method for High-Precision Wet-Chemical Processing: *J. O. Dukovic, P. C. Andricacos, L. T. Romankiw,* and *J. Horkans,* IBM Research Div., T. J. Watson Research Center, Yorktown Heights, NY 10598

The steady-state bath control (SSBC) method has been developed for maintaining constant chemical composition in plating baths and other chemical processing solutions. The method employs a system of replenishing solutions which are formulated and doses in accordance with a comprehensive material balance, with total replenishment volume proportional to process service. The concentrations of all bath species are fixed, eliminating bath "aging," and enabling uninterrupted, drift-free operation for high-precision manufacturing. Applications to permalloy and copper electroplating are described.

207 Innovations in Automatic Hoist System Control for the Metal Finishing Industry: *R. J. Van Kirk,* Technic, Inc., Pawtucket, RI 02860

We present information about control systems which are being used for automated control of process times, sequences, and bath parameters in the metal finishing industry. Included is information about the latest PLC process monitoring/control software and MS-DOS based software to provide just-in-time random loading capabilities. Also included is information about additional features such as SPC/SQC data bases and automatic process control of plating baths.

208 Equipment for Electrodepositing CMA Coatings and Materials: *P. Leisner* and *T. C. Dörge,* Cntr. of Adv. Electroplating, DK-2800 Lyngby, Denmark

Electrodeposition is an important alternative to PVD techniques for preparation of composition modulated alloy (CMA) coatings. Electrodeposition of CMA coatings is closely related to pulse plating. A flexible computer-aided pulse plating system has been developed and further improvements of the system include simultaneous feedback from the plating process.

209 Precision Electroformed Neutron Penumbral Imaging Apertures: *N. Elliott, S. Armstrong,* and *P. Gobby,* Los Alamos Natl. Lab., Los Alamos, NM 87545

Computer-aided electroplating similar to work performed earlier has been used to fabricate precision parts for the nova laser ring coded-aperture microscope (RAM). Parts produced to date have an RMS deviation from desired diameter of 40 nm and an RMS straightness of approximately 4 nm over a length of 60 mm. This is roughly an order of magnitude improvement over parts produced previously by precision machining and electroplating. The design of the apertures requires a continuously varying radius of curvature. Because of this design, some subtle but significant changes were required to the fabrication technique used.

210 Transient Plating-Rate Distribution on Resistive Thin Films with Point Contact Terminals: *S. Mehdizadeh,* and *J. O. Dukovic,* IBM Res. Div., T.J. Watson Res. Cntr., Yorktown Heights, NY 10598

A numerical model has been developed to compute the transient thickness profile on a wafer with a thin conducting "seed layer" to which the plating current is supplied by low-contact-area terminals. The potential was assumed to obey the flux-continuity equation both within the electrolyte and the thin film, with surface and concentration overpotentials acting at the interface. The metal-ion concentration was assumed to obey the steady-state diffusion equation within a boundary layer. Solutions are obtained for contact-terminal arrangements that give rise to 2D and 3D formulations of the problem. Although the current density initially can be as high as its transport limit near the contact point, the nonuniformity quickly declines as the conductance of the growing deposit increases.

211 Experimental Strategy: Application of Taguchi's Quality Engineering Method to Zinc Phosphate Coating Uniformity: *S.-M. Lin* and *T.-C. Wen,* Dept. of Chemical Engineering, National Cheng Kung University, Tainan, Taiwan 70101, China

Plating process quality can be improved at no additional cost or even at a savings by Taguchi's quality engineering approach. The experimental strategy described in this paper is different from traditional experimental design, in that it is concerned with reducing variance in the manufactured product by determining the best settings for the manufacturing process parameters without tightening tolerances on them.

Wednesday PM

212 Application of Ring-Disk Electrodes to Alloy Electrodeposition: *P. C. Andricacos,* IBM Research Div., T.J. Watson Research Center, Yorktown Heights, NY 10598

A combination of ring-disk electrodes with stripping voltammetry permits the determination of plated-alloy composition and bath current efficiency with a high degree of accuracy and precision and at a low cost. This method has been successfully applied to such systems as NiFe and PbSn that are of interest in the fabrication of computer components. This paper reviews results obtained to date with emphasis on the development on stripping media and conditions for various alloy systems. Other application including depth profiling, multilayered deposit analysis, and *in situ* measurements also are discussed.

213 Galvanic Corrosion during Pulse-Current Plating of Cu-Ni Alloys: *S. Roy, M. Matlosz,* and *D. Landolt,* Laboratoire de metallurgie chimique, Dept. des matériaux, Ecole polytechnique Fédérale de Lausanne, CH-1015, Lausanne, Switzerland

Copper and nickel have been codeposited by pulse-current at a rotating cylinder from a citrate bath. Polarization data for copper and nickel and pulse-current experiments indicate that galvanic corrosion occurs during the off-time. A simple mathematical model was developed to predict the composition of electrodeposits. The model shows that copper deposits at the mass transfer limiting current throughout the pulse and nickel is alternately deposited and dissolved.

214 Electrodeposition of Mo Rich, Ni-Mo Alloys onto Rotating Cylinders: *E. J. Podlaha, M. Matlosz,* and *D. Landolt,* Ecole Polytechnique Fédérale de Lausanne, Dept. des Matériaux, Laboratoire de métallurgie chimique, CH-1015 Lausanne, Switzerland

Mo rich, bright, compact, adherent, metallic Ni-Mo alloys, containing over 50 w/o Mo have been electrodeposited from an aqueous solution. The Mo concentration was determined by x-ray fluorescence spectroscopy and the absence of oxygen was verified by Auger electron spectroscopy. Electrodeposition experiments were performed on rotating cylinder electrodes and demonstrate that the Mo content of the alloy is strongly influenced by convective transport. Higher Mo concentration could thus be achieved than previously reported for induced codeposition of Ni-Mo alloys.

215 Alternative to Cadmium Plating: Tin/Low Zinc Alloy: *S. Schachameyer, T. R. Halmstad,* and *R. Bauer,* Eaton Corp., Milwaukee, WI 53216, and *J. Newman,* Master Lock, Inc., Milwaukee, WI 53212

The search for cadmium plating alternatives accelerated in 1992 due to the EEC directive 91/338/EC, OSHA's release of CFR 1919.1027 (New Cd Standard) and EPA's Project 33/50. Eaton Corp. and Master Lock Co. joined partnership to do searching, evaluating, and ultimately implementing a Tin-1% nominal Zn alloy to replace cadmium. Electrochemical impedance spectroscopy and corrosion tests showed that Tin-Zinc exhibits improved corrosion resistance on steel without a chromate, compared to chromated cadmium on steel. The coating also exhibits many other useful engineering properties of cadmium for a universal replacement.

216 Periodic Passivation of CuP Anodes during Electrodeposition of Cu from Acid-Sulfate Electrolyte: *G. S. Frankel, J. O. Dukovic,* and *J. Horkans,* IBM Res. Div., T.J. Watson Res. Cntr., Yorktown Heights, NY 10598

The behavior of Cu-0.1%P anodes used in electrodeposition of Cu from acid sulfate baths was studied. Rotating disk electrodes electrolyzed anodically at constant current in solutions containing organic additives exhibited passivation events during which the electrode potential increased by 15-20 V. The events were of limited duration (about 20 min) and were separated by a regular and reproducible period that depended on many experimental parameters and was on the order of hours in length. The passivation events were observed only in baths that contained organic additives. The period between events decreased as the organic additive content increased, as the current density increased, and as the rotation rate decreased.

217 Direct Electrodeposition of Inherently Conducting Polymers into and onto Microporous Membranes as Continuous Films: *P. Kathirgamanathan,* Industrial Unit for Specialty Electronic Polymers and Materials, Chem. Dept., Univ. Coll. London, London WC1H 0AJ, England

Electrical signal and communication cables are currently shielded by either metal braids and/or aluminum laminated polyester, μ-metals (for low frequency magnetic shielding), carbon loaded polyesters, etc. Direct electrodeposition of inherently conducting polymers into and onto microporous membranes yield conductive materials with conductivities as high as 10 S/cm which are suitable for cable shielding applications. The materials have been produced by an electrochemical method using a partially immersed cylindrical horizontally revolving electrodes with the assistance of ultrasound. Production and electrical, mechanical, and electromagnetic shielding characteristics of poly(pyrrole) and poly(aniline)-impregnated microporous polyethylenes and polyurethanes are discussed.

218 Anodizing of Aluminum with Microexplosive Air Agitation: *K. Okuno* and *H. Satoh,* Okuno Chemical Industries Co. Ltd., Tsurumi-ku Osaka 538, Japan

As to agitation for anodizing, we have found many advantages in using air bubbles diffused from porous ceramic pipes in place of conventional air agitation. This method, called Microexplosive air agitation, provides excellent effects against burning prevention, so that it can apply high current density for anodizing. Furthermore, this method has a remarked effect on improving uniformity, suppressing surface roughness, and hardness of anodizing film. Good effects are expected for the plating process.

height. The impact of these trends and the resulting material requirements for present and future head designs are discussed.

231 Fundamental Experiment on Submicron Track Width Recording Utilizing Highly Permeable Magnetic Film: *Y. Nakamura* and *H. Muraoka,* Res. Institut. of Electric. Commun., Tohoku Univ., Aoba-ku, Sendai 980, Japan

To accomplish ultrahigh areal density recording, submicron track width recording was examined. Utilizing a new configuration of a single pole head with a Co-Cr/Ni-Fe double-layered medium, perpendicular magnetic recording was performed with sliding contact recording on a hard disk. The track width of write-head was less than 1 μm. Bitter method proved that the actual written track width on a medium was about the same track width of the write-head. The clear read-back waveform was obtained on an oscilloscope without averaging or any other special signal processing. Its carrier-to-noise ratio was over 30 dB. With a separated high resolution read-head, the signal over 100 kFRPI was confirmed. These results suggest that ultrahigh track density is realized without deterioration of the linear density.

232 Omega Flat Head Structure with 120 Turns: *D. D. Tang,* IBM Almaden Research Center, San Jose, CA 95120, and *L. T. Romankin,* IBM T.J. Watson Research Center Yorktown Heights N.Y. 10598

The present day pancake vertical inductive heads are approaching their track limit due to the inability to produce more turns without increasing the separation between the P1 and P2 yoke. Increasing the separation beyond ~30 μm makes it very difficult, if not impossible, to do the necessary lithography over these very large vertical steps. This paper reports on design, fabrication, and testing of a novel planar thin film head which spreads the yoke in the plane of the slider and thereby permits up to 120 turns which are tightly wound around the yoke in a helical fashion. Experimental results show that coil resistance and inductance are much lower per turn in the flat head than in the pancake head. Thus, it is possible to build planar inductive heads in which tracks can be narrowed perhaps to as low as 2 μm, while still maintaining an adequate signal using the existing electronics.

233 A Pinched-Gap Magnetic Recording Thin-Film Head: *U. Cohen,* Palo Alto, Ca 94303

An inductive pinched-gap thin-film head (TFH) device with contacting pole-tips along its sides or edges, thereby precisely confines a pinched-gap segment.[1] The contacting sides effectively eliminate all flux lines emanating from side edges and corners during write operations. These include the track-edge noise-producing nonparallel lines. The write magnetic field is precisely confined to across the pinched-gap segment. The written track width is accurately defined by the width of the pinched-gap segment and is practically independent of the pole-tips width. The track has a high degree of magnetization coherency and is virtually free of track-edge noise. The pole-tips must be saturated, during write operations, to maintain adequate write field. The improved SNR facilitates substantial increase of the track density. Using photolithographic etching of gap-vias, it is possible to control precisely the width of the pinched-gap segment (and track) down to ≤1 μm. Very narrow pinched-gap TFH write element can be combined with an MR read element to achieve extraordinaryly high recording densities.

1. U. Cohen, Pat. pending.

Monday PM

234 Modeling of Anomalous Codeposition of Binary Iron-Group Alloys: *J. B. Talbot* and *K. Y. Sasaki,* Dept. of AMES/Chem. Eng., Univ. of California, San Diego, La Jolla, CA 92093-0310

The electrodeposition of the iron-group alloys is characterized by the phenomenon of anomalous codeposition, in which the less noble metal deposits preferentially. Thin films of NiCo and FeCo were electroplated galvanostatically from simple sulfate baths containing 0.5*M* of the less noble metal and 0.1*M* of the more noble metal at pH3 on a rotating-disk electrode. The one-dimensional diffusion model of Grande and Talbot, which previously described NiFe deposition under similar conditions, was extended to determine its viability as a general model for the iron-group alloy deposition. This model assumes that the metallic monohydroxide, MOH^+, controls the codeposition. Comparison of the experimental data and model results indicates that this model is inadequate to characterize NiCo and FeCo electrodeposition. Modifications of the model are discussed.

235 Boric Acid Complexation in the Electrodeposition of Nickel-Iron Alloys: *T. M. Harris,* Dept. of Chem., Univ. of Tulsa, Tulsa, OK 74104-3189, *G. M. Whitney* and *I. M. Croll,* IBM, San Jose, CA 95193, and *R. H. Schad,* Dept. of Chem., Univ. of Tulsa, Tulsa, OK 74104-3189

Boric acid commonly is added to baths for the electrodeposition of Permalloy thin-film heads. The role of boric acid in nickel and nickel-iron alloy electroplating has been debated for many years. In potentiodynamic tests, boric acid greatly extends the potential range for deposition (of nickel, iron, and nickel-iron alloys) without precipitation. The same behavior is observed with ammonium chloride. The basic form of this compound, ammonia, is known to complex both nickel and iron. A detailed comparison of the effects of these two additives indicates that boric acid acts as a complexant for both nickel and iron, but that the complexes form only in the vicinity of the cathode, where the pH is higher.

236 Potential Modulation Near-Normal Incidence Reflection Absorption UV-Visible Spectroscopy under Forced Convection: Absorbing Reactant and Product: *M. Zhao* and *D. A. Scherson,* Dept. of Chem., Case Western Reserve Univ., Cleveland, OH 44106-7078

A spectroelectrochemical technique has been developed to determine the UV-visible spectral properties of electrogenerated species at a rotating-disk electrode using potential modulation. The present contribution extends the theoretical treatment described previously to a spectral region in which the absorption of the reactant may not be neglected, and compares the predictions with experimental data. The agreement between theory and experiment using the oxidation of iron (II) hexacyanide as a probe reaction was excellent providing further evidence that the results obtained from this method are indeed quantitative even when the absorption due to the reactant is not negligible.

237 Corrosion and Passivation of Permalloy Thin Films: *G. Dagan* M. Tomkiewicz, Dept. of Physics, Brooklyn College of CUNY, Brooklyn, NY 11210 and *M. C. A. Fantrini,* Instituto de Fisica, Universidade de Sao Paulo, CP 20516, 01498, Sao Paulo, Brazil

Corrosion and passivation of permalloy ($Ni_{0.8}Fe_{0.2}$) thin films were studied via the potentiodynamic behavior in different electrolytes. The corroded surfaces were characterized using Auger electron spectroscopy, scanning electron microscopy and x-ray diffraction. The results show an anisotropic preferential etching in the <200> direction. *In situ* measurements of the spectral response show that passive films formed by air annealing are n-type Fe_2O_3 and Fe_3O_4 and that the films formed by anodic oxidation are p-type NiO.

238 LIGA Microstructures from a NiFe Alloy: Preparation by Electroforming and Their Magnetic Properties: *A. Thommes, W. Stark, K. Leyendecker,* and *W. Bacher,* Kernforschungszentrum Karlsruhe, Instit für Mikrostrukturtechnik, D-7500 Karlsruhe, Germany and *H. Liebscher* and *C. Jakob,* Technische Universität Ilmenau, D-O-6300 Ilmenau, Germany

A sulfate-based electrolyte together with the electroplating procedure was developed for manufacturing LIGA microstructures from permalloy. A flow cell was used for alloy deposition into microstructures with a maximum height of 200 μm and aspect ratios up to 20. The composition gradient over the structural height is almost negligible regardless of the lateral geometry. Coercivity of permalloy microprisms was determined to be <10 Oe; the corresponding saturation moment was about 1200 G.

239 Material and Processing Aspects of FeAlN High Moment Thin-Film Heads: *S. Wang, F. Liu, K. Maranowski* and *M. H. Kryder,* Dept. of ECE, Carnegie Mellon Univ., Pittsburgh, PA 15213-3890

FeAlN single and multilayer films with excellent magnetic properties previously were obtained on thin glass substrates by the authors. To fabricate thin-film recording heads suitable for high coercivity media and high data rates, these materials should be deposited on substrates used in head-slider fabrication such as alumina-TiC and hard-cured photoresists. Magnetic properties of FeAlN films are not only affected by sputtering parameters but also dependent on the substrates. Therefore, different sputtering conditions are necessary to obtain optimized films on various substrates. Substrate roughness, underlayer, and substrate temperature during deposition appear to be critical. A mainly dry process has been developed to fabricate the head wafers. Sputtered 2 μm thick FeAlN-based films are ion beam etched into pole pieces. Multiturn Cu coils and leads are electroplated. Fabricated heads function well at the wafer level. The core inductances measured by a network analyzer are flat up to 50 MHz (measurable range). Closure domains are eliminated, but multiple domains with a couple of 180° domain walls parallel to the easy axis defined during head fabrication are observed. Edge-curing walls also are observed.

240 Sputtered FeN Based Material for High Density Recording Applications: *M. A. Russak, C. V. Jahnes, J.-W. Lee, M. E. Re, B. C. Webb,* and *E. Klokholm,* IBM Research Div., T.J. Watson Research Center, Yorktown Heights, NY 10598

This paper summarizes our recent work with FeN based laminated materials for thin film head applications. These materials are attractive candidates for recording head applications as storage systems require higher storage densities and faster data transfer rates because they can be engineered to have high $4\pi M_s$ tunable coercivities and anisotropics as well as excellent high frequency performance.

241 Gradient Field Method for the Magnetoresistive Characterization of Thin Film Structures: *P. L. Trouilloud, F. Suits, C. Jahnes, M. A. Russak, E. J. Spada,* and *J. W. Chang,* IBM Research Div., T.J. Watson Research Center, Yorktown Heights, NY 10598

Magnetoresistance measurements can be used during manufacturing to help characterize some of the basic magnetic parameters of thin-film magnetic structures. A first approach is to measure the response to external applied fields that are uniform over the thickness of the sample. The object of this paper is to investigate the use of gradient fields such as those generated by currents flowing through the magnetic structures or in close proximity to them.

242 Properties of Sputtered Alumina Overcoats for Inductive Thin-Film Heads: *C. A. Ross*, Komag Inc., Milpitas, CA 95035, and *R. Malmhall,* Dastek, Inc., San Jose, CA 95119

Thick films of sputtered alumina commonly are used for encapsulation of thin-film heads. The properties of the alumina can have significant effects on the magnetic behavior of the plated Permalloy magnetic circuit. The plated Permalloy used in heads generally has a relatively high negative magnetostriction, so any stress induced by the alumina overcoat affects the magnetic performance of the head. We have measured the internal stress, composition, hydroxide etch rate, hardness, and elastic modulus of RF sputtered alumina sheet films as a function of deposition parameters including target power, substrate bias, and gas pressure. When alumina is sputtered over a head, topographically induced resputtering alters the composition and etch rate of the alumina immediately around the head by an amount which depends on bias. We have used the relationships between etch rate, composition, and stress for sheet films, measurements on the alumina in devices and finite element modeling to understand the effect of the overcoat on the stress in the Permalloy pole pieces of the head.

243 A Studless Thin-Film Head Produced by Deep Alumina Etching: *U. Cohen,* Palo Alto, CA 94303

satellite peaks which are typical of super lattices, which in turn are closely related with the giant magnetoresistive effect.

THE DEGRADATION OF ELECTRONIC DEVICES DUE TO DEVICE OPERATION AS WELL AS CRYSTALLINE AND PROCESS-INDUCED DEFECTS

Electronics

Monday AM

255 The Electronics and the Dielectric Science and Technology, SiO_2/Si Interface Structures and Reliability Characteristics: *A. Ishitani, E. Hasegawa, K. Akimoto, M. Tsukiji,* and *N. Ohta,* ULSI Device Development Laboratories, NEC Corp., 1120 Shimokuzawa, Sagamihara, Kanagawa 229, Japan

Reliability degradation of thin SiO_2 films is caused by a structural transition layer of SiO_2 at the SiO_2/Si interface. The structural transition layer is clearly detected by using synchrotron radiation for the first time. *Ab initio* molecular orbital calculations are carried out to simulate Si-Si bond formation in SiO_2 due to conduction electron capture. Based on the experimental results and theoretical analysis, a new model for dielectric breakdown mechanism is proposed.

256 Elimination of Oxide Defects on Czochralski Si by Pouring Deionized Water on a Rotating Wafer: *M. Itsumi* and *S. Aoyama,* LSI Laboratories NTT, Atsugi-Shi, Kanagawa 243-01, Japan

Oxide defects on Czochralski Si can be eliminated by pouring deionized water onto a rotating (6000 rpm) oxidized wafer. Electrostatic measurement reveals that electrons are produced during rotation. The resulting charge corresponds to a field across the oxide above several MV/cm. We propose that electrons produced by friction between the water and the SiO_2 induce this high field, and that an oxide defect receives excessive electron conduction. This conduction changes the chemical state of the defect.

257 N_2O-Based Metal Oxide Semiconductor Gate and Tunneling Dielectrics for Complimentary Metal Oxide Semiconductor Ultralarge Scale Integrated Application: *D.-L. Kwong,* Microelectronics Res. Cntr., Dept. of Electrical and Computer Engineering, The Univ. of Texas at Austin, Austin, TX 78712

A novel technique for the fabrication of ultrathin metal oxide semiconductor (MOS) gate and tunneling dielectrics for ultralarge scale integrated (ULSI) applications has been developed using oxidation of Si or nitridation of SiO_2 in N_2O ambient. These processes are extremely attractive for ultrathin gate oxides due to simplicity, oxide thickness uniformity, and controllability, and manufacturability. In addition, because of nitrogen incorporation at the SiO_2/Si interface during oxidation, the hot carrier immunity in MOSFETs with N_2O gate oxides is significantly enhanced. In this talk, the motivation of this work and a comparison between N_2O oxides and reoxidized nitrided SiO_2 is presented first. This is followed by a discussion of N_2O oxidation process/kinetics as well as the chemical/electrical properties of N_2O oxides. Then results are presented to demonstrate the superior performance and reliability of N_2O oxides over the control oxides, with particular focus on time-dependent dielectric breakdown (TDDB) characteristics and MOSFET hot carrier immunity. The potential of N_2O oxides for NVM applications also are discussed and demonstrated. Finally, the issues of defect density, thickness scaling, and process control and manufacturability are discussed with projections toward future trends.

258 Influence of Fluorine Atoms on Reliability of Dielectric Thin Films: *A. Yokozawa,* ULSI Device Development Laboratories, NEC Corp., 1120 Shimokuzawa, Sagamihara, Kanagawa, 229 Japan, *Y. Mochizuki,* Fundamental Research Laboratories, NEC Corp., 34 Miyukigaoka, Tsukuba, Ibaraki, 305 Japan, *E. Hasegawa* and *A. Ishitani,* ULSI Device Development Laboratories, NEC Corp., 1120 Shimokuzawa, Sagamihara, Kanagawa, 229 Japan, *T. Takada*, Fundamental Research Laboratories, NEC Corp., 34 Miyukigaoka, Tsukuba, Ibaraki, 305 Japan

The influence of fluorine (F) atoms on the electrical reliability of SiO_2 films is investigated. The TDDB measurements indicate that F atoms degrade the reliability of SiO_2 films. *Ab initio* molecular orbital calculations are performed for an $F^- + SiO_4$ model system. Those results suggest that F atoms enhance oxygen desorption and successive Si-Si bond formation in SiO_2 films. Increase in Si-Si bonds induces large leakage current through the films, resulting in dielectric breakdown.

Monday PM

259 Overview of Device Degradation Due to Crystallographic Defects: *Y. Takano* and *N. Fuma,* Dept. of Mat. Sci. and Technol., Science Univ. of Tokyo, Noda-shi, Chiba 278, Japan

Recent results about crystallographic defects formation causes, their device degradation effects and preventing methods for the defect formation are shown. The defects are divided into four groups, microdefects, defects in ion-implanted and annealed layer, contaminated impurities, and dislocations. This paper focuses on (*i*) contaminated impurities effects for the crystallographic defects and deep levels formation, and (*ii*) dislocations generated at edges of As-implanted and annealed layers.

260 Correlation of Substrate "D-defects" with MOS Breakdown Sites Via EBIC, FIB, and TEM: *J.-G. Park, H. Kirk,* and *G. A. Rozgonyi,* Dept. of Mat. Sci. & Eng., North Carolina State Univ., Raleigh, NC 27695-7916, *S.-P. Choi,* and *C.-S. Lee,* Samsung Electronics, Youngin-Gun, Kvunaki-Do, Korea, *D. M. Lee*, MEMC, St. Peters, MO 63376

The impact of "D-defects" in CZ silicon on MOS capacitors was investigated by measuring SiO_2 breakdown voltage as a function of crystal pulling speed and oxide film thickness. In addition, the D-defect morphology was observed by MOS/EBIC and focused ion beam plus HRTEM. D-defects are most likely vacancy-related defects which induce a localized SiO_2 perturbation during thermal oxidation.

261 Impact of Oxygen-Related Defects on the Electrical Characteristics and the Degradation of Si n^+p Junctions: *C. Claeys, E. Simoen,* and *J. Vanhellemont*, IMEC, B-3001 Leuven, Belgium

We discuss the effect of oxygen-related defects on the forward and reverse characteristics of junctions fabricated in p-type Si wafers with different interstitial oxygen concentration [O_i] and for different preheat-treatments. As shown by a combination of both electrical and analytical techniques (TEM, FTIR spectroscopy, DLTS, low-frequency noise), there is a clear effect of the SiO_x precipitates on the performance of the diodes. Furthermore, the degradation of the I-V curves, which is observed after operating the diode in the breakdown regime is most pronounced in epitaxial wafers, while a beneficial effect of the presence of oxygen is observed.

262 Effect of Bulk Microdefects Induced in Silicon by Heat-Treatment on the Leakage Current of PN Junctions: *Y. Murakami, Y. Satou,* and *H. Furuya,* Central Res. Inst., Mitsubishi Materials Corp., Omiya, Saitama 330, Japan, *H. Abe*, Mitsubishi Materials Silicon Corp., Noda, Chiba 278, Japan, and *T. Shingyouji,* Central Res. Inst. Mitsubishi Materials Corp., Omiya, Saitama 330, Japan

The effect of bulk microdefects induced in silicon by heat-treatment on the leakage current of pn junctions have been investigated. The effect of bulk microdefects under the depletion region can be explained quantitatively by considering the diffusion equation of minority carriers. When bulk microdefects are incorporated within the depletion region, the generation component increases markedly, and the effect of OSF dominates rather than the effect of oxygen precipitates.

263 Reduction of Epitaxial Stacking Faults Formed at the Edge of the N+ Buried Layer: S. Nagalingam, *K. Briggs, D. Jacy,* and *D. Massetti,* Silicon Systems, Inc., Santa Cruz, CA 95060

In developing a defect-free epitaxial (epi) layer we have observed the generation of epi stacking faults at the edge of the N+ buried layer. These defects appear to form as a result of the different epitaxial regrowth rates of the various crystal planes bounding the laterally confined amorphous layer which is formed by the high dose buried layer implant. The density of these epi stacking faults can be reduced by either annealing the heavily implanted buried layer in an N_2 only ambient prior to oxidation or by etching 1200 A of the silicon surface with an HCl etch prior to epi growth.

264 Hydrogen Annealing of Silicon Wafer: *S. Samata, M. Numano, T. Amai,* and *Y. Matsushita,* Semiconductor Manufacturing Engineering Center, Toshiba, 72 Horikawa-cho, Saiwai-ku, Kawasaki-shi, Kanagawa, 210, Japan; *H. Kobayashi, A. Yamamoto,* and *T. Kawaguchi,* Semiconductor Manufacturing Engineering Center, Toshiba, 1 Komukai Toshiba-cho, Saiwai-ku, Kawasaki-shi, Kanagawa 210, Japan, *S. Nadahara* and *K. Yamabe,* ULSI Laboratory, Toshiba, 1 Komukai Toshiba-cho, Saiwai-ku, Kawasaki-shi, Kanagawa 210, Japan

High temperature hydrogen annealing of Si was studied. Surface BMD was drastically reduced by hydrogen annealing. The effect of oxide breakdown failure reduction by hydrogen annealing lasted through device fabrication process. Using silicon wafer without oxide breakdown failure achieved by hydrogen annealing, relation between surface microroughness and TDDB was studied, and it was concluded that surface microroughness affected mean time to failure of constant voltage TDDB. Oxygen precipitation was formed in hydrogen annealed wafer.

Tuesday AM

265 Reliability Issues Due to Hot-Electron Effects in GaAs-Based MESFETs and HEMTs: *E. Zanoni, C. Tedesco, A. Neviani,* and *G. Meneghesso,* Dipt. di Elettronica e Informatica, Univ. di Padova, 35131-Padova, Italy

In submicrometer GaAs MESFETs and HEMTs hot-electron phenomena can induce several detrimental effects, possibly affecting the reliability of these devices. In particular, impact-ionization effects can trigger device breakdown and burnout, cause an unacceptable increase in drain current or induce kinks in the I-V characteristics. We show that hot-electron phenomena can be characterized by measurements of the impact-ionization induced gate current and by spectroscopic analysis of the radiation emitted by the devices. Permanent degradation effects are observed in unpassivated and SiO_2-passivated devices after hot-electron accelerated tests, inducing decrease in drain current and increase in drain parasitic resistance and in transconductance frequency dispersion.

266 Temperature Dependent Performance Simulation and Failure Mechanisms of Heterostructure Field Effect Transistors and Inverter Circuits: *J.-S. Kuo* and *A. Christou,* CALCE Electronics Packaging Research Center, University of Maryland, College Park, MD 20742

A model for the temperature dependence of current-voltage characteristics of the AlGaAs/GaAs heterostructure field-effect transistor is developed. The temperature dependence of forward-transfer characteristics of two different HFET-based inverters are analyzed by the developed temperature dependent model and AIM-SPICE. The current-voltage characteristic collapses caused by the failure mechanisms, such as AlGaAs/GaAs interdiffusion and gate degradation, are simulated with the developed temperature dependent model.

267 Study of SiO_2/InP Structure Prepared by Direct Photo Chemical Vapor Deposition: *Y. K. Su, S. C. Shei, C. J. Hwang,* and *M. Yokoyama,* Dept. of Electrical Engineering, National Cheng Kung Univ., Tainan, Taiwan, China

281 Temperature-Dependent Electron-Beam-Induced Current Studies of MOS Capacitor Structures: *H. R. Kirk, J. G. Park,* and *G. A. Rozgonyi,* Dept. of Mat. Sci. & Eng., North Carolina State Univ., Raleigh, NC 27695-7916; and *D. M. Lee,* MEMC, St. Peters, MO 63376

A temperature dependent analysis of MOS capacitors used as EBIC probes of the defect electrical properties of the bulk Si, Si/SiO_2 interface, and the SiO_2 layer is presented. Three sources of EBIC contrast are described: (*i*) localized recombination at extended bulk defects, (*ii*) electron beam enhancement of SiO_2 leakage currents at localized defect sites, and (*iii*) spatial variation of the flatband voltage. New results using MOS/EBIC(T) probes include the study of the electrical activity of near-surface misfit dislocations and the detection of "D" defects at the Si/SiO_2 interface which cause low values of BV_{ox} in DRAM cells.

282 Eliminating Metal-Sputter Contamination in Ion Implanter for Low Reverse-Bias Current, 450°C-Annealed Junction: *K. Tomita, T. Migita, S. Shimonishi, T. Shibata, T. Ohmi,* and *T. Nitta,* Dept. of Electronic Engineering, Faculty of Engineering, Tohoku Univ., Sendai 980, Japan

Metal-sputter contamination caused by a high energy ion beam was found to be proportional to the ion dose, and to degrade the characteristics of low temperature annealed pn junctions. By installing sputtering protection boards made of silicon, metal contamination sputtered behind and in front of the wafer in the ion implanter have been suppressed. As a result, we have successfully formed ultrashallow, low reverse-current pn junctions at an annealing temperature as low as 450°C.

283 Electric Field Effect on FeB/Fe_i Dissociation/Re-association: *H. Kikuchi, A. Agarwal, S. Koveshnikov,* and *G. A. Rozgonyi,* Dept. of Mat. Sci. and Eng., North Carolina State Univ., Raleigh, NC 27695-7916

The dependence of the properties of Fe-contaminated p-type silicon structures on their operation conditions (reverse bias, temperature) has been investigated using DLTS. Fe-B pair dissociation resulting in device degradation has been initiated at room temperature in the presence of a reverse bias. The depth profiles of the Fe_i indicate that enhanced dissociation takes place only within the depletion region. Although the dissociation reaction resulting in device degradation is initiated by an increase in temperature, it can be enhanced and sustained by the electric field, even at room temperature.

THIRD INTERNATIONAL SYMPOSIUM ON CLEANING TECHNOLOGY IN SEMICONDUCTOR DEVICE MANUFACTURING

Electronics/Dielectric Science and Technology

Monday AM

284 Aspects of the Etching of Silicon Dioxide in Fluoride Bearing Solutions: *C. W. Pearce,* AT&T Microelectronics, Allentown, PA 18103, *B. C. Chung,* AT&T Bell Laboratories, Princeton, NJ 08540

This paper overviews various aspects of the wet etching of oxides by solutions containing hydrofluoric acid. In particular, the role of water as a necessary ingredient for the formation of fluoride species in the wet etching process is discussed and contrasted to buffered etch solutions employing ammonium fluoride. Based on the model for the etching of silicon oxides, an etch mechanism for doped and undoped oxides is presented and discussed.

285 Modeling of the Hydrogen Passivation Kinetics of Si in Dilute HF Solutions: *S. Verhaverbeke, M. Meuris, H. Schmidt, P. Mertens,* and *M. Heyns,* IMEC, Kapeldreef 75, B-3001 Leuven, Belgium

When an Si surface with a native oxide is treated in a HF solution to remove the native oxide, the surface is left with a hydrogen passivation. In this paper, the kinetics of this hydrogen passivation formation is modeled. The hydrogen passivation occurs as follows. At first, the native oxide is etched away, then the first monolayer of the Si substrate is etched and as a result the hydrogen passivation occurs. In order to model the hydrogen passivation formation, at first, the SiO_2 etch rate was modeled as a function of the fluoride concentration, and then the Si etch rate was modeled. From this modeling, we could see that the selectivity of the hydrogen passivation formation with respect to the thermal oxide etching improves when lowering the fluoride concentration. This was confirmed experimentally.

286 Hydrogen Passivation of HF-Last Cleaned (100) Silicon Surfaces: An FTIR Study: *H. Bender, S. Verhaverbeke,* and *M. M. Heyns,* IMEC, Kapeldreef 75, B-3001 Leuven, Belgium

HF-last cleanings of silicon result in superior dielectric characteristics. Infrared spectroscopy can yield information on the surface micro-roughness through investigation of the relative amount of mono-, di- and trihydrides and their direction of polarization. The characterization with attenuated total reflection infrared spectroscopy (ATR) of the hydrogen passivation of (100) silicon surfaces is discussed as a function of the chemical treatment (HF/H_2O, HF/isopropylalcohol, BHF). The relative strength of the symmetric and asymmetric dihydride peaks of shown to depend on the pH of the etching solution. The stability of the surfaces against oxidation and the build-up of a CH_x contamination layer during storage of the samples in cleanroom air are studied by time-resolved ATR. A new attenuated total reflection sample preparation method is proposed.

287 HF *In Situ* Tank Used in HF-Last Cleaning: *P. Patruno, D. Levy,* and *A. Fleury,* SGS-THOMSON Microelectronics, 38192 Crolles, France, *A. Tonti,* SGS-THOMSON Microelectronics, Agrate Brianza, Italy, and *F. Tardif,* LETI, CEA, Grenoble, France

The effect of a wet chemical cleaning process used as HF-last cleaning in an automated wet bench, is investigated, in a special tank design incorporating the capability for *in situ* displacement by DI water of extremely diluted solution of HF. The performance of this tank is compared to the one we get on a conventional acid tank associated to its dedicated rinse tank to which the wafers are transferred. Surface microroughness (AFM), chemical contamination (TXRF) are measured. Particle contamination with a laser particle counter, lifetime of minority carrier (SPV) and contact angle are monitored as well.

288 Effect of HF-Last Clean Process Sequence on Gate-Oxide Quality: *D. Dimitrelis, L. Kroonblawd, G. Harper, H. Conte,* and *E. deMuizon,* VLSI Technology, Inc., San Jose, CA 95131

We measured the dependence of the electrical breakdown yield of 1.2-mm^2 17.5-nm-thick polycide/oxide/silicon capacitors on the process sequence of the HF-last clean prior to the gate oxidation. We discuss the effects of chemical purity, rinse, and drying process on gate-oxide quality. The gate-oxide quality has been determined by breakdown yield under stress in fields in excess of 7.5 MV/cm. Use of ultrahigh purity hydrofluoric acid for the wet clean results in a twofold increase in electrical breakdown yield. Subsequent deionized-water cascade-overflow rinse results in a tenfold decrease in particle density when compared with a dump-rinse increasing electrical breakdown yield by approximately 10%. The final drying process (spin/rinse or IPA-vapor) does not appear to affect electrical breakdown yield.

289 Contamination Reduction in Dilute HF by Adding HCl: *I. Oki, H. Shibayama,* and *A. Kagisawa,* Sharp Corp., VLSI Research Laboratories, 2313-1 Ichinomoto-cho, Tenri City, Nara 632, Japan

We have shown the following advantages of Si wafer cleaning by HCl added dilute HF. (*i*) The adhesion of particles and impurity metals from solution is suppressed. (*ii*) The cleaning efficiencies of metallic contaminants on Si surface are improved. The oxidation of Si surface by HCl and the oxide etching by HF are considered to be the main reason for these advantages which results in reliability improvement of thin oxide films.

Monday PM

290 Effects of Residual Iron Contamination Introduced during Wet Chemical Processing on Thin Oxide Breakdown and Reliability Characteristics: *W. B. Henley, L. Jastrzebski,* and *N. F. Haddad,* Center for Microelectronics Research, Univ. of South Florida, Tampa, FL 33620

The effects of residual iron contamination introduced during wet chemical processing on subsequent thermal oxide characteristics are investigated. Empirical and modeling studies describing the effects of iron contamination on the breakdown and reliability characteristics of thin silicon gate oxides is studied. Iron concentration is measured using a diffusion length technique applicable to real-time line monitoring. The density of gate oxide weak spots is given as a function of iron contamination level for oxide thicknesses ranging from 75 to 200 Å. Reduction of oxide thickness from 20 to 10 nm requires a reduction in iron contamination by 100 times. Iron contamination limits concerning gate oxide integrity are established.

291 Surface Recombination Velocity and Recombination Lifetime in Iron-Contaminated Silicon: *A. Buczkowski, F. Shimura,* and *G. A. Rozgonyi,* Dept. of Mat. Sci and Eng., North Carolina State Univ., Raleigh, NC 27695-7916

A theoretical simulation of available experimental data on recombination lifetime and surface recombination velocity in silicon samples contaminated with iron has been performed. Both n-type and p-type samples have been studied based on experimental data, determined primarily by deep level transient spectroscopy and photoconductance decay, for samples intentionally doped with iron. Differences observed for n- and p-type silicon, as well in the absolute value of bulk lifetime and the surface recombination velocity, along with their temperature dependencies, are explained. The effect of iron contaminants present in concentrations typical of modern silicon device material has been evaluated by comparing the theoretical lifetime results to the experimental data. Finally, the problem of true bulk lifetime determination by transient photoconductance is discussed in terms of the total recombination process which proceeds via both bulk and surface recombination centers.

292 Metal Contamination Monitoring in a Semiconductor Manufacturing Environment: *E. E. Fisch,* IBM Technology Products, Essex Junction, VT 05452

A repeatable accurate method for monitoring metal contamination introduced by silicon wafer cleaning was developed and tested in a manufacturing environment. It is based on diffusion length mapping using the commercially available electrolytic metal tracer (ELYMAT). Decreased diffusion lengths are an excellent indicator of the presence of metal bulk contamination. Quantitative comparisons with total reflection x-ray fluorescence spectroscopy (TXRF) on intensionally iron-contaminated wafers and extensive in-line monitor tests were used to develop the final monitoring method. Its advantages include reproducibility to less than 5%, cleanliness of the measurement, monitor reuse, and high resolution wafer maps which often provide diagnostic clues to the metal contamination origin.

293 Control of Manufacturing Cleaning Operations Using Surface Photovoltage Techniques: *A. M. Hoff,* Cntr. for Microelectron. Res., Univ. of S. Florida, Tampa, FL 33620-5350 and *E. J. Persson, J. Chacon,* and *B. DeSelms,* AT&T Microelectronics, Orlando, FL 32819

The use of surface photovoltage (SPV) techniques to monitor and control spray processor cleaning in a manufacturing environment is described. The principal advantages of the SPV technique are that it provides short-loop feedback on process quality and that the fabrication of electronic test structures is not required. Results from the implementation of SPV monitoring techniques show that iron contamination may be tracked and controlled at a sensitivity level well below that required by ULSI technologies.

294 Heavy Metal and Organic Cleaning Efficiency Optimization and Monitoring for Real-Time, In-Line Process Control by Surface Photovoltage: *L. Jastrzebski* and *W. Henley,* Cntr. for Microelectronics, Univ. of South Florida, Tampa FL 33620, *J. Lagowski,* Semiconductor Diag-

309 Effects of Surface Iron on Recombination Lifetime and Its Removal from Silicon Surfaces: *H. Park* and *C. R. Helms,* Stanford Electronics Lab., Stanford Univ., Stanford, CA 94305 and *M. Trans* and *B. B. Triplett,* Intel Corp., Santa Clara, CA 95052-8125

Experiments on photoconductivity recombination lifetime of the wafers showed a very low lifetime for silicon wafers with SC1-last surfaces, a relatively high lifetime for silicon wafers with SC2-last surfaces, and a high lifetime for silicon wafers with HF-last surfaces. In addition, vacuum-evaporated iron caused a severe degradation in the lifetimes irrespective of the cleans used, indicating lifetime degradation is related to initial iron concentration, not merely to final iron concentration after cleaning.

310 The Relation Between Sodium Contamination and Dielectric Breakdown in MOS Structures: *B. Vermeire, S. Verhaverbeke, P. W. Mertens,* and *M. M. Heyne,* IMEC, B-3001 Leuven, Belgium

The effect of a low level (10^{11} atom/cm^2) of sodium contamination on the gate oxide characteristics was investigated. Some sodium was removed during oxidation. The remaining sodium correlates well with the mobile charge observed in the oxide. No influence was found on the current-voltage characteristics and only a minor effect on the breakdown distribution on Epi-wafers could be noted for the contamination levels under investigation. A tail in the charge-to-breakdown (Q_{BD}) Weibull plots is found for the Na-contaminated epitaxial wafers, which indicates that Na can cause reliability problems. This tail is not seen for Cz-wafers where other defects mechanisms are important.

311 Control of Native Oxides on Deep-Submicron Contact-Hole-Bottom Surfaces: *N. Aoto, M. Nakamori,* and *H. Hada,* ULSI Device Development Laboratories, NEC Corp., 1120 Shimokuzawa, Sagamihara, Kanagawa 229, Japan, *T. Kun*io, Microelectronics Research Laboratories, NEC Corp., 1120 Shimokuzawa, Sagamihara, Kanagawa 229, Japan, *Y. Teraoka* and *I. Nishiyama,* Optoelectronics Research Laboratories, NEC Corp., 34 Miyukigaoka, Tsukuba, Ibaraki 305, Japan and *E. Ikawa,* ULSI Device Development Laboratories, NEC Corp., 1120 Shimokuzawa, Sagamihara, Kanagawa 229, Japan

The effects of cleaning and treatments on contact-hole bottom Si surfaces were investigated by XPS and TDS. Suboxide-rich native oxides are formed on dry-etch-damaged Si surfaces and are removed by chemical dry etching (CDE). The suboxide-rich native oxide layers still exist after DHF treatment, resulting in high contact resistance. After the oxide removal, native oxidation of the bottom Si surfaces immediately occurs under clean-room air exposure, while oxidation is suppressed in N_2 atmosphere.

Tuesday PM

312 Prevention of Particle Deposition in HF Solution: *A. Saito, K. Ohta, H. Itoh,* and *H. Oka,* Production Engineering Research Laboratory, Hitachi, Ltd. 292 Yosida-cho, Totsuka-ku, Yokohama 244, Japan

It is a serious problem for LSI fabrication that particles very easily adhere to the Si wafer in hydrofluoric acid (HF) solution. We have clarified that it is because the zeta potential of the Si wafer and particle becomes high. As one example of our technology "zeta potential control", we have developed a new method using anionic surfactants. When the surfactant is added to the HF solution, the number of deposited particles becomes less than one fifth.

313 A New Method for Simultaneous Characterization of Process Cleanliness and True Particle Removal Efficiency: *N. E. Henelius* and *O. J. Anttila,* Okmetic Ltd., Sinimäentie 12, FI-02630 Espoo, Finland and *H. Ronkainen* and *J. M. Molarius,* VTT Semiconductor Laboratory, Olarinluoma 9, FI-02200 Espoo, Finland

Many experiments in wafer cleaning technology rely on comparing wafer particle counts before and after processing steps. The number of particles often change dramatically, but there are more difficult cases where the variations appear slight. They need to be analyzed in greater detail by separating the effects of true particle removal efficiency and process cleanliness. A new method for rapidly accomplishing this, utilizing powerful PC-based software and a modern light point defect counter, is presented here for the first time. Other applications related to crystal material quality include improved analysis of COPs, stacking faults and carrier lifetime.

314 Electrokinetic Characteristics of Nitride Wafers in Aqueous Solutions and Their Impact on Particulate Deposition: *D. Jan* and *S. Raghavan,* Materials Science Dept., Univ. of Arizona, Tucson, AZ 85721

The electrokinetic characteristics of LPCVD and PECVD silicon nitride films cleaned in aqueous solutions of interest to semiconductor processing have been measured using a streaming potential technique. The results show that the isoelectric point of the nitride films is sensitive to the cleaning treatment. The pH dependence of PSL particle deposition on the wafers follows the zeta potential-pH profile of the wafers indicating the importance of electrostatic interactions in particulate contamination.

315 Particulate Evaluation of Post-Ash Cleaning: *S. D. Hossain* and *M. F. Pas,* Texas Instruments, 0.5 μm Process Engineering, Semiconductor Group, Dallas, TX 75243

Particulate evaluation of wet cleaning processes using SCI (NH_4OH:H_2O_2:H_2O) at 50, 60, and 80°C is reported for post-ash silicon wafer cleaning. The ratio of SCI used is 1:2:10 for this work. Using various sequences with and without heated SCI, a comparison is made of particulate removal. These particulates originate from position implant or plasma etch, and O_2 ash steps in device processing. Particle evaluation is done using the ESTEK WIS-8500. Using sequences of heated SCI, ozonated piranha baths (O_3/P), acid spray piranha solutions (P), room temperature SCI with megasonic (SCI), and HF cleaning, results are obtained showing the effectiveness of these sequences on particulate removal. The data show O_3/P to have the lowest defect density removal of efficiency relative to all other processes studied. The defect density removal of heated SCI increased as the temperature of SCI is increased for both ion-implanted and plasma-etched samples. Defect densities are much lower overall for these samples which are etched and ashed than for the ion-implanted samples.

316 A Design of Experiments Approach to an Optimized SC-I/Megasonic Clean for Sub 0.15 Micron Particle Removal: *P. J. Resnick, C. L. J. Adkins, P. J. Clews, E. V. Thomas,* and *S. T. Cannaday,* Sandia National Lab., Albuquerque, NM 87185

A statistical design of experiments approach has been employed to evaluate the particle removal efficacy of the SC-I/megasonic clean for sub 0.15 μm particles. The effects of megasonic input power, solution chemistry, bath temperature, and immersion time have been investigated. Immersion time was not observed to be a statistically significant factor. The NH_4OH/H_2O_2 ratio was significant, but varying the molar H_2O_2 concentration had no affect on inorganic particle removal. Substantially diluted chemistries, performed with high megasonic input power and moderate-to-elevated temperatures, can be effective for small particle removal.

317 Behavior of Ultrafine Metallic Particles (*ca.* ~10 nm) on Silicon Wafer Surfaces: *H. Morinaga, T. Futatsuki, T.A Ohmi, E. Fuchita, M. Oda* and *C. Hayashi,* Dept. of Electronics, Faculty of Engineering, Tohoku University, Aramaki, Aoba-ku, Sendai 980, Japan

Ultrafine particles (UFP) with diameters of several to several hundreds of nanometers were adhered onto the Si surface and the removal efficiency of the UFPs using various cleaning solutions was investigated. It has been found that the conventional cleaning methods are unacceptable at removing Au UFPs with diameters of less than several tens of nanometers. In addition, it has been found that particle removal by chemical etching, such as DHF-H_2O_2, causes increased surface roughness due to local chemical reactions.

318 Separate Detection of Particles and Bubbles in Liquid: *K. Takeda, Y. Itoh,* and *A. Hiraiwa,* Central Research Laboratorty, Hitachi, Ltd. Kokubinji, Tokyo 185, Japan, *K. Yasuda,* Advanced Research Laboratory, Hitachi, Ltd. Hatoyama, Saitama 350-03, Japan and *K. Suda,* Hitachi Electric Engineering, Co. Ltd. Kanda, Tokyo, 100, Japan

We developed a novel liquid-phase particle counting technology for monitoring deionized water and cleaning solution used in deep submicron LSI process. This technology separately detects particles from bubbles in liquids, and has a sensitivity of detecting 38 nm particles. It is based on electrophoresis and light scattering, and was proven effective by experiments with ultrasonically generated bubbles.

Wednesday AM

319 Chemical Vapor Cleaning Technologies for Dry Processing in Semiconductor Manufacturing: *D. A. Bohling, S. E. Beck, B. S. Felker, A. G. Gilicinski, J. C. Ivankovits, J. G. Langan,* and *S. W. Rynders,* Air Products and Chemicals, Inc., Allentown, PA 18195, *J. A. T. Norman, D. A. Roberts,* and *G. Voloshin,* Schumacher Co., Carlsbad, CA 92008, M. A. George and *D. M. Hess,* Lehigh University, Bethlehem, PA 18015, and *A. Lane,* Texas Instruments, Dallas, TX 75265

Chemical vapor cleaning is a methodology for removing metallic contamination from semiconductor surfaces. It is the process where a gas phase coordinating or chelating ligand reacts with a surface metal species and forms a volatile coordination compound. This metal coordination compound then desorbs from the surface at relatively low temperatures. This paper reviews the processing issues surrounding chemical vapor cleaning and describes current results and trends for this technology area.

320 The Effects on Surfaces of Silicon and Silicon Dioxide Exposed to 1,1,1,5,5,5-Hexafluoro-2,4-Pentanedione: *S. E. Beck, A. G. Gilicinski, B. S. Felker, J. G. Langan, D. A. Bohling,* and *J. C. Ivankovits,* Air Products and Chemicals, Inc., Allentown, PA 18195-1501 and *M. A. George,* Dept. of Chemical Engineering, Lehigh Univ., Bethlehem, PA 18015

This study explores the effects of chemical vapor cleaning (CVC) with 1,1,1,5,5,5-hexafluoro-2,4-pentanedione (hfac) on surface roughness and chemical by-products deposited on the surfaces of Si and SiO_2. These surfaces are not significantly roughened due to their exposure to hfac. We did find that fluorine is deposited on the surfaces during treatment. The fluorine may not be from the hfac ligand, but may be from impurities within the reagent.

321 Reaction of 1,1,1,5,5,5-Hexafluoro-2,4-Pentadione (HFAC) with Surfaces of CuO and Cu_2O Studied by X-Ray Photoelectron Spectroscopy: *M. A. George* and *D. W. Hess,* Dept. of Chemical Engineering, Lehigh Univ., Bethlehem, PA 18015, *S. E. Beck, J. C. Ivankovits, D. A. Bohling,* and *B. S. Felker,* Air Products and Chemicals, Inc., Allentown, PA 18195, and *A. P., Lane,* Texas Instruments, Dallas, TX 75265

X-ray photoelectron spectroscopy (XPS) was used to study the interaction of hexafluoroacetylacetonate (1,1,1,5,5,5-hexafluoro-2,4-pentanedione or HFAC) with copper oxide (Cu_2O and CuO) surfaces. This study shows that similar mechanisms are responsible for the creation of a volatile metal-organic coordination compound ($Cu(HFAC)_2$) on CuO and Cu_2O. However an additional reaction pathway is found in the interaction with Cu_2O, which leaves $Cu^{(0)}$ metal on the surface. These mechanisms are important to chemical vapor etching and chemical vapor cleaning processes based on HFAC chemistry, both of which exploit these chemical reactions.

322 Removal of Al from Silicon Surfaces Using UV/Cl_2: *C. Daffron, K. Torek,* and *J. Ruzyllo,* Electronic Materials and Processing Research Laboratory, The Pennsylvania State University, University Park, PA 16802 and *E. Kamieniecki,* QC Solutions, Inc., Lexington, MA 02173

A gas-phase UV/Cl_2 cleaning process applied using a commercial dry cleaning module has demonstrated the ability to remove aluminum contaminant from a silicon wafer surface. The greatest amount of aluminum removal

resistance of anhydrous HF/CH_3OH etched surfaces was found to be sensitive to process parameters.

337 Comparison of Vapor-Phase and Wet Chemical Pregate Oxide and Precontact Cleans: *C. W. Draper* and *V. E. Anyanwu,* AT&T Engineering Research Center, Princeton, NJ 08542-0900, *J. H. Eisenberg, G. J. Felton, P. K. Roy, S. Chittipeddi*, and *P. F. Bechtold,* AT&T Bell Laboratories, Allentown, PA 18103, *G. Hagner*, *D. Cooper,* and *D. Syverson,* FSI International Chaska, MN 55318-1096, *B. Witowski, B. Van Eck* and *M. Gordon,* SEMATECH, Austin, TX 78741.

We report the results of an evaluation comparing wet chemical and vapor-phase cleaning at the pregate oxide and precontact levels. The gate oxide is a 9 nm, 0.35 μm CMOS application, while the precontact clean is at the titanium silicide level in advance of the titanium and aluminum alloy thin film depositions. The vias are 1 μm in diameter with BPTEOS and TEOS dielectrics. Results for zone tester lots indicate that equivalent or superior performance can be achieved with the vapor-phase clean.

338 Cleaning of Silicon Surface after RIE Using UV/Ozone and HF/CH_3OH: *D. K. Hwang* and *J. Ruzyllo,* Electronic Materials Processing and Research Laboratory, The Pennsylvania State University, University Park, PA 16802 and *E. Kamieniecki,* QC Solutions, Inc., Lexington, MA 02173

Polymer-like films deposited by a CHF_3/O_2 RIE can be effectively removed by a UV/ozone clean followed by a HF/CH_3OH etch. The UV/ozone and HF/CH_3OH process were performed *in situ* using a prototype cluster tool compatible commercial apparatus. XPS results show that amount of carbon and fluorine at the Si surface following the clean has been greatly reduced SCA results indicate that the RIE processed and unprocessed surfaces following the UV/ozone and HF/CH_3OH clean were similar.

339 Removal of Fe and Al by Pyrochemical Cleaning: *Y. Limb, B. Y. Nguyen,* and *P. Tobin,* Motorola Inc., APRDL, Austin, TX 78721

A new HCl-based thermal cleaning process which we call pyrochemical cleaning was developed. The cleaning efficiency of this new cleaning process was examined by intentionally introducing contaminants on the wafer surface and measuring with a total reflection x-ray fluorescence (TXRF) spectrometer the residual contaminant concentration after the cleaning. The results showed that the new cleaning process is effective in removing metallic contaminants including Fe and Al. The reliability of Al-contaminated gate oxide dramatically improved when pyrochemical cleaning was utilized.

340 The Interaction of Hydrogen, H, Plasmas with Ga-Baed III-V Semiconductor Surfaces: *Z. Lu, S. Habermehl, N. Deitz, G. Lucovsky,* and *K. J. Bachmann,* North Carolina State University, Raleigh, NC 27695-8202 and *R. M. Osgood, Jr.,* Columbia Univ., New York, NY 10027

This paper describes the interaction of H-plasmas with Ga-baed semiconductor (GaAs, GaP, GaSb) surfaces. Surface sensitive techniques such as AES, XPS, and LEED are used *in situ* to characterize these surfaces in integrated ultrahigh vacuum processing systems. Our results consistently demonstrate: (*i*) a significant reduction of surface carbon and oxygen; as well as (*ii*) surface ordering on the aforementioned surfaces after interaction with the H-plasma. Changes in surface band bending are correlated with passivation and damage by exposure to the H-plasma.

Thursday AM

341 A New Cleaning Concept for Particle and Metal Removal on Si Surfaces: *M. Meuris, S. Verhaverbeke, P. W. Mertens, H. F. Schmidt, A. Rotondaro,* and *M. M. Heyns,* IMEC, B-3001 Leuven, Belgium and *A. Philipossian,* Digital Equipment Corp., Hudson, MA 01749

The IMEC-clean concept is proposed. It is a simple two-step cleaning. In the first step a chemical oxide of about 1.5 nm is grown. In the second step this chemical oxide is removed, providing the cleaning action by undercutting and lift-off of the particles. It is demonstrated that the IMEC-clean has a high particle and metal removal efficiency, combined with a minimal Si surface roughness. This results in excellent dielectric breakdown performance of gate oxides grown after this cleaning treatment.

342 Prevention of Microroughness on the Si Wafer Surface in Buffered Oxide Etchant by a Surfactant Addition: *M. Miyamoto, N. Kita, S. Ishida,* and *T. Tatsuno,* Morita Chemical Industries Co., Ltd., Yodogawa-ku, Osaka, 532, Japan

The generation of microroughness on the Si wafer surface in buffered oxide etchant (BOE) was prevented by several 10 ppm additions of surfactant. The prevention effect is caused by the surfactant molecules which suppress the dissolution of Si into BOE from Si wafer. The microroughness was suppressed by lowering NH_4F concentration in BOE.

343 Ultrathin Oxide Formation Using Chemical Oxide Passivation: *K. Nakamura, T. Futatsuki, K. Makihara,* and *T. Ohmi,* Dept. of Electronic Engineering, Faculty of Engineering, Tohoku Univ., Sendai 980, Japan

We have investigated electrical characteristics of metal oxide semiconductor (MOS) diodes with ultrathin oxide films including the chemical oxides used as a passivation film of silicon surface. The ultrathin oxide films including the chemical oxides formed in sulfuric acid-hydrogen peroxide mixture (SPM), O_3/H_2O, and hot H_2O_2 are superior to those including the chemical oxides formed in APM and hydrochloric acid-hydrogen peroxide-water mixture (HPM) in reliability. The chemical oxides formed by different methods are different in the etching rate of oxide.

344 Peculiarities of Hot Phosphoric Acid Used in the Etching of Silicon Nitride: *W. Syverson* and *M. J. Fleming,* IBM Technology Products, Essex Junction, VT 05452

The etching of silicon nitride using hot phosphoric acid is a common practice among many semiconductor producers. Although the process appears straightforward, knowledge of the actual mechanics and peculiarities of the process is typically limited. This paper details the aspects of chemical transformations during heating, the importance of DI water makeup, nitride and oxide etch rates, acid contaminant levels, and wafer foreign material levels as well as the importance of adequate DI water rinsing of the wafers after exposure to phosphoric acid.

345 Impact Study of the Use of ULSI, VLSI, and and MOS, Grade Chemicals in the RCA Cleaning Process on MOS and Bipolar Devices: *F. Tardif, J. P. Joly,* and *T. Lardin,* LETI (CEA-Technologies Avancées), F38041 Grenoble Cedex, France, *A. Tonti, P. Patruno,* and *D. Levy,* SGS/Thomson, F38190 Crolles, France, and *W. Sievert,* Riedel-de Haën, D3016 Seelze-1, Germany

The use of commercial metal oxide semiconductor (MOS), very large scale integration (VLSI), and ultralarge scale integration (ULSI) grade chemicals in the RCA cleaning process are evaluated here in terms of MOS minority carrier lifetimes and of 7 nm dry gate oxide yield. In these tests, the generation lifetime is clearly correlated to the purity of the chemicals used during the last cleaning step before oxidation (SC2). The results obtained on 7 nm thin dry oxide show that defectivity is affected in the first order by the particles present before oxidation.

346 Contamination Removal by a Wafer Spin Cleaning Process with an Advanced Chemical Distribution System: *N. Yonekawa, S. Yasui, F. Kunimoto, F. W. Kern, Jr.,* and *T. Ohmi,* Dept. of Electronic Engineering, Faculty of Engineering, Tohoku Univ., Sendai 980, Japan

We describe our study on the single-wafer spin cleaning system. The spin cleaning process was evaluated in comparison with the batch process. The metal removal test has revealed that cleaning time and chemical consumption are reduced drastically in the spinning method, compared with the batch method. The spin cleaning efficiency is dependent on two parameters: chemical flow rate and cleaning time. The spinning method has proved effective in removing organic impurities and particles.

347 Characterization of Quick Dump Megasonic Cleaner for VLSI Planarization RIE Post-Clean Process: *P. Wang* and *D. Bell,* Motorola, Mesa, AZ 85202

In this study, megasonic cleaning was applied to the multilevel metal planarization RIE etchback process. The characterization of a newly designed quick dump megasonic cleaner for VLSI post-planarization RIE treatment was studied. A new megasonic cleaning process with optimized parameter conditions were obtained. The new process significantly reduced the planarization post-cleaning defectivity level. The results were confirmed by patterned planarization monitor wafer inspection, and the yield of snake/comb wafers.

348 The Effect of HI-Cleaning Prior to Silicon Wafer Bonding: *Y. Backlund, K. Ljungberg,* and *A. Söderbärg,* Dept. of Technology, Electronics Div., Uppsala Univ., S-75121 Uppsala, Sweden

We have studied the effects of different aqueous HF-etches on the initial bonding of silicon wafers. The surface morphology was characterized by atomic force microscopic (AFM) and electron spectroscopic for chemical analysis (ESCA) measurements and is strongly dependent on the HF-etch procedure. The best result for a spontaneous and voidless bond is to use a 10% HF-solution without a subsequent water rinse. Water rinsing yields rougher surfaces and introduces particles. Etching in a buffered HF-solution was destructive for the bond process.

349 The Effect of Dissolved Oxygen and Dissolved Ozone in Ultrapure Water on N^+-Doped Polyerystalline Silicon to N^+-Doped Crystalline Silicon Contact Resistance: *M. J. Satterfield, B. Anthony, G. Huffman,* and *F. Walczyk,* Motorola, Inc., Austin, TX 78721

The effect of dissolved oxygen and dissolved ozone has been studied on integrated N^+-doped polycrystalline to N^+-doped crystalline silicon contact resistance devices. Dissolved ozone in concentrations of 15 ppb or higher sharply increases the contact resistance of this structure. Dissolved oxygen in concentrations as high as 3 ppm has no statistical effect on the contact resistance of this structure.

Thursday PM

350 Silicon Surface-Roughening by the Decompositon of Hydrogen Peroxide: *H. F. Schmidt, M. Meuris, P. W. Mertens, S. Verhaverbeke,* and *M. M. Heyns,* IMEC, B-3001 Leuven, Belgium, *L. Hellemans* and *I. Snauwaert,* Lab. Chem. Biolog. Dynamica, Katholieke Universiteit Leuven, B-3001 Heverlee, Belgium, and *K. Dillenbeck,* Ashland Chemical Inc., Columbus, OH 43216

The decomposition of hydrogen peroxide is a problem for the stability and therefore the suitability of hydrogen peroxide based cleaning solutions in the semiconductor industry. Nonuniform attack of the silicon surface happens especially in the SCI step of the widely used RCA-cleaning procedure. The effect of hydrogen peroxide decomposition is correlated to wafer surface-roughening by light-scattering studies, AFM, and SEM measurements. Also direct correlations between gate oxide integrity and decomposition roughness are presented.

351 A Study of Various Pretreatments and Their Effect on Electrical Characteristics of Subsequently Grown Film: *K. Morinville, R. Kauffman, R. C. Hawthorn,* and *D. Korn,* Micron Semiconductor, Boise, ID 83709

As device geometry shrink and dielectric films become thinner, the surface condition of the wafers prior to the growth/deposition of subsequent films becomes more relevant. In the past, cleans were optimized for strictly particle performance and ionic contamination. Surface roughness was not considered as important, nor was it measurable. We investigate here new ways of conditioning the surface prior to the growth/deposition of thin dielectric films.te

provided where battery specific energy and specific power requirements are bounded for three classes of electric vehicles over ranges of vehicle acceleration, range, and battery mass fraction.

366 Electric Vehicle Battery Performance Projections from Research Cell Measurements: *L. Redey, T. Rauworth, J. Prakash,* and *D. R. Vissers,* Argonne National Lab., Argonne, IL 60439

A method that combines physical and mathematical modeling has been developed and used successfully to measure performance parameters of small engineering research cells that are needed for performance calculations and to calculate performance of full-size battery designs from the measured values. The method is useful for R&D of various battery systems and provides an expedient means for reliable performance merit analysis of battery designs and performance projections. Considerable time and cost savings can be achieved because the method minimizes the need for fabrication of an experimentation with full-size cell design options. The paper describes results with $Na/NiCl_2$ cells as an example.

367 Abusive Testing of Ovonic Nickel-Metal Hydride Electric Vehicle Batteries: *D. A. Corrigan, S. Venkatesan, M. A. Fetcenko, S. K. Dhar,* and *S. R. Ovshinsky,* Ovonic Battery Co., Troy, MI 48084

Tolerance to electrical abuse is a key criterion for modern electric vehicle applications where string voltages can exceed 300 V. The unique ability of Ovonic nickel-metal hydride batteries to withstand overcharge, through an oxygen recombination mechanism, and overdischarge, through a hydrogen recombination mechanism, has been demonstrated. This operational ruggedness, together with high energy density (80 Wh/kg, 200 Wh/L), high power (200 W/kg), and high cycle life (1000 cycles), makes Ovonic NiMH batteries the enabling technology for electric vehicle.

IONIC AND CONDUCTING POLYMERS AND THEIR APPLICATIONS TO ENERGY TECHNOLOGY

Energy Technology/Battery

Monday AM

368 Nafion 105: Properties and Use in Polymer Electrolytge Fuel Cells: *T. A. Zawodzinski Jr., J. Valerio, M. S. Wilson,* and *S. Gottesfeld,* Electronics Materials and Device Research, Los Alamos National Laboratory, Los Alamos, NM 87545

Nafion 105, a 5 mil thick form of Nafion with EW = 1000 g/eq, has been characterized with respect to water uptake and transport properties and tested in polymer electrolyte fuel cells. The membrane water uptake from the vapor phase is enhanced relative to that of other perfluorosulfonic acid materials. This contributes to high conductivity (roughly 70% greater than Nafion 117) of the membrane exposed to saturated water vapor. Various transport properties of this material are reported.

369 Oxygen Reduction at Electrocoated Nafion-Modified Ni-Carbon Composite Electrodes in Alkaline Solution: The Effect of Temperature: *G. M. Swain* and *B. J. Tatarchuk,* Dept. of Chem. Eng., Auburn Univ., Auburn, AL 36849

Perfluorosulfonic acid ionomer membranes are currently receiving much study due to their ion exchange properties, particularly for use in fuel cells. Nafion™ has received much of the focus in the literature because of its inherent properties which include high oxygen solubility, high chemical stability, and high proton conductivity. The performance of the polymer membrane is highly dependent on the procedure used to clean and coat the film. We report here on the temperature dependence of the oxygen reduction reaction (ORR) in alkaline solution at a novel high surface area, light weight Ni-carbon composite electrode modified with an electrocoated Nafion film. The electrocoating presumably involves an electrostatic attraction between the negatively charged sulfonate ligands of the polymer and the positively charged electrode surface (9 V) producing a higher degree of interfacial contact between the polymer and the electrode. The ORR was studied using linear sweep voltammetry, chronoamperometry, and ac impedance analysis.

370 Catalyzation of Membrane-Electrode Assemblies: *M. W. Verbrugge,* Physical Chemistry Dept., General Motors NAO Research and Development Center, Warren, MI 48090-9055

A method that allows one to selectively electrodeposit catalyst within the thin active layer of a membrane-electrode assembly is described. The method is based on the unique chemistry of the membrane/gas-diffusion-electrode interface, where metal deposits tend to concentrate if dilute-electrolyte solutions are used for deposition; it is the membrane/gas-diffusion-electrode interfaces that form the active layers in a membrane-electrolyte fuel cell. Examples of copper and platinum deposition from aqueous solutions of copper sulfate and tetrammine platinum (II) chloride, respectively, demonstrate the generality and effectiveness of the method. Electron probe microanalysis, backscattered electron images, and electrochemical experiments are used to characterize the catalyzed membrane-electrode assemblies.

371 Elucidation of Mass-Transport Phenomena in H_2/Air PEMFCs by Analysis of Dependence of Performance on Platinum Loading: *A. C. Ferriera* and *S. Srinivasan,* Cntr. for Electrochem. Sys. and Hydrogen Res., Texas A&M Univ., College Station, TX 77843-3402

A major challenge in proton exchange membrane fuel cell technology, particularly for the electric vehicle application, is to attain the desirable power densities (at least 0.35 W/cm^2) with H_2/air as the reactants at atmosphere pressure. The main problem in attaining this goal is that mass-transport overpotentials (*i*) increase the slope of the linear region of the cell potential *vs.* current density plot, and (*ii*) cause a departure from linearity of this plot at a current density of about 500 mA/cm^2. We focus on an elucidation of the effect of Pt loading (low and high) on the mass-transport behavior. The results show that with increase of Pt loading there is (*i*) an increase of the open-circuit potential; (*ii*) an increase of the exchange current density for oxygen reduction; (*iii*) a decrease in the slope of the linear region of the **E** *vs.* **i** plot; and (*iv*) an increase in the current density at which departure from linearity occurs in this plot. This behavior is akin to the effect of increase of pressure in respect to reduction in mass-transport limitations and can be rationalized on the basis of enhancing the kinetics of oxygen reduction, by increasing the sites for the reaction and by increasing the partial pressure of oxygen.

372 Microelectrode Investigation at the Pt/Aciplex-S Membrane Interface: O_2 Reduction Kinetics, Mass Transport, and Ohmic Parameters: *M. Wakizoe, S. Srinivasan, A. Parthasarthy,* Cntr for Electrochem. Sys. and Hydrogen Res., Texas A&M Univ., College Station, TX 77843-3402

Microelectrode technique was developed previously in our laboratory to determine the electrode kinetics parameters for oxygen reduction, mass-transport parameters for oxygen, and the conductivities of membranes from cyclic voltammetric and chronoamperometric measurement at the Pt/Nafion-117® interface. This method was applied for determination of the parameters at the Pt/Aciplex®-S membrane interface. The results reveal similar values on the Tafel parameters for oxygen reduction at the Pt/Nafion interface. However, there are differences in the mass-transport parameters. The values of the diffusion coefficient for oxygen are higher for Aciplex-S membrane than for Nafion, but the reverse is the case in the value of solubilities. The value of the product dc is twice as high for Aciplex-S membrane as for Nafion membrane. Studies are in progress to make a more detailed analysis of these parameters at the Pt/Aciplex-S membrane, as was done for the Pt/Nafion interface.

Tuesday AM

373 Design and Synthesis of p- and n-Dopable Polymers for Energy Storage Devices: *J. P. Ferraris,* Dept. of Chemistry, Univ. of Texas at Dallas, Richardson, TX 75083, *A. Rudge* and *S. Gottesfeld,* Los Alamos National Lab., Electronic Research Group, Los Alamos, NM 87545

Recently we have reported a new configuration for electrochemical supercapacitors based on p- and n-dopable conducting polymers. To elucidate those factors that enabled facile reversible doping, we have investigated a series of polythiophene derivatives by cyclic voltammetry, electrochemical quartz crystal microbalance techniques, and molecular modeling. The results are discussed in terms of the symmetry of the frontier orbitals and the steric and electronic requirements of the substituents.

374 Photocured Gelled Electrolytes for Li Battery Applications: *G. Nagasubramanian, D. Shen, R. Surampudi,* and *G. Halpert,* JPL, Pasadena, CA 91109

Some UV cured gelled electrolytes (GEs) of different compositions were prepared and their electrochemical properties were investigated. Different compositions of organic liquids such as ethylene carbonate (EC) + propylene carbonate (PC), ethylene carbonate + diethyl carbonate (DEC) containing $LiAsF_6$ as salt were used as solvents. Both Quick Cure and EnviBar based photocurable polymers were used as host materials. While the bulk conductivity of these electrolytes is stable near 10^{-3} the interfacial resistance increased with time indicating a reactive Li/polymer interface. Flat polymer thin cells containing Li anode, GE, and TiS_2 cathode were made and charge/discharge characteristics studied. Cathode composition and thickness are studied to optimize the C/D behavior.

375 Conducting Polymer/Graphite Fiber Composites for High Charge Density Battery Electrodes: *B. M. Coffey, P. V. Madsen, T. O. Poehler,* and *P. C. Searson,* Dept. of Mat. Sci., John Hopkins Univ., Baltimore, MD 21218

A novel method of preparing high charge density polymer electrodes by electrodeposition of conducting polymers into a commercially available graphite fiber matrix (Toray TGP-H-120) has been developed. The graphite composite provides a 40:1 increase of available surface area over projected surface area and offers advantages of single-step preparation and improved dimensional stability compared to pelletized polymer electrodes. The charge density and stability of polypyrrole, polyaniline, and poly-3-methyl thiophene composite electrodes have been determined. Charge capacities in excess of 6.5 mAh g^{-1} (3.8 mAh cm^{-3}) have been obtained.

376 *In Situ* Spectroelectrochemical Studies on Poly(1,8-Diaminonaphthalene): *S.-M. Park* and *M. Ruan,* Dept. of Chemistry, Univ. of New Mexico, Albuquerque, NM 87131, and *Y.-B. Shim,* Dept. of Chemistry, Pusan National University, Pusan, Korea

A functionalized conducting polymer, poly(1,8-diaminonaphthalene), has been studied employing *in situ* spectroelectrochemical techniques. Results indicate that the polymer has an absorption band maximum attributable to the polymer at 357 nm. When oxidized, a broad absorption band with its maximum at about 550 nm attributable to polarons appears. The band does not disappear completely upon reduction. This result may be because its ground state structure contains a significant amount of quinoid structure, which is isoelectronic with the bipolaron and not easily reduced. This assumption also explains why the polymer shows conductivity even in the reduced state. Spectra were obtained when the polymer is doped with Ag^+ and a new absorption band appeared at 478 nm. The Ag^+-doping increases the conductivity of the polymer significantly.

377 Sulfonated Polyaniline: A Conducting Polymer Electrode for Ion Transfer Batteries: *R. Koetz, C. Barbero,* and *M. C. Miras,* Paul Scherrer Institut, CH-5232 Villigen PSI, Switzerland

The suitability of sulfonated polyaniline (SPAN) as cation insertion material for battery and electrochromic applications is investigated. The polymer is synthesized by sulfonation of polyaniline with fuming sulfuric acid. The

configuration. Complementary electrochromic cells with the tungsten oxide-PB couple previously have been based on Li^+ or K^+-conducting electrolytes. A repetitively cycling cell has not been reported previously with a proton-conducting solid polymer electrolyte. Repeated reduction and oxidation of the current system over 20,000 cycles has been demonstrated, indicating many switchings without apparent degradation or irreversible side reactions. The sustained high overall coloration efficiency of the devices confirms the insertion/extraction of protons into and out of both WO_3 and PB films. The effect of cell size on the switching response is discussed.

389 Digital Simulation of an Electrochromic Device: *J. C. Lopez Tonazzi* and *C. L. Pershing,* Advanced Technology Center, Donnelly Corp., Tucson, AZ 85712-1108

A digital simulation model of an electrochromic device based on a two mixed conductor intercalation type electrodes is presented. The input parameters describe the thermodynamic, electrochemical, and optical properties of each electrode and electrolyte based on usually accepted models. Different transient techniques can be simulated (*i.e.,* potential sweeps, potential steps, current interruptions, etc.) giving as outputs concentration profiles *vs.* time, current *vs.* potential (time), percent transmittance *vs.* potential (time), etc. The program can simulate the usual three-electrode configuration to study each electrode separately. The simulation can be used as a framework for the design of this type of electrochromic devices.

390 Spectroelectrochemistry of Reversible Electrodeposition Electrochromic Materials: *J. P. Ziegler* and *B. M. Howard,* McDonnell Douglas Technologies Inc., San Diego, CA 92127

We present the first detailed spectroelectrochemical data taken on an electrochromic material based on the reversible electrodeposition of bismuth. McDonnell Douglas Technologies Inc. is investigating the system for potential use in military display systems. The electrodeposited bismuth system has been shown previously to yield devices with high contrast and rapid switching speed. Here we investigate the system spectroelectrochemistry as a function of chemical formulation and relate it to corresponding display properties such as coloration efficiency.

Tuesday AM

391 Electrochromic Devices for Optical Modulation in the Thermal Infrared: *S. F. Cogan, R. D. Rauh,* and *J. D. Klein,* EIC Lab., Inc., Norwood, MA 02062

We have demonstrated for the first time a complete charge-balanced electrochromic device for optical modulation in the thermal infrared. The devices incorporate infrared transparent substrates and microgrid electrical contacts. Electrochromic infrared reflectance modulation is accomplished by the reversible electrochemical lithiation of crystalline WO_3 thin films, while charge balance is provided by an infrared passive amorphous WO_3 counter-electrode. Such devices could be used to construct walls and panels for thermal management of enclosed structures such as buildings and satellites.

392 Electrochemical, Chemical, and Optical Characterization of Electrochromic $Li_\delta Nb_2O_5$ ($0 \leq \delta \leq 1.5$): *P. C. Yu,* PPG Industries, Inc., Chemicals Div., Monroeville, PA 15146; *T. E. Haas,* Dept. of Chemistry, Tufts Univ., Medford, MA 02155, and *R. B. Goldner,* Electro-Optics Technology Center, Tufts Univ., Medford, MA 02155

Thin films of niobium oxide, Nb_2O_5, demonstrated electrochromic behavior on the electrochemical insertion (reduction) and removal (oxidation) of lithium. Long-term electrochemical cycling (1,100 cycles) of $Li_\delta Nb_2O_5$/ITO/glass (*vs.* Li/Li^+) showed that similar amounts of charge (mC/cm^2) were measured for each of the cathodic (insertion of Li^+) and anodic (extraction of Li^+) cycles at a scan rate of 10 mV/s. Coulometric titrations of $Li_\delta Nb_2O_5$ ($0 \leq \delta \leq 1.5$) showed a hysteresis behavior for the insertion and removal of lithium. Using galvanostatic intermittent titration techniques (GITT), the diffusion coefficients of Li were $(9.9 \pm 0.2) \times 10^{-13}$ cm^2/s for $d\delta = (3.1 \pm 0.2) \times 10^{-3}$ in as-deposited $Li_\delta Nb_2O_5$ and $(2.2 \pm 0.2) \times 10^{-12}$ cm^2/s for $d\delta = (1.5 \pm 0.2) \times 10^{-3}$ in $Li_{0.3+\delta}Nb_2O_5$. Nb_2O_5 film thicknesses were 2500 – 500 Å. Optical transmittance and reflectance were measured for $Li_\delta Nb_2O_5$ ($0 \leq \delta \leq 1.5$) on ITO and Al substrates, respectively. At a wavelength of 550 nm, the coloration efficiency for $Li_{0.6}Nb_2O_5$/ITO/glass was 12 cm^2/C. Surface analysis using Auger electron spectroscopy indicated little difference in the chemistry of as-deposited, lithiated, and delithiated $Li_\delta Nb_2O_5$ ($0 \leq \delta \leq 0.8$); Auger peak energies of Nb and O showed no appreciable shifts. Structural analysis, utilizing x-ray and electron diffraction techniques, demonstrated that the films were amorphous.

393 Switchable Glazing Using a Suspension of TiO_xN_y Particles: *Y. Saito, M. Hirata, H. Tada, M. Hyodo,* and *H. Kawahara,* Central Research Laboratory, Nippon Sheet Glass Co., Ltd., 1, Kaidoshita Konoike, Itami 664, Japan

Dipole particle suspension (DPS) device using TiO_xN_y particles, which formed particle chains under an electric field, was fabricated. The transmittance change increased with an increase of the particle volume. It was considered that induced dipole moment of the smaller particles ($<1.1 \times 10^3$ μm^3) was insufficient for the complete particle chain formation. The response time of bleaching and coloring were approximately 2 and 13 s. A good switching behavior above 1×10^4 times was observed without aggregation and sedimentation.

394 Electrochromic Performance of Polyaniline Films Polarized in a pH 3 Electrolyte: *A. Hugot-Le Goff,* and *M. C. Bernard,* UPR 15 du CNRS "Physique des Liquides et Electrochemie", Université Pierre et Marie Curie, 75252 Paris Cedex 05, France

The electrochromic properties of polyaniline (PANI) films polarized in a pH 3 medium (HCl 0.001*M* + KCl 1*M*) were studied. The polymer is characterized by Raman spectroscopy as a function of the polarization potential and of the working time. The decomposition of the Raman spectra gives a semi-quantitative evaluation of the oxidation and protonation rates. The optical properties of the different PANI forms are characterized by optical multichannel analysis (OMA). At the same time, one can follow the coloration kinetics when the bleached polymer is polarized at a higher potential where a colored form is stable. The main absorption bands in PANI are due to polaronic absorption connected to the protonation rate at ≈3 eV and to exciton-like absorption connected to the oxidation rate at ≈2 eV. In the pH 3 solution, one can anodically form a material which has in the same time high protonation and oxidation rates, and a very broad optical absorption in the visible range. One can then obtain values of optical density higher than in the very acid media, which are generally used, without polarizing the sample at a too anodic potential at which degradation mechanisms are fast. The PANI electrochromic properties and its degradation mechanisms are followed during long voltammetric cyclings.

395 Fractal Porosity and Lithium Ion Kinetics in Electrochromic Li_xWO_3 Thin Films: *D. K. Benson, J.-G. Zhang, C. E. Tracy, A. W. Czanderna, S. K. Deb,* NREL, Golden, CO 80401

The microporosity in thermally evaporated thin films of WO_3 has been studied by small angle x-ray scattering and by water vapor adsorption/desorption using a quartz crystal microbalance. The pore structure was interconnected and had a fractal dimension of *ca.* 2.6 depending upon the parameters of deposition process. Electrode impedance spectroscopy of these WO_3 films during electrochromic lithium-ion insertion showed a low frequency Warburg impedance slope consistent with the 2.6 fractal dimension.

396 Electrodeposition of Nickel Oxyhydroxide Films Through Polymer Masks: *M.-C. Yang, C.-K. Lin, C.-L. Su,* and *T.-C. Chou,* Dept. of Chemical Engineering, National Cheng Kung University, Tainan, Taiwan, China

Nickel oxyhydroxide films were electrodeposited through gelatin masks, whose thickness may control the thickness and the optical transmittance of the deposited electrochromic film. The electrodeposited films, prepared with gelatin masks, had higher stability. Other behavior of nickel oxyhydroxide during electrodeposition and its electrochromic phenomena are described.

397 On the Structural Properties of Electrochromic NiO_x: *M. C. A. Fantini,* Instituto de Física, USP, 01498-970 São Paulo, (SP) Brazil, *I. C. Faria, R. M. Torresi,* and *A. Gorenstein,* Instituto de Física, UNICAMP, 13083-970 Campinas, (SP) Brazil

The structural properties of RF-sputtered electrochromic NiO_x thin films were investigated by x-ray diffraction (XRD). The degree of crystallinity, the preferred orientation, and the lattice parameters were analyzed for as-grown, bleached, and colored states in LiOH, NaOH, KOH, and CsOH aqueous electrolytes. The XRD results were correlated to the cyclic voltammetry, transmittance, stress, and mass variation results. Films with preferred orientation in the <101> direction of the NiO hexagonal unit cell showed better electrochromic performance. The degree of crystallinity does not determine the optical variation under cycling, but determines the stress in the film. All the results indicate the participation of the alkaline ion in the electrochromic reaction.

Tuesday PM

398 Application of a Solid Polymer Electrolyte in One-Square-Foot Electrochromic Devices: *R. D. Varjian, M. Shabrang, S. J. Babinec,* The Dow Chemical Co., Midland, MI 48674

Solid polymer electrolytes generally have respectable conductivities near ambient temperature making them better suited to electrochromic devices than inorganic solid-state ionic conductors. However, electrochromic devices incorporating solid polymer electrolytes have experienced stability problems. We describe here the performance of electrochromic devices using a proprietary polysulfonic acid electrolyte. The devices have an operating temperature range of −8 to 90°C. Performance of devices with viewing areas from 10 to 1000 cm^2 is discussed.

399 Characterization of Nonstoichiometric Nickel Oxide Thin Film Electrodes for Electrochromic Devices: *B. Scrosati* and *S. Passerini,* Dipartimento di Chimica, Università di Roma 00185 Roma, Italy

Thin film, nonstoichiometric nickel oxide is an interesting intercalation electrode with unique electrochemical and optical properties which can be successfully exploited for the realization of improved displays and windows of relevant technological interest. The correlation between the intercalation process of lithium in the nickel oxide host structure and the optical response of the electrode have been discussed in previous papers. In this work we have continued the characterization of the electrode with the aim of reaching a better understanding of the lithium intercalation reaction and of its implications in the evolvement of the structural and electronic properties of the host nickel oxide compound.

400 Electrochromic Reactions in MnO_2 Films Polarized in Neutral Solution: *A. Hugot-Le Goff, M. C. Bernard, S. Cordoba-Torresi,* and *T. B. Vu,* UPR 15 du CNRS "Physique des Liquides et Electrochimie", Université Pierre et Marie Curie, 75252 Paris Cedex 05, France

The electrochromic reactions in manganese oxides can be followed *in situ* by Raman Spectroscopy. Two discharge waves are observed during the voltammetric cycles showing the presence of two reduction reactions, but in fact, their identification is complicated by the three valences of Mn, the large number of its identified oxides/oxyhydroxides, and the possible formation of intermediate nonstoichiometric compounds. Another worry for the use of Raman spectroscopy is that almost all the manganese compounds are very sensitive to the laser beam. As a consequence we started with the characterization of a large number of reference samples (MnO_2, Mn_3O_4, Mn_2O_3, MnOOH, MnO), either mineralogical specimens or pellets prepared from commercial powders, and studied their stability under the laser beam. The

application, automotive or architectural glass. In each case, some specific technological problems are encountered.

415 Solar Modulation in an Electrochromic Window Using Polyaniline, Prussian Blue, and Tungsten Oxide: *B. P. Jelle* and *G. Hagen,* Dept. of Applied Electrochemistry, The Norwegian Institute of Technology, N-7034 Trondheim, Norway

We have made electrochromic windows using the three color changing materials polyaniline (PANI), Prussian blue (PB), and tungsten oxide (WO_3) glued together with a solid polymer electrolyte. Transmission spectra in the 290-3300 nm wavelength region at different applied potentials were recorded, and the windows show good light modulation, *e.g.,* a change in transmission from 0.79 (−1800 mV) to 0.15 (+1400 mV) at 1000 nm. Altogether, the windows are able to regulate as much as 50% of the total solar energy.

HIGH TEMPERATURE BEHAVIOR OF CERAMICS, INTERMETTALICS, AND COMPOSITES

High Temperature Materials

Monday PM

416 The Effect of Substrate Grain Growth on High Temperature Oxidation of Pure Nickel: *R. A. Rapp* and *J. Shen,* Dept. of Materials Science & Engineering, The Ohio State Univ., Columbus, OH 43210

High temperature oxidation has been studied for pure Ni with predeformation by cold rolling. The oxidation kinetics at 900°C showed a sequence of stages with protective behavior for the predeformed Ni. Some local detachments at the Ni/NiO interface intersecting with grain boundaries for the substrate were revealed by scanning electron microscopy (SEM) for predeformed samples. The predeformation eliminated the appearance of square pits that appeared on the surface of oxidized annealed samples. Most of the observed effects of predeformation can be interpreted fairly well by the Pieragi-Rapp model for the role of an epitaxial semicoherent metal/scale interface.

417 The Stability of a Protective Oxide Scale on a Binary Alloy with Scale Dissolution or Evaporation: *G. Wang,* Dept. of Materials Science and Engineering, The Ohio State Univ., Columbus, OH 43210

The stability of the solute oxide scale on a single-phase binary alloy in a corrosive environment with oxide dissolution or evaporation is analyzed by taking the dissolution/evaporation into consideration in the Wagner theory. The incubation time for the transition from a continuous protective solute oxide scale to a discontinuous nonprotective scale is estimated as a function of the diffusional parameters and the dissolution or evaporation parameters. Examples are given for several interesting situations.

418 The Effect of Yttrium on the Oxide Spalling Behavior of Cast Ni-30Cr Alloy: *Y. Zhang* and *D. A. Shores,* Corrosion Research Cntr., Dept. of Chem. Engng. & Mat. Sci., Univ. of Minnesota, Minneapolis, MN 55455

Cast Ni-30Cr and Ni-30Cr-0.5Y alloys were oxidized at 1000°C in pure O_2 for 20 h, then were thermally cycled between 1000°C and different lower temperatures. Acoustic emission signals collected throughout the experiment showed that Y greatly decreases the scale cracking and spalling. Scanning electron microscopic (SEM) and energy dispersive x-ray spectroscopic (EDAX) analyses after oxidation showed that continuous Cr_2O_3 scales were formed on both Y-bearing and Y-free alloys after a short time, but after a longer time and with thermal cycling, a NiO outer layer formed. Yttrium decreased the depletion of Cr in the substrate and retarded the formation of NiO. The NiO outer scale creates a new interface with the Cr_2O_3 scale at which additional stress may be generated during cooling due to the thermal expansion difference between Cr_2O_3 and NiO. The role of NiO in stress generation and cracking has not been explored previously.

419 The Formation of α-Al_2O_3 Scales on β-NiAl at 1400 and 1500°C: *B. A. Pint* and *L. W. Hobbs,* H. H. Uhlig Corrosion Lab., MIT, Cambridge, MA 02139

β-NiAl oxidation has been characterized at 1400 and 1500°C. Without a reactive element addition such as Y or Zr, β-NiAl forms a nonadherent α-Al_2O_3 scale. However, reactive elements are not as effective at these high temperatures as at lower temperatures. Zr alloy additions sufficient to improve scale adhesion also result in large volume fractions of ZrO_2 in the outer scale. These particles are believed to be detrimental in both isothermal and cyclic oxidation.

420 The Effect of Oxidation Time on the Grain Boundary Segregation of Zr in α-Al_2O_3 Scales Grown on β-NiAl: *B. A. Pint, A. J. Garratt-Reed,* and *L. W. Hobbs,* H. H. Uhlig Corrosion Lab., MIT, Cambridge, MA 02139

β-NiAl with an alloy addition of 0.23 weight percent (w/o) Zr was oxidized at 1200°C for times ranging from 40 min to 100 h. Using high-resolution FEG-STEM/XEDS, the average Zr segregation on α-Al_2O_3 grain boundaries near the gas interface peaked at approximately 16 h before dropping to a steady-state value. A model is proposed in which the boundaries supersaturate prior to the formation of ZrO_2 particles at longer times.

421 Oxidation-Resistant Boron- and Germanium-Doped Silicide Coatings for Titanium: *B. V. Cockeram* and *R. A. Rapp,* Dept. of Materials Science and Engineering, The Ohio State Univ., Columbus, OH 43210

A halide-activated pack cementation method has been used to codeposit either silicon and boron, or else silicon and germanium in a single step to produce a boron- or germanium-doped silicide diffusion coating on commercially pure titanium. Isothermal oxidation tests at 700-1000°C have shown excellent oxidation resistance, significantly superior to any other diffusion coating on pure titanium. Additionally, preliminary data on the application of the coating technique to titanium-aluminide alloys are discussed.

422 High Temperature Oxidation of Alloys in the Presence of HF Vapor: *M. McNallan* and *Y. W. Chang,* Dept. of CEMM, Univ. of Illinois at Chicago, Chicago, IL 60607, and *E. Dewing,* and *D. Creber,* Alcan R&D Cntr., Kingston, ON, K7L 4Z4, Canada

A series of high temperature chromium and aluminum containing alloys have been exposed to an oxidizing environment consisting of air containing approximately 1.2% HF vapor at 1000°C. The alloys suffer both internal attack and oxidation with the formation of a porous oxide scale. The alloys were ranked according to their susceptibility to overall and internal attack. The aluminum-containing alloys were subject to severe internal attack, while some of the chromium-containing alloys were more resistant to this environment. The mechanisms of the accelerated attack are discussed.

423 The Simultaneous Oxidation-Sulfidation Resistance of a Cr-Nb Alloy: *J. C. Duncan* and *L. W. Hobbs,* H. H. Uhlig Corrosion Lab., MIT, Cambridge, MA 02139

A Cr-40 weight percent (w/o) Nb alloy was studied to evaluate its promising mixed oxidation sulfidation resistance at 800 and 900°C. Sulfidation experiments at low P_{S_2} also were conducted. Pure Cr and pure Nb were exposed to identical conditions for comparison. Corrosion kinetics showed an improvement in the alloy over catastrophic chromium sulfidation and niobium oxidation.

Tuesday AM

424 Strength Retention of NT154 Silicon Nitride Exposed to High Temperature Oxidation and Hot Corrosion Environments: *T. E. Strangman,* Allied Signal Auxiliary Power, Phoenix, AZ 85072-2180 and *D. S. Fox,* NASA-Lewis Research Center, Cleveland, OH 44135-3191

The status of environmental life prediction for silicon nitride for advanced gas turbine applications is presented. Strength retention in flexure specimens following 1-3300 h exposures to high temperature oxidation and hot corrosion environments has been measured. Results are used to calibrate a life prediction model. Predicted component life is dependent upon engine design (stress, temperature, pressure, fuel/air ratio, gas velocity and inlet air filtration), mission usage [fuel sulfur content, location (salt in air) and times at duty cycle power points], and material parameters. Protective coatings may be required to extend ceramic component life in such aggressive environments.

425 Lifetime Prediction of Engineering Ceramics and Composites in High Temperature Corrosion Environments: *M H. Van de Voorde,* European Communities Joint Research Centre, Institute for Advanced Materials, 1755 ZG Petten, The Netherlands

High performance ceramics and composites are potential candidate materials for modern technologies in the future. Not much scientific information is available on the reliability of nonoxide ceramics and new ceramic composites, in industrial applications; this is particularly so for high temperature corrosion degradation. This paper describes (*i*) the effect of high temperature gaseous and hot corrosion on ceramic properties; (*ii*) the corrosion failure mechanisms in industrial simulative operating conditions; (*iii*) a method to predict the life time of ceramic materials/components for environmental effects; (*iv*) the development of protective coatings for high temperature corrosion resistant ceramics and composites. Suggestions are made to catalyze international collaboration in the complex R&D field, to the welfare of the worldwide engineering ceramics community (ceramics producers, designers and industrial users).

426 Environmental Effects on the Flexure Strength of HIPed Silicon Nitride at Elevated Temperatures: *A. A. Wereszczak, K. Breder, M. K. Ferber,* and *T. P. Kirkland,* Oak Ridge National Lab., Oak Ridge, TN 37831-6064, and *P. Khandelwal,* Allison Gas Turbine Div., General Motors Corp., Indianapolis, IN 46206-0420

Parallel dynamic fatigue studies were conducted in air or inert (argon or nitrogen) environments on two hot isostatically pressed silicon nitrides (cold isostatically pressed or injection molded GTE-PY6) using 4-point-flexure at elevated temperatures. Flexure strength was dependent on the stressing rate for tests conducted in air, signifying slow crack growth susceptibility. Tests in inert environments revealed flexure strength to be independent of the stressing rate. Failure mechanisms and how they relate to the mechanical performance of the materials at elevated temperatures in ambient or inert environments are discussed. (Research sponsored by the U. S. DOE, Assistant Secretary for Energy Efficiency and Renewable Energy, Office of Transportation Technologies, as part of the High Temperature Materials Laboratory User Program, under contract DE-AC05-84OR21400 with Martin Marietta Energy Systems, Inc.)

427 High Temperature Subcritical Crack Growth of SiC/SiC Composites: *C. F. Windisch, Jr., R. H. Jones,* and *C. H. Henager, Jr.,* Pacific Northwest Laboratory, Richland, WA 99352

Time-dependent crack growth measurements of ceramic composites in varying PO_2 environments were conducted on materials consisting of chemical vapor infiltration (CVI) SiC reinforced with Nicalon fibers having C-interfaces. Crack velocities are determined as a function of applied stress intensity and time for varying O_2 levels. Results are presented for crack velocity-stress intensity relationships in pure Ar and in Ar plus 2,000, 5,000, 10,000, and 20,000 ppm O_2 atmospheres at 1100°C. A 2-D micromechanics model is used to represent the time-dependence of observed crack bridging events and is able to rationalize the observed phenomena.

perature, and HBr temperature and concentration have been achieved already. The combined results reveal the spatial distribution of non-LTCE and make possible comparisons with the predictions of models of chemically reacting flows.

442 Ripening of Y_2O_3 Particles in W-5 Weight Percent Y_2O_3 Composites: *X. Zheng, R. A. Rapp,* Dept. of Materials Science and Engineering, The Ohio State Univ., Columbus, OH 43210, *V. Mehrotra, H. S. Betrabet,* and *P. D. Goodell,* Philips Labs., North American Philips Corp., Briarcliff Manor, NY 10510

Tungsten-Y_2O_3 composites are potential electrode materials for discharge lamps because Y_2O_3 can lower the work function of tungsten. Dispersed Y_2O_3 particles ripen at high temperature to reduce interfacial energy. In this work, Y_2O_3 distributions in W-5 weight percent Y_2O_3 composites were measured experimentally as a function of time after exposure at 2200°C. The distributions, measured in 2-dimensional cross sections, were converted to 3-dimensional distributions using the Johnson-Saltykov method. Lifshitz-Slyozov-Wager theory was applied to the ripening process and reasonable agreement between the theoretical calculations and the experimental measurements was achieved.

443 The High Temperature Corrosion of Tungsten by Carbon Dioxide: *G. M. Forsdyke,* GE Lighting Ltd., Advanced Tech. Dept., Leicester LE4 7PD, England, *D. M. Jenkins* and *J. S. Ogden,* Dept. of Chemistry, Univ. of Southampton, Southampton SO9 5NH, England

The corrosion of tungsten by carbon dioxide has been investigated together with the corrosion of tungsten by carbon dioxide in the presence of tin(II) chloride and in the presence of chlorine. The results show that at 1442 K the rate of tungsten mass loss is linearly dependent on the concentration of carbon dioxide with tin(II) chloride being present. Similarly, the variation of the rate of tungsten mass loss with temperature is also a linear function when there is no tin(II) chloride present.

444 Wall Blackening in Metal Halide Lamps Containing Scandium or Rare-Earth Iodide: *W. van Erk,* Philips Lighting BV, 5600 JM Eindhoven, The Netherlands, *P. H. L. M. Cobben* and *P. Bennema,* R.I.M. Lab. of Solid State Chemistry, Faculty of Sciences, Univ. of Nijmegen, 6525 ED Nijmegen, The Netherlands

In metal halide lamps containing rare-earth or scandium iodide no regenerative tungsten cycle is possible. Tungsten is deposited on the vessel wall in the form of crystals. The loss of light transmission due to this is a.o dependent on the number density of crystals. This density depends on the electrode temperature, on the vessel wall temperature, and on the iodine pressure.

445 Damage to the Cathodes of HPS Lamps Suffered during Sealing: *F. Nagel,* Tungsram, Co. Ltd., H-1340 Budapest, Hungary, and *M. Farkas-Jahnke,* Res. Instit. for Tech. Phys. of HAS, H-1047 Budapest, Hungary

Electrodes of HPS lamps frequently are contaminated during sealing by aluminum/or AlO_x/and calcium. Morphology and composition changes of the surfaces of the W-wires and the emissive materials were detected by scanning electron microscope and electron probe microanalysis. X-ray diffraction investigations proved that the contaminates react with the emissive material, resulting in different tungstate-aluminates with a lattice similar to that of Ba_2SrWO_6, but having a somewhat compressed unit cell.

446 Aging of Ba_2SrWO_6 Cathode Emissive Material Used in HPS Lamps: *F. Nagel,* Tungstam Co., Ltd., H-1340 Budapest, Hungary, *M. Farkas-Jahnke* and *L. Petrás*,Res. Instit. for Techn. Phys. of HAS, H-1047 Budapest, Hungary

Correlation between the inclination for decomposition of Ba_2SrWO_6 used as electrode emissive material in HPS lamps and certain properties of the polycrystalline material, (color, morphology of the crystallites, stoichiometry, structure, surface composition, and structure, impurities) was investigated on as-produced and aged samples. X-ray diffraction methods, scanning electron microscope, electron beam microanalysis, and electron diffraction were used to detect differences in stoichiometry, impurity content, and surface composition of stable and decomposed samples, respectively.

Tuesday AM

447 Measurement of Enhanced Thulium Abundance in Metal Halide Discharge Lamps: *M. J. Shea, W. M. Keeffe, C.W. Struck,* Osram Sylvania, Danvers, MA 01923, and *A. E. Feuersanger,* GTE Lab., Waltham, MA 02154

Complexing between Tm and Sc in metal halide lamps with fills consisting of NaI, ScI_3, LiI, TmI_3, Hg, and Ar has been investigated. Spectroscopic data suggest that the ratio of Tm abundance to Sc abundance N_{Tm}:N_{Sc} in the arc of a lamp is 37 times what is expected from the vapor pressures of TmI_3 and ScI_3. Direct evidence of such a complex, $ScTmI_4^+$, was observed in Knudsen cell mass spectrometer measurements.

448 Analysis and Thermochemistry of the Vapor of the NaBr-$DyBr_3$ System: *K. Hilpert,* Institute of Reactor Materials, Research Centre Jülich (KFA), D-5170 Jülich, Germany, and *M. Miller,* Technical University of Wroclaw, 50-370 Wroclaw, Poland

The vapor of the NaBr-$DyBr_3$ system was investigated under equilibrium conditions in the temperature range between 763 and 1009 K by using Knudsen effusion mass spectrometry. The gaseous species NaBr, $(NaBr)_2$, $DyBr_3$, $(DyBr_3)_2$, $NaDyBr_4$, and Na_2DyBr_5 were detected in the vapor. Enthalpy and entropy changes were determined for the dissociation reactions of the heterocomplexes. The data are discussed with respect to their significance for chemical vapor transport in metal halide lamps.

449 Study of the Heterocomplexes in the Vapor of the Na-Sn-Br-I System and Their Relevance for Metal Halide Lamps: *K. Hilpert,* Institute of Reactor Materials, Research Centre Jülich (KFA), D-5170 Jülich, Germany, *M. Miller,* Technical University of Wroclaw, 50-370 Wroclaw, Poland, *U. Niemann,* Philips GmbH Research Laboratory Aachen, D-5100 Aachen, Germany

The vapor of the Na-Sn-Br-I system was investigated under equilibrium conditions in the temperature range between 623 and 913 K by the use of Knudsen effusion mass spectrometry. The gaseous species NaBr, NaI, $(NaBr)_2$, NaBrI, $(NaI)_2$, $SnBr_2$, SnBrI, SnI_2, $NaSnBr_3$, $NaSnBr_2I$, $NaSnBrI_2$, and $NaSnI_3$ were detected in the vapor. Enthalpy and entropy changes resulted for the dissociation reactions of the homo- and heterocomplexes. Gas phase equilibria important for the development of metal halide lamps were computed from these results and ancillary data.

450 Modeling Multicomponent Metal Halide Systems: *S. A. Mucklejohn,* GE Lighting Ltd., Advanced Tech. Dept., Leicester LE4 7PD, England, and *A. T. Dinsdale,* National Physical Lab., Div. of Materials Metrology, Teddington, Middlesex TW11 0LW, England

Multicomponent metal halide systems can be employed in high intensity discharge lamps to produce white light sources with high efficiencies and good color-rendering properties. To exploit fully the potential of such systems it is necessary to know their chemical behavior at temperatures between 300 and 1500 K. Models for the thermodynamic properties of binary metal halide systems are discussed together with methods for combining these data to represent the properties of multicomponent systems.

451 An Assessment of the Thermochemical Parameters for the Lanthanide Triiodides: *S. A. Mucklejohn,* GE Lighting Ltd., Advanced Tech. Dept., Leicester LE4 7PD, England, *R. Devonshire* and *D. L. Trindell,* Dept., of Chemistry, High Temperature Science Lab., The Univ. of Sheffield, Sheffield S3 7HF, England

The published values for the thermodynamic properties that characterize the lanthanide triiodides have been reviewed and critically assessed together with the corresponding vapor pressures. The analysis covers values that were not available when previous assessments of the properties of the lanthanide triiodides were reported. A comprehensive set of thermochemical parameters has been derived from this assessment for the gaseous and condensed phase species.

452 Coherent Anti-Stokes Raman Scattering (CARS) Studies of Metal Halides: *D. L. Trindell, S. Greiff,* and *R. Devonshire,* Dept. of Chemistry, High Temperature Science Lab., Univ. of Sheffield Brook Hill, Sheffield S3 7HF, England

Coherent anti-Stokes Raman scattering (CARS) has been used to investigate the vibrational-rotational spectroscopy of metal halides. CARS spectra of liquid $SnCl_4$ have been obtained, as have spectra arising from coherent Stokes Raman scattering (CSRS) and other higher order Raman processes. CARS studies of vapor-phase $SnCl_4$ and $NbCl_5$ have produced high resolution spectra of the respective ν_1 bands, the first reported spectra of high temperature metal halide vapors.

453 Incandescent Radiation from Clusters: A Novel Type of Light Source: *R. Scholl,* Philips GmbH Forschuugslaboratorium Aachen, D-5100 Aachen, Germany

Incandescent radiation of nanometer-sized particles (clusters) can be utilized in a novel type of light source. A regenerative chemical cycle is used to form rhenium or tungsten clusters inside a high pressure microwave discharge, which heats the particles to 4700 K (rhenium) or 3800 K (tungsten). Continuous emission spectra of the clusters are peaked in the visible range. The result is a novel light source with color-rendering properties above R_a = 95 and efficacies of about 60 lm/W.

Tuesday PM

454 On The Lithium Loss of LiI Containing Metal-Halide Lamps: *F. Nagel,* Tungsram, Co., Ltd., H-1340 Budapest, Hungary, and *L. Bencze,* Roland Eötvös Univ., Budapest, Hungary

The lithium loss of metal-halide lamp-arc tubes cannot be extrapolated from the well-known sodium loss taking into account the ion radii only. The tendency of Li to produce a covalent bond can be decisive. The result of experimental investigation is: Li^+ ion current is significantly lower than Na^+ current tested in 150 W arc tubes containing 1:1 (molar ratio) LiI and NaI. We used the 1:1 mix for the test, since it is impossible to produce a LiI lamp with the same temperature distribution as a NaI lamp. In the 1:1 arc tube the Li ion current was *ca.*. 60% of the Na ion current in arc tubes containing LiI and NaI only (as iodides + Ar + Hg). The presence of rare earth (Dy + Ho 1:1 + CsI) iodides reduces this ratio, pointing to stable Li-complexes. Before starting the experiments, we tested again our experimental arrangement used to investigate sodium-loss, since W. M. Keeffe and V. D. Meyer have reported on neutrals (at the LS5 York Conference, investigating Sc-Na lamps) and ions coming from the arc tube. The result of our investigation shows; all their findings are artifacts caused by two mistakes in their experimental arrangement as follows: (*i*) high energy modulation caused by asymmetric ballast, and (*ii*) reevaporation of neutralized ions from the hot ion source, caused by the missing shielding-focusing plates between the arc tube and the ion source.

455 On the Chemical Processes in Zr Containing Fluorescent Tube Emission Mix: *F. Nagel,*[a] [a]Tungsram Co. Ltd., H-1340 Budapest, Hungary, *M. Farkas-Jahnke,* Res. Inst. of Tech. Phys., H-1047 Budapest, Hungary, and *J. Mészáros*[a]

The emission mix is produced during the pumping process by decomposition of Ba-Sr-Ca carbonates. The oxides react immediately with zirconia producing Perovskite type zirconate. Tungstates, mixed Perovskite tungstate-zirconates are produced on the tungsten-mix interface. Enrich-

paper reviews advances in this phosphor made possible through the use of encapsulating coatings.

469 Electroluminescence and Photoluminescence of Cerium-Activated Alkaline Earth Thiogallate Thin Film: *S. S. Sun* and *R. T. Tuenge,* Planar Systems, Inc. Beaverton, OR 97006, *J. Kane* and *M. Ling,* David Sarnoff Res. Ctr. Princeton, NJ 08450

Thin films of cerium-activated alkaline earth thiogallate were investigated for the fabrication of blue-emitting thin-film electroluminescent (TFEL) devices. The films were prepared by RF sputtering from various thiogallate targets having composition of $M_{1-x}Ga_2S_4:Ce_x$, where M = Ba, Ca, Sr, and $0.01 < x < 0.1$. The EL emission peak wavelengths measured for the cerium-activated strontium, calcium, and barium thiogallate TFEL devices were 445, 460, and 452 nm, respectively. Photoluminescent emission spectra measured for each thiogallate thin film showed identical peak wavelength to the EL emission. The optimum cerium concentration for EL emission intensity for strontium and calcium thiogallate films is 0.04 and 0.06 atomic ratio, respectively. The EL brightness of the calcium thiogallate devices is almost twice of those measured from the strontium thiogallate devices. The brightness variation, however, is due mainly to the difference in lumen equivalent of the emission intensity.

470 Factors Affecting the Conductivity of Copper-Coated DCEL Phosphor: *L. F. Tsang,* Dept. of Electronic Engineering, Hong Kong Polytechnic, Hong Kong, *J. Anderson,* Dept. of Electronic Engineering, University of Ulster, Ulster, Northern Ireland, *N. Brown,* Dept. of Chemistry, University of Ulster, Ulster, Northern Ireland

Performance of a powder DCEL[1] device depends on the conductivity of its copper-coated ZnS phosphor, but little effort has been spent on its study. We report a series of experiments of whose results are used to analyze the forming and aging behavior in DCEL device. Factors affecting the conductivity of copper-coated DCEL phosphor are found to be its temperature, coating solution temperature, and gaseous atmosphere. Based on these results, new theories about forming and effect of gaseous atmosphere on a DCEL device, as well as how to produce a long lifetime DCEL phosphor are discussed.

471 Electroluminescence of Decatungstoeurropate Dispersion Layers: *T. Yamase* and *K. Uheda,* Research Laboratory of Resources Utilization, Tokyo Institute of Technology, 4259 Nagatsuta Midori-ku, Yokohama 227, Japan

ITO/$[EuW_{10}O_{36}]^{9-}$/Mylar/ITO electroluminescence (EL) cells have been fabricated with the $[EuW_{10}O_{36}]^{9-}$ layer with 40-80 μm thickness, as the emissive medium. The spectral distribution of EL, induced by the applied negative voltage pulse, indicates the presence of three emission envelopes of nitrogen plasma, oxygen-to-tungsten (O $\rightarrow$ W) ligand-to-metal charge transfer (LMCT) emission, and Eu^{3+} f-f emission for every dispersion layer of Ca^{2+}, Sr^{2+}, or Ba^{2+} salt of $[EuW_{10}O_{36}]^{9-}$ and $Na_9[EuW_{10}O_{36}] \cdot 32\ H_2O$ pellet. Typical operating conditions are $-0.7 \sim -1.2$ kV at 100-300 Hz. A high porosity of the $[EuW_{10}O_{36}]^{9-}$ layer allows a voltage drop to occur in the layer, resulting in a significant contribution of the nitrogen plasma to the total emission. Comparison of transient behavior among three emissions exhibits an accumulation of charges inside the $[EuW_{10}O_{36}]^{9-}$ layer which induces an internal field. Such charges once trapped are released and accelerated by external field or by internal field after the applied pulse is turned off until enough kinetic energy is acquired to excite $[EuW_{10}O_{36}]^{9-}$

Wednesday PM

472 Synthesis and Properties of Thulium-Activated, Niobium-Activated, and Self-Activated Yttrium Tantalate X-Ray Phosphors: *V. B. Reddy,* Osram Sylvania Inc., Towanda, PA 18848, and *W. J. Zegarski,* E.I. DuPont DeNemours, Towanda, PA 18848

Monoclinic fergusonite rare-earth tantalates exist in two crystallographic forms. The fergusonite M′ form of yttrium tantalate is a superior luminescent host compared to the M form of yttrium tantalate. Based on this host, several phosphors were developed and are used currently in commercial x-ray intensifier screens. The niobium-activated phosphors are used in Quanta Fast Detail screens, thulium-activated phosphors in Quanta Detail and self-activated phosphor in the newly developed Ultra-Vision™ screens. We describe here the synthesis of these phosphors and details some of the synthesis modifications that improved the phosphors' brightness. The effect of flux materials on the luminescence efficiency, particle size, and morphology of niobium-activated, thulium-activated, and self-activated yttrium tantalate phosphors are presented. The effect of small levels of dopants, such as alkali, alkaline earth, and Group III elements, on the luminescent properties of these phosphors also are highlighted.

473 A Study of the Rare-Earth Tantalate Phosphor Formation Reaction: *D. B. Hedden* and *W. J. Zegarski,* DuPont Co., Electronics Dept., Towanda, PA 18848, and *C. C. Torardi,* DuPont Co., Central R&D, Wilmington, DE 19880

Our studies of the M′-fergusonsite rare-earth tantalate phosphor ($RTaO_4$, R = rare earth) formation reaction have shown that, contrary to previous beliefs, the flux is an important reactant. Through a combination of techniques (DTA, TGA, XRD, reaction quenching studies, and mass balance), we have shown that the flux reacts with the refractory constituent oxides to give intermediates that then react to give product and regenerate flux. The oxide/flux reaction systems are more efficient than direct reaction of the oxides, showing the importance of intermediate formation. The details of these reaction systems are discussed.

474 Factors Influencing Light Output and Modulation Transfer Function of Gd_2O_2:S:Tb Screens for Radiation Therapy Verification Imaging: *C. G. A. Hill,* Levy Hill Labs. Ltd., Cheshunt, Herts, EN8 9TJ England, *D. W. Mah,* Dept. of Medical Biophysics, Univ. of Toronto, Dept. of Clinical Physics, Princess Margaret Hospital, Toronto, ON, Canada M4X 1K9, *J. A. Rowlands,* Dept. of Medical Biophysics, Univ. of Toronto, Toronto, ON, Canada M4N 3M5, and *J. A. Rawlinson,* Dept. of Medical Biophysics, Univ. of Toronto, Dept. of Clinical Physics, Princess Margaret Hospital, Toronto, ON, Canada M4X 1K9

Relative light output measurements of Gd_2O_2S:Tb phosphor screens irradiated using megavoltage x-ray beams will be presented. The effects of phosphor grain size, mass thickness, reflective layers and beam energy have been quantified. Measurements of the resolution as quantified by the modulation transfer function (MTF) of these screens also are presented.

475 Properties of Titanium-Activated Hafnia in Intensifying Screens: *P. S. Bryan, L. C. Roberts, P. M. Lambert, C. M. Towers,* and *G. S. Jarrold,* Research Lab., Eastman Kodak Co., Rochester, NY 14650-2033

Potential improvements in conventional screen/film radiography can be obtained by the use of phosphors having x-ray absorption that is greater than that of currently used commercial materials. We describe the reinvestigation of titanium-activated hafnia (density = 9.7 g/cm^3) as a phosphor for medical intensifying screens.

476 Titanium-Activated Hafnium Germanate: Synthesis and Luminescence: *P. M. Lambert, S. A. Ferranti, C. M. Towers,* and *G. S. Jarrold,* Research Lab., Eastman Kodak Co., Rochester, NY 14650-2033

A new phosphor, titanium-activated $HfGeO_4$, has excellent x-ray absorption properties. The material exhibits an efficient broad-band emission, centered at 425 nm, which is only weakly quenched at high titanium levels. The phosphor can be prepared conveniently from the component oxides, or a coprecipitated precursor gel, with the assistance of a flux.

Thursday AM

477 Infrared Emitting Rare-Earth Aluminum Oxide Phosphors: *H. Tamaki* and *M. R. Royce,* Nichia America Corp., Lancaster, PA 17601

The properties of chromium-activated rare-earth aluminum oxide phosphors with a perovskite crystal structure were measured under cathode ray excitation. These materials described by the molecular formula $RAlO_3$:Cr (R = Y, La, Gd) have distinctive emissions in the infrared region (650-850 nm). Other chromium activated rare-earth aluminates were prepared in various stoichiometric proportions and discussed. These phosphors can be used in the cathode ray tubes for liquid crystal light valves.

478 Measurement of Adhesion of Electrophoretically Deposited Phosphor Coatings: *M. J. Shane,* Materials Science Program, Univ. of California at San Diego, La Jolla, CA 92093-0310, *J. B. Talbot* and *M. Le,* Dept. of AMES (Chemical Engineering), UCSD, La Jolla, CA 92093-0310, *E. Sluzky,* Hughes Aircraft Co., Industrial Products Div., Carlsbad, CA 92008, and *K. R. Hesse,* Escondido, CA 92028

The performance of cathode-ray tube (CRT) screens depends upon the uniformity, density, and adhesion of the phosphor layer. Our objective is to develop a quantitative measure of the adhesion of electrophoretically deposited phosphor coatings to improve the processing and resulting characteristics of luminescent screens for CRTs. The effect of the amount of hydroxide binder material on the adhesion properties of the particulate screens was investigated. Also, the microstructure of the phosphor/adhesive deposits was investigated using standard microscopic techniques.

479 Aging and Thermoluminescence in Flying Spot Scanner CRT Phosphors: *M. S. Waite* and *C. Brass,* Rank Brimar Ltd., Middleton, Manchester M24 1SN, England

The aging of Ga-modified P46 scanner phosphors from various sources has been investigated in telecine CRTs at 25 kV and 50 μA/cm^2. Aging is accompanied by an increase in saturation tendency, suggesting that loss of active Ce (III) centers is a principal mechanism. Glow curves for scanner phosphor screens contain a new peak at 650-700 K after electron beam aging. The characteristics of the peak indicate significant trapping of carriers by native defects in the phosphors.

480 High Resolution Phosphor Screens by Electrophoretic Deposition: *R. P. Rao* and *D. C. Ketchum,* Thomas Electronics, Inc., Wayne, NJ 07470

With the increasing demand of miniaturization of equipment and technical advancements, we need tiny cathode-ray tubes (CRTs) with high resolution, high brightness, low cost, and long life. These screens can be optimized by careful selection of the best phosphor (1-2 μ) and by precision control of the screen density, Green- and red-emitting silicate phosphor screens (1-1.5 mg/cm^2) are coated by an electrophoretic process. Isopropyl alcohol bath with nitrates of La, Mg, or Al as dissociating salts and glycerol as binder are used. Some of the results obtained on various parameters are presented and discussed.

481 Photo- and Low-Voltage Cathodoluminescence of Mn^{+2}-Activated $ZnGa_2O_4$ Phosphors: *L. E. Shea, R. K. Datta, and J. J. Brown, Jr.,* CACM, 301 Holden Hall, Virginia Tech., Blacksburg VA 24061-0256

The synthesis and photoluminescence mechanism of $ZnGa_2O_4:Mn^{2+}$ are presented. Monitored at 450 nm, $ZnGa_2O_4$ exhibits an absorption band at 245 nm; monitored at 506 nm $ZnGa_2O_4:Mn^{2+}$ exhibits absorption bands at 245 and 283 nm. Under 254 nm excitation, $ZnGa_2O_4$ exhibits broad-band emission extending from 360 to 610 nm, peaking at 450 nm. This emission is gradually quenched, as a new band emerges, peaking at 506 nm, as Mn^{2+} is incorporated into the lattice ($Zn_{1-x}Mn_xGa_2O_4$), where $x = 0.006$ at maximum intensity. Activator sensitization and host to activator energy transfer is suggested.

stimulation of the CA1 region of the hippocampus was obtained using repetitive fast-scan voltammetry (100 V/s). The selectivity of the enzyme-generated response was demonstrated by perfusing the tissue slice with buffer that either contained or omitted 3 m*M* NAD^+ (the enzyme cofactor), thus allowing the formation of NADH as a function of glutamate concentration. Additional confirmation of the identity of the signal is derived from the voltammetry observed during stimulation.

496 Utility of Blocked Electrodes for Electroanalysis in Bioactive Media: *S. E. Creager,* and *K. A. Groat,* Dept. of Chemistry, Indiana University, Bloomington, IN 47405

Electro-oxidation of hydroxymethylferrocene (HMFc) has been studied at gold electrodes coated with self-assembled monolayers of alkanethiols. The alkanethiol layer dramatically decreases the rate of electron transfer such that an overpotential of several hundred millivolts must be applied to oxidize HMFc. The monolayer also dramatically decreases the background current due to charging the electric double layer. It is shown that alkanethiol-coated electrodes can be used to achieve very selective and sensitive detection of HMFc in a model bioactive medium, specifically a 2 day-old yeast fermentation broth in a commercial growth medium.

497 Voltammetry of H_2O_2 and Anthracene in CO_2 Using Chemically Modified Microelectrodes: *S. F. Dressman, E. F. Sullenberger,* and *A. C. Michael,* Dept. of Chemistry, Univ. of Pittsburgh, Pittsburgh, PA 15260

Voltammetric experiments using polymer-coated, self-contained, electrochemical probes have been performed in CO_2 to detect H_2O_2 and anthracene. For the H_2O_2 studies, a redox polymer consisting of pendant osmium atoms attached to a cross-linked poly(vinylpyridine) backbone was used to immobilize horseradish peroxidase onto an electrochemical probe. The results showed that electroenzymatic reduction of H_2O_2 had occurred in low density CO_2 (30°C, 850 psi). Additionally, a poly(ethylene oxide) electrode film was used to monitor both the oxidation and the reduction of anthracene in supercritical CO_2 (32°C, 1250 psi).

498 Catalytic Dechlorinations in Bicontinuous Microemulsions: *J. F. Rusling, S. Zhang, S. Schweizer,* and *G. N., Kamau,* Dept. of Chemistry (U-60), University of Connecticut, Storrs, CT 06269-3060

Bicontinuous microemulsions are clear, stable mixtures of oil, water, and surfactant which have good conductivity, solubilization, and mass transport properties for electrochemical reactions. We used microemulsions of cationic surfactant, dodecane, and water with metal complex catalysts for dechlorination of organohalide pollutants. Enhanced efficiency was obtained for nonpolar reactants. Applications to difficult-to-reduce organohalides, such as mixtures of chlorinated biphenyls and DDT, are discussed.

Wednesday PM

499 Fluorescence of Probes in Clay-Surfactant Films: *M. F. Ahmadi* and *J. F. Rusling,* Dept. of Chem., Univ. of Conn., Storrs, CT 06269-3060

Fluorescence spectra of pyrene derivatives in composite films of cationic surfactants and clay colloids on electrodes were studied. Changes in viscosity of composite films with temperature and electrode potential were probed by pyrene and 1,3-di(1-pyrenyl)propane. Results suggests that an increase in mobility of the alkyl chains in these lamellar films accompanies the transition from gel to liquid crystal state, explaining increases in diffusion rates above T_c.

500 Electrochemistry in Cavitating Liquids: *L. A. Coury, Jr.* and *C. R. S. Hagan*; Dept. of Chemistry, Duke University, Durham, NC 27708-0348, *Honghua Zhang*; AndCare, Inc., Durham, NC 27701

Electrochemical experiments at Pt electrodes during sonication are described. Steady-state limiting currents which correspond to effective rotation rates of 160,000 rpm in rotating disk voltammetry are shown. Effects of solution temperature, viscosity, concentration, cell geometry and ultrasonic amplitude are addressed. Steady-state voltammetry at scan rates of 25 V/s is demonstrated. Changes in the surfaces of glassy carbon electrodes after sonication in various solvents are also discussed.

501 Electrochemical Synthesis and Characterization of Superconducting Niobium Nitride Powders and Niobium Nitride Powder Precursors: *T. L. Wade, R. M. Crooks, D. M. Smith, G. Garza,* Dept. of Chemistry, University of New Mexico, Albuquerque, NM 87131, and *J. O. Willis,* Superconducting Technol. Cntr., Los Alamos National Lab., Los Alamos, NM 87545

Anodic dissolution of Nb foil in liquid NH_3 produced an insoluble precursor. The calcination product of this precursor was a superconducting NbN powder with a T_c and T_c^{mid} of 14.75 and 13.6 K, respectively. The precursor was characterized by Fourier transform infrared (FTIR) spectroscopy and the calcined powder by x-ray diffraction (XRD), elemental analysis, and surface area analysis. The superconducting properties were analyzed using a superconducting quantum interference device (SQUID) magnetometer.

502 Magnetic Ion Exchange Polymer Composites: *J. Leddy* and *S. Amarasinghe,* Dept. of Chemistry, Univ. of Iowa, Iowa City, IA 52242

Magnetically modified electrodes are formed by mixing suspensions of 1 μm polystyrene-coated magnetic particles and the cation exchange polymer, Nafion, on an electrode centered in a circular magnet. Once the solvents evaporate and the circular magnet is removed, the magnetic particles are trapped in the Nafion, stacked as magnetic pillars. When compared to Nafion films, larger flux enhancements are found for paramagnetic species. Potential shifts consistent with the stabilization of the paramagnetic component of a redox couple are observed cyclic voltammetrically.

503 Solid Polymer Electrolytes for the Paired Electrochemical Synthesis of Organic Compounds: *O. J. Murphy, J. K. Jeng, C. E. Salinas, H. Hu,* and *G. D. Hitchens,* Lynntech, Inc., College Station, TX 77840

The electrochemical synthesis of xylitol and sorbitol from aqueous solutions of xylose and glucose, respectively, was investigated using a solid polymer electrolyte-based electrochemical reactor. This approach avoids the tedious and expensive removal of supporting electrolytes from the product solution. Xylitol was produced at a current efficiency as high as 40% and xylonic acid at a current efficiency of 45% using a Tosflex IE-SF34 anion exchange membrane. The corresponding current efficiencies for sorbitol and gluconic acid were 15 and 40%, respectively. Electroreduction of the sugars is hindered since only the linear form of the sugars can be readily electroreduced with available electrocatalysts. However, the linear form of the sugars are present only at low concentrations during mutarotation which can be influenced considerably by the pH at the electrode/solid polymer electrolyte interface.

504 New Composite Solid Electrolytes with $t_{Li}^+ = 1$: *E. Peled, D. Golodnitsky, C. Menachem, A. Ardel,* and *Y. Lavi,* School of Chemistry, Tel-Aviv Univ., Tel-Aviv 69978, Israel

New composite solid electrolytes (CSEs), based on interfacial conduction of Li^+ at the grain boundaries of small solid LiI and LiBr crystals, were developed and characterized. Thin films (50-200μ), produced by casting, have high conductivity (up to 10^{-3} $\Omega^{-1}cm^{-1}$ at 120°C), low and stable (on storage) Li/CSE interfacial resistance and excellent mechanical stability. The effect of the CSE composition (Li halide, high surface area oxide matrix, PEO, and other polymers) on its properties are discussed.

Thursday AM

505 Electrochemistry in Ambient Temperature Chloroaluminate Ionic Liquids: An Overview for the Uninitiated: *R. A. Osteryoung,* Dept. of Chemistry, North Carolina State Univ., Raleigh, NC 27695-8204

Aspects of chemistry in ambient temperature ionic liquids, consisting of mixtures of either N-(1-butyl)pyridinium chloride (BuPyCl) or 1-ethyl-3-methylimidazolium chloride (ImCl) with aluminum chloride are described. These solvents may be characterized by the solvolysis equilibrium

$$2\ AlCl_4^- = Al_2Cl_7^- + Cl^-$$

The solvolysis equilibrium constants for both the BuPyCl and ImCl aluminum chloride based solvents are the same, having a value of $\sim 10^{-17}$. These systems possess Lewis acidity and basicity due to the presence of the Lewis acid, $Al_2Cl_7^-$, in systems containing excess aluminum chloride, and of the Lewis base, Cl^-, in systems containing excess organic chloride. The Brønsted (proton) acidity of proton in these ionic liquids also depends on the underlying Lewis acidity of the solvent. This talk discusses aspects of the solvents electrochemical window, and presents examples of the electrochemical behavior of inorganic and organic solutes which respond to Lewis and Brønsted melt acidity variations.

506 Electrochemical Reduction of Azobenzene and Azoxybenzene from Molten Acetamide at 85°C: *R. Saraswathi,* USIC, M. K. University, Madurai, Tamilmadu, India 625021, *R. Narayan,* Chemistry Dept., I. I. T. Madras 600 036, India

Azobenzene present as the transisomer in molten acetamide is reducible both at the mercury and glassy carbon electrodes. Two reduction steps are observed with mercury electrodes. The first is a quasi-reversible reduction to hydrazobenzene which is oxidized in the anodic sweep. No assignment could be made for the second reduction step. Azoxybenzene undergoes a four-electron, four-proton irreversible reduction to hydrazobenzene. Polarograms are distorted by a surface process with high concentrations of azoxybenzene, particularly in alkaline melt. The observations are relevant to account for the observations made when nitrobenzenes undergo reduction in the amide melts.

507 Electrochemical Measurements of Diffusion Coefficients of Redox-Labeled Poly(ethyleneglycol) Dissolved in Poly(ethyleneglycol) Melts: *O. Haas,* Paul Scherrer Instit., CH-5232 Villigen PSI Switzerland, *Ch. Velasquez, Z. Porat,* and *R. W. Murray,* Kenan Labs. of Chemistry, Univ. of North Carolina, Chapel Hill, NC 27514-3290

Ferrocene-labeled monomethyl poly(ethyleneglycol) (MPEG) with molecular weights of 1900 and 750 was used as an electrochemical diffusion probe in poly(ethyleneglycol) melts. Cyclic voltammetry and chronoamperometry were used in connection with microdisk electrodes to measure the diffusion coefficient of redox-tagged molecules using melted poly(ethyleneglycol) as a solvent. The molecular weight of the solvent polymer was 750, 2000, and 20000. Results form the temperature dependency of the probe diffusion process and of the viscosity and conductivity of the host polymer electrolyte are presented and discussed.

508 Clusters and Complexes in Polymer Electrolytes: Extended X-Ray Absorption Fine Structure Studies: *J. McBreen, I.-C. Lin, X. Q. Yang,* and *H. S. Lee,* Brookhaven National Lab., Upton, NY 11973

EXAFS studies were done on $RbBr(PEO)_8$, $ZnBr_2(PEO)_8$, and the mixed salt complexes $[xZnBr_2 + (1-x)LiBr](PEO)_{12}$ and $[xZnBr_2 + (1-x)CaBr_2](PEO)_{12}$. There is evidence for Rb_xBr_x cluster formation in the RbBr-PEO electrolytes. The additions of LiBr and $CaBr_2$ to the $ZnBr_2$-PEO electrolyte results in the formation of immobile $ZnBr_4^=$ species. The implications regarding mixed salt conduction are discussed.

509 A Study of Anodic Processes at Carbon Electrodes in Alumina-Cryolite Melts by Means of Cyclic Voltammetry: *S. S.*

521 The Concentration Profile of Oxygen Vacancies in the Passive Film on Tungsten: *E. Sikora,* Center for Advanced Materials, The Pennsylvania State Univ., University Park, PA 16802, *A. Goossens,* Dept. of Chemistry, Univ. of California at Berkeley, Berkeley, CA 94720 and *D. D. Macdonald,* Center for Advanced Materials, The Pennsylvania State Univ., University Park, PA 16802

To investigate semiconductor properties of the anodic films formed on tungsten in phosphoric acid and phosphate buffer solutions, various electrochemical and optical techniques (electrochemical impedance, capacitance transient, and reflectance response) have been employed. Mott-Schottky analysis was used to obtain the donor density N_D, as a function of the film formation potential and the pH of the solution. The results demonstrate the existence of a linear relationship between the steady-state film thickness and the applied voltage, as predicted by the point defect model. The relationships between the donor density and the film formation potential and the pH of solution are discussed.

522 New Water Insoluble Polyphosphazenes as Polymer Electrolytes: *I. I. Selvaraj, S. Chaklanobis,* and *V. Chandrasekhar,* Dept. of Chemistry, IIT, Kanpur 20816, India

New ion conducting polymer electrolytes based on polyphosphazene macromolecular systems are described. The polymer electrolyte poly(bis(4-n-octyl phenoxy ethoxy ethoxy)phosphazene) (PEEP) has remarkable solubility properties. It is insoluble in water unlike MEEP, poly[bis(methoxy ethoxy ethoxy)phosphazene], and also is soluble in a variety of organic solvents ranging from hexane to chloroform. The synthesis, characterization, and conductivity studies of the polymer-salt complexes at varying temperature with different O:Li ratio are reported. The maximum conductivity of PEEP-$LiClO_4$ is 4.3×10^{-7} S cm^{-1} at 333 K.

Thursday PM

523 Modeling of the Electronic Structure of Passive Oxide Films: *J. Sikora* and *D. D. Macdonald,* Center for Advanced Materials, The Pennsylvania State Univ., University Park, PA 16802

A mathematical model of the electronic structure of a semiconductor type passive oxide film has been formulated. The model is based on the point defect model and semiconductor theory. A computer program has been developed to obtain numerical solutions to the model. Our numerical simulations have been compared with experimental data obtained for anodic films formed on tungsten in phosphoric acid and phosphate buffer solutions. The numerical solutions show that, in the steady-state, the electric field strength is constant and the relation between the film thickness and applied voltage is linear, as initially assumed in the point defect model. For the steady-state solutions, all possible different types of defect concentration profiles have been discussed and interpreted physically.

524 Voltammetric Studies of Tetrasulfonated Phthalocyanines in Aqueous Electrolyte on Tin-Doped Indium Oxide Electrodes: *Z. Zhang, S. L. Gupta, D. A. Tryk,* and *E. B. Yeager,* Case Center for Electrochemical Sciences, Dept. of Chemistry, Case Western Reserve Univ., Cleveland, OH 44106

The cobalt and iron tetrasulfonated phthalocyanines (TsPc) irreversibly adsorb on ordinary pyrolytic graphite (OPG) and give voltammetric peaks corresponding to the adsorbed species. No redox peaks are observed for the dissolved species, however. In present study, tin-doped indium oxide (ITO) was used as the electrode and the well-defined solution-phase redox peaks were observed in cyclic voltammograms. No adsorption of the macrocycles was observed on the ITO. The O_2 reduction onset potential was the same as that for the adsorbed CoTsPc on OPG.

525 Poisioning Effects on the Kinetic Behavior of the Hydrogen Evolution Reaction at Pt Electrodes in Alkaline Solution: *L. Gao, B. E. Conway,* and *J. Barber,* Dept. of Chemistry, University of Ottawa, Ottawa, ON, Canada K1N 6N5

The kinetics of the HER are sensitively influenced by adsorption of catalyst poisons such as As, thiourea, etc., which decrease the coverage of the overpotential-deposited, adsorbed H intermediate. The adsorbed poisons will not only competitively occupy the available adsorption sites but also interact with the H atoms already covering the surface, *e.g.,* through surface dipole repulsion. The involvement of poisons in the kinetics and the mechanisms of the HER has been investigated by making theoretical calculations of the rates of the electrochemical processes involved, considering both the coverage of poison, θ_p, and the lateral interaction factor, g. With introduction of the poison reagent thiourea NH_2-CS-NH_2 (1 ppm) into the solution, open-circuit potential relaxation, ac impedance, and cyclic voltammetry experiments were carried out. It was found that most of the surface sites (*ca.* 93%) were occupied by the poison molecules, which lead to a decreased coverage of the H intermediate and an insignificant pseudocapacitance. From calculations based on the rate constants evaluated from the simulation of the potential relaxation transients, it is concluded that the HER mechanism changes from that of rate-limiting H desorption to one determined by the initial H discharge step. This corresponds to a lower steady state coverage by H.

526 Electrochemical Studies of Closo-2,3,-dicarbaundecaborane on a Glassy Carbon Electrode in Dichloromethane Using a Novel Method: *I. S. El-Hallag* and *M. M. Ghoneim,* Dept of Chemistry, Faculty of Science, Tanta Univ., Tanta, Egypt, and *J. Kennedy,* Dept. of Chem., Leeds Univ., Leeds, LS2 9JT, England

Convolution and deconvolution voltammetry were used to evaluate the rates of heterogeneous charge transfer of closo-2,3-dicarbaundecaborane [closo-2,3-$C_2B_9H_{11}$] using a glassy carbon electrode and CH_2Cl_2 as solvent. This technique allows correction for uncompensated resistance and double-layer capacitance, as well as determination of the diffusion coefficient, D, and symmetry coefficient, α, from a single cyclic voltammogram. Chronopotentiometry also was used for evaluation of the diffusion coefficient, D. A direct test of the parameters was made by digital simulation using the Condesim program (from PAR, Princeton Applied Research) by superposition of the simulated votammograms on the measured data using the average experimentally determined values of the electrochemical parameters.

POROUS SILICON

Physical Electrochemistry/Dielectric Science and Technology/ Electronics/Luminescence and Display Materials

Wednesday AM

527 Light Emission Properties of Anodized and Oxidized Porous Silicon: *S. M. Prokes* and *O. J. Glembocki,* NRL, Washington, DC 20375

The PL and Raman spectra of PorSi has been examined for anodized and extensively oxidized samples. Results indicate no blue-shifting of the red PL with increased oxidation, and a persistent red PL for samples comprised of an oxide. Thus, an oxide-related luminescence has been suggested as a possible mechanism in this case. The Raman results show the presence of both an amorphous silicon phase, and a significantly red-shifted Si-Si line. In oxidation, the Si-Si line shifts by 26 cm^{-1}, to a position above that of bulk silicon, indicating that the Raman shift cannot be the result of particle size, but may be due to strain.

528 The Luminescence and Its Quenching from Porous Silicon Formed in a Nonaqueous Electrolyte: *P. A. Kohl, E. K. Propst,* and *M. Rieger,* School of Chemical Engineering, Georgia Institute of Technology, Atlanta, GA 30332-0100

Porous silicon layers which electroluminesce in aqueous solutions have been formed by oxidation of (100) silicon in acetonitrile (MeCN)-HF solutions. The porous layers are generally >1 μm in size, and the luminescence corresponds to the presence of silicon dihydride, not to the presence of siloxene. The luminescence can be quenched by replacing the surface hydride with a fluoride. The pores are formed by first producing (111) facets, a monohydride surface which does not luminesce, followed by etching at the base of the facets. Replacement of the hydride with a fluoride results in quenching of the luminescence.

529 Luminescence Quenching of Porous Silicon: *M. J. Sailor, D. Fisher, J. Harper,* and *J. M. Lauerhaas,* Dept. of Chemistry, Univ. of California at San Diego, La Jolla, CA 92093-0506

A series of experiments aimed at probing the range of energy relaxation processes available to luminescent porous Si is presented. Physisorbed molecules that can quench the luminescence include benzene, hexane, and alcohols. The degree of quenching of physisorbed molecules can be tuned somewhat via surface chemical transformations of the porous Si. Chemisorbed halogens also quench luminescence. Data involving interfacial charge and energy transfer reagents are presented.

530 Steady-State and Time-Resolved Spectroscopy of Visibly Emitting Porous Si: *S. V. Gaponenko, I. N. Germanenko, E. P. Petrov, A. P. Stupak,* and *A. L. Gurskii,* Institute of Physics, Academy of Sciences of Belarus, Minsk 220072, Belarus, and *G. V. P. Bondarenko, V. E. Borisenko,* and *A. M. Dorofeev*, Minsk Radioengineering Institut, Minsk 220069, Belarus

Spectroscopic properties of porous Si aged in air during several years are studied. Samples show noticeable shift of steady-state emission spectrum with porosity and excitation wavelength. Emission bands shifts to shorter wavelengths with increasing excitation intensity and to longer wavelength with time obeying nonexponential decay in the microsecond time range. A model of decay based on discrete (Poissonian) distribution of trap states is advanced and important parameters of radiative and nonradiative processes are evaluated.

531 Photoluminescence and *In Situ* Photomodulated Infrared Spectroscopy of Porous Silicon: *V. M. Dubin, J.-N. Chazalviel,* and *F. Ozanam,* Laboratoire de Physique de la Matière Condensée, CNRS-Ecole Polytechnique, 91128 Palaiseau-Cedex, France

Photomodulated infrared absorption and photoluminescence of porous silicon have been recorded simultaneously in nitrogen ambient and during etching in HF. Different behavior is observed when porous silicon is kept as-prepared in HF, or when it is exposed to air. As-prepared porous silicon in HF exhibits green luminescence and a correlated large free-carrier infrared absorption. This gives evidence for a large free-carrier lifetime, and for a direct recombination of photocreated electron-hole pairs in the luminescence process.

532 The Influence of Preparative Method on the Surface Reactivity of Luminescent Silicon: *J. L. Coffer* and *R. R. Chandler,* Dept. of Chemistry, Texas Christian University, Ft. Worth, TX 76129

In this work, the role of the preparative technique employed to fabricate luminescent porous silicon is analyzed in terms of the materials' chemical reactivity and physical stability. Specifically, we compare the amine-induced PL response of anodically etched porous silicon to that of stain-etched porous silicon as well as that of Si nanocrystallites. Results are analyzed in terms of the observed magnitude of binding constants, saturable PL intensity, and reversibility upon acid addition.

533 Some Possible Effects of c-Si Hydrogenation during Porous Si Fabrication: *I. A. Aisenberg* and *S. V. Nosenko,* IPTM, Chernogolovka, 142432 Moscow District, Russia

We have drawn attention to the process of c-Si hydrogenation during porous Si formation as electrolytically in HF-based solution as by remote hydrogen plasma treatment. The process of H-induced microclearage of c-Si during hydrogenation may take an important part in the formation of a porous

cata-Politecnico di Milano, I-20133 Milano, Italy, L. Battezzati, Dip. Chimica Inorganica, Univ. di Torino, Torino, Italy, *E. Lanzoni*, Instit. di Metallurgia, Univ. degli Studi di Bologna, Bologna, Italy, and *M. V. Ivanov,* Inst. Phys. Chem., Academy of Sciences, Moskow, Russia

Ni-P [P ~ 7 × 10 weight percent (w/o)], and Co-P (P ~ 4 × 5 w/o) ACD coatings were prepared and their corrosion and wear resistance characterized. Structure, morphology, composition, and microhardness were investigated. The correlation of bath composition, nature, and concentration of stabilizers and brighteners [Te^{4+}, Se^{4+}, organic thioamines (OTA)] with deposit structure, brightness, and functional properties was established. As plated (AP) ACD Ni-P is x-ray amorphous and has a crystalline Ni matrix with dispersion of phosphides after heat-treatment (HT); ACD Co-P is crystalline and Te^{4+} additions give bright layers with strong (10.0) and (11.0) P.O. which also show interesting magnetic properties, with higher coercivity than mat thin films. Thermal analyses of Ni-P deposits reveal two crystallization peaks related to dispersed precipitation of phosphides; OTA and Te^{4+} additions have structural effects as shown by the appearance of high temperature peaks; Co-P deposits show a typical peak, Te^{4+} additions cause the appearance of a high temperature peak. The highest corrosion and wear resistances are shown by Ni-P with OTA additions. In AP Ni-P hardness decreases as P content increases; the reverse behavior is observed in HT Ni-P samples; wear resistance and microhardness are correlated only in the AP state; HT does not improve abrasion resistance.

548 Electroless Deposition in the Electronic Industry: A Review: *C. J. Sambucetti,* IBM T.J. Watson Research Cntr., Yorktown Heights, NY 10598

We review the electroless deposition processes which had major impact in different aspects of the electronic and computer component manufacturing. The review is divided in to two sections. The first section is dedicated to the electroless deposition of base metals such as copper, nickel, and cobalt and their uses. The second section covers the electroless deposition of noble metals for surface finish, contacts, connectors, and chip attachment applications. We focus on the chemistry of the processes, the chemical composition evolution and improvements, and their relation to some particular media on which the pre-electroless activation is applied: for example, glass-epoxy boards, polyimides, Teflon, ceramic, as well as silicon substrates for integrated circuits.

549 Electroless Metal Deposition for Microelectronics: *V. M. Dublin,* Laboratoire de Physique de la Matière Condensée, CNRS-Ecole Polytechnique, 91128 Palaiseau-Cedex, France

Electroless metal deposition is potentially a much simpler, less costly, and more reproducible technique than the other metal deposition processes widely used in microelectronics. Micro- and nanostructures were obtained by selective electroless metal deposition. Ohmic contacts to silicon, diffusion barrier to silicon, and refractory metal silicides were also manufactured by selective electroless metal (NiP, Re, Pd) deposition. Electroless metal [NiP, Ni-Cu(P), Cu, Ni] deposition have been investigated for via and contact hole filling, Al cladding, conductor pattern and pillar formation, soldering to Al and Si.

550 STM Patterning and AFM Imaging of Self-Assembled Monolayer Films with Selective Electroless Metallization: *S. L. Brandow,* Dept. of Chem., Univ. of Colorado, Boulder, CO 80309 and *W. J. Dressick, T. S. Koloski, C. S. Dulcey, J. M. Calvert, C. R. K. Marrian, F. K. Perkins,* and *E. A. Dobisz,* NRL, Washington, DC 20375-5347

The scanning tunneling microscope (STM) as a source of low energy electrons for patterning self-assembled monolayer films is demonstrated. The STM patterned organosilane films are then used as templates for subsequent organic reactions and for selective electroless (EL) metal deposition. The EL metal deposit allows observation of the latent image in the monolayer film, and also provides a plasma hard etch barrier for pattern transfer into the substrate. AFM characterization of the EL metal particle size, a critical factor in the ultimate resolution of the process, is discussed.

551 Patterned Self-Assembled Films for Selective Electroless Metallization: *J. M. Calvert,[a] W. J. Dressick,[a] C. S. Dulcey,[a] M. S. Chen,[b] J. H. Georger, Jr.,[b,c] G. S. Calabrese,[c] T. S. Koloski,[a]* and *S. L. Brandow,[d]* [a]NRL, Washington, DC 20375-5348, [b]Geo-Centers, Inc., Ft. Washington, MD 20744, [c]Shipley Co., Marlborough, MA 01752, [d]Dept. of Chem., Univ. of Colorado, Boulder, CO 80309

A new approach for selective electroless (EL) metallization is described. Surfaces are modified with a ligand-bearing organosilane monolayer film, catalyzed with a chloride-stabilized aqueous Pd(II) catalyst solution, and then immersed in an EL plating bath to obtain metallization. This process involves fewer steps and displays improved selectivity compared to process involving conventional Pd/Sn catalysts. Fabrication of high resolution metal patterns by lithographic patterning of the organosiliane films is demonstrated.

552 A New Series of Inorganic Additives for Electroless Copper Plating Solutions: *H. Akahoshi, M. Kawamoto,* and *A. Takahashi,* Hitachi Research Laboratory, Hitachi, Ltd., 7-1-1 Omika-cho, Hitachi-shi, Ibaraki-ken 319-12 Japan

Influence of the oxoacid anions on mechanical properties and surface grain structure of electroless copper deposits is illustrated as a new series of ductility promoting agents. Oxoacid anions of group IIIb, IVb, and VIb elements were examined and group IVb elements especially silicate and germanate ions were found to improve ductility. They were as effective as cyanide or 2,2'-bipyridyl.

553 Characterization of the Copper-Poly(tetrafluoroethylene) Interface: *R. R. Rye, G. W. Arnold,* and *A. J. Ricco,* Sania National Laboratories, Albuquerque, NM 87185

Using Rutherford backscattering spectroscopy (RBS) and x-ray photoelectron spectroscopy (XPS) we have shown that strong adhesion of electrolessly deposited Cu to etched poly(tetrafluoroethylene) (PTFE) results from penetration of all species (tin oxide from the sensitization step, Pd from the nucleation step, and electrolessly deposited Cu) into the porous, carbon-rich, 3000 Å deep chemically etched layer. Yield strength measurements of the deposited Cu films show near-cohesive failure in PTFE with both failure surfaces yielding only C(1s) and F(1s) XPS peaks characteristic of virgin PTFE with a small amount of the C(1s) peak characteristic of etched PTFE. (This work was supported by the U.S. Department of Energy under contract No. DE-AC04-76DP00789.)

554 Morphology of Electrolessly Deposited Pd Membranes and Its Effects on Hydrogen Permeability: *J. Shu, B. P. A. Grandjean, S. Kaliaguine,* Dept. of Chem. Eng., Laval Univ., Ste-Foy, Quebec, Canada G1K 7P4

Palladium was electrolessly deposited on porous stainless steel substrate from both concentrated and dilute Pd-containing baths. SEM and XRD analyses revealed the formation of different morphologies due to the deposition kinetics. Poorly adhered palladium particles with large dimensions of 0.42 μM were formed by repeated deposition from the dilute bath. Dense palladium membranes with microcrystalline sizes of *ca.* 108 Å were deposited from the concentrated bath. The latter composite membrane was permselective to hydrogen.

555 Modelization of Chemical Bath Deposition of Cadmium Sulfide Films: *D. Lincot* and *R. Ortega-Borges,* Laboratoire d'Electrochimie Analytique et Appliquee, ENSCP 75 231 Paris Cedex 05

In situ quartz crystal microbalance technique has been used for the study of the growth kinetics of cadmium sulfide thin films by chemical bath deposition from ammonia-thiourea solutions. The formation of CdS appears to obey a ion by ion mechanism, based on successive adsorption of thiourea molecules and cadmium ions on the surface. The reaction involves the decomposition of a surface intermediate complex between thiourea and cadmium hydroxide, in opposition with the commonly accepted dissociation route. In particular, no free sulfide formation is required. The model, which has been derived, allows for the first time, to fit quantitatively the influence of the main parameters on the growth rate of CdS films by chemical bath deposition.

556 The Electroless Catalytic Properties of an Efficient Cr-Based Barrier for Cu Diffusion: *M. D. Bruni,* CNET/CNS, TPM/MAD, Chemin du Vieux Chine, 38243 Meylan, France

This paper reviews the problems encountered in applying barrier metal technology to Si processing, particularly where Cu is the conductor. The properties of such key barrier metals are discussed, Cu deposition seeding was performed on a thin Cr-based seed layer inside PPQ (polyphenylguinoxalime) as well as PECVD oxide openings using a commercial Cu electroless solution. The Cr-based surface acts as a Cu diffusion barrier, allows a good adhesion of Cu and a correct deposition seeding. The effectiveness of the Cr based layer as diffusion barrier was investigated by RBS analysis. The barrier is thermally stable up to 320°C. An examination of the metallic surface after different plasma treatments was carried out using FE-AES. The Cr based layer does not, usually, require a preliminary sensitization and/or activation operation, as it does not oxidize much and remains catalytic. However we observed that, the properties of the Cr-based layer are damaged, during structures patterning, leading to irreproducibility or sporadic plating. It is thus, demonstrated that the main reason for the loss of the catalytic property for Cu electroless deposition is the oxidation state. In order to restore the Cr catalytic properties a short fluorinated plasma step, compatible with the insulator structure, is recommended.

ELECTROCHEMISTRY IN NONAQUEOUS MEDIA

Physical Electrochemistry/Organic and Biological Electrochemistry/Battery

Monday AM

557 Electrochemistry of Aromatic Ketones in a Room-Temperature Molten Salt: *G. T. Cheek,* Dept. of Chemistry, US Naval Academy, Annapolis, MD 21402-5026

Investigations are continuing into the electrochemical behavior of benzophenone and fluorenone in the aluminum chloride: 1-ethyl-3-methylimidazolium chloride molten salt system. Recent results have shown that both the voltammetric properties and the electrolysis products depend greatly on melt acidity, which can be varied over a tremendous range in this solvent. In general, chloroaluminate species have the ability to remove oxygen from some of the electrolysis products, and the 1-ethyl-3-methylimidazolium cation can serve as as proton donor in other cases.

558 Redox Chemistry of Tetrathiafulvalene in Ambient Temperature Molten Salts: *M. T. Carter,* Dept. of Chemistry, Kenan Laboratories, University of North Carolina, Chapel Hill, NC 27599, *R. A. Osteryoung,* Dept. of Chemistry, North Carolina State University, Raleigh, NC 27695

The electrochemical behavior of tetrathiafulvalene (TTF) in an ambient temperature molten salt composed of 1-ethyl-3-methylimidazolium chloride mixed with aluminum chloride is described. TTF is oxidized in successive electron transfers to the cation radical, TTF^+ and the dication, TTF^{2+}. Neutral TTF is stable in basic melt (excess ImCl) and the electron transfers are well-behaved as examined by pulse voltammetry. However, TTF^{2+} adsorbs onto the glassy carbon working electrode, complicating some cyclic voltammetry experiments. In acidic melts (excess $AlCl_3$) TTF is oxidized to mono- and dication probably by HCl impurity. The diffusion coefficients of these species suggest formation of a slowly diffusing $AlCl_3$ adduct. Preliminary results for the formation of electronically conductive charge transfer salts in basic media are also presented.

Although superconductivity was discovered in 1911, the first superconductor derived from an organic compound, tetramethyltetraselenafulvalenium hexafluorophosphate (superconducting transition temperature (T_c) of 0.9 K at 6.5 kbar) was reported in 1980. In a relatively short time since then, radical cation-based superconductors have been synthesized with T_c's near 13 K and, more recently, radical anion salts of Buckminsterfullerene have been prepared that possess T_c's as high at 33 K. The design, synthesis, and characterization of organic superconductors are summarized briefly. Electrocrystallization has played a key role in the synthesis of organic conducting materials and is a major topic of discussion.

573 *In Situ* Spectroelectrochemical Studies on Metallophthalocyanines in Nonaqueous Solvents: *S.-i Mho, B. Ortiz,* and *S.-M. Park,* Dept. of Chemistry, Univ. of New Mexico, Albuquerque, NM 87131, and *N. Doddapaneni,* Sandia National Labs., Albuquerque, NM 87185

Spectroelectrochemical studies have been conducted on a few selected metallophthalocyanines, *i.e.,* cobalt, iron, and magnesium as well as a free base, in nonaqueous solvents including pyridine, dimethylsulfoxide, and dichloromethane. Results indicate that the Soret bands are relatively independent of experimental variations whereas the Q-bands are heavily dependent on many experimental parameters. Vibrational structures on the Q-bands are individually affected by addition or extraction of electrons to or from the phthalocyanines. This observation is explained by the Jahn-Teller splitting introduced when they undergo redox processes. The conventional catalytic (EC′) mechanism is not operative for oxygen reduction.

574 Electrochemical and Spectroelectrochemical Properties of Brominated Metalloporphyrins: *F. D'Souza, A. Villard, E. Van Caemelbecke,* and *K. M. Kadish,* Dept. of Chem., Univ. of Houston, Houston, TX 77204-5641, and *P. Tagliatesta, P. Bianco, A. Antonini,* and *T. Boschi,* Dipart. di Scienze e Tecnologie Chimiche, II Universita' degli Studi di Roma, 00173, Italy

The synthesis and electrochemical/spectroelectrochemical characterization of $(TPPBr_x)Co$ and $(TPPBr_x)FeCl$ are reported where $TPPBr_x$ represents the derived dianion of a tetraphenylporphyrin bearing 0, 6, 7, or 8 Br groups on the β-pyrrole positions of the porphyrin macrocycle. Each $(TPPBr_x)Co$ complex undergoes three one-electron oxidations and up to nine one-electron reductions depending upon the degree of Br substitution. The half-wave potentials for these electrode reactions are all shifted positively in potential with respect to the metal and ring centered electrode reactions of unsubstituted (TPP)Co. The singly oxidized and the singly reduced products are both stable on the cyclic and thin-layer voltammetric time scales but further reductions beyond $[(TPPBr_x)Co^{I}]^-$ lead to a stepwise elimination of the Br groups giving $[(TPP)Co^{I}]^-$ as the ultimate reduction product in solution.

575 The Role of Solvent and Electrolyte in Governing the Reactivity of Electrogenerated Anionic Nucleophiles: *D. H. Evans,* and *M. E. Niyazymbetov,* Dept. of Chemistry and Biochemistry, University of Delaware, Newark, DE 19716

A common strategy in electro-organic synthesis is to generate anions by cathodic electrolysis of appropriate precursors (*e.g.,* C-H, S-H, N-H or P-H acids) and allow the anions to react subsequently with electrophiles, *e.g.,*alkyl halides or Michael acceptors. It is of interest to determine what conditions will lead to the greatest nucleophilic reactivity of the electrogenerated anions. In this study, we have investigated a variety of solvents and electrolytes and have found that the irreversible oxidation potential of the nucleophile is a useful predictor of nucleophilic reactivity. Conditions giving the greatest ease of oxidation also produce the highest nucleophilicity.

MICROELECTRODES AND MICROENVIRONMENTS: FUNDAMENTALS AND APPLICATIONS

Physical Electrochemistry/Sensor/Corrosion

Monday AM

576 Electrochemistry at Collector-Generator Assemblies: Direct Experimental Evidence on the Dichotomic Nature of Diffusion at Microelectrodes: *C. Amatore* and *B. Fosset,* Ecole Normale Supérieure, Dépt. de Chimie, URA CNRS 1679, 75231 Paris Cedex 05, France and *K. M. Maness* and *R. M. Wightman,* Dept. of Chemistry, University of North Carolina, Chapel Hill, NC 27599-3290

A model based on conformal mapping is presented to describe and analyze the behavior of electrochemiluminescence (ECL) generation at double band microelectrodes. Simulations show that when these devices are operated in ECL mode, the current reaches steady state much faster than when they are operated in collector-generator mode, because of the important feedback of the electroactive species in the near vicinity of the electrodes. The limiting current thus achieved is exactly twice that determined in the collector-generator mode. In contrast, the ECL flux reaches steady state at much larger times because it requires the establishment of diffusion layers whose thickness greatly exceeds the gap and electrode widths. Experimental verification of the model are provided by ECL of $Ru(bpy)_3(PF_6)_2$ and 9,10-diphenylanthracene at double band electrodes.

577 Steady-State Currents at Electrodes with Rotationally Invariant Surfaces: Conical and Spherical Segment Electrodes: *C. G. Zoski,* Dept. of Chemistry, University of Rhode Island, Kingston, RI 02881, *A. J. Bard and M. V. Mirkin,* Dept. of Chemistry, University of Texas, Austin, TX 78712

Microelectrodes of many shapes have been described in the literature. Recently attention has been focused upon microelectrodes shaped as a spherical segment or as a cone. One reason for this growing interest is the simplicity of their fabrication compared to that of a true hemisphere or disk. Additionally, spherical and conical shaped ultramicroelectrodes are more ideally suited for use as electrochemical probes in applications including scanning electrochemical microscopy and intracellular measurements. Theory for the behavior of these electrodes is noticeably absent from the literature, although expressions for the diffusion-limited current have been proposed. Solutions to the problem of steady-state transport to a spherical segment and a blunt conical electrode under reversible, quasi-reversible, and irreversible conditions are discussed. Comparisons with analogous transport to hemispherical and disk microelectrodes are also made.

578 Effects of Microelectrode Geometry: *K. B. Oldham,* Trent Univ., Peterborough, ON, Canada

Uncertainty about the shapes of microelectrodes makes it important to understand how voltammetry is influenced by the sizes and shapes of ultrasmall electrodes. Two aspects of this topic addressed: (*i*) how the short-time chronoamperometric response of a microelectrode to a large potential step is affected by the electrode geometry; and (*ii*) how the steady-state voltammogram (the long-time current dependence on electrode potential) reflects the geometry of the electrode and its environment.

579 Migration, Diffusion, and Microelectrodes: A New Modeling Approach Applied to Pitting Corrosion: *M. W. Verbrugge,* Physical Chemistry Dept., General Motors NAO Research and Development Center, Warren, MI 48090-9055, *D. R. Baker,* Mathematics Dept., General Motors NAO Research and Development Center, Warren, MI 48090-9055, and *J. Newman,* Materials Sciences Div., Lawrence Berkeley Laboratory, and Dept. of Chemical Engineering, University of California, Berkeley, CA 94720

We develop a methodology for treating coupled diffusion and migration with an arbitrary number of facile homogeneous reactions and the participation of an arbitrary number of species in the heterogeneous electrode reaction. The technique should find wide application in microelectrode analyses. As an example problem, the anodic dissolution of nickel in chloride medium is treated for a stagnant solution and the hemispherical cavity geometry common to the dissolution of passivating, corrosion-resistant metals.

Monday PM

580 Probing the Chemical Microenvironment around Biological Cells with Carbon-Fiber Microelectrodes: *R. M. Wightman, J. A. Jankowski, T. J. Schroeder, E. L. Ciolkowski,* and *J. M. Finnegan,* Dept. of Chemistry, Univ. of North Carolina at Chapel Hill, Chapel Hill, NC 27599-3290

Voltammetric electrodes fabricated from individual carbon fibers are sufficiently small that they can be used to measure secretion of molecules from single biological cells. We have examined secretion of catecholamines from bovine adrenal medullary cells grown in culture. Secretion appears as a series of concentration packets, and each concentration packet corresponds to the contents of a single intracellular vesicle. Measurements made with cyclic voltammetry enable the concentration and identification of the secreted catecholamine. Amperometric measurements allow the temporal characteristics of the secretion to be observed.

581 Neurotransmitter Dynamics at Single Nerve Cells and Nerve Cell Processes: *A. G. Ewing, R. Zhou, G. Chen,* and *T. Chen,* Penn State University, University Park, PA 16802

Voltammetric microelectrodes can be used to monitor catecholamines released from single nerve cells. Design and application of submicron carbon electrodes has allowed detection of approximately 150,000 molecules of dopamine released from single vesicles in pheochromocytoma cells. In addition, pharmacological studies on vesicular release of norepinephrine and epinephrine has provided dynamic evidence for the effect of autoreceptors on single adrenal cells. Finally, voltammetric methods have been used to monitor quantal release of dopamine from nerve cell bodies in invertebrates.

582 The Effect of Analyte Charge on the Electron-Transfer Properties of Carbon-Fiber Microelectrodes as Determined with Electrochemically Generated Luminescence: *W. G. Kuhr, P. Hopper,* and *P. Pantano,* Dept. of Chemistry, Univ. of California, Riverside, CA 92521

The surfaces of carbon-fiber microelectrodes were electrochemically treated to produce different levels of surface oxides in the following manner: after normal polishing, the carbon surface was activated by applying a cyclic potential sweep from −0.2 to 2.0 V at a frequency of 50 Hz for 3 s in solutions of varying pH: 1*M* HCl, Ph 7.4 and pH 12.0 phosphate buffers. Electrochemically generated chemiluminescence (ECL) of luminol and $Ru(bpy)_3^{2+}$ were imaged at these surfaces through a fluorescence microscope using a Peltier-cooled, Thompson 7895B CCD. The oxide layer produced by electrochemical pretreatment produced a significant diminution (on the order of 50%) in luminol ECL intensity. This reduction in observed ECL is attributed to the electron-electron repulsion existing between the oxide species on the electrode surface and the negative charge present on the analyte. $Ru(bpy)_3^{2+}$ oxidation was facilitated by oxygen functionalities, as evidenced by an increase in ECL intensity, leading to the conclusion that $Ru(bpy)_3^{2+}$ and luminol are oxidized at different sites on the carbon fiber surface.

583 Electrochemical Behaviors of Dopamine at IDA and Polymer-Modified IDA Electrodes: *O. Niwa,* NTT Basic Res. Lab., Tokai, Ibaraki 319-11, Japan, *M. Morita,* NTT Basic Res. Lab., Musashino, Tokyo 180, Japan, and *H. Tabei,* NTT Basic Res. Lab., Tokai, Ibaraki 319-11, Japan

The highly sensitive and selective detection of dopamine in the presence of L-ascorbic acid was carried out using interdigitated array (IDA) microelectrodes, with and without a coating of Nafion/polyester ionomer bilayer film. A low detection limit of 10 n*M* was obtained for dopamine as a result of high redox cycling. Dopamine was detected selectively in the presence of 100 times its concentration of L-ascorbic acid using the bilayer film modified IDA electrodes.

This paper describes motivations for measuring ultraslow diffusion of redox solutes in solid and semi-solid polymer electrolyte solutions, and experimental aspects of measuring such diffusion. Example measurements draw upon the use of variable concentrations of electrolyte, of electrolytes that are strongly ether oxygen-coordinated, of solute dimension and poly(ether) derivatization, and of poly(ether) chain length in order to manipulate diffusion rates, and upon the use of microband electrode assemblies and ultraslow potential scans to minimize solid solvent resistance effects.

598 AC Admittance Techiques Using Ultramicroelectrodes in Media of High Resistance: *M. Fedurco, W. R. Fawcett,* and *M. Opallo,* Dept. of Chemistry, University of California, Davis, CA 95616

The ac admittance technique has been applied at ultramicroelectrodes to the study of fast electron transfer reactions in highly resistive organic solvents. The importance of carrying out the meassurements at very high frequencies where linear mass transfer conditions are maintained is discussed. The results of applying this method to several simple electron transfer reactions involving organic molecules such as buckminsterfullerene and benzophenone are presented.

599 Electrochemistry at Microelectrodes in Supercritical Chlorodifluoromethane: *D. E. Tallman* and *S. A. Olsen,* Dept. of Chemistry, North Dakota State University, Fargo, ND 58105

Platinum disk microelectrodes are being used to probe the electrochemistry of ferrocene and other test redox systems in supercritical chlorodifluoromethane (CDFM). CDFM is a moderately polar medium which has been used for supercritical fluid extraction and chromatography. With millimolar concentrations of tetra-n-butyl ammonium tetrafluoroborate as supporting electrolyte, reversible to quasi-reversible cyclic voltammograms can be obtained under homogeneous fluid conditions. The influence of density and dielectric constant (as controlled by pressure) on the voltammetric behavior of ferrocene and cobaltocene is described.

600 Electrochemical Studies in Nonconventional Conditions: *M. I. Montenegro, M. F. Bento, M. D. Geraldo,* and *M. J. Medeiros,* Dept. de Química, Universidade do Minho, Largo do Paço, 4719 Braga Codex, Portugal, *D. Pletcher,* Dept. of Chemistry, The University, Southampton, England, and *C. Amatore,* Ecole Normale Superieure, Paris, France

The advent of microelectrodes has catalyzed the interest in the application of electrochemical techniques in many fields. It is intended to demonstrate the possibilities offered by microelectrodes by presenting examples of studies performed in nonconventional conditions. It is shown that it is possible to gain insight into the mechanisms and kinetics of reactions of industrial interest which are, in practice, carried out in conditions such that the concentration of electroactive species is very high. The examples used for illustrating this point are the Monsanto reaction, the reduction of formaldehyde, and the methoxylation of furan. Examples are also presented on the influence of the nature and concentration of electrolyte in the electrochemical behavior of some organic compounds. Finally, an analytical application of microelectrodes in nonpolar solvents is considered. A simple and straightforward analytical procedure is presented for the determination of residual styrene in polysterene used in yoghurt packaging, using gold microelectrodes and linear sweep voltammetry.

601 A New Kind of Viscometer Based on the Electrochemical Measurement of Diffusion-Limited Currents at Microelectrodes and Microelectrode Arrays: *S. Fletcher* and *R. L. Deutscher,* CSIRO Institute of Minerals, Energy, and Construction, Div. of Mineral Products, Port Melbourne 3207, Victoria, Australia, and *V. A. Vicente-Beckett,* Dept. of Applied Chemistry, Royal Melbourne Institute of Technology, Melbourne, Victoria 3001, Australia

The present paper describes the principle and mode of operation of a new kind of viscometer which is capable of working in very viscous media or very small volumes of solution. The device works by recording the diffusion-limited currents of specially selected electroactive ions on microelectrodes and microelectrode arrays, and then converting the results into solution viscosities by applying the Stokes/Einstein relation. Proof-of-concept experiments are described in which the voltammetry of the potassium hexacyanoferrate (II/III) couple is investigated in glycerol + water mixtures. It is shown that, using conventional linear scan rates of applied potential (10 mV s^{-1}) and conventional microdisks (r_0 = 3.5 μm), it is possible to measure viscosities up to 100 mPa s without difficulty. It is also shown that viscosities greater than 4800 mPa s can be measrued when non-steady-state techniques and very large arrays are employed.

602 Electrocatalysis with Metal Microparticles in a Synthetic Glassy Carbon Host: *R. L. McCreery, N. Pocard, D. Alsmeyer, M. Huston, W. Huang,* and *M. Callstrom,* Dept. of Chemistry, The Ohio State Univ., Columbus, OH 43210

A synthetic route to glassy carbon (GC) involving an organometallic precursor results in thin films of modified glassy carbon denoted X-GC6, where X is Pt, Fe, halogen, etc. If X is initially single atoms of Pt(O), the final material contains small Pt clusters with average diameters of 8-15 Å. While the GC host is similar to conventional GC in mechanical, electrical, and electrochemical properties, the metal catalyst provides efficient electrocatalysis of hydrogen evolution (HER) and oxygven reduction. Evidence that the HER is mechanistically different on small Pt particles compared to bulk polycrystalline Pt is presented.

603 Electrified Microheterogeneous Catalysis: With and Without Zeolite-Supported Microelectrodes: *D. R. Rolison,* NRL, Surface Chemistry Branch, Washington, DC 20375-5342, and *J. Z. Stemple,* Pfizer Central Research, Groton, CT 06340

The intersection of electrochemical processes with aluminosilicate zeolites has led to studies exploring the effect of the zeolitic contribution, as based on molecular discrimination (size, shape, and charge selectivity) or on the catalytic nature of the zeolite, to the ionic and electron-transfer reactions of interest to electrochemists. Dispersion electrolysis in pure solvent permits characterization of supported microelectrodes or supported molecular catalysts for electro-organic reactions at low ionic strengths. The partial oxidation of propene was chosen as a model redox reaction, in that it is comprised of molecularly simple reactants and products, and is normally achieved by thermal, not electrochemical, means. This reaction was studied in pure water at three types of microheterogeneous dispersions: (*i*) Pt-Y (zeolite-supported microelectrodes); (*ii*) $Pd^{II}Cu^{II}$-NaY (zeolite-supported molecular catalyst); and (*iii*) $Pd^{II}Cu^{II}$/Pt-Y (zeolite-supporting microelectrodes and molecular catalyst).

Wednesday PM

604 Nanometer-Scale Electrochemical Synthesis of Electronic Materials Using the Scanning Tunneling Microscope: *W. Li, G. Hsiao, S. Lee, J. A. Virtanen,* and *R. M. Penner,* Institute for Surface and Interface Science, Dept. of Chemistry, University of California, Irvine, CA 92717-2025

Metal (Cu, Ag, Cd, etc.) and semiconductor (*e.g.,* CdSe) nanodisks having diameters of ≈100-200 Å and heights of 20-40 Å are synthesized in the STM by the reduction of metal ions at graphite surfaces. These structures are produced by confining the electrochemical reaction, which generates the semiconductor or metal as an insoluble product, to a nanometer-scale area of the sample surface. The spatial selectivity of the synthesis reaction derives from a unique two-step mechanism in which a reactive site (*i.e.,* a defect) is produced at the point of tunneling on the sample surface within 5 μs of the application of a bias pulse. Nucleation of the semiconductor or metal phase is then observed to occur on the high coordination sites of the defect and the subsequent growth of this structure is diffusion limited. Metal depositions onto Si(111) surfaces may be accomplished by field evaporation from the STM tip. Nanometer-scale Schottky barriers are thereby formed.

605 Toward the Refinement of Nanoband Electrodes: Chemically Enhanced Metal Nucleation as Studied by Scanning Probe Microscopy: *D. J. Dunaway* and *R. L. McCarley,* Dept. of Chemistry, Louisiana State University, Baton Rouge, LA 70803

Preparation of ultrathin metal films (d_{film} < 1 μm) on insulators is of great importance in many areas including catalysis, electronic device fabrication, microscopy and electrochemistry due to the unique properties exhibited by such thin films. Early stages of metal nucleation and growth are affected by the interaction of the metal with substrate, *e.g.*, surface wettability or affinity. We describe here the characteristics of thin (10-100 Å) evaporated Au films deposited onto SiO_2/Si (111) and onto monolayers of $(CH_3O)_3Si(CH_2)_3X$ (X = −SH, $-NH_2$ and $-CH_3$) on SiO_2/Si(111). Atomic force microscopy (AFM) images of Au deposited on the X = −SH monolayer indicate that adhesion of the Au to the thiol surface is affected by the deposition protocol. Interaction of the AFM tip with mobile Au crystallites on bare SiO_2Si(111) surfaces causes rows of crystallites to be formed in the scan area. The nature of the substrate-Au and tip-Au interactions is discussed in light of these results.

606 Imaging the Modification of Au(111) Monoatomic Steps with the Atomic Force Microscope: *J. C. Brumfield, C. A. Goss, E. A. Irene,* and *R. W. Murray,* Kenan Laboratories of Chemistry, University of North Carolina, Chapel Hill, NC 27599-3290

AFM images of Au(111) films on mica substrates show crystalline plateaus averaging 230 nm across and separated by *ca.* 20 nm deep valleys. Images obtained at relatively low (≈20 nN) tip-sample forces reveal well-defined monoatomic high (0.24 nm) terraces on top of individual crystallites. Scanning the tip at high forces results in selective removal of Au atoms at and near monoatomic terrace edges. A model is presented for the estimation of AFM tip dimensions from high resolution step profiles of monoatomic terrace edges. The results suggest that the contact mechanics of the Au surface are a function of defect density within and near the tip-sample contact area.

607 Luminescence Imaging of Electrode Microenvironments: *R. C. Engstrom* and *J. E. Vitt,* Dept. of Chemistry, Univ. of South Dakota, Vermillion, SD 57069

The formation and relaxation of the diffusion layer at platinum/iridium microelectrode tips was studied with fluorescence imaging techniques. Electrogenerated hydrogen ion or hydroxide ion converted a fluorescent indicator (either quinine or fluorescein) in bulk solution to the fluorescent form near the microelectrode tip. As predicted by theory, the diffusion layer established itself and reached a steady state within a few hundred milliseconds. The structure of the diffusion layer was spherically symmetrical, and its size was dependent on current density.

608 Observations of Corrosion Pit Initiation on Aluminum Using Microelelctrodces: *K. Hebert* and *Y. Tak,* Dept. of Chemical Engineering, Iowa State Univ., Ames, IA, and *I. Obi,* KDK Corp., Takahagi, Japan

Microelectrodes have been used to measure current transients associated with the appearance of individual micron-size corrosion pits on aluminum. The electrodes were 50 μm diam Al wires encased in epoxy. Electrochemical measurements were coupled with topographic observations using scanning electron microscopy. The birth of a corrosion pit was accompanied with an abrupt increase of current, from the passive current of about 10 nA, to around 50 nA, in a time of no more than 1 ms. Current noise was only significant after pits initiation.

609 Disk Microelectrodes Fabricated by Excimer Laser Micromachining: *B. J. Seddon* and *H. H. Girault,* Laboratoire d'electrochimie, Institut de Chimie Physique 3, Ecole Polytechnique Federale de Lausanne, CH-1015 Lausanne, Switzerland

Disk microelectrodes, as single devices or in arrays, have been developed in a planar format using conventional screen printing methods, dielectric encapsulation and laser photoablation micromachining. The microelec-

forming equipment used to decompose CCl_4, and has shown sensitivity in the 300 ppm range while not displaying any degradation due to the HCl. Measurements with the sensor have been performed which verify that the steam-reforming equipment can decompose a minimum of 90% of the CCl_4.

STATE-OF-THE-ART PROGRAM ON COMPOUND SEMICONDUCTORS XIX

Electronics

Thursday AM

623 InGaAs/GaAs Light Emittors for Optical Interconnections: *P. Van Daele, F. Vermaerke, P. De Dobbelacre, G. Vermeire, J. Blondelle, B. Dhoedt, R. Baets,* and *P. Demeesler,* University of Gent, Interuniversity MicroElectronic Center IMEC, Laboratory of Electromagnetics and Acoustics, B-9000 Gent, Belgium

For high density interconnections over short distances (a few millimeters to a few meters), optical losses in optical fibers or in free space are less important then, *e.g.,* for long distance communications. The wavelength region between 900 and 1000 nm, as covered by the InGaAs/(Al)GaAs material system is very attractive since cheap Si-detectors can still be used. The GaAs substrate is transparent and due to the strain QW laser diodes and LED's are expected to have high performance and high reliability. The requirements on the laser diodes can be very different depending on the application. Low threshold current and high speed is, for example, required when looking at short distance optical interconnects where closely packed arrays of laser diodes are used. For most of the applications no extreme performances are required and a fast processing scheme using self-aligned etching and isolation steps that we present, will result in high yield and reproducibility and is therefore very interesting. Also LEDs are interesting for optical interconnections because of their stability and robustness. The use of InGaAs(Al)GaAs LEDs, transmitting through the GaAs substrate, allows for the integration of diffractive lenses on the back side of the device. Such a configuration is extremely useful for parallel high density free space optical interconnects. Again processing details are presented together with typical characteristics.

624 New Advances in Compound Semiconductor Epitaxial Growth: *F. Briones,* CNM-CSIC, Madrid Spain

Growth of GaAs and InP based alloy compounds have advanced to higher levels of process control using the latest growth reactors for MOCVD and MBE. This paper covers the progress in these techniques as well as advances in characterization and *in situ* monitoring for the growth of these high quality materials.

625 10 × 16 GaAs/AlGaAs Multiquantum Well Infrared Detector Array: *J.-M. Li, H.-Q. Zheng, Y.-P. Zeng,* and *M.-Y. Kong,* Institute of Semiconductors, Chinese Academy of Sciences, Beijing 100083, China

10 × 16 GaAs/AlGaAs quantum well infrared detectors arrays with a peak responsivity at 9.4 μm have been achieved with front-side normal illumination based on a waveguide with a doubly periodic grating coupler. The GaAs/AlGaAs quantum well structures were grown in a Riber 32P MBE system and consisted of a 2 μm undoped AlAs waveguide cladding layer and 50 periods of 5.0 nm quantum wells (Si: 1×10^{18} cm^{-3}) separated by 32 nm thick undoped $Al_{0.28}Ga_{0.72}As$ barriers. The multiple quantum well structure is sandwiched between a doped (Si: 3×10^{18} cm^{-3}) 1.5 μm bottom and 1.0 μm top GaAs layer for electrical contacts. The detectors are made into arrays of 180 μm × 180 μm square mesas chemically etched down to the bottom contact layer. Crossed gratings of square symmetry and cavities of approximately cylindrical shape were fabricated by RIE into upper contact layer of the mesa. A peak detectivity $D^* = 1.3 \times 10^{10}$ cm $Hz^{1/2}/W$ and high responsivity $R_p = 0.37$ A/W have been obtained at $\lambda_p = 9.4$ μm and $T = 77$ K with front-side normal illumination. The dark current densities of the detectors in the array were smaller than 6.2×10^{-6} A/cm^2 with the detectors biased (3.2 V) for maximum detectivity.

626 Thermally Stable Schottky Contact on InGaP/GaAs: *K. Shiojima, K. Nishimura, T. Aoki,* and *F. Hyuga,* NTT LSI Laboratories, 3-1, Morinosato Wakamiya, Atsugi-shi, Kanagawa 243-01, Japan

The formation of a GaAs cap thicker than 70 Å on an InGaP film can successfully suppress the interfacial reaction between gate metal and InGaP during a post-ion implantation annealing at 800°C. WSiN/GaAs-cap (70 Å)/InGaP (200 Å) GaAs-sub Schottky contacts with a barrier height as high as 0.7 eV and break down voltage of 3 V were formed with 30 keV Si ion implantation.

627 The Role of Molecular Beam Epitaxy in the Fabrication of Low Threshold Vertical Cavity Surface Emitting Lasers: *M. T. Asom,* AT&T Bell Laboratories, Breinigsville, PA 18031

This paper presents a detailed study on the role of molecular beam epitaxy in the growth and fabrication of vertical cavity surface emitting lasers. We show that by selecting an appropriate growth temperature and the composition of Al, and controlling the unintentionally impurity doping density, we can obtain high quality and high reflectivity Bragg mirrors. The effects of three and two dimensional doping schemes on the resistance of p-type mirrors are presented. Finally, we describe a combination of growth parameters that have resulted in low threshold current and voltage, and highly uniform devices at 850 and 980 nm.

628 Photodissociation of Trimethylindium and Trimethylgallium on GaAs at 193 nm Studied by Angle-Resolved XPS and UPS Photoelectron Spectroscopy: *M. Kawasaki, S. Shogen, M. Ohashi, S. Hashimoto,* and *Y. Matsumi,* Institute for Electronic Science, Hokkaido University, Sapporo 060, Japan

Trimethylindium (TMIn) and trimethylgallium (TMGa) are exposed to a GaAs (100) substrate at 150 K, which mostly adsorb in their molecular form on the substrate. Partial dissociative adsorption is observed. An increase of the substrate temperature from 150 to 300 K induced the In-C bond cleavage of the adsorbed TMIn to generate methyl radicals that react with Ga species of the substrate to form the Ga-C bonds. The 193 nm irradiation of TMIn adsorbed on the GaAs at 150 K induces the In-C bond cleavage. A signal assigned to In appeared due to formation of In metals on the surface. Upon laser irradiation, the absolute intensity of the C1s signal decreased to 40% of the original intensity. Carbon containing were species ejected from TMIn into the gas phase by 193 nm irradiation while In atoms remained on the substrate. Irradiation at 351 nm caused no change in the x-ray photoelectron spectra of the adsorbed species. These results imply that photodissociation is not due to photoabsorption of the GaAs substrate but that of the adsorbed species on the substrate. Photoirradiation of 514.5 nm on TMIn adsorbed on GaAs at 150 K induces pyrolytic cleavage of the In-C bond.

629 Barrier Thickness Dependence of Lasing Characteristics in InGaAsP Strained Multiquantum Well Structure: *S. Suzaki, K. G. Ravikumar, T. Sekiguchi, T. Banno,* and *R. Yamauchi,* Optical Device Section, Advanced Technology R&D Center, Fujikura Ltd., 1440, Mutsuzaki, Sakura, Chiba 285, Japan

Recently, strained multiquantum well (MQW) structures have been extensively investigated for high power, high efficiency LDs[1] and TE/TM polarization controlled optical switches. Large well volume ratio in a MQW structure, with a barrier thick enough to avoid coupling between wells, is preferable for high optical confinement as well as high gain. The barrier thickness becomes the more important parameter, because it also acts as a confining medium for the strain in the well. We have reported the barrier thickness dependence of InGaAs/In(GaAs)P strained MQW structure, and showed that suitable barrier thickness for high crystal quality was about twice the strained well thickness.[2] Here, we report the barrier thickness and strain quantity dependence of threshold current density in InGaAsP ($\lambda_g = 1.7$ μm)/InGaAsP ($\lambda_g = 1.15$ μm) strained MQW structure. The strained MQW structure grown by Lp-OMVPE on a p-InP substrate is comprised of 3 periods of 6 nm thick $In_{0.65}Ga_{0.35}A_{0.89}P_{0.11}$ compressively strained (1%) well layer and 5-20 nm thick InGaAsP barrier layers embedded in InP cladding layers. The fine crystal quality was obtained for 10 nm barrier from the results of photoluminescence measurement. 600 μm long broad area laser diodes were fabricated with this wafer and pulse lasing characteristics were measured. The minimum threshold current density (J_{th}) of 600 A/cm^2 as well as maximum differential quantum efficiency was obtained in the case of 10 nm barrier. The best J_{th} value was around 290 A/cm^2 for 1800 μm device. These results show that the strain in the well is relaxed in the case of thin barrier, leading to uniform strain in well layers, due to which J_{th} increased. By increasing the barrier thickness, which here acts as a confining medium for strain in the well, the crystal quality is improved, and J_{th} is decreased. However, in the case of thicker barrier, more than twice the well thickness, J_{th} is increased due to the decrease of optical confinement. In conclusion, suitable barrier thickness for minimum J_{th} and maximum quantum efficiency in 1% compressively strained MQW structure is around twice the well thickness.

1. P. J. A. Thijs *et al., IEEE J. Quantum Electron.,* **22,** 1426 (1991).
2. S. Suzaki *et al., Jpn. J. Appl. Phys.,* **32,** L408 (1993).

Thursday PM

630 Low Specific Contact Resistivity GaAsSb p-Type Ohmic Contacts for AlGaAs/GaAs Based Devices: *K. Ikossi-Anastasiou, M. S. Ahmed,* and *Z. M. Khwaja,* Solid State Laboratory, Dept. of Electrical and Computer Engineering, Louisiana State University, Baton Rouge, LA 70803-5901

A molecular beam epitaxy graded GaAsSb superlattice with Au/Zn/Au metallization produced ohmic contacts to P type AlGaAs/GaAs heterojunction bipolar transistors (HBTs), with specific contact resistivity in the 10^{-7} $-cm^2$ range. A two layer transmission line model for the multilayer structure indicates that the interface that dominates the measured resistivity is the GaAs/GaAsSb and not the GaAsSb/metal interface. This suggests that even better ohmic contacts could be realized with optimization of the GaAsSb graded layer.

631 Gate Recess Etch Contributions to Source Resistance: *G. T. Cibuzar,* Microelectronics Laboratory, University of Minnesota, Minneapolis, MN 55455

Fabrication of microwave MESFETs and MODFETs usually involves gate recessing to reduce the source resistance. Gate recessing involves either a wet chemical or an RIE-based process followed by metallization. Normally there exists a small length δ of the channel on each side of the gate which has been recessed but is not covered by the gate metallization. This region has a high sheet resistance and can greatly affect the source resistance. We present a technique for quantifying this contribution R_δ to the source resistance using common test structures such as ohmic contact transmission lines and variable dimension FETs. Results show that for 27 MESFETs spread across a 3 in. wafer, each with gate and channel lengths of 1 and 3 μm, respectively, and with δ measured by SEM to be 0.2 μm, the contribution of R_δ to the measured source resistance is almost 50%.

632 Defect Characterization and Hydrogenation of MOCVD-Grown InP on GaAs and Ge Substrates: *B. Chatterjee* and *S. A. Ringel,* Dept. of Electrical Engineering, The Ohio State University, Columbus, OH 43210, *R. Hoffman,* NASA Lewis Research Center, Cleveland, OH 44135

The growth of InP on GaAs and Ge substrates is of current interest for integration of high speed electronic and photonic devices and for low-cost space-based solar cells. Inherent in such heteroepitaxial structures are misfit and threading dislocations resulting from lattice mismatch. This paper presents an investigation of the electronic properties of these dislocation, correlations to their microstructural properties, and the use of atomic hydrogen to

luminescence measurements) are used to investigate the C_{60}/metal system as well. Reflectance measurements show absorption at 450 nm on the aluminum/C_{60} material. Soft x-ray photoelectron spectroscopy of C_{60} monolayers on metal surfaces is used to show that the C_{60} cage is intact up to a surface anneal temperature 650-750 K. The hydrophobic nature of C_{60} can be used to reduce the sticking probability of water vapor to C_{60} covered metal surfaces. (This work was performed under the auspices of U.S. Department of Energy, by Lawrence Livermore National Laboratory under Contract No. W-7405-ENG-48.)

642 Fragmentation and Delayed Ionization of Fullerenes: *K. R. Lykke,* Materials Science/Chemistry Div., Argonne National National Laboratory, Argonne, IL 60439, *P. Wurz,* Physikalisches Institut. Universitat Bern, CH-3012 Bern, Switzerland

Two major processes result from high internal excitation of fullerenes: fragmentation and delayed ionization. Both of these processes have macroscopic analogues, namely, evaporation and thermionic electron emission from hot surfaces. We discuss recent results on each of these mechanisms for energy loss from extremely excited species.

643 Mass Spectrometric Characterization of Fullerenes and Metallofullerenes: *S. W. McElvany, J. H. Callahan, H. H. Nelson,* and *M. M. Ross,* Chemistry Div., Code 6113, Naval Research Laboratory, Washington, DC 20375

Mass spectrometry has been vital in both the analysis and characterization of fullerenes and their derivatives and also in obtaining insights into the formation mechanisms of these species. Rapid thermal desorption coupled with negative ion chemical ionization is extremely sensitive in the analysis of both fullerenes and endohedral metallofullerenes. This technique has recently been used to detect and characterize large odd-numbered carbon clusters (C_{119}, C_{129}, and C_{139}) and their apparent production through ozone-catalyzed coalescence reactions. Studies are underway to characterize and optimize the reactions that form these unique species. Laser desorption/vaporization can also be used in the analysis of fullerenes but under certain laser/sample conditions, laser-induced surface and/or plasma reactions result in the production of gas-phase species which are not in the initial sample. One example is the production of metallofullerenes from laser vaporization of metal/fullerene mixtures. Although the formation mechanism of metallofullerenes remains unresolved, laser desorption studies of cyclocarbon precursors which yielded fullerenes provided the first evidence that coalescence of cyclic carbon species may play an important role in the formation of fullerenes.

644 Factors Affecting Fullerene Formation: *M. T. Bowers, G. von Helden, N. G. Gotts* and *E. Porter,* Dept. of Chemistry, University of California, Santa Barbara, CA 93106

Over the past 6 or 7 years there have been a number of mechanisms put forward to explain the surprising appearance of C_{60} Buckminster fullerene and other similar carbon cage compounds of smaller and larger sizes. These mechanisms have focused on constructing fullerenes from "component parts," mainly 5 and 6 member ring networks, although condensation of larger monocyclic rings has also been proposed. The puzzling aspect of these mechanisms is that component parts either do not appear at all at small carbon sizes or cease to be important in the carbon isomer distribution before fullerenes begin to appear. Recently, however, we have shown that collisional heating of large mono, bi and tricyclic ring systems causes them to rearrange very efficiently to fullerenes. In this paper we present our first data on how efficiently this process proceeds for negatively charged carbon clusters and the effect of both metal atoms and hydrogen on the carbon growth mechanism.

645 Determination of the London Penetration Depth in Superconducting Rb_3C_{60} with Pulsed EPR: *K.-P. Dinse,* Technische Hochschule Darmstadt, Institut für Physikalische Chemie, Physikalische Chemie III, D-64287 Darmstadt, Germany, *D. M. Wang, R. Bramley,* and *J. W. White,* Research School of Chemistry, The Australian National University, Canberra, Australia

Alkali-doped superconducting fullerenes exhibit a strong EPR signal, observable above and below T_c. Although the origin of the multicomponent signal has not yet been fully characterized, pulsed EPR investigations have clearly established the presence of localized spins in the bulk of the sample. This result prompted us to use these spins as local field probes for the magnetic flux in the vortex state of the superconductor. From the temperature-dependent width of the echo-detected EPR signal the vortex-induced field variance was determined and interpreted in terms of the London penetration length λ. Its low-temperature extrapolated value in the system Rb_3C_{60} was found as $\lambda(0) = 480(40)$ nm, well in the range predicted from a correlation of the charge carrier density and T_c.

646 Electrochemistry of Crown-Ether Fulleroids at Very Negative Potentials: *L. Echegoyen, Q. Xie,* and *F. Arias,* Dept. of Chemistry, University of Miami, Coral Gables, FL 33124, *S. R. Wilson* and *Y. Wu,* Dept. of Chemistry, New York University, Washington Square, NY 10003

The cyclic and Osteryoung square wave voltammetries (CV and OSWV) of some substituted C_{60}s have been obtained in a toluene:acetonitrile solvent mixture, as previously described. Some of the structures studied are shown below. The most interesting observation is a larger than expected peak potential separation between the fourth and fifth electron reductions of these molecules. They are separated by an extra 110 mV over the expected 400 mV typically observed for C_{60} and its derivatives. These results are interpreted in terms of removal of the triply degenerate LUMO of C_{60} resulting from the presence of the substituents. Other results to be presented include the formation of supramolecular complexes of C_{60} with a series of water soluble calixarenes along with ESR studies of C_{60}^{2-}. In the calixarene work, several new complexes have been formed and detected between a series of water soluble calix-[6]- and calix-[8]-arenes. The ESR work has clearly established the presence of an aggregate of C_{60}^{2-}.

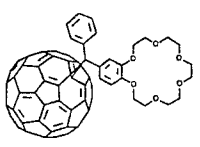

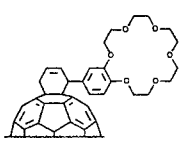

Tuesday AM

647 Methods for the Synthesis and Purification of M @ C_{60}: *J. M. Alford, M. D. Diener,* and *R. E. Smalley,* Dept. of Chemistry, Rice University, Houston, TX 77251-1892

Encapsulated metal fullerenes, such as La @ C_{60}, promise to provide researchers with an exciting new class of exotic materials. However, the macroscopic synthesis and purification of these new molecules has proven to be difficult and time consuming. We report here on various new techniques for the bulk production of M @ C_{60}. These methods include both direct laser vaporization of graphite-metal oxide targets and conventional arc vaporization of graphite-metal oxide rods. In both cases the vaporization is carried out in a high temperature furnace where the fullerenes and metal fullerenes are separated from the waste carbon soot by a gas phase filtering system utilizing a flowing carrier gas and high temperature filters such as ceramic or graphite fiber cloth. The resulting fullerene-metal fullerene mixture is air sensitive and must be kept under an inert gas environment. When handled under anaerobic conditions, the M @ C_{60} can be resublimed, and we are now investigating the feasibility of purifying the M @ C_{60} by fractional sublimation along a temperature gradient using either a high vacuum or a diffusion controlled process.

648 Chemistry of the Fullerenes: The Manifestation of Strain in a Class of Aromatic Molecules: *R. C. Haddon,* AT&T Bell Laboratories, Murray Hill, NJ 07974-0636

Within the π-orbital axis vector (POAV) theory the total rehybridization required for closure of the fullerenes is approximately conserved. This allows for the development of a structure-based index of strain in the fullerenes, and it is estimated that about 90% of the heat of formation of the carbon atoms in C_{60} may be attributed to a combination of σ-strain and steric inhibition of resonance. Application of this analysis to the geometries of structurally characterized organometallic derivatives of C_{60} and C_{70} shows that the reactivity exhibited by the fullerenes may be attributed to the relief of a combination of local and global strain energy which is unique to this class of molecules. C_{60} is of ambiguous aromatic character with anomalous magnetic properties, but with the reactivity of an aromatic molecule, moderated only by the tremendous strain inherent in the spheroidal structure.

649 Solubility Studies of C_{70}: *R. S. Ruoff, A. Chwang, R. Malhotra, D. Tse,* and *D. Lorents,* Molecular Physics Laboratory, SRI International, Menlo Park, CA 94025

The room temperature solubility of C_{70} in a variety of pure solvents has been determined by calibrated HPLC. Comparison to the solubility of C_{60}[1] in the same solvent set is given. Technological implications are discussed. The temperature dependence of solubility of C_{70} in several solvents has been determined between 190 K and the normal solvent boiling points. Comparison to the temperature dependence of the solubility of C_{60}[2] in the same solvent set is given. Technological implications are discussed.

1. R. S. Ruoff, D. Tse, R. Malhotra, and D. C. Lorents, *J. Phys. Chem.,* **97,** 3379 (1993).
2. R. S. Ruoff, R. Malhotra, D. L. Huestis, and D. Tse, *Nature,* **362,** 140 (1993).

650 Solvent-Induced Spectral Shift Studies of C_{60}: *R. S. Ruoff, A. Chwang, R. Malhotra, D. Tse,* and *D. Lorents,* Molecular Physics Laboratrory, SRI International, Menlo Park, CA 94025

C_{60} is not purple in all solvents. For example, in 1-chloronaphtohalene, 1-methylnapthalene, and 1,2,3,5-tetramethylbenzene, dilute C_{60} solutions are essentialy yellow. We present a correlation of C_{60} spectral shift with the room temperature solubility[1] of C_{60} in a variety of solvents. Stronger solvents cause stronger spectral shifts. The simple explanation for the "dramatic" color change is given, based on the spectral response of the human eye.[2]

1. R. S. Ruoff, D. Tse, R. Malhotra, and D. C. Lorents, *J. Phys. Chem.,* **97,** 3379 (1993).
2. Vol. 19, McGraw-Hill Encyclopedia of Science & Technology, 6th ed., pp. 249-254, New York, (1987).

651 Adsorption Isotherm Studies of C_{60} and C_{70}: *R. S. Ruoff, A. Chwang, R. Malhotra,* and *D. Lorents,* Molecular Physics Laboratory, SRI International, Menlo Park, CA 94025

Room temperature adsorption isotherms of pure C_{60}, pure C_{70}, and C_{60}, C_{70} mixtures are presented. The solid phase sets are a group of activated carbons;[1] graphite powder; and alumina. The solvents employed include (among others) toluene and 1,2 dichlorobenzene. The technological implications of these studies and what they teach us about chromatography with activated carbon stationary phase (a "tour de force" for separation of C_{60}, but not C_{70} and larger fullerenes, Ref. 2) are discussed, along with suggested methods for improvement to this chromatographic[2] method.

1. We thank the American Norit Company for donation of a variety of activated carbons for this study.

2. W. A. Scrivens, P. V. Bedworth, and J. M. Tour, *J. Am. Chem. Soc.,* **114,** 7917 (1992).

652 Encapsulation of Uranium in Supergiant Fullerenes: *R. S. Ruoff,*[a] *S. Subramoney,*[b] *D. Lorents,*[a] and *D. Keegan,*[a] [a]Moleculare

istry, University of Delaware, Newark, DE 19716, *S. A. Lerke,* Sterling Winthrop Pharmaceuticals, Malvern, PA 19355, *P. J. Fagan,* Central Research and Development Department, E. I. du Pont de Nemours and Co., Inc., Experimental Station, Wilmington, DE 19880-0328

The overall cathodic electrode reactions of many compounds comprise a series of electron transfer and protonation reactions. The thermodynamic reversible potential of the overall reaction is a function of the standard potentials of the electron transfer steps and the pK_a values of the species in the scheme. In principle, the reduction of C_{60} to $C_{60}H_2$ (and more fully hydrogenated forms) can be analyzed within this framework. Rough estimates of the reversible potentials for the $C_{60}/C_{60}H_2$ system were obtained from earlier data for t-BuC_{60}^-, t-BuC_{60}, and t-BuC_{60}H. Acid-base equilibria for $C_{60}H_2/C_{60}H^-$/C_{60}^{2-} in DMSO were studied by voltammetry.

661 Spectroscopic Characterization of Electrochemically Prepared Fullerene Films: *P. W. Faguy* and *W. N. Richmond,* Dept. of Chemistry, University of Louisville, Louisville, KY 40292, *F. Xu, A. Borman,* and *T. F. Guarr,* Dept. of Chemistry, University of Kentucky, Lexington, KY 40506-0055

Electrochemical reduction of C_{60} in acidic nonaqueous media yields a mixture of soluble reduced fullerenes $C_{60}H_n$. Surprisingly, however, repetitive cycling under these conditions leads to the deposition of electroactive layers on the electrode surface. The characteristics of such films suggest that they can also be formulated as reduced fullerene derivatives, but these insoluble materials may be oligomeric or polymeric in nature. Preliminary laser desorption mass spectral data indicate the formation of new high MW species, including several peaks at integer multiples of 720. The films are also being probed by *in situ* as well as *ex situ* IR spectroscopy (using germanium windows); these results are discussed in detail. The electrochemical and spectroscopic properties of the films are sensitive to both the proton concentration and the switching potential employed during deposition. The incorporation of various redox-active species (*i.e.,* ferrocene, $Ru(NH_3)_6^{2+}$) serves to stabilize the electrochemical response of the films by providing a mechanism for the release of trapped charge.

662 Electrochemical Properties of Reduced Fullerenes: *T. F. Guarr, M. S. Meier, V. K. Vance,* and *M. Clayton,* Dept. of Chemistry, University of Kentucky, Lexington, KY 40506-0055

Although the preparation of $C_{60}H_{36}$ via Birch reduction of C_{60} is well known, chemical reduction of C_{60} under milder conditions has only very recently been shown to lead to less highly reduced fullerenes such as $C_{60}H_2$ and $C_{60}H_4$.[1] Gel permeation chromatography then provides a convenient route to isolation of these materials in reasonable purity ($C_{60}H_4$ is obtained as a mixture of three isomers). Electrochemical oxidation of $C_{60}H_2$ in 80/20 toluene/CH_3CN (E_p = +1.13 V vs. Fc^+/Fc) is chemically irreversible at all accessible sweep rates and yields C_{60} via a $2H^+$, $2e^-$ process. Four reversible one-electron reductions of $C_{60}H_2$ (with half-wave potentials 120-170 mV more negative than those of C_{60}) are observed at relatively fast sweep rates (> *ca.* 1 V/s). However, at slower sweep rates, a decrease in the magnitude of the anodic return waves is accompanied by the appearance of several new peaks attributable to redox processes of the parent fullerene. Addition of even a single electron to $C_{60}H_2$ is sufficient to induce conversion to C_{60}. The formation of C_{60} (following reoxidation) has been confirmed by C_{18} HPLC.

1. M. S. Meier, V. K. Vance, P. L. Corbin, and M. Clayton, *J. Org. Chem.,* Submitted.

663 Magnetic Properties of Some Solid C_{60} Salts: *M. T. Jones, P. Boulas, R. Subramanian, W. Kutner,* and *K. M. Kadish,* Dept. of Chemistry, University of Houston, Houston, TX 77204-5641.

The results from an investigation of the static magnetic susceptibility and ESR properties of a variety of chemically synthesized solid salts of C_{60}^{n-} anions,[1] of the general formula $(D^+)_nC_{60}^{n-}$, where D^+ includes the methylpyridinium, methylquinolinium, and tetraalkylammonium cations, are presented. A comparison of the *g* vlaues and ESR linewidths with previously reported data indicate predominant 1:1, $n = 1$, stoichiometry of the salts.[2,3] The ESR linewidths of the solid salts are thermally activated. The determined activation energies are compared to those previously reported. Static magnetic susceptibility measurements show antiferromagnetism at low temperature in some of the salts studied. A comparison of these resutls with those obtained from the ESR studies will be presented.

1. P. Boulas, R. Subramanian, W. Kutner, M. T. Jones, and K. M. Kadish, *J. Electrochem. Soc.,* **140,** L130 (1993).
2. D. Dubois, M. T. Jones, and K. M. Kadish, *J. Amer. Chem. Soc.,* **114,** 6446 (1992).
3. R. Rataiczak, R. Subramanian, W. Koh, K. M. Kadish, and M. T. Jones, *Synthetic Metals,* In press.

664 Solvent, Supporting Electrolyte and Substituent Effects on the Electrochemistry of Fullerenes: *K. M. Kadish,* Dept. of Chemistry, University of Houston, Houston, TX 77204-5641

The redox properties of "simple" and derivatized fullerenes have now been reported under a variety of experimental conditions. Redox potentials have been measured in numerous solvent/supporting electrolyte mixtures, as neutral or doped films at an electrode surface and as inclusion complexes in a matrix such as cyclodextrin. This paper summarizes recent electrochemical data from our laboratory as well as from those of others and attempts to present a self-consistent picture as to the most important factors which influence the reversible half-wave potentials. Compounds to be discussed included not only C_{60} and C_{70} but also derivatives such as $C_{60}H_2$ and $C_{70}H_2$, $C_{60}(R)_n$ and $C_{70}(R)_n$ where R is a given alkyl group and $n = 2$ or 4. Many of the electroreduced fullerenes have been characterized by UV-visible, ESR, IR and/or Raman spectroscopy and data on several of these electrogenerated species are presented.

665 Regioselective Electrosynthesis of Alkylated C_{60} Derivatives: A Novel Method for Controlled Functionalization of Fullerenes: *K. M. Kadish, C. Caron, R. Subramanian, F. D'Souza, W. Kutner* and *M. T. Jones,* Dept. of Chemistry, University of Houston, Houston TX 77204-5641

A new electrosynthetic method for the selective alkylation of fullerenes was developed. The method consists of first generating the C_{60}^{2-} dianion by bulk electroreduction of the neutral C_{60} compound in an aprotic solvent solution, followed by reacting this dianion with an alkyl halide to yield selectively R_pC_{60} where R = CH_3–, CH_3CH_2–, $CH_3(CH_2)_2$– and *n*-$CH_3(CH_2)_3$–; $p = 2$ or 4. For the doubly alkylated products, either a mixture of the 1, 2- and 1, 4-R_2C_{60} regioisomers or a single isomer was obtained, depending upoon the reaction conditions and the nature of the alkyl addend. Up to four reversible, one-electron electroreductions were detected by cyclic voltammetry (CV) and differential pulse voltammetry (DPV) for the alkylated products, isolated by semi-preparative gel permeation HPLC. The $E_{1/2}$ values of these electroreductions were examined as a function of the nature and number of alkyl addends. The alkylation products were characterized by HPLC on a "Buckyclutcher I" column, UV-vis spectroscopy and spectroelectrochemistry as well as by ^1H and ^{13}CNMR spectroscopy. A prevailing alkylation mechanism was proposed.

Wednesday PM

666 A Computational Model for Fullerene Chemistry: *B. Doust, D. A. Jelski,* and *J. R. Bowser,* Dept. of Chemistry, State University of New York, College at Fredonia, Fredonia, NY 14063, *T. F. George,* Dept. of Chemistry and Physics, Washington State University, Pullman, WA 99164

The complexity of fullerene chemistry suggests that a simple computational model of fullerene reactivity is important. Toward this end, we are developing an extended Hückel model for fullerene chemistry which will be fit to the experimental and *ab initio* thermodynamic and electronic structure data. The initial application of the model will be to calculate structure activity relationships, particularly Drago-Wayland measures fo Lewis acid-base chemistry. The reactivity differences between pure fullerene and variously addended species are investigated. An attempt is made to untangle the bewilderingly complex array of isomers which fullerene adducts present.

667 Theoretical Studies of Fullerene Derivatives: *K. Raghavachari,* AT&T Bell Laboratories, Murray Hill, NJ 07974

Chemical modifications of fullerenes have resulted in the formation of a variety of functionalized fullerenes. In this work, we investigate the structures and properties of fullerene derivatives by means of semiempirical, *ab initio* Hartree-Fock, and density functional studies. Both exohedral and endohedral derivatives are considered. The bonding in the derivatized fullerenes is compared to that in C_{60}. Spectroscopic properties and chemical reactivities of the derivatives are discussed.

668 Evaluation of Linear and Nonlinear Optical Properties of Fullerenes: *A. Rosén* and *E. Westin,* Dept. of Physics, Chalmers University of Technology and University of Göteborg, S-412 96 Göteborg, Sweden

Electronic and optical properties of fullerenes and especially C_{60} have been studied using local density approximations and a numerical LCAO approach. Energy dependent linear and nonlinear polarizabilities have been evaluated using a sum over states approach with single particle wavefunctions, dipole matrix elements, and energy levels determined from the ground state calculations. The induced dipole moment was calculated using an external field in the Hamiltonian. By repeating such calculations for different field strengths, the static linear and nonlinear polarizabilities of C_{60} have been evaluated. To approximately treat the dynamic polarizabilities, the static field results were used to determine an effective parameter in a simplified random phase approximation (RPA) approach. After inclusion of screening, broadening, and Lorentz local field factors, the dispersion of the linear dielectric function for films of C_{60} is well described. The evaluated nonresonant third order nonlinear polarizabilities are however two orders of magnitude larger than the experimental values. This discrepancy is analyzed by evaluation of energy dependent free and screened values of the third order nonlinear polarizabilities for third harmonic generation (THG) degenerate four wave mixing (DFWM), and electric field induced harmonic generation (EFISH).

669 Fullerene Annealing and Fragmentation: A Tale of Handles and Sticks: *G. E. Scuseria,* Rice Quantum Institute and Dept. of Chemistry, Rice University, Houston, TX 77251-1892

We have investigated the process of fullerene annealing and fragmentation using various theoretical methods and present the energy barriers of a wide range of reactions. Our theoretical predictions imply that many of the assumptions frequently made about fullerenes, that their carbon is trivalent and that they are composed of five- and six-membered rings, may not be valid under certain experimental conditions. These results may be useful in designing experimental processes to control the fullerene surface.

670 Pinching Reactions of Carbon Rings: *D. L. Strout* and *G. E. Scuseria,* Dept. of Chemistry and Rice Quantum Institute, Rice University, Houston, TX 77251-1892

Recently, it has been shown that fullerenes can be synthesized from monocyclic carbon rings with 18, 24, or 30 carbon atoms. To understand these formation processes it becomes necessary to understand the mechanisms whereby large monocyclic rings form networks of pentagons and hexagons. The mechanisms and energetics of such ring "pinching" reactions are investigated by theoretical means. The Hartree-Fock self-consistent field method is employed, as well as a recently proposed hybrid of Hartree-Fock and density functional methods.

Above the orientational order-disorder transition at ~260 K, C_{60} molecules undergo a hindered rotation in their face-centered cubic (FCC) lattice sites with pronounced deviation from spherical symmetry. Through an analysis of the symmetry-adapted spherical harmonic coefficients, determined from a synchrotron x-ray study,[1] we have extracted a meanfield single particle potential, $V(\omega)$, where (ω) represents the set of Euler angles describing the molecular orientation in the crystal frame. The potential shows a barrier height of −46 meV as the C_{60} molecule is rotated about a <111> axis starting with its twofold axes along the cube axes of the crystal. A potential minimum occurs at −98° which brings pentagons essentially into [110] directions. Other details of the orientational potential function are discussed. (This research was supported by the NSF on DMR92-08450 and by the State of Texas at the Texas Center for Superconductivity at the University of Houston.)

1. P. C. Chow *et al., Phys. Rev. Lett.,* **69,** 2943 (1992).

682 Indenyl Iridium Complexes of C_{60} and C_{70}: *J. R. Shapley,* School of Chemical Sciences and Materials Research Laboratory, University of Illinois, Urbana, IL 61801

Substitution of the labile cyclooctene ligand in the indenyliridium(I) compound $(\eta^5\text{-}C_9H_7)Ir(CO)(C_8H_{14})$ with C_{60} provides the compound $(\eta^5\text{-}C_9H_7)Ir(CO)(C_{60})$, which has been isolated as a green-black solid following chromatography over neutral alumina. The structure of the [Ir-C_{60}] complex is assigned as having the C_{60} ligand bonded to the iridium center in a π-fashion (*i.e.,* at a 6, 6 junction) by a combination of ^1H and ^{13}C NMR, Raman, and UV-Vis data and comparison with other mono-substituted C_{60} derivatives. The properties of the [Ir-C_{60}] complex have been probed by a number of physicochemical techniques, including, substitution kinetics, cyclic voltammetry, and laser flash photolysis. An analogous [Ir-C_{70}] complex has been prepared in the same manner and isolated as a brown solid. The ^1H NMR spectrum of this complex suggests that the iridium atom is coordinated to one of the double bonds radiating from the five-membered ring end caps of the C_{70} structure. The barrier to restricted rotation about this Ir-η^2-C_{70} bond has been measured as *ca.* 22 kcal/mol.

683 Reactions of C_{60} and C_{70} with Main-Group and Transition Metals in N-Methylimidazole: *J. P. Selegue, S. Dev.,* and *T. G. Guarr,* Dept. of Chemistry, University of Kentucky, Lexington, KY 40506-0055, *J. W. Brill* and *E. Figueroa,* Department of Physics & Astronomy, University of Kentucky, Lexington, KY 40506-0055

Recent success in raising the superconducting transition temperature (T_c) of alkali metal fullerides, A_3C_{60}, by the intercalation of ammonia suggests that fulleride salts with larger, ligated metal cations $[ML_n]^{n+}$ may provide a systematic approach to new superconducting fullerene phases. Dissolving metal reactions of C_{60} with Mg, Ca, Ba, Mn, and Fe (all at 90°C) or Cu and Zn (at room temperature) metals in neat N-methylimidazole (Melm) produce deeply colored solutions containing fulleride anions. The reaction of Cu powder with C_{60} also proceeds in pyridine. Dissolving-metal reductions of C_{70} with Cu (room temperature) or Mg (90°C) proceed similarly in N-methylimidazole. Reduction in volume *in vacuo* and precipitation with ethyl ether yields very insoluble, brown to black powders or microcrystals of the fulleride salts. Metal analyses are generally consistent with the formulas $[M(Melm)_x]^{2+}[C_{60}]_2^-$ (x = 6 for Mg, Ca, Ba, Mn, and Fe, x = 4 for Cu and Zn). ESR spectra display the characteristic signal of C_{60}^-, sometimes superimposed over the $[M(Melm)_x]^{2+}$ signal. Variable-temperature magnetic moment measurements are in progress.

684 Synthesis and Characterization of Decamethylmanganocenium Fulleride Salts: *J. P. Selegue* and *S. Dev,* Dept. of Chemistry, University of Kentucky, Lexington, KY 40506-0055, *J. W. Brill, E. Figueroa, L. DeLong,* and *Q. Chen,* Dept. of Physics & Astronomy, University of Kentucky, Lexington, KY 40506-0055

The electron-accepting ability of the fullerenes makes them attractive candidates for the formation of charge-transfer salts, perhaps with "organic metal" conducting properties. The reaction of decamethylmanganocene, $[Mn(Cp^*)_2](Cp^* = \eta^5 - C_5Me_5)$, with C_{60} in toluene or benzene gives a dark brown solution from which a black solid is precipitated upon addition of pentane. C_{70} leads to a very similar product. Elemental analyses, infrared, NMR, ESR, and mass spectrometric data are most consistent with the formulations $[Mn(Cp^*)_2][C_{60}]_2$ and $[Mn(Cp^*)_2][C_{70}]_2$. Magnetic susceptibilities of these compounds were measured at temperatures between 5 and 300 K by using a Faraday balance. Samples of $[Mn(Cp^*)_2][C_{60}]_2$ unexposed to the air obey a Curie-Weiss law, $\chi = \chi_\infty + C/(T \cdot \theta)$, with $\chi_\infty = 4.5 \times 10^{-4}$ emu · mol^{-1}, C = 0.516 emu · K · mol^{-1} and $\theta = -1.27$ K. The Curie constants are consistent with the presence of one $[Mn(Cp^*)_2]^+$ (S = 1), one C_{60}^- (S = 1/2) and one neutral C_{60}(S = 0) per formula unit. The negative values of θ indicate that there is (very weak) antiferromagnetic coupling between $[Mn(Cp^*)_2]^+$ and $[C_{60}^-]$ or $[C_{70}^-]$.

685 Progress in Higher Fullerene Purification and Investigations on New C_{60} Derivatives: *F. Diederich, A. Herrmann, L. Isaacs, C. Thilgen,* and *A. Wehrsig,* Laboratorium für Organische Chemie, ETH-Zentrum, CH-8092 Zürich, Switzerland, *G. Calzaferri* and *D. Herren,* Institut für Anorganische, Analytische und Physikalische Chemie, Universität Bern, CH-3000 Bern 9, Switzerland

The preparative HPLC-separation of C_{60} and the larger carbon spheres C_{70}, C_{76}, C_{2v}- and D_3-C_{78}, and C_{84} was improved and quantified by the use of a tetrachloro-phthalimidopropyl modified silica π-acceptor phase. Reactions of C_{60} with ethyl and tert-butyl diazoacetates in refluxing toluene led to the formation of three (alkoxycarbonyl)methylene-bridged C_{60} isomers which can be thermally equilibrated into single compounds. Based on NMR data, the thermodynamically most stable isomers are bridged at the 6-6 ring junction (1) whereas the remaining isomers are bridged at the 6-5 junction (2, 3). The assignment of an open transannular bond, leading to a 1,6-methano[10]annulene-type structure, to the 6-5 ring bridged structures and of a closed transannular bond to the 6-6 ring bridged strucures is supported by the ^{13}C NMR chemical shift of the bridgehead carbon atoms and $^1J(C, H)$ of the methylene bridge atoms. With the synthesis of carboxylic ester derivates of C_{60}, versatile reagents for the attachment of a fullerene residue have been developed. In further studies, covalent fullerene-crown ether derivatives are prepared, which combine the metal complexing ability of crown ethers with the high electron affinity of C_{60}.

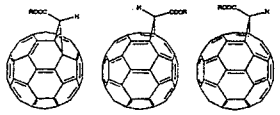

1 2 3

686 Exploring the Reactivity of Fullerenes C_{60} and C_{70}: *A. L. Balch, J. W. Lee, B. C. Noll,* and *M. M. Olmstead,* Dept. of Chemistry, University of California, Davis, CA 95616

Our group has been successful in the past in discretely derivatizing fullerenes with organometallic reagents and structurally characterizing these fullerene adducts utilizing various spectroscopic techniques including single crystal x-ray diffraction. We have previously reported on the addition of iridium complexes to the surface of fullerenes C_{60} and C_{70}.[1,2] Recently, we also presented our work on the first structural characterization of the C_{60} radical anion in a single crystal form.[3] Our work on the double addition product of C_{60} showed that the second addition preferably adds at the site furthest from the first addition.[4] As for the double addition to C_{70}, we have reported on the selective crystallization of one particular isomer which seems to be favored merely by intermolecular packing forces.[5] We present results on further investigation on the reactivity of C_{60} and C_{70} which leads to higher addition products. We also present other latest findings in this fast developing field.

1. A. L. Balch, V. J. Catalano, and J. W. Lee, *Inorg. Chem.,* **30,** 3980 (1991).
2. A. L. Balch, V. J. Catalano, J. W. Lee, M. M. Olmstead, and S. R. Parkin, *J. Am. Chem. Soc.,* **113,** 8953 (1991).
3. A. L. Balch, J. W. Lee, B. C. Noll, M. M. Olmstead, W. R. Fawcett, M. Fedurco, Paper 2119, Honolulu, HI, Meeting of the Electrochemical Society, May 16-21, 1993; A. L. Balch, J. W. Lee, B. C. Noll, and M. M. Olmstead, *J. C. S. Chem. Comm.,* Submitted.
4. A. L. Balch, J. W. Lee, B. C. Noll, and M. M. Olmstead, *J. Am. Chem. Soc.,* **114,** 10984 (1992).
5. A. L. Balch, J. W. Lee, and M. M. Olmstead, *Angew. Chem. Int. Ed. Engl.,* **31,** 1356 (1992).

687 Design and Operation of an Inexpensive Fullerene Synthesis Reactor: *A. G. Hill,* Dept. of Chemical Engineering, University of Southwestern Louisiana, Lafayette, LA 70504-4130, *P. A. Dooley,* Canal Carbon Black Operations, Cabot Corp., Franklin, LA 70538

The design and operation of a modified Kratchmer-Huffman fullerene reactor is described. The main body of the reactor consists of a joint of 2 in. I.D. annealed Pyrex glass pipe and a water-jacketed 2 in. stainless steel pipe spool section that are joined together with flanges and gasketed by an ordinary piece of cork gasket. The jacketed section of pipe is about 10 in. long. The glass pipe section was used with lengths in the range of 20-28 in. The two ends of the reactor are closed up with the positive electrode assembly on one end and the negative electrode assembly on the other end. The electrode assemblies entered the reactor through 1 in. thick blocks of SBR rubber. The reactor was used with gouging rods as a source of graphite. These rods are commonly available at welding supply stores. The particular rods used were 5/32 in. diameter (Profax Arc Gouging Carbons 4G DC). The power source for the reactor is an ordinary electric welding machine (Lincoln AC-225 arc welder). The reactor was operated with a continuous bleed of helium at a pressure of about 75 Torr. Presence of fullerenes in the reactor product was verified by HPLC and FTIR analysis.

688 Hydrogen Addition and Cycloaddition to C_{60} and C_{70}: *M. F. Meidine, R. Roers, A. Darwish, H. W. Kroto, R. Taylor,* and *D. R. M. Walton,* School of Chemistry, University of Sussex, Brighton, England BN1 9QJ

Toward hydrogenation with di-imide, both C_{60} and C_{70} show behavior parallel to that reported for hydrogenation with diborane: two isomers of $C_{70}H_2$ and a number of isomers of $C_{60}H_4$ are evident in the ^1H NMR spectra. The monoadducts formed between pentamethylcyclopentadiene and each of C_{60} and C_{70} have been prepared and characterized by ^{13}C NMR spectroscopy. The behavior of C_{70} in this reaction is compared with its behavior in other additions and in hydrogenation, and conclusions are drawn concerning the intrinsic reactivity of C_{70}.

Friday AM

689 Production of Fullerenes in Nitrogen Media: *O. M. Vovk, L. A. Vaschenko, O. A. Boryak, M. V. Kosevich, G. V. Andrievsky,* and *V. S. Shelkovsky,* B. Verkin Institute for Low Temperature Physics and Engineering of The Academy of Science of Ukraine, Kharkov 310164, Ukraine

An investigation of fullerene production with the arc-technique as a function of gas media type media (Ar, N_2, He) has been carried out. We have found that N_2 can be effectively used for arc-synthesis of fullerenes. A comparison between N_2, He, and Ar has shown that the yield of benzene-soluble products increases as: Ar < N_2 < He. The dependence of fullerene yields *vs.* gas pressure displays maxima at about 60-100 Torr for the 3 gases studied. The sublimation rate of the graphite rods increases by more than an order of magnitude from Ar to He to N_2, respectively. The benzene extracts of products have been analyzed by means of fast atom bombardment (FAB) and plasma desorption (252 Cf PD) mass spectrometry ("SELMI" instruments, Sumy, Ukraine). The most abundant ions in the mass spectra obtained in both ionization modes in all cases were m/z = 720 (C_{60}) and m/z 840 (C_{70}).

704 Characterization of Plasma-Enhanced Chemical Vapor Deposited Diamond-Like-Carbon Films: *G. Sreenivas, S. S. Ang, W. D. Brown, R. K. Ulrich,* and *S. Nasrazadani,* Dept. of Electrical, Chemical, and Mechanical Engineering, University of Arkansas, Fayetteville, AR 72701

The electrical, mechanical, optical, and chemical properties of plasma-enhanced chemically vapor deposited (PECVD) diamond-like-carbon (DLC) films with nitrogen trifluoride have been investigated. These DLC films have an increased deposition rate, a higher refractive index, a lower bulk resistivity and a lower optical bandgap compared to films deposited in methane. The surface morphology of these films were studied using scanning electron microscope. DLC films have been applied to test structures to evaluate their potential applications.

705 Solar Cells: Solution Optimized n-GaAs/Aqueous Polyselenide Photoelectrochemistry: *F. Forouzan* and *S. Licht,* Dept. of Chemistry, Clark University, Worcester, MA 01610

GaAs/aqueous polyselenide photoelectrochemical solar cells (PECs) have shown stable high efficiency solar to electrical conversion. This work demonstrates results to optimize photoelectrochemical characteristics of n-GaAs/polyselenide PEC. Optimization included investigation of effects of pH and selenium to selenide ratio while determining the distribution of species in the photoelectrolyte. The aqueous polyselenide equilibrium is highly complex generating a series of species of the form $Se_x = (x = 1\text{-}4)$, as well as H_2Se, HSe^-, and HO^-. Equilibrium constants and the distribution of species present in this photoelectrolyte have been determined spectroscopically. Thermodynamic determination of the speciation in solution is used to purposefully modify polyselenide photoelectrolytes and thereby the n-GaAs PEC behavior. These results indicate that solution phase optimization can enhance open-circuit voltage, and specific design of the distribution of species in solution can modify observed photoelectrochemical phenomena.

706 Blanket Tungsten Deposition by APCVD: *U. V. Patel, M. S. Haque, H. A. Naseem,* and *W. D. Brown,* University of Arkansas, Fayetteville, AR 72701

A recent trend in submicron VLSI technology is to use CVD tungsten as contact/via stud and interconnect layer. This study describes CVD of blanket tungsten at atmospheric pressure in a single wafer chamber. Statistically designed experiments were performed to study the effects of process parameters on resistivity, deposition rate, adhesion to silicon, and preferred orientation of the deposited film. The hydrogen reduction method was used for this study. Deposition rate and resistivity shows a good correlation with deposition temperature.

707 AuTi Metallization of CVD Diamond Substrates for Multichip Module Applications: *P. Chilakamarri, I. Meyyappan, H. Naseem,* and *W. D. Brown,* University of Arkansas, Fayetteville, AR 72701

Tenaciously adherent Au/Ti metallization was sputter deposited on CVD diamond substrates for potential use as interconnects in multichip module technology. Adhesion value up to 12 Kpsi was achieved with temperatures as low as 150°C, by preconditioning the diamond surface using *in situ* sputter etch technique. Carbide precipitates were identified at the metal-diamond interface by AES, at 400°C, while previously reported temperatures were above 800°C. Interdiffusion was observed at 400°C as revealed by sheet resistance measurements, optical micrographs, EDX, and AES techniques.

708 Deposition of a-SiN_x:H:F Films by PECVD for Use in Multijunction a-Si:H Based Solar Cells: *S. G. Kizzar, H. A. Naseem,* and *W. D. Brown,* Dept. of Electrical Engineering, University of Arkansas, Fayetteville, AR 72703

A study of a-SiN_x:H:F films deposited by PECVD from SiH_4 and NF_3 feed gases has been undertaken to determine their suitably as an i-layer for the upper p-i-n cell of a multijunction structure. This research has concentrated on varying the power density and feed gas flow rates. Hydrogen dilution of the feed gases was also studied. Optical and electrical measurements to determine bandgap energy, photoresponse, atomic composition, and defect density have been performed. Preliminary results show that increasing either the power or NF_3 flow rate increases the bandgap while hydrogen dilution improves the photoresponse by a factor of two or more.

709 Silane Assisted PECVD of Fluorinated, Hydrogenated Germanium Carbon Alloy, *P. R. Moffitt, H. A. Naseem,* and *W. D. Brown,* Dept. of Electrical Engineering, University of Arkansas, Fayetteville, AR 72701

Thin amorphous films of fluorinated, hydrogenated, germanium carbon alloy show promise for use in high efficiency, multijunction solar cells, but only hydrogenated alloys have been studied to date. This study explores growth of thin films of a-GeC:H, F alloy by PECVD deposition using GeF_4, CH_4, and H_2 as source gases. The addition of small amounts of SiH_4 as a source of sacrificial silicon atoms increases the film growth rate by up to six-fold without any silicon being incorporated in the film. Results from optical bandgap, FTIR, and EDS measurements are presented.

710 Preparation of Tl-Ba-Ca-Cu-O Thin Films by Laser Ablation and Low Temperature Annealing: *S. Afonso, I. N. Chan, Y. Q. Tang, F. T. Chan,* and *G. S. Salamo,* Dept. of Physics, University of Arkansas, Fayetteville, AR 72701 USA

$Tl_2Ba_2Ca_2Cu_3O_{10}$ (Tl-2223) and $Tl_1Ba_2Ca_2Cu_3O_9$ (Tl-1223) films with good superconducting properties have been produced by a two-step process. The BaCaCuO precursor films are first deposited by a eximer Ar-F laser. Tl is then introduced through low temperature diffusion. The films exhibit T_c of 115-121 K and J_c as high as 10^6 A/cm^2 at 77 K. Experimental details are presented. The influence of annealing conditions on the film quality is also discussed. (This work was supported by University of Arkansas HiDEC program, ARPA, and Conductus, Inc.).

711 Preparation of Superconducting $TlSr_2(Ca, Cr)Cu_2O_7$ Thin Films with Zero Resistance up to 100 K by Laser Ablation: *K. Y. Chen, Y. Q. Tang, I. N. Chan, Y. J. Shi, Z. Y. Chen, A. Pigg, Z. Z. Sheng, G. J. Salamo,* and *F. T. Chan,* Dept. of Physics, University of Arkansas, Fayetteville, AR 72701

Superconducting $TlSr_2(Ca, Cr)Cu_2O_7$ thin films have been prepared on single crystal MgO and $LaAlO_3$ substrates by laser ablation and post-annealing process. The films exhibit T_c up to 100 K and are highly c-axis oriented. Critical current density of 1×10^6 A/cm^2 at 77.7 K was obtained for the sample on $LaAlO_3$. The effect of different annealing processes on T_c is discussed. (This work was supported by University of Arkansas HiDEC program, DARPA, and Conductus, Inc.)

712 Deposition of Polycrystalline Silicon by PECVD at Low Temperatures: *M. R. Sathish Kumar, H. A. Naseem,* and *W. D. Brown,* Dept. of Electrical Engineering, University of Arkansas, Fayetteville, AR 72701

Polycrystalline silicon thin film transistors have a great potential in active matrix large screen flat panel displays because of their high carrier mobility. Low temperature deposition will allow low cost substrates to be used for such applications. Plasma-enhanced chemical vapor deposition using SiH_4, SiF_4, and H_2 as feed gases is being investigated at our University. Fluorine is expected to enhance crystallinity and improve film stability and quality. Statistical design of experiments will be used to study the effects of various deposition parameters on crystallinity, hydrogen content, surface morphology, and transport properties.

713 Defects Structure of ZnO/Ag Ceramic-Metal Two-Phase Material: *S. Jiang* and *J. B. Wagner, Jr.,* Center for Solid State Science, Arizona State University, Tempe, AZ 85287-1704

A new low-voltage varistor of ZnO/Ag ceramic-metal two-phase material with a very high nonlinear coefficient α has been developed in our lab. The abnormal electrical properties and the defect structure in various oxygen pressures were studied. AC impedance spectroscopy was used to study the electrical characteristics and the depletion layer of ZnO/Ag. Microstructural study showed that metallic silver segregates near grain boundary while a very small amount of silver is dissolved in ZnO to form a grain boundary layer barrier.

714 A New Apparatus for Measuring the Ultimate Strain of Thin Films: *G. Zhao* and *R. K. Ulrich,* Dept. of Chemical Engineering, University of Arkansas, Fayetteville, AR 72701

A four-point bending apparatus was built and tested that imparts controlled strain to thin inorganic films deposited on a substrate and enables that strain to be quantitatively measured at the onset of film cracking. With this apparatus, the strain being inflicted on the film does not have to be measured directly but can be calculated from the applied force, the Young's modulus, and the geometry of the substrate as long as the film is much thinner than the substrate. The onset of cracking was detected with an electrochemical method that gave sharp and reproducible indications of film failure.

715 Bubble Formation and Growth in Liquid Encapsulated Laser Chemical Vapor Deposition: *Q. J. Chen* and *S. D. Allen,* Tulane Laser Microfabrication Laboratory, Tulane University, New Orleans, LA 70118

We have reported liquid encapsulated laser chemical vapor deposition (LLCVD), by which high quality aluminum is deposited on Si substrates from triisobutylaluminum(TIBA) using a 514.5 nm cw Ar^+ laser. A liquid precursor allows for a fast deposition rate and provides a wide range of available precursors. We discovered that the deposition of aluminum from TIBA was always associated with a small bubble found at the irradiation site. We describe the LLCVD initiation study via the bubble formation and growth.

716 Laser Assisted Particle Removal of Micron Sized Contaminants on Silicon Surfaces: *L. A. Pollack, S. J. Lee,* and *S. D. Allen,* Tulane Laser Microfabrication Laboratory, Tulane University, New Orleans, LA 70118

Laser-assisted particle removal (LAPR) is new surface cleaning technique which involves the removal of particles from silicon surfaces. The contaminated silicon is dosed with water vapor which acts as an energy transfer medium. Pulsed radiation incident on the substrate then causes an explosive evaporation of the medium and the effective propulsion of the particles from the surface. We report on the removal of polystyrene and Al_2O_3 particles, as well as the potential for removing metal contaminants.

717 Laser Fabricated Fiber Optic Taps and Application to Sensors: *C. H. Lee* and *S. D. Allen,* Tulane Laser Microfabrication Laboratory, Tulane University, New Orleans, LA 70118

We demonstrated the rapid fabrication of high quality taps in the cladding of silica-based multimode and single mode optical fibers using a cw CO_2 laser ablative chemical etching process (LACE) operated at 10.6 μm. Previous experimental results have shown directed beam output with controllable output power from a single tap without disturbing guided mode patterns in the fiber. In this presentation the characteristics of such taps, the fabrication process, and the initial attempt to apply these taps to sensors are described.

718 Diagnostics and Mechanisms in Laser Chemical Vapor Deposition of Tungsten: *X. F. Zhang* and *S. D. Allen,* Tulane Laser Microfabrication Laboratory, Tulane University, New Orleans, LA 70118

Laser chemical vapor deposition (LCVD) of W uses a highly focused laser as the heat source to induce localized deposition of W on silicon substrates. In order to understand the geometry and the mechanisms of deposition in micron range, we study the substrate surface temperature distribution as well as the gas phase temperature distribution above the laser heated surface. The local concentration of both reactant and product species in a complex flow geometry is investigated, and the theoretical calculations are compared with experimental data.

EXTENDED DEADLINE SYMPOSIA PROGRAMS AND ABSTRACTS

Tuesday, October 12, 1993

JOINT RECENT NEWS PAPER SESSION
Dielectric Science and Technology/Electronics

D. E. Bailey, Chairman; L. K. White, Vice-Chairman
Rosella Room, 4th Floor

Monday, October 11, 1993

MICROMACHINING AND 3-D NANOSTRUCTURES
New Technology Subcommittee

N. McDonald, Chairman: D. Polla, Vice-Chairman
St. Charles A, 3rd Floor

M. Mehregany, Chairman; C. O. Bozler, Vice-Chairman

Tuesday, October 12, 1993

MICROMACHINING AND 3-D NANOSTRUCTURES
New Technology Subcommittee

S. K. Jones, Chairman: M. G. Allen, Vice-Chairman
St. Charles A, 3rd Floor

J. L. Shaw, Chairman; D. L. Kendal, Vice-Chairman

electron field emission into a vacuum. This paper explores the technical issues related to the success of FEA technology, the advantages and disadvantages of various proposed field emitter array displays, and reviews the current status of FEA display technology.

733 Hydroxide Etching of Silicon: Mechanisms and Structural Constraints: *D. L. Kendall,* University of New Mexico, Center for High Technology Materials, Albuquerque, NM 87131

The different etching mechanisms that have been proposed to explain the anisotropic etching of silicon are treated, with emphasis on work that needs to be done to finally accurately measure and explain the extremely large variations of the (111) etch rate in various basic solutions and additives, as well as the concomitant effects on the other low index crystal planes and on the masking oxides. The potential and observed effects of various defects on the dissolution of the silicon are also discussed. The practical implications of these factors in producing a wide variety of micromachined structures are also discussed in generic terms. These include deep grooves, V-grooves, mesa corners, groove corners, shallow micromirrors, cantilever beams, thin diaphragms, tall studs, super thin studs and wires, porous studs, stepped wall structures, and other forms.

734 Fabrication of Binary Optics in Silicon and Fused Silica Using Electron Beam Lithography and Reactive Ion Etching: *S. M. Shank, F. T. Chen, D. Mikolas,* and *H. G. Craighead,* School of Applied Engineering Physics, Cornell University, Ithaca, NY 14853, *F. Hass* and *D. A. Honey,* USAF Photonics Center, Rome Laboratory, Griffiss AFB, NY 13441

The fabrication of multilevel reflective and transmissive binary optics using high resolution electron beam lithography and reactive ion etching (RIE) in silicon and fused silica is described. The precise control of the wavefront phase requires precise etch depth control. For Si substrates, precisely controlled etching is achieved using thin film deposition of SiO and Cl_2RIE for four- and eight- level grating and mirrors. For fused silica substrates, the use of $CF_4/H_2O/O_2$ RIE is characterized to evaluate its use for four- and eight- level binary lenses. The effect of surface morphology on the optical performance of the devices is discussed.

735 Surface-Micromachined Vacuum Electronic Devices: *Q. Mei* and *D. L. Polla,* Dept. of Electrical Engineering, University of Minnesota, Minneapolis, MN 55455

Silicon surface micromachining methods have been used to fabricate vacuum microelectronic devices with integral vacuum cavities. Both tungsten and polysilicon microdiodes have been formed in 2 μm deep recessed trenches with silicon nitride encapsulation membranes. Device fabrication is based on the selective removal of a sacrificial oxide through on-chip chemical etch delivery channels and subsequent sealing in a 10^{-6} Torr electron beam evaporation chamber. Stable current *vs.* voltage characteristics have been obtained. Current *vs.* voltage characteristics in self-sealed tungsten emitter devices, for example, show good diode behavior with a current of 26 μA when biased in the forward direction with 50 V and less than −1 nA of reverse current. Surface analysis methods including atomic force microscopy, x-ray photoelectron spectroscopy, and ultraviolet photoelectron spectroscopy have been used in developing unit fabrication steps.

736 Nonlinear Vibrations of Submicron-Scaled, Single Crystal Silicon: *J. A. McMillan* and *N. C. MacDonald,* School of Electrical Engineering, Cornell University, Ithaca, NY 14853-5401.

In this paper we present results of studies of the nonlinear vibrations in micromachined resonators. We have fabricated resonators out of single crystal silicon (SCS) beams and also beams made of a composite of SCS and silicon nitride. These devices have minimum linewidths of 100 nm and resonant frequencies as high as 14 MHz. We have examined the structural nonlinearities that are a result of large amplitude deflections. Resonating structures can find applications as sensing devices by taking advantage of the sensitivity of the resonant frequency to changes in the structure or its surrounding atmosphere. These results are important for understanding the source of the nonlinear behavior and the limitations imposed on the amplitude of deflection and on the design of the resonator.

737 High Temperature Effects on a Micromachined Gated Field Emitter: *D. C. Perng* and *A. Feinerman,* EECS Dept., University of Illinois at Chicago, Chicago, IL 60607-7053

A silicon-gated tip has been fabricated on the middle of a microbridge 80 μm wide, 100 μm thick, and 5 mm long. This microbridge has resistance ~20 Ω and can be heated over 800°C easily. The leakage current from gate to cathode increases as temperature increases. The emission current follows Fowler-Nordheim plot at room temperature. The onset voltage of emission drops from 340 to 275 V as the tip was cleaned by heating the bridge. The high temperature characteristics of silicon field emission is under investigation.

738 Fabrication of Uncoated and Coated Silicon Field Emitter Arrays: *C. A. Ball, F. F. Lee, G. E. McGuire, W. D. Palmer,* and *D. Temple*, MCNC, Center for Microelectronic Systems Technologies, Research Triangle Park, NC 27709-2889

Fabrication of gated and ungated field emission structures using silicon as a cathode material has the advantage of compatibility with standard MOS and bipolar technologies. In addition, in such emitter structures there is no thermal mismatch between emitters and the underlying substrate, and, perhaps most importantly, silicon emitters can be sharpened in a controlled and repeatable manner via an oxidation process. Ungated and gated field emitter devices are fabricated in MCNC using orientation dependent etching and reoxidation sharpening techniques for the formation of the tips, silicon dioxide evaporation for the gate-cathode interelectrode insulator formation, and a lit-off process for the gate metal delineation. This fabrication process results in sharp (< 20 nm radius of curvature) emitters which have yielded electron emission currents of the order of microampers per tip with the gate to cathode voltage of less than 100 V. In this paper, issues concerning the statistical control of the fabrication process, critical in view of a need for reliable large (> 10,000 tips) arrays, as well as the integration of low work function coatings into the silicon emitter processing sequence are discussed. (The work has been supported in part by the Advanced Research Projects Agency, Contributions of David G. Vellenga, Lindsey Yadon, Xuefeng Liu, and Mark Kellam, all of MCNC, are also gratefully acknowledged.)

739 Grain Growth Mechanism of Doped Amorphous Silicon "Slit Nano Wire": *Y. Wada,* Advanced Research Laboratory, Hitachi, Ltd., Hatoyama, Saitama 350-03, Japan, *T. Kure, T. Kobayashi, T. Yoshimura, Y. Sudo,* and *Y. Goto,* Central Research Laboratory, Hitachi, Ltd. Kokubunji, Tokyo 185, Japan, *S. Kondo,* Advanced Research Laboratory, Hitachi, Ltd., Hatoyama, Saitama 350-03, Japan.

Grain growth mechanism of amorphous silicon (a-Si) layers in a 10 nm "slit nano wire" structure is studied, which are *in situ* doped with a phosphorus concentration of 1×10^{20} cm^{-3}. The fabrication processing steps of a-Si nano wire consist of delineating a 100 nm wide patterns by E-beam lithography, microwave dry etching of a 100 nm deep trenches in silicon substrate, conformable filling of the trenches by HLD SiO_2, slight etch-back of the HLD SiO_2 to form less than a 10 nm wide slit patterns, conformable deposition of doped amorphous silicon (a-Si) in the slit, followed by etch-back of the a-Si layer. The grain growth mechanism of the a-Si layer is studied as functions of annealing temperature between 525 and 580°C, and annealing time between 1 and 200 h. The activation energies of nucleation and grain growth are derived. Experimental results indicate that nucleation speed is slower than that in planar structure by several factors of magnitude. They also suggest that the driving force of the grain growth is the crystalline energy. Therefore, by choosing appropriate annealing conditions of the a-Si layer, the poly-Si grains grow to more than several μm in length.

740 Characterization of Properties of Silicon Probes of Nanometer Curvature: *J. Liu* and *J. Hren,* Dept. of Materials Science and Engineering, North Carolina State University, Raleigh, NC 27695-7907, *A. Stepanova* and *E. Givargizou,* Institute of Crystallography, Russian Academy of Sciences, Moscow, Russia

Highly curved field electron emitters of needle-shape or the edges of thin films have been fabricated recently for potential device applications in the emerging field of vacuum microelectronics. Silicon has been one material of choice because of the wealth of microelectronic experience that can be applied to fabricating emitter arrays. However, the operational environment of practical devices often results in instabilities and catastrophic failures, which causes can be traced to the unusual chemical reactivity of nanometer scale silicon, particularly in consort with the high electric fields and high current densities. Fortunately, fundamental data can be obtained from needle-shaped emitter prototypes that permit extensive characterization both under operational conditions and afterwards (FEM, FIM, SEM, and TEM) In addition, results of beneficial surface modification by SiC film formation are reported.

741 Nanomechanisms: Materials, Structures, and Devices: *N. C. MacDonald,* School of Electrical Engineering, Cornell University, Ithaca, NY 14853-5401

We discuss the fabrication and operation of micro instruments with integrated nanometer-scale tips. Such micro instruments include scanning tunnelling microscopes, atomic force microscopes, scanned-probe instruments, electron beam instruments, atom and molecular manipulators, and neural probes. The rapid advances in the microminiaturization of mechanical systems for scanned probe devices including integrated tips and integrated actuators are reviewed. Large, dense arrays of stationary or moving tips for field emission or for scanned-probe applications including the transport of atoms have been fabricated. Array architectures offer potential for smart, programmable (electrically or mechanically) tip-arrays; array cathodes for electron beam instruments; array sensors; and information storage systems with nm scale per bit storage. Materials properties of interest include internal friction, fatigue, wear, and adhesion. A short video presentation shows nanomechanisms in motion.

742 Fabrication and Surface Modification of Nanoscale Silicon Field Emitters: *J. J. Hren* and *J. Liu,* Dept. of Materials Science and Engineering, North Carolina State University, Raleigh, NC 27695, E. I. Givargizou, Institute of Crystallography, Russian Academy of Sciences, Moscow, Russia, *H. F. Gray,* Naval Research Laboratory, Washington, DC 200375

Nanoscale single crystal silicon field emitters were fabricated for applications such as vacuum microelectronics. The fabrication consists of localized eutectic deposition of Si onto a single-crystalline substrate via a chem-

central 200-300 Å thick thin-film-edge emitter is sandwiched between two gate electrodes, of which one is above the gate and the other below the gate. The thin-film-edge emitter structure miniaturizes capacitance because emission occurs along the emitter film-edge, thus permitting the use of very narrow gate electrodes. The transconductance is maximized because the radius of curvature is low due to the thinness of the emitter film. These two factors imply improved ft and fmax. The edge field emitter is essentially a line of closely spaced point emitters. We report the details of fabrication as well as device characterization of the thin-film-edge emitter vacuum transistor.

751 Microfabrication and Bio-Instrumentation: *M. Madou,* Microfabrication Applications, Palo Alto, CA 94306

In fast succession bulk micromachining, surface micromachining, and LIGA (from the German words; Litbografie, Galvanoformung and Abformung) have emerged as viable new manufacturing tools. Whereas bulk and surface micromachining are still focused on Si, LIGA does not necessarily involve Si at all. With the latter technology plastic, ceramic, and metal shapes can be made with unprecedented aspect ratios and precision. It is our opinion that one of the best matches for these new manufacturing technologies is bio-instrumentation. Often, size, response time, dead volume, and contamination avoidance are key in this application. The new technologies listed above, especially LIGA, will provide improved products in areas like fluid handling systems, diagnostics, catheters, filters, micro-PCR, drug delivery systems, microsurgery tools, stitching devices for skin, organs, and nerves, microphoresis devices, etc. In this paper these new fabrication tools are compared and illustrated with examples. Interesting and challenging microstructures for electrochemists are explored.

752 Microelectromechanical Systems: *M. Mehregany,* Electronics Design Center, Dept. of Electrical Engineering and Applied Physics, Case Western Reserve University, Cleveland, OH 44106

Miniaturization of mechanical systems promises unique opportunities for progress of science and technology in new directions and is expected to lead to an entirely new industry. Micromechanical devices and systems are inherently smaller, lighter, faster, and usually more precise than their macroscopic counterparts. Furthermore, since they are fabricated by integrated circuit processing *(i.e.,* microfabrication) techniques, they can be integrated with electronics to develop high performance closed-loop-controlled microelectromechanical systems (MEMS). In the most general form MEMS would consist of mechanical components, sensors, actuators, and electronics, all integrated in the same environment. An overview of MEMS, with emphasis on related research as Case Western Reserve University, is presented.

INDEX TO AUTHORS

Authors of Recent News Papers are not in this index

APPLICATION FOR ADMISSION
The Electrochemical Society, Inc.

Please fill out completely and mail to:
Secretary, The Electrochemical Society, Inc.
10 S. Main St.
Pennington, NJ 08534-2896
U.S.A.
Phone: 609-737-1902

Office use only

Date Recd. _____ $_____

Notice of Ackn._____

Checked:_____

Approved:_____

Please Print

1. Name: (Last) _____ (First) _____ (M.I.)_____

Business Affiliation:_____

Mailing Address: (Check One): ❑ Business ❑ Home_____

_____

City:_____ State/Province:_____ Zip/Postal Code:_____

Country:_____

Daytime Telephone: (_____)_____ Daytime Fax: (_____)_____

2. Date of Birth: (Month)_____ (Day) _____ (Year) _____

3. LOCAL SECTION affiliation:

___Canadian (60)
___Chicago (10)
___Cincinnati (12)
___Cleveland (15)
___Columbus (20)
___Detroit (25)
___European (27)
___Georgia (30)
___Japan (33)
___Metropolitan N.Y. (35)
___Midland (Mich.) (40)
___National Capital (45)
___New England(05)
___North Texas (55)
___Pacific Northwest (65)
___Philadelphia (70)
___Pittsburgh (75)
___San Francisco (85 & 86)
___South Texas (88)
___So. Calif.-Nevada (90)
___Southern Wisconsin (92)
___Twin Cities (96)
___None (99)

4. DIVISION/GROUP interests:
(Note primary interest(s) with the number 1 and secondary interest(s) with the number 2.)

___Battery (AO)
___Corrosion (BO)
___Dielectric Science & Technology (CO)
___Electrodeposition (DO)
___Electronics (EO)
___Energy Technology (GO)
___High Temperature Materials (HO)
___Industrial Electrolysis & Electrochemical Engineering (IO)
___Luminescence & Display Materials (KO)
___Organic & Biological Electrochemistry (FO)
___Physical Electrochemistry (JO)
___Sensor (LO)

5. Education: Institution | Dates Attended | Major Subject | Degree Earned

_____

_____

_____

6. Work Experience: (current, followed by previous)
Employer | Dates | Position

_____

_____

_____

_____

7. Membership Class: _____Student _____Active
(See reverse side for membership class and dues information. Note options for Date of Election, Active Life Membership, and Nonmember Meeting Registration Credit .)

8. Payment Information: Amount: $ _____
❑ Check enclosed payable to The Electrochemical Society, Inc., in U.S. Dollars, drawn on a U.S. Bank.
❑ VISA/MC #: _____ Exp. Date_____

9. Recommendations:
(**Student Member** applicants must obtain only one faculty member signature, including title and institution. **Active Member** applicants must be recommended by two Active Members in good standing; if obtaining signatures is inconvenient, please list their names and addresses.)

_____
Name (please print) | Signature | Address

_____
Name (please print) | Signature | Address

10. I hereby certify that the above statements are correct, and agree, if elected to the Society, to be governed by its Constitution and Bylaws and to promote the objectives of the Society as stated in its Constitution.

_____ _____
Applicant's Signature | Date

Rev. 5/93

SYMPOSIUM LISTING

San Francisco, California, May 22-27, 1994

Alternate Vehicle Fuels
Application of Surface Analysis Methods to Environmental/Material Interactions II
Battery/Energy Technology Joint General Session
Compatability of Biomedical Implants
Contamination Control and Defect Reduction in Semiconductor Manufacturing III
Corrosion General Session
Dielectric Science and Technology/Electronics Joint General Session
Dielectric Science and Technology/Electronics Joint Recent News Paper Session
Disposal and Handling of Non-Nuclear Hazardous Materials
Electrochemical Impedance Analysis of Geometrically Awkward and Mathematically Complex Structures
Electrochemistry and Materials Science of Cathodic Hydrogen Absorption and Adsorption
Electrochemistry and Solid-State Science Education at the Graduate and Undergraduate Levels
Electrode Materials and Processes for Energy Conversion and Storage III
Electrodeposition of Bulk, Thin-Film, and Surface Compounds
Fifty Years of Industrial Electrochemistry: The Industrial Electrolysis and Electrochemical Engineering Divisions 50th Anniversary Symposium
Fullerenes: Chemistry, Physics, and New Directions IV
Fundamentals of Electrochemical Process Design: A Tutorial
General Society Student Poster Session
In Situ Spectroscopy
Industrial Electrolysis and Electrochemical Engineering General Session
Ionic and Mixed Conducting Ceramics II
Large Area Wafer Growth and Processing for Electronic and Photonic Devices
Microstructures and Microfabricated Systems
Molten Salts IX
Nuclear Waste Disposal and Recycling
Organic Electrochemistry Symposium in Honor of Professor T. Shono
Organic and Biological Electrochemistry General Session
Organic Electrosynthesis: Pilot and Production Scale Processes
Physical Electrochemistry General Session
Plasma Processing X
Quantum Confinement: Physics and Applications
Sensor General Session
Silicon Materials Science and Technology VII
Silicon Nitride and Silicon Dioxide Thin Insulating Films
Silicon-on-Insulator Technology and Devices VI
Solid Electrolyte Sensors
State-of-the-Art Program on Compound Semiconductors XX
Water Purification by Photocatalytic, Photoelectrochemical, and Electrochemical Processes

Please keep in mind that BOTH a 75-word and extended abstract are required and must be submitted no later than December 1, 1993 to be considered for inclusion in the program. Refer to pages 64-72 of the June 1993 issue of ***Interface*** for the Call for Papers which includes complete symposium descriptions, the Abstract Form, and specific extended abstract preparation and mailing instructions. Contact: The Electrochemical Society, Inc., 10 South Main Street, Pennington, NJ 08534-2896, phone: 609-737-1902, for additional information.

THE ELECTROCHEMICAL SOCIETY CONTRIBUTING MEMBERS

BENEFACTOR MEMBERS

International Business Machines Corp.
Armonk, NY

Olin Corporation
Stamford, CT

PATRON MEMBERS

AT&T Bell Laboratories
Murray Hill, NJ

Dow Chemical Company
Central Research
Midland, MI

Eltech Systems Corporation
Chardon, OH
Fairport Harbor, OH

Eveready Battery Co., Inc.
Danbury, CT

Fujitsu Limited
Tokyo, Japan

Hitachi, Ltd.
Central Research Laboratory
Tokyo, Japan

Saft Research & Development Center
Hunt Valley, MD

Texas Instruments Inc.
Dallas, TX

SUSTAINING MEMBERS

The Aerospace Corp.
Los Angeles, CA

Alupower, Inc.
Warren, NJ

AMP Inc.
Harrisburg, PA

Analog Devices, Inc.
Norwood, MA

Ballard Power Systems, Inc.
North Vancouver, B.C., Canada

Battelle Memorial Institute
Columbus, OH

Boeing Co.
Seattle, WA

Central Electrochemical Research Institute
Tamilnadu, India

Comalco Aluminium Ltd.
Melbourne, Victoria, Australia

COMSAT Laboratories
Clarksburg, MD

Corning Incorporated
Corning, NY

CSIRO Division of Mineral Products
Port Melbourne, Victoria, Australia

E. I. Du Pont de Nemours & Co., Inc.
CR&D Engineering Laboratories
Wilmington, DE

Duracell Research Center
Needham, MA

ECO Energy Conversion
Somerville, MA

EG&G Princeton Applied Research Corp.
Princeton, NJ

Electrochemical Technology Corp.
Seattle, WA

Electronics and Telecommunications Research Institute
Chung Nam, Korea

Exxon Research & Engineering Co.
Engineering Technology Division
Florham Park, NJ

General Electric Co.
Corporate Research & Development
Schenectady, NY

OFFICERS OF THE SOCIETY

PRESIDENT
Robert P. Frankenthal

VICE PRESIDENTS
Kathryn R. Bullock
James A. Amick
Dennis W. Hess

SECRETARY
James McBreen

TREASURER
Ralph E. White

EXECUTIVE SECRETARY
Roque J. Calvo

DIVISIONS AND GROUPS OF THE SOCIETY

Battery

Frank R. McLarnon, Chairman
Samuel C. Levy, Vice-Chairman
Sid A. Megahed, Treasurer
Curtis F. Holmes, Secretary
Bruno Scrosati, Division Advisor

Corrosion

Hugh S. Isaacs, Chairman
Barry R. MacDougall, Vice-Chairman
Martin W. Kendig, Secretary-Treasurer
Donald B. Deal, Division Advisor

Dielectric Science and Technology

Robin A. Susko, Chairman
John R. Susko, Vice-Chairman
Henry G. Hughes, Treasurer
Y. H. Wong, Secretary
D. Noel Buckley, Division Advisor

Electrodeposition

Keith G. Sheppard, Chairman
Milan Paunovic, Vice-Chairman
Dexter D. Snyder, Secretary-Treasurer
Bruno Scrosati, Division Advisor

Electronics

George K. Celler, Chairman
Wayne E. Bailey, First Vice-Chairman
Hisham Z. Massoud, Second Vice-Chairman
S. N. G. Chu, Treasurer
Donald B. Deal, Secretary
D. Noel Buckley, Division Advisor

Energy Technology

Albert R. Landgrebe, Chairman
Bruce A. Parkinson, Vice-Chairman
Kimio Kinoshita, Treasurer
Krishnan Rajeshwar, Secretary
David A. Shores, Division Advisor

High Temperature Materials

Subhash C. Singhal, Chairman
William B. Johnson, Senior Vice-Chairman
Karl E. Spear, Junior Vice-Chairman
Ashok Khandkar, Secretary-Treasurer
John P. Dismukes, Division Advisor

Industrial Electrolysis and Electrochemical Engineering

Richard D. Varjian, Chairman
Eric J. Rudd, Vice-Chairman
Robert F. Savinell, Secretary-Treasurer
Donald B. Deal, Division Advisor

Luminescence and Display Materials

Thomas F. Soules, Chairman
William M. Yen, Vice-Chairman
Alok M. Srivastava, Secretary
David A. Shores, Division Advisor

Organic and Biological Electrochemistry

Fred M. Hawkridge, Chairman
Norman L. Weinberg, Vice-Chairman
Franklin A. Schultz, Secretary-Treasurer
William H. Smyrl, Division Advisor

Physical Electrochemistry

Brian E. Conway, Chairman
Daniel A. Scherson, Vice-Chairman
Shimshon Gottesfeld, Secretary-Treasurer
William H. Smyrl, Division Advisor

Sensor

Michael A. Butler, Chairman
H. V. Venkatasetty, Vice-Chairman
Antonio J. Ricco, Secretary-Treasurer
John P. Dismukes, Group Advisor